

# **ADAPTIVE FAULT LOCATION IN POWER SYSTEM NETWORKS BASED ON SYNCHRONIZED PHASOR MEASUREMENTS**

BY

**ALI H. AL-MOHAMMED**

A Dissertation Presented to the  
DEANSHIP OF GRADUATE STUDIES

**KING FAHD UNIVERSITY OF PETROLEUM & MINERALS**

DHAHRAN, SAUDI ARABIA

In Partial Fulfillment of the  
Requirements for the Degree of

## **DOCTOR OF PHILOSOPHY**

In

**ELECTRICAL ENGINEERING**

**OCTOBER 2012**

**KING FAHD UNIVERSITY OF PETROLEUM AND MINERALS**

**DHAHRAN, SAUDI ARABIA**

**DEANSHIP OF GRADUATE STUDIES**

*This thesis, written by*

**ALI HASSAN AL-MOHAMMED**

*under the direction of his Thesis Advisor, and approved by his Thesis Committee, has been presented to and accepted by the Dean of Graduate Studies, in partial fulfillment of the requirements for the degree of*

**DOCTOR OF PHILOSOPHY IN ELECTRICAL ENGINEERING**

***Thesis Committee:***



Prof. Mohammad A. Abido (Chairman)



Prof. Ibrahim M. Elamin (Member)



Prof. A. H. Abdurrahim (Member)



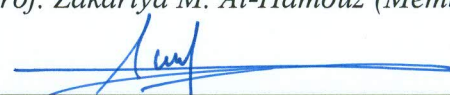
Prof. Zakariya M. Al-Hamouz (Member)



Dr. Ali A. Al-Shaikhi  
EE Department Chairman



Prof. Salam A. Zummo  
Dean of Graduate Studies



Dr. Mohamed Deriche (Member)

Date: 30/1/13

This Thesis is dedicated to

**The soul of my Father**

**The soul of Prof. Mohamed M. Mansour**

**Dear Mother**

**Brothers** *Tawfiq, Sami, Yaseen and Mohammed*

**Sisters**

**Beloved wife**

**Sons** *Hassan, Mohammed and Abdurrahman*

and

**Daughters** *Fatimah and Zahra'a*

## **Acknowledgement**

All praise is for Almighty Allah for having guided me at every stage of my life. Acknowledgement is due to King Fahd University of Petroleum and Minerals for providing support for this work.

I wish to express my deep appreciation to my thesis advisor Professor Mohammad A. Abido for his guidance throughout the course of this work. His suggestions as to how this work should be carried out were very helpful and his encouragement only made my small achievements ever possible.

I also wish to thank the other members of my doctoral committee Professor Ibrahim M. Elamin, Professor A. H. Abdurrahim, Professor Zakariya M. Al-Hamouz and Dr. Mohamed Deriche for their interest and guidance. Thanks are due to my department chairman, Dr. Ali A. Al-Shaikh and other faculty members for their support.

I also wish to acknowledge my roommate and close friend Engr. Mohammed H. Al-Mubarak who provided me with the moral support necessary to go through this work. He made the PHD program at KFUPM a very pleasant one.

A special thank is due to SEC top management and all my job superiors and partners for their valuable assistance and continuous encouragement.

I will always be indebted to my family for instilling in me the self-confidence and perseverance to pursue graduate studies. I am grateful to my late father, mother, sisters and brothers Tawfiq, Sami, Yaseen and Mohammed for their tacit encouragement throughout my academic career. Last, but not the least, I wish to thank my wife, sons and daughters for their patience, encouragement and support.

# Contents

<b>Acknowledgement</b>	<b>ii</b>
<b>List of Tables</b>	<b>x</b>
<b>List of Figures</b>	<b>xvii</b>
<b>Abstract (English)</b>	<b>xxii</b>
<b>Abstract (Arabic)</b>	<b>xxiii</b>
<b>Nomenclature</b>	<b>xxiv</b>
<b>Chapter 1 Introduction</b>	<b>1</b>
1.1 Importance of locating faults.....	3
1.2 Fault location techniques and algorithms .....	6
1.3 Factors affecting fault location accuracy .....	7
1.4 Motivation .....	9
1.5 Thesis objectives .....	11
1.6 Contributions .....	12
1.7 Organization of the thesis .....	13

<b>Chapter 2</b>	<b>Literature Review</b>	<b>14</b>
2.1	Fault location utilizing two-end synchronized measurements .....	15
2.2	Fault location on three-terminal and multi-terminal lines .....	20
2.3	Fault location on series-compensated lines .....	21
2.4	Adaptive fault location .....	22
2.5	Fault location in power system networks .....	25
<b>Chapter 3</b>	<b>Synchronized Phasor Measurements and Their Applications</b>	<b>30</b>
3.1	Historical overview .....	31
3.2	Classical definition of a phasor .....	32
3.3	Phasor measurement concepts .....	33
3.4	Synchrophasor definition and measurements .....	34
3.5	A generic PMU.....	35
3.6	Global positioning system (GPS) .....	38
3.7	Phasor measurement systems .....	39
3.8	Applications of phasor measurements .....	42
<b>Chapter 4</b>	<b>Optimal PMU Placement (OPP) Problem Formulation</b>	<b>44</b>
4.1	Introduction .....	47
4.2	OPP problem formulation .....	48
4.3	Extended OPP problem formulation .....	50
4.4	Justifying OPP problem for fault location application .....	51
<b>Chapter 5</b>	<b>Differential Evolution (DE) Algorithm for Solving OPP Problem</b>	<b>54</b>
5.1	DE optimization algorithm .....	55

5.1.1	DE fundamentals .....	56
5.1.2	DE key operators .....	58
5.2	DE application to OPP problem .....	60
5.2.1	Application to IEEE 14-bus test system .....	61
5.2.2	Application to IEEE 30-bus test system .....	63
5.2.3	Application to IEEE 39-bus test system .....	65
5.2.4	Application to IEEE 57-bus test system .....	67
5.2.5	Comparison with other optimization techniques .....	69
5.3	DE application to the extended OPP problem .....	71
5.3.1	Application to IEEE 14-bus test system .....	71
5.3.2	Application to IEEE 30-bus test system .....	77
5.3.3	Application to IEEE 39-bus test system .....	81
5.3.4	Application to IEEE 57-bus test system .....	86
5.3.5	Comparison with other optimization techniques .....	91
5.4	Application to a 115 kV system from SEC transmission network .....	92
5.5	Reducing DE search space .....	98
5.5.1	Virtual buses reduction rules .....	99
5.5.2	Base case .....	101
5.5.3	Selection of “don’t place” buses (Case I and II) .....	102
5.5.4	Selection of “must place” buses (Case III) .....	109
5.6	DE performance analysis .....	113
5.6.1	DE design with a variable scaling factor (Case IV) .....	113
5.6.2	DE design with another mutation scheme (Case V) .....	116

5.6.3	Selection of population size and crossover rate .....	120
<b>Chapter 6</b>	<b>Transmission Line Parameter Identification using PMU Synchronized Measurements</b>	<b>122</b>
6.1	Introduction .....	123
6.2	Transmission line parameter identification methods .....	126
6.2.1	Single measurement method .....	126
6.2.2	Double measurement method .....	128
6.2.3	Multiple measurement method using linear regression .....	129
6.3	Simulation results.....	131
6.3.1	Results with noise-free measurements .....	132
6.3.2	Results with biased and non-biased noise .....	133
<b>Chapter 7</b>	<b>Determination of Thevenin's Equivalent (TE) using PMU Measurements</b>	<b>137</b>
7.1	Algorithm description .....	138
7.2	Simulation results .....	141
<b>Chapter 8</b>	<b>Adaptive PMU-based Fault Location Algorithms for Two-terminal Lines</b>	<b>147</b>
8.1	Introduction .....	147
8.2	Proposed adaptive fault location algorithm # 1 (AFLA-1) .....	149
8.3	Simulation results of AFLA-1 .....	159
8.3.1	Data generation and conditioning .....	159
8.3.2	Accuracy analysis .....	160
8.3.3	Influence of the fault resistance .....	164
8.3.4	Influence of fault inception angle .....	166



8.3.5	Influence of the pre-fault loading .....	167
8.3.6	Error analysis .....	169
8.4	Proposed adaptive fault location algorithm # 2 (AFLA-2) .....	172
8.5	Simulation results of AFLA-2 .....	175
8.5.1	Data generation and conditioning .....	177
8.5.2	Accuracy analysis .....	177
8.5.3	Influence of the fault resistance .....	181
8.5.4	Influence of fault inception angle .....	183
8.5.5	Influence of the pre-fault loading .....	184
8.5.6	Error analysis .....	186
8.6	Comparison with nonadaptive algorithm for two-terminal lines .....	196
<b>Chapter 9</b>	<b>Adaptive PMU-based Fault Location Algorithm for Three-terminal Lines</b>	<b>198</b>
9.1	PMU-based parameter estimation of a three-terminal line .....	199
9.1.1	Line sections having the same parameters per unit length .....	200
9.1.2	Line sections having different parameters .....	202
9.2	Description of the proposed algorithm .....	204
9.3	Simulation results .....	210
9.3.1	Data generation and conditioning .....	211
9.3.2	Accuracy analysis .....	213
9.3.3	Influence of the fault resistance .....	213
9.3.4	Influence of fault inception angle .....	229
9.3.5	Influence of the pre-fault loading .....	232

9.4	Comparison with nonadaptive algorithm for three-terminal lines .....	233
<b>Chapter 10</b>	<b>Adaptive PMU-based Fault Location Algorithm for Series-compensated Lines</b>	<b>236</b>
10.1	Series capacitor location .....	241
10.2	Series capacitor scheme .....	241
10.2.1	Voltage-current relationship of MOV .....	243
10.2.2	Internal and external faults .....	244
10.3	PMU-based parameter estimation of a SCL .....	245
10.4	Description of the proposed algorithm .....	250
10.4.1	Fault location subroutine $S_A$ .....	252
10.4.2	Fault location subroutine $S_B$ .....	255
10.4.3	Selection procedure .....	257
10.5	Simulation results .....	257
10.5.1	Data generation and conditioning .....	258
10.5.2	Accuracy analysis .....	262
10.5.3	Influence of the fault resistance .....	265
10.5.4	Influence of fault inception angle .....	267
10.5.5	Influence of the pre-fault loading .....	267
10.5.6	Influence of the compensation degree .....	269
10.6	Comparison with nonadaptive algorithm for series-compensated lines .....	271
<b>Chapter 11</b>	<b>RTDS Implementation of the Proposed PMU-based Fault Locator</b>	<b>273</b>
11.1	Real-time digital simulator (RTDS) .....	273

11.1.1	RTDS hardware .....	274
11.1.2	RTDS software .....	277
11.2	RTDS applications .....	279
11.3	Experimental work and simulation results .....	281
11.4	Comparison with RTDS simulation results .....	295
<b>Chapter 12</b>	<b>Conclusions and Future Work</b>	<b>298</b>
12.1	Summary and conclusions .....	298
12.2	Future work .....	303
<b>References</b>		<b>306</b>
<b>Extracted papers</b>		<b>322</b>
<b>Appendices</b>		<b>324</b>
A.	NASPI's synchrophasor applications table .....	324
B.	IEEE test systems .....	325
<b>Vita</b>		<b>328</b>

# List of Tables

3.1	PMU deployment in different parts of the world .....	43
5.1	OPP of IEEE 14-bus Test System .....	62
5.2	OPP of IEEE 30-bus Test System .....	64
5.3	OPP of IEEE 39-bus Test System .....	66
5.4	OPP of IEEE 57-bus Test System .....	68
5.5	Number of PMUs from DE and other Optimization Algorithms .....	70
5.6	Case-I OPP of IEEE 14-bus Test System .....	73
5.7	Case-II OPP of IEEE 14-bus Test System .....	73
5.8	Effect of the Maximization of PMU Measurement Redundancy (Case-I and Case-II OPP) .....	74
5.9	Case-III OPP of IEEE 14-bus Test System .....	74
5.10	Case-IV OPP of IEEE 14-bus Test System .....	75
5.11	Case-I OPP of IEEE 30-bus Test System .....	78
5.12	Case-II OPP of IEEE 30-bus Test System .....	78
5.13	Case-III OPP of IEEE 30-bus Test System .....	79
5.14	Case-IV OPP of IEEE 30-bus Test System .....	79
5.15	Case-I OPP of IEEE 39-bus Test System .....	82
5.16	Case-II OPP of IEEE 39-bus Test System .....	83
5.17	Case-III OPP of IEEE 39-bus Test System .....	84
5.18	Case-IV OPP of IEEE 39-bus Test System .....	84
5.19	Case-I OPP of IEEE 57-bus Test System .....	87
5.20	Case-II OPP of IEEE 57-bus Test System .....	87
5.21	Case-III OPP of IEEE 57-bus Test System .....	88
5.22	Case-IV OPP of IEEE 57-bus Test System .....	89
5.23	Number of PMUs from DE and other Optimization Algorithms .....	91
5.24	Case-I OPP of SEC 115 kV System .....	95
5.25	Case-II OPP of SEC 115 kV System .....	95

5.26	Case-III OPP of SEC 115 kV System .....	96
5.27	Case-IV OPP of SEC 115 kV System .....	96
5.28	IEEE 14-bus system-Case I .....	103
5.29	IEEE 30-bus system-Case I .....	104
5.30	IEEE 39-bus system-Case I .....	104
5.31	IEEE 57-bus system-Case I .....	105
5.32	IEEE 14-bus system-Case II .....	107
5.33	IEEE 30-bus system-Case II .....	108
5.34	IEEE 39-bus system-Case II .....	108
5.35	IEEE 57-bus system-Case II .....	109
5.36	IEEE 14-bus system-Case III .....	111
5.37	IEEE 30-bus system-Case III .....	112
5.38	IEEE 39-bus system-Case III .....	112
5.39	IEEE 57-bus system-Case III .....	113
5.40	IEEE 14-bus system-Case IV .....	115
5.41	IEEE 30-bus system-Case IV .....	115
5.42	IEEE 39-bus system-Case IV .....	115
5.43	IEEE 57-bus system-Case IV .....	116
5.44	IEEE 14-bus system-Case V .....	118
5.45	IEEE 30-bus system-Case V .....	119
5.46	IEEE 39-bus system-Case V .....	119
5.47	IEEE 57-bus system-Case V .....	120
6.1	Actual Line Parameters .....	132
6.2	Calculated Line Parameters .....	132
6.3	Percentage Error in the Calculated Line Parameters .....	132
6.4	Methods Performance When Noise and Bias Errors Appear in the Measurements .....	136
8.1	Parameters of the 115 kV, 60 Hz SEC Network .....	160
8.2	AFLA-1: Fault Location Estimates for Single-Line-to-Ground Faults .....	161
8.3	AFLA-1: Fault Location Estimates for Line-to-Line Faults .....	162

8.4	AFLA-1: Fault Location Estimates for Line-to-Line-to-Ground Faults .....	163
8.5	AFLA-1: Fault Location Estimates for Three-Phase Faults .....	163
8.6	AFLA-1: Influence of the Fault Resistance on the Algorithm's Accuracy for Single-Line-to-Ground Faults (Actual FL: 0.8 p.u.) .....	164
8.7	AFLA-1: Influence of the Fault Resistance on the Algorithm's Accuracy for Line-to-Line Faults (Actual FL: 0.8 p.u.) .....	165
8.8	AFLA-1: Influence of the Fault Resistance on the Algorithm's Accuracy for Line-to-Line-to-Ground Faults (Actual FL: 0.8 p.u.) .....	165
8.9	AFLA-1: Influence of the Fault Resistance on the Algorithm's Accuracy for Three-Phase Faults (Actual FL: 0.8 p.u.) .....	166
8.10	AFLA-1: Influence of the Fault Inception Angle on the Algorithm's Accuracy (Actual FL: 0.6 p.u.) .....	167
8.11	AFLA-1: Influence of the Pre-fault Loading at Terminal A on the Algorithm's Accuracy (Actual FL: 0.6 p.u.) .....	168
8.12	AFLA-1: Influence of 2% Voltage Magnitude Error on Fault Location Estimates for Single-Line-to-Ground Faults .....	169
8.13	AFLA-1: Influence of 2° Voltage Angle Error on Fault Location Estimates for Single-Line-to-Ground Faults .....	170
8.14	AFLA-1: Influence of 2% Current Magnitude Error on Fault Location Estimates for Single-Line-to-Ground Faults .....	171
8.15	AFLA-1: Influence of 2° Current Angle Error on Fault Location Estimates for Single-Line-to-Ground Faults .....	172
8.16	AFLA-2: Fault Location Estimates for Single-Line-to-Ground Faults .....	178
8.17	AFLA-2: Fault Location Estimates for Line-to-Line Faults .....	179
8.18	AFLA-2: Fault Location Estimates for Line-to-Line-to-Ground Faults .....	180
8.19	AFLA-2: Fault Location Estimates for Three-Phase Faults .....	180
8.20	AFLA-2: Influence of the Fault Resistance on the Algorithm's Accuracy for Single-Line-to-Ground Faults (Actual FL: 0.8 p.u.) .....	181
8.21	AFLA-2: Influence of the Fault Resistance on the Algorithm's Accuracy for Line-to-Line Faults (Actual FL: 0.8 p.u.) .....	182
8.22	AFLA-2: Influence of the Fault Resistance on the Algorithm's Accuracy for Line-to-Line-to-Ground Faults (Actual FL: 0.8 p.u.) .....	182
8.23	AFLA-2: Influence of the Fault Resistance on the Algorithm's Accuracy for Three-Phase Faults (Actual FL: 0.8 p.u.) .....	183

8.24	AFLA-2: Influence of the Fault Inception Angle on the Algorithm's Accuracy (Actual FL: 0.6 p.u.) .....	184
8.25	AFLA-2: Influence of the Pre-fault Loading at Terminal A on the Algorithm's Accuracy (Actual FL: 0.6 p.u.) .....	185
8.26	AFLA-2: Influence of 2% Voltage Magnitude Error on Fault Location Estimates for Single-Line-to-Ground Faults (MMLR) .....	187
8.27	AFLA-2: Influence of 2° Voltage Angle Error on Fault Location Estimates for Single-Line-to-Ground Faults (MMLR) .....	188
8.28	AFLA-2: Influence of 2% Current Magnitude Error on Fault Location Estimates for Single-Line-to-Ground Faults (MMLR) .....	189
8.29	AFLA-2: Influence of 2° Current Angle Error on Fault Location Estimates for Single-Line-to-Ground Faults (MMLR) .....	190
8.30	AFLA-2: Influence of 2% Voltage Magnitude Error on Fault Location Estimates for Single-Line-to-Ground Faults (SM) .....	191
8.31	AFLA-2: Influence of 2° Voltage Angle Error on Fault Location Estimates for Single-Line-to-Ground Faults (SM) .....	192
8.32	AFLA-2: Influence of 2% Current Magnitude Error on Fault Location Estimates for Single-Line-to-Ground Faults (SM) .....	193
8.33	AFLA-2: Influence of 2° Current Angle Error on Fault Location Estimates for Single-Line-to-Ground Faults (SM) .....	194
8.34	AFLA-2: Influence of Line Parameters and System Impedance Variation on the Algorithm's Accuracy (Actual FL: 0.6 p.u.) .....	197
9.1	Parameters of the 500 kV Three-terminal Network .....	211
9.2	Fault Location Estimates for Single-Line-to-Ground Faults on Section A .	214
9.3	Fault Location Estimates for Line-to-Line Faults on Section A .....	215
9.4	Fault Location Estimates for Line-to-Line-to-Ground Faults on Section A	216
9.5	Fault Location Estimates for Three-Phase Faults on Section A .....	216
9.6	Fault Location Estimates for Single-Line-to-Ground Faults on Section B .	217
9.7	Fault Location Estimates for Line-to-Line Faults on Section B .....	218
9.8	Fault Location Estimates for Line-to-Line-to-Ground Faults on Section B	219
9.9	Fault Location Estimates for Three-Phase Faults on Section B .....	219
9.10	Fault Location Estimates for Single-Line-to-Ground Faults on Section C .	220
9.11	Fault Location Estimates for Line-to-Line Faults on Section C .....	221
9.12	Fault Location Estimates for Line-to-Line-to-Ground Faults on Section C	222

9.13	Fault Location Estimates for Three-Phase Faults on Section C .....	222
9.14	Influence of the Fault Resistance on the Algorithm's Accuracy for Single-Line-to-Ground Faults (Actual FL: 0.4 p.u. from Terminal A) .....	223
9.15	Influence of the Fault Resistance on the Algorithm's Accuracy for Line-to-Line Faults (Actual FL: 0.4 p.u. from Terminal A) .....	223
9.16	Influence of the Fault Resistance on the Algorithm's Accuracy for Line-to-Line-to-Ground Faults (Actual FL: 0.4 p.u. from Terminal A) .....	224
9.17	Influence of the Fault Resistance on the Algorithm's Accuracy for Three-Phase Faults (Actual FL: 0.4 p.u. from Terminal A) .....	224
9.18	Influence of the Fault Resistance on the Algorithm's Accuracy for Single-Line-to-Ground Faults (Actual FL: 0.4 p.u. from Terminal B) .....	225
9.19	Influence of the Fault Resistance on the Algorithm's Accuracy for Line-to-Line Faults (Actual FL: 0.4 p.u. from Terminal B) .....	225
9.20	Influence of the Fault Resistance on the Algorithm's Accuracy for Line-to-Line-to-Ground Faults (Actual FL: 0.4 p.u. from Terminal B) .....	226
9.21	Influence of the Fault Resistance on the Algorithm's Accuracy for Three-Phase Faults (Actual FL: 0.4 p.u. from Terminal B) .....	226
9.22	Influence of the Fault Resistance on the Algorithm's Accuracy for Single-Line-to-Ground Faults (Actual FL: 0.4 p.u. from Terminal C) .....	227
9.23	Influence of the Fault Resistance on the Algorithm's Accuracy for Line-to-Line Faults (Actual FL: 0.4 p.u. from Terminal C) .....	227
9.24	Influence of the Fault Resistance on the Algorithm's Accuracy for Line-to-Line-to-Ground Faults (Actual FL: 0.4 p.u. from Terminal C) .....	228
9.25	Influence of the Fault Resistance on the Algorithm's Accuracy for Three-Phase Faults (Actual FL: 0.4 p.u. from Terminal C) .....	228
9.26	Influence of the Fault Inception Angle on the Algorithm's Accuracy (Actual FL: 0.4 p.u. from Terminal A) .....	229
9.27	Influence of the Fault Inception Angle on the Algorithm's Accuracy (Actual FL: 0.4 p.u. from Terminal B) .....	230
9.28	Influence of the Fault Inception Angle on the Algorithm's Accuracy (Actual FL: 0.4 p.u. from Terminal C) .....	230
9.29	Influence of the Pre-fault Loading at Terminal A on the Algorithm's Accuracy (Actual FL: 0.4 p.u. from Terminal A) .....	232
9.30	Influence of the Pre-fault Loading at Terminal B on the Algorithm's Accuracy (Actual FL: 0.4 p.u. from Terminal B) .....	233



9.31	Influence of the Pre-fault Loading at Terminal C on the Algorithm's Accuracy (Actual FL: 0.4 p.u. from Terminal C) .....	233
9.32	Three-terminal Lines: Influence of Line Parameters and System Impedance Variation on the Algorithm's Accuracy (Actual FL: 0.4 p.u. from Terminal A) .....	235
10.1	Weighting Coefficients .....	254
10.2	Share Coefficients .....	255
10.3	Parameters of the 400 kV Series Compensated Network .....	261
10.4	Fault-location Estimates for Single-Line-to-Ground Faults on Sections A-X & B-Y .....	262
10.5	Fault-location Estimates for Line-to-Line Faults on Sections A-X & B-Y .	263
10.6	Fault-location Estimates for Line-to-Line-to-Ground Faults on Sections A-X & B-Y .....	264
10.7	Fault-location Estimates for Three-Phase Faults on Sections A-X & B-Y .	264
10.8	Influence of the Fault Resistance on the Algorithm's Accuracy for Single-Line-to-Ground Faults on Section B-Y (Actual FL: 0.6 p.u. from Terminal A) .....	265
10.9	Influence of the Fault Resistance on the Algorithm's Accuracy for Line-to-Line Faults on Section B-Y (Actual FL: 0.6 p.u. from Terminal A) .....	266
10.10	Influence of the Fault Resistance on the Algorithm's Accuracy for Line-to-Line-to-Ground Faults on Section B-Y (Actual FL: 0.6 p.u. from Terminal A) .....	266
10.11	Influence of the Fault Resistance on the Algorithm's Accuracy for Three-Phase Faults on Section B-Y (Actual FL: 0.4 p.u. from Terminal A) .....	267
10.12	Influence of the Fault Inception Angle on the Algorithm's Accuracy (Actual FL: 0.6 p.u. from Terminal A) .....	268
10.13	Influence of the Pre-fault Loading at Terminal A on the Algorithm's Accuracy (Actual FL: 0.6 p.u. from Terminal A) .....	269
10.14	Influence of the Compensation Degree on the Algorithm's Accuracy (Actual FL: 0.6 p.u. from Terminal A) .....	270
10.15	SCLs: Influence of Line Parameters and System Impedance Variation on the Algorithm's Accuracy (Actual FL: 0.6 p.u. from Terminal A) .....	272
11.1	Parameters of the 400 kV Network Implemented in RSCAD .....	282
11.2	RTDS: Influence of the Fault Type and Location on the Algorithm's Accuracy .....	294

11.3	RTDS: Influence of the Fault Resistance on the Algorithm's Accuracy (FL=0.6 p.u.) .....	294
11.4	RTDS: Influence of the Fault Inception Angle on the Algorithm's Accuracy (FL=0.6 p.u.) .....	295
11.5	Influence of the Fault Type and Location on the Algorithm's Accuracy ...	296
11.6	Influence of the Fault Resistance on the Algorithm's Accuracy (FL=0.6 p.u.) .....	296
11.7	Influence of the Fault Inception Angle on the Algorithm's Accuracy (FL=0.6 p.u.) .....	297

# List of Figures

2.1	Two-end Synchronized Fault-location Arrangement using PMUs .....	17
2.2	Transmission line compensated with SCs and MOVs installed at midpoint	21
2.3	Transmission line compensated with SCs and MOVs installed at both ends .....	21
2.4	Illustration of a distorted voltage analysis using wavelet transform .....	28
3.1	Phasor representation of a sinusoidal waveform .....	33
3.2	PMU block logic diagram .....	36
3.3	Hierarchy of the phasor measurement systems and levels of phasor data concentrators .....	40
4.1	Topological observability rules .....	50
5.1	Flow chart of a typical DE optimization process .....	60
5.2	IEEE 14-bus: DEA convergence for $F=0.9$ and different values of $CR$ .....	62
5.3	IEEE 14-bus: DEA convergence for $F=0.8$ and different values of $CR$ .....	63
5.4	IEEE 14-bus: DEA convergence for $F=0.7$ and different values of $CR$ .....	63
5.5	IEEE 30-bus: DEA convergence for $F=0.9$ and different values of $CR$ .....	64
5.6	IEEE 30-bus: DEA convergence for $F=0.8$ and different values of $CR$ .....	65
5.7	IEEE 30-bus: DEA convergence for $F=0.7$ and different values of $CR$ .....	65
5.8	IEEE 39-bus: DEA convergence for $F=0.9$ and different values of $CR$ .....	66
5.9	IEEE 39-bus: DEA convergence for $F=0.8$ and different values of $CR$ .....	67
5.10	IEEE 39-bus: DEA convergence for $F=0.7$ and different values of $CR$ .....	67
5.11	IEEE 57-bus: DEA convergence for $F=0.9$ and different values of $CR$ .....	68
5.12	IEEE 57-bus: DEA convergence for $F=0.8$ and different values of $CR$ .....	69
5.13	IEEE 57-bus: DEA convergence for $F=0.7$ and different values of $CR$ .....	69
5.14	DEA Convergence for $F=0.7$ and Different values of $CR$ (IEEE 14-bus, Case-I) .....	75
5.15	DEA Convergence for $F=0.7$ and Different values of $CR$ (IEEE 14-bus, Case-II) .....	76
5.16	DEA Convergence for $F=0.7$ and Different values of $CR$ (IEEE 14-bus, Case-III) .....	76

5.17	DEA Convergence for $F=0.7$ and Different values of $CR$ (IEEE 14-bus, Case-IV) .....	76
5.18	DEA Convergence for $F=0.7$ and Different values of $CR$ (IEEE 30-bus, Case-I) .....	80
5.19	DEA Convergence for $F=0.7$ and Different values of $CR$ (IEEE 30-bus, Case-II) .....	80
5.20	DEA Convergence for $F=0.7$ and Different values of $CR$ (IEEE 30-bus, Case-III) .....	81
5.21	DEA Convergence for $F=0.7$ and Different values of $CR$ (IEEE 30-bus, Case-IV) .....	81
5.22	DEA Convergence for $F=0.7$ and Different values of $CR$ (IEEE 39-bus, Case-I) .....	85
5.23	DEA Convergence for $F=0.7$ and Different values of $CR$ (IEEE 39-bus, Case-II) .....	85
5.24	DEA Convergence for $F=0.7$ and Different values of $CR$ (IEEE 39-bus, Case-III) .....	85
5.25	DEA Convergence for $F=0.7$ and Different values of $CR$ (IEEE 39-bus, Case-IV) .....	86
5.26	DEA Convergence for $F=0.7$ and Different values of $CR$ (IEEE 57-bus, Case-I) .....	89
5.27	DEA Convergence for $F=0.7$ and Different values of $CR$ (IEEE 57-bus, Case-II) .....	90
5.28	DEA Convergence for $F=0.7$ and Different values of $CR$ (IEEE 57-bus, Case-III) .....	90
5.29	DEA Convergence for $F=0.7$ and Different values of $CR$ (IEEE 57-bus, Case-IV) .....	90
5.30	One line diagram of SEC 115 kV system .....	93
5.31	DEA Convergence for $F=0.7$ and Different values of $CR$ (SEC system, Case-I) .....	97
5.32	DEA Convergence for $F=0.7$ and Different values of $CR$ (SEC system, Case-II) .....	97
5.33	DEA Convergence for $F=0.7$ and Different values of $CR$ (SEC system, Case-III) .....	97
5.34	DEA Convergence for $F=0.7$ and Different values of $CR$ (SEC system, Case-IV) .....	98
6.1	$\pi$ -type equivalent circuit of a single line .....	127

6.2	Phasor voltages at bus-38 and associated random noise .....	134
7.1	Phasor diagram for the first set of measurements .....	139
7.2	Phasor diagram for the second set of measurements .....	139
7.3	Sampling of 1 <sup>st</sup> set of PMU phasor measurements at bus 30 & bus 38 .....	142
7.4	Sampling of 2 <sup>nd</sup> set of PMU phasor measurements at bus 30 & bus 38 .....	143
7.5	Sampling of 3 <sup>rd</sup> set of PMU phasor measurements at bus 30 & bus 38 .....	144
7.6	Z circles at bus 30 .....	145
7.7	Z circles at bus 38 .....	145
7.8	Determination of $Z_{th}$ at bus 30 .....	146
7.9	Determination of $Z_{th}$ at bus 38 .....	146
8.1	Superimposed network of a transmission line .....	151
8.2	Curve of voltage for AG fault at 170 km from bus A .....	153
8.3	Curve of voltage for BG fault at 50 km from bus A .....	153
8.4	Curve of voltage for CG fault at 100 km from bus A .....	154
8.5	Curve of voltage for ABC fault at 40 km from bus A .....	154
8.6	Curve of voltage for ABC fault at 120 km from bus A .....	155
8.7	Curve of voltage for ABC fault at 180 km from bus A .....	155
8.8	Curve of voltage for AC fault at 15 km from bus A .....	156
8.9	Curve of voltage for AB fault at 110 km from bus A .....	156
8.10	Curve of voltage for BC fault at 175 km from bus A .....	157
8.11	Curve of voltage for BCG fault at 35 km from bus A .....	157
8.12	Curve of voltage for ABG fault at 90 km from bus A .....	158
8.13	Curve of voltage for ACG fault at 165 km from bus A .....	158
8.14	Flow chart of AFLA-1 .....	159
8.15	AFLA-1: Effect of fault inception angle on FL accuracy (Actual FL: 0.6 p.u.) .....	167
8.16	AFLA-1: Effect of pre-fault loading on FL accuracy (Actual FL: 0.6 p.u.) .....	168
8.17	A faulted power system .....	173
8.18	Transmission line model in post-fault .....	173
8.19	Thevenin equivalent model of the faulted system .....	173

8.20	Flow chart of AFLA-2 .....	176
8.21	AFLA-2: Effect of fault inception angle on FL accuracy (Actual FL: 0.6 p.u.) .....	184
8.22	AFLA-2: Effect of pre-fault loading on FL accuracy (Actual FL: 0.6 p.u.) .....	185
8.23	FL error with 2% error in voltage magnitude (AG-10) .....	194
8.24	FL error with 2% error in current magnitude (CG-10) .....	195
8.25	FL error with 2° error in voltage angle (BG-10) .....	195
8.26	FL error with 2° error in current angle (CG-10) .....	195
8.27	Influence of parameter variation on FL accuracy in two-terminal lines .....	197
9.1	A three-terminal transmission network .....	199
9.2	Steady state $\pi$ equivalent model of a three-terminal transmission network .....	200
9.3	Flow chart showing the algorithm to identify the faulted section .....	206
9.4	Faulted three-terminal system in $\pi$ equivalent model .....	207
9.5	Flow chart of the proposed AFLA for a three-terminal line .....	210
9.6	Sampling of voltage and current phasors at terminal A, B, C .....	212
9.7	Effect of fault inception angle on FL accuracy (Actual FL: 0.4 p.u. from A) .....	231
9.8	Effect of fault inception angle on FL accuracy (Actual FL: 0.4 p.u. from B) .....	231
9.9	Effect of fault inception angle on FL accuracy (Actual FL: 0.4 p.u. from C) .....	231
9.10	Influence of parameter variation on FL accuracy in three-terminal lines ...	235
10.1	Series capacitor of a gapped scheme .....	242
10.2	Series capacitor of a gapless scheme .....	242
10.3	One line diagram of a series compensated line .....	246
10.4	Positive sequence network of the system during normal operation .....	246
10.5	Diagram of a line compensated with series capacitors equipped with MOVs .....	251
10.6	Subroutine $S_A$ - scheme of SC line under $F_A$ .....	251
10.7	Subroutine $S_B$ - scheme of SC line under $F_B$ .....	251
10.8	Test system with a SC line .....	258

10.9	Sampling of 1 <sup>st</sup> set of PMU phasor measurements at bus A & bus B .....	259
10.10	Sampling of 2 <sup>nd</sup> set of PMU phasor measurements at bus A & bus B .....	260
10.11	Sampling of 3 <sup>rd</sup> set of PMU phasor measurements at bus A & bus B .....	261
10.12	Effect of fault inception angle on FL accuracy (Actual FL: 0.6 p.u. from A) .....	268
10.13	Effect of load variation on FL accuracy (Actual FL: 0.6 p.u. from A) .....	269
10.14	Effect of compensation degree on FL accuracy (Actual FL: 0.6 p.u. from A) .....	270
10.15	Influence of parameter variation on FL accuracy in SCLs .....	272
11.1	Existing RTDS simulator .....	276
11.2	A two terminal 400 kV transmission network for RTDS implementation ..	281
11.3	A faulted system at a distance d (p.u.) from terminal A .....	282
11.4	A 400 kV transmission system model in RSCAD .....	284
11.5	Fault control logic .....	285
11.6	Subsystem for calculation of line parameters .....	285
11.7	Subsystem for calculation of fault location .....	286
11.8	Pre-fault voltages at terminal A .....	287
11.9	Pre-fault currents at terminal A .....	287
11.10	Pre-fault voltages at terminal B .....	288
11.11	Pre-fault currents at terminal B .....	288
11.12	Pre-fault voltage and current phasors at terminal A and B .....	289
11.13	Symmetrical components of pre-fault voltage and current phasors at A and B .....	289
11.14	Waveforms pertaining to AG fault .....	290
11.15	Waveforms pertaining to BC fault .....	291
11.16	Waveforms pertaining to CAG fault .....	292
11.17	Waveforms pertaining to ABC fault .....	293

## Abstract

**Name** : Ali H. Al-Mohammed  
**Title** : Adaptive Fault Location in Power System Networks Based on Synchronized Phasor Measurements  
**Major Field** : Electrical Engineering  
**Date of Degree** : October 2012

*The phasor measurement unit (PMU), using synchronization signals from the satellite global positioning system, is considered to be a key measuring device in the future of power systems. A PMU is characterized with its unique ability to provide synchronized phasor measurements of voltages and currents from widely separated locations in an electric power network. PMUs have recently evolved into mature tools and can now be deployed in a variety of power system applications including the field of fault location.*

*Although PMUs have the potential to revolutionize the way electric power systems are monitored and controlled, their installation shall be optimized due to cost factor. This thesis addresses the two main issues in any PMU initiative, namely PMU placement and intended system application. A new formulation for the optimal PMU placement (OPP) problem is proposed considering not only the new PMUs to be installed but also the existing ones to be retained or relocated. This formulation takes into account various practical constraints and limitations such as achievement of full network observability, the list of system buses at which PMUs must be installed and the list of system buses at which PMU installation shall be avoided. An optimization technique based on differential evolution algorithm (DEA) is proposed and coded in MATLAB for solving OPP problem. To benchmark the proposed DEA, its optimal solutions are compared to the published solutions obtained using other optimization techniques for different IEEE test systems.*

*Realizing the importance of accurate and swift fault location on a power network, this thesis also proposes new PMU-based adaptive fault location algorithms for two-terminal-, three-terminal- and series-compensated transmission networks. To improve the fault location accuracy, the proposed algorithms utilize only PMU synchronized measurements and do not require any data to be provided by the electric utility. In these algorithms, the transmission line parameters and Thevenin's equivalent of the system at designated terminals are determined online to reflect the actual operating conditions of the system. Fault-location accuracy evaluation of the proposed algorithms is performed considering various factors such as fault position, fault type, fault resistance, fault inception angle, pre-fault loading and line compensation degree. The proposed algorithms have been simulated using both PSCAD/EMTDC and MATLAB and practically implemented using RTDS simulator. A real-life system is used to test the proposed algorithms for OPP problem and PMU-based adaptive fault location. Simulation results revealed that the developed algorithms produce reliable and high-quality solutions.*

**Doctor of Philosophy Degree**  
**King Fahd University of Petroleum and Minerals**  
**Dhahran, Saudi Arabia**



## خلاصة الرسالة

اسم الطالب : علي حسن ياسين المحمد  
عنوان الرسالة : التحديد التكميلي لمواقع الاعطال في شبكات الأنظمة الكهربائية باستخدام وحدات قياس الأطوار المتزامن للكميات الكهربائية  
التخصص : هندسة كهربائية  
تاريخ الشهادة : أكتوبر 2012 م

تعتبر وحدات قياس الأطوار المتزامن للكميات الكهربائية (Phasor Measurement Units) المعتمدة على النظام العالمي لتحديد المواقع (GPS) من أهم أدوات القياس التي ستشكل مستقبل أنظمة الطاقة الكهربائية. وتتميز هذه الوحدات بقدرتها الفريدة على قياس أطوار الجهد والتيار بشكل متزامن في الزمن الحقيقي لمواقع متباعدة في شبكات الكهرباء. وشهد تصنيع هذه الوحدات تطورا ملموسا في السنوات القليلة الماضية مما أتاح استخدامها في تطبيقات كثيرة وواحدة ومنها استخدامها في تحديد مواقع الأعطال.

وعلى الرغم من أن وحدات القياس هذه لها القدرة على أحداث ثورة في طريقة المراقبة والتحكم بأنظمة الطاقة الكهربائية إلا أن تركيبها في الشبكات يجب أن يدرس ويقنن من حيث المكان والعدد لاعتبارات اقتصادية. تبحث هذه الرسالة مشكلة إيجاد الوضع الأمثل لوحدات قياس الأطوار المتزامن في الشبكات الكهربائية وتعرض صياغة جديدة لهذه المشكلة لا تأخذ بعين الاعتبار الوحدات الجديدة المراد تركيبها فقط وإنما تشمل أيضا الوحدات القائمة التي ربما تبقى في مكانها أو تنقل لمكان آخر في الشبكة تبعا للحل الأمثل. كما تأخذ هذه الصياغة بعض القيود والمحددات العملية بعين الاعتبار كالقدرة على ملاحظة حالة النظام بشكل كامل والمواقع التي يجب تركيب وحدات قياس بها أو تلك التي ينبغي تحاشي تركيب الوحدات بها لاعتبارات مختلفة. كما تعرض الرسالة حل المشكلة المذكورة آنفا باستخدام خوارزم يحاكي طريقة التطور التفاضلي (Differential Evolution) تم برمجته باستخدام لغة (MATLAB) بحيث يمكن ملاحظة حالة النظام باستخدام أقل عدد من هذه الوحدات مع تحقيق جميع القيود والمحددات العملية. ولتأكيد جودة الحل تم مقارنة حلول هذه الطريقة مع الحلول المنشورة التي تم الحصول عليها باستخدام طرق أخرى لأنظمة قياسية مختلفة.

وإدراكا لأهمية موضوع تحديد مواقع الأعطال في شبكات الكهرباء بشكل دقيق وسريع اشتملت هذه الرسالة كذلك على اقتراح خوارزميات تقوم بتحديد مواقع الأعطال بشكل تكيفي بالاعتماد فقط على قياسات الجهد والتيار المأخوذة من وحدات قياس الأطوار المتزامن حيث تقوم هذه الخوارزميات بحساب البارامترات المطلوبة في الزمن الحقيقي دون الحاجة لأن يتم تزويد هذه البارامترات من قبل شركات الكهرباء إذ لا يتم عندئذ أخذ حالة التشغيل الفعلية للنظام بنظر الاعتبار. ويمكن تطبيق هذه الخوارزميات على خطوط لها نهايتان أو ثلاث نهايات طرفية وكذلك الخطوط المزودة بمعوصلات القدرة المفاعلة المربوطة على التسلسل. ولتقييم اعتمادية الخوارزميات المقترحة تم دراسة تأثير عدد من العوامل كمكان العطل ونوعه ومقاومته ووقت بداية حدوثه وأحمال ما قبل العطل ونسبة تعويض القدرة المفاعلة على دقة الحل المتحصل عليه. تم برمجة هذه الخوارزميات باستخدام لغة (MATLAB) وتمثيل الشبكات باستخدام برنامج (PSCAD/EMTDC) كما تم تطبيق محدد الأعطال المقترح باستخدام محاكي في الزمن الحقيقي. طبقت جميع الخوارزميات المقترحة على شبكة نظام كهربائي حقيقي ومن خلال النتائج التي تم الحصول عليها يمكن الاستنتاج أن هذه الخوارزميات تمتاز باعتماديتها ودقتها العالية سواء في إيجاد الوضع الأمثل لوحدات القياس المتزامن أو في تحديد مواقع الأعطال.

درجة الدكتوراه في الفلسفة  
جامعة الملك فهد للبترول والمعادن  
الظهران ، المملكة العربية السعودية

# Nomenclature

## List of Abbreviations

PMU	: Phasor Measurement Unit
WAMS	: Wide-area Measurement System
GPS	: Global Positioning System
DFR	: Digital Fault Recorder
RTDS	: Real-time Digital Simulator
SCADA	: Supervisory Control and Data Acquisition
CT	: Current Transformer
VT/PT	: Voltage Transformer/Potential Transformer
EHV	: Extra High Voltage
SCL	: Series-compensated Line
SC	: Series Capacitor
MOV	: Metal-oxide Varistor
FACTS	: Flexible AC Transmission Systems
DC	: Direct Current
HV	: High Voltage
FL	: Fault Locator (Location)
DCR	: Differential Current Ratio
FTU	: Feeder Terminal Unit
GA	: Genetic Algorithm
WT	: Wavelet Transform
ANN	: Artificial Neural Network
DWT	: Discrete Wavelet Transform
SCDR	: Symmetrical Component Distance Relay
DFT	: Discrete Fourier Transform
PDC	: Phasor Data Concentrator
UTC	: Coordinated Universal Time

NASPI	: North American Synchrophasor Initiative
EMS	: Energy Management System
OPP	: Optimal PMU Placement
DE	: Differential Evolution
EA	: Evolutionary Algorithm
MMLR	: Multiple Measurements using Linear Regression
TE	: Thevenin Equivalent
AFLA	: Adaptive Fault Location Algorithm
CLDC	: Current Limiting Damping Circuit

### **List of Symbols**

$N_b$	: Number of buses
$C_i$	: Installation cost of a new PMU
$C_r$	: Removal and relocation cost of an existing PMU
$n_k$	: A binary number to indicate PMU installation at/removal from bus 'k'.
$W_k$	: Penalty factor for bus unobservability.
$U_k$	: A binary number to indicate unobservability of bus 'k'.
$S_{MP}$	: A set of "must place" buses, if any, at which PMUs must be placed
$S_{DP}$	: A set of "do not place" buses, if any, at which installation of PMUs shall be avoided
$S$	: A candidate solution represented by a set of binary numbers indicating PMU installation at system buses.
$W_1$	: A design factor to maximize PMU measurement redundancy
$W_2$	: Penalty factor for bus unobservability.
$R_k$	: An integer number to indicate bus 'k' observability redundancy index.
$E_A, E_B$	: Equivalent source voltage at terminal A, B
$Z_{SA}, Z_{SB}$	: Equivalent source impedance at terminal A, B
$Z$	: Line impedance

$Y$	: Line admittance
$V_A$	: Phase voltages at bus A during normal operation
$V_B$	: Phase voltages at bus B during normal operation
$I_A$	: Phase currents at bus A during normal operation
$I_B$	: Phase currents at bus B during normal operation
$i$	: The $i^{\text{th}}$ sequence, $i=0,1,2$ , namely zero, positive and negative sequence
$\Delta V_{Ai}$	: The $i^{\text{th}}$ sequence of superimposed voltage at terminal A
$\Delta V_{Bi}$	: The $i^{\text{th}}$ sequence of superimposed voltage at terminal B
$\Delta I_{Ai}$	: The $i^{\text{th}}$ sequence of superimposed current at terminal A
$\Delta I_{Bi}$	: The $i^{\text{th}}$ sequence of superimposed current at terminal B
$Z_i$	: The $i^{\text{th}}$ sequence impedance of the line between terminals A and B
$Y_i$	: The $i^{\text{th}}$ sequence admittance of the line between terminals A and B
$R_f$	: Fault resistance
$I_{fi}$	: The $i^{\text{th}}$ sequence of fault current
$Z_{Asi}$	: The $i^{\text{th}}$ sequence of terminal A equivalent source impedance
$Z_{Bsi}$	: The $i^{\text{th}}$ sequence of terminal B equivalent source impedance
$L$	: The total length of the line
$D$	: Distance between bus A and fault point F
$L_A$	: Length of section A
$L_B$	: Length of section B
$L_C$	: Length of section C
$Z_A, Y_A$	: Impedance, admittance of section A
$Z_B, Y_B$	: Impedance, admittance of section B
$Z_C, Y_C$	: Impedance, admittance of section C
$i_v$	: The instantaneous current through the MOV
$I_c$	: The MOV coordination current
$V_v$	: The instantaneous voltage across the MOV
$V_p$	: The MOV protective level voltage usually defined at $I_c$

$\alpha$	: A parameter related to the manufacturing process of the MOV material
$V_{pi}, I_{pi}$	: The $i^{th}$ phasor measurement of positive sequence voltage and current at terminal $P$ at $i^{th}$ moment
$V_{qi}, I_{qi}$	: The $i^{th}$ phasor measurement of positive sequence voltage and current at terminal $Q$ ; $i=1, 2, \dots, N$ , $N$ being the total number of measurement sets, with each set consisting of $V_{pi}, I_{pi}, V_{qi}, I_{qi}$
$V_{ri}$	: The voltage at the left side of location $R$
$V_{si}$	: The voltage drop across the series compensation device at location $R$
$I_{ri}$	: The current flowing through the series compensation device at location $R$
$Z_c$	: The characteristic impedance of the line
$\gamma$	: The propagation constant of the line
$Z_{pr}, Z_{qr}$	: The equivalent series impedance of the line segment $PR$ and $QR$
$Y_{pr}, Y_{qr}$	: The equivalent shunt admittance of the line segment $PR$ and $QR$
$l_1, l_2$	: Length of the line segment $PR$ and $QR$ in mile or km
$z_1, y_1$	: Positive sequence series impedance and shunt admittance of the line per mile or km respectively
$N$	: Total number of measurement sets
$x_{2i-1}, x_{2i}$	: $i=1, 2, \dots, N$ , variables used to represent voltage across the compensation device, i.e. $V_{si} = x_{2i-1}e^{jx_{2i}}$
$x_{2N+1}, x_{2N+2}, x_{2N+3}$	: Positive sequence transmission line series resistance, series reactance and shunt susceptance per unit length respectively
$X_k, X_{k+1}$	: Variable vector before and after $k^{th}$ iteration
$k$	: Iteration number starting from 1
$\Delta X$	: Variable update
$H$	: Matrix composed of the derivatives of the function with respect to the unknown variables
$d_{FA}$	: Unknown distance to fault [p.u.] on the section A-X
$R_{FA}$	: Unknown fault resistance for fault on section A-X
$V_{Ap}, I_{Ap}$	: Fault loop voltage and current for fault on section A-X

$I_{FA}$	:	Total fault current for fault on section A-X
$Z_{1LA}$	:	Positive sequence impedance of the line section A-X
$a_1, a_2, a_0$	:	Weighting coefficients (Table 10.1)
$V_{A1}, V_{A2}, V_{A0}$	:	Positive, negative and zero sequence components of side-A voltage
$I_{A1}, I_{A2}, I_{A0}$	:	Positive, negative and zero sequence components of side-A current
$Z_{0LA}$	:	Zero sequence impedance of the line section A-X
$a_{F1}, a_{F2}, a_{F0}$	:	Share coefficients (Table 10.2)
$I_{Ai}$	:	$i^{th}$ sequence component of current at bus A
$I_{Xi}$	:	$i^{th}$ sequence component of current at point X
$d_{FB}$	:	Unknown distance to fault [p.u.] on the section B-Y
$R_{FB}$	:	Unknown fault resistance for fault on section B-Y
$V_{Bp}, I_{Bp}$	:	Fault loop voltage and current for fault on section B-Y
$I_{FB}$	:	Total fault current for fault on section B-Y
$Z_{1LB}$	:	Positive sequence impedance of the line section B-Y
$I_{Bi}$	:	$i^{th}$ sequence component of current at bus B
$I_{Yi}$	:	$i^{th}$ sequence component of current at point Y

# CHAPTER 1

## Introduction

The electrical grids are amongst the most complex systems worldwide. The power system planners and operators work hard to operate the system in a reliable manner to provide the safe and satisfied electric power to the customers. With the introduction of free marketing and deregulation of the power system, the economic factors are added to the power system operation, leading to new uncertainties and challenges to large interconnected power system. Power systems continue to be stressed as they are operated in many instances at or near their full capacities. In such a situation, power system protection and control becomes an important safeguard of power system and also the key enabler to meet the challenges of the electrical grid in the 21<sup>st</sup> century. [1]

Nowadays, electric power systems are growing in size and complexity. As a result, they will be always exposed to failures of their components. In the case of a failure, the faulty element should be disconnected from the rest of the healthy system in order to

minimize the damage of the faulty element and to remove the emergency situation for the entire system. This action, which is accomplished by a set of automatic protective relaying devices, should be taken quickly and accurately. At the same time, it is very important for the utility to identify the fault location as fast as possible for improving the service reliability. If a fault location cannot be identified quickly and this produces prolonged line outage during a period of peak load, severe economic losses may occur and reliability of service may be questioned. In recent years, fault-location research studies become greatly important and the problem has attracted widespread attention among researchers in power system technology because of all the above-mentioned circumstances. [2]

Transmission and distribution lines experience faults that are caused by storms, lightning, snow, freezing rain, insulation breakdown and, short circuits caused by birds and other external objects. In most cases, electrical faults manifest in mechanical damage, which must be repaired before returning the line to service. Power line faults must be located accurately to allow maintenance crews to arrive at the scene and repair the faulted section as soon as possible. Rugged terrain and geographical layout cause some sections of power transmission lines to be difficult to reach. Therefore, robustness of the accurate fault location determination under a variety of power system operating constraints and fault conditions is an important requirement. [2, 3]

In modern society, customers are more sensitive to the outages. Therefore, more efficient methods for fault location, supply restoration and high-quality customer service, which reduce the overall costs, are required. Fast location of the faulted section in power networks results in minimizing the inconvenience caused to the affected customers. This is becoming more important as there is an increasing emphasis placed on quality and



reliability of supply and, therefore, fault location is considered to be one of the first functions to be integrated into modern substation control system. [2, 4]

The lessons learned from several recent major blackouts revealed that current protection systems were not always sufficient to stop an uncontrolled cascading failure of the power system and, therefore, the application of existing protection system should be revisited. Phasor measurement units (PMUs) using synchronization signals from the satellite global positioning system (GPS) have recently evolved into mature tools with the potential to revolutionize the way electric power systems are monitored and controlled. Since PMUs were introduced into power system thirty years ago, their values have been proved by their extensive applications in power system operation and planning. In recent years, varieties of PMU application areas, including the area of fault location, have been studied, proposed and implemented with their significant benefits. At present, a large number of PMUs have been installed and the wide area measurement system (WAMS) that gathers real-time phasor measurements by PMUs across broad geographical areas has been gradually implemented. [1]

## **1.1 Importance of locating faults**

The process aimed at locating a fault with the highest possible accuracy is known as fault location. A fault locator is mainly supplementary protection equipment applying fault-location algorithms for estimating the distance to fault. When locating faults on a line having more than one section as in the case of a three-terminal or a multi-terminal line, the fault-location function consists in this case of two steps. The faulted section has to be first identified and, secondly, location of a fault on this section has to be determined. [2]

Practically speaking, a fault-location function is possible to be implemented into four main options, namely microprocessor-based protective relays, digital fault recorders (DFRs), stand-alone fault locators and post-fault analysis programs. The first option is commonly used in practice and, in this case, high computational capability and communication with remote sites of modern relays are utilized at almost no additional cost. Moreover, the second option enables easy and cheap incorporation of the fault-location function. The third option is only applied in the case of using sophisticated fault-location algorithms and under the condition that higher cost of the implementation is accepted. The fourth option is related to post-fault analysis programs with included fault-location algorithms which are used mainly for verification of operation of protective relays. [2]

Faults on transmission and distribution lines could be either temporary or permanent. Temporary faults are the most dominant on overhead lines. As temporary faults are self cleared, the power-supply continuity is not permanently affected. In the case if a permanent fault occurs, the related protective relaying equipment enables the associated circuit breakers to isolate the faulted sections. If a certain line is taken out of service due to a permanent fault, the connected loads are either not supplied or, if possible, the other lines are forced to supply the loads which used to be supplied by the tripped line. In addition, a series of cascading trips can possibly happen if successively larger and larger parts of the system are taken out of service. This can lead even to blackouts of large power systems in some unfavorable cases as has happened recently in some countries. In order to avoid or at least minimize such blackouts, a special care ought to be paid in equipping power systems with protection and control devices especially

when we take into account the fact that contemporary power systems operate closer and closer to their operating limits. [2]

In the case of permanent faults, the power supply can be restored only after the maintenance crew finishes the repair of the damage caused by such faults. For this purpose, the fault position shall be known or else the whole line has to be inspected to find the damage place. Therefore, it is quite significant that the location of a fault is either known or can be estimated with reasonably high accuracy. This not only allows saving money and time for the inspection and repair but also provides a better service due to the possibility of faster restoration of power supply. Furthermore, this enables the blackouts to be minimized. In the case of temporary faults, the fault location is also important as it can help to pinpoint the weak spots on the line and, hence, maintenance schedules can be planned for avoiding further problems in the future. [2]

Fault locators perform a valuable service even when helicopters are immediately available for patrol following unsuccessful reclosing because trouble cannot always be found with a routine patrol with no indication of where the fault occurred. For instance, tree growth could reduce clearances, resulting in a flashover during severe conductor sagging. However, by the time the patrol arrives the conductors have cooled, increasing the clearance to the tree, and the weak spot is not obvious. The importance of fault locators is more obvious on long lines, in rough terrain where foot patrols are relied upon. Fault locators can also help where maintenance jurisdiction is divided between different companies or divisions within a company. Moreover, fault locators are valuable even where the line has been restored either automatically or non-automatically since they allow rapid arrival at the site before the evidence is removed or the 'trail becomes cold'.

Examples of this category include faults caused by cranes swinging into the line, brushfires, damaged insulators and vandalism. Furthermore, the knowledge that repeating faults are occurring in the same area can be valuable in detecting the cause. Weak spots that are not obvious may be found because a more thorough inspection can be focused in the limited area defined by the fault locator. [2]

## **1.2 Fault location techniques and algorithms**

Power system faults can be located naturally by foot patrols or by patrols equipped with different transportation means and binoculars. In addition, calls from witnesses of damages on the power line or customer can provide the required knowledge about the fault position. However, such primitive ways are time-consuming and do not satisfy the requirements imposed on fault location. Therefore, faults shall be located automatically. Automatic fault location, which is based on determining the physical location of a fault by processing the voltage and current waveform values, can be classified into the following four main categories [2]:

- Techniques based on fundamental-frequency currents and voltages, mainly on impedance measurement
- Techniques based on traveling-wave phenomenon
- Techniques based on high-frequency components of currents and voltages generated by faults
- Knowledge-based (artificial intelligence) approaches

Travelling-wave methods consider the voltage and current waves travelling at the speed of light from the fault location towards the line terminals. These methods, although accurate,

are not widely used since they are expensive and complex for implementation due to the requirement of high sampling frequency. The technique based on high-frequency components of currents and voltages generated by faults is also costly and complex for implementation due to the requirement of specially tuned filters for measuring high-frequency components and, therefore, not widely used. Knowledge-based techniques are still in the development stage and, recently, a lot of efforts have been focused on such techniques. [2]

The technique based on fundamental frequency currents and voltages exhibits numerous advantages and is considered the most popular in real applications. Varieties of fault-location algorithms have been developed so far. The majority of them are based on an impedance principle, making use of the fundamental frequency voltages and currents. Depending on the availability of the input signals, they can be categorized as [2]:

- One-end algorithms
- Two-end algorithms
- Multi-end algorithms

### **1.3 Factors affecting fault location accuracy**

There are different factors that affect the accuracy of fault-location methods. Generally speaking, without specifying the fault-location method, the main factors can be listed as follows [2]:

- Inaccurate compensation for the reactance effect in the case of fault-location algorithms using one-end measurements.

- Inaccurate fault-type (faulted phases) identification for fault-locating algorithms based on considering the natural fault loops (phase-to-earth or phase-to-phase loops), similarly as applied in distance relays.
- Inaccuracy of / uncertainty about the line parameters, particularly for the zero-sequence impedance. It is often difficult to obtain the accurate zero-sequence impedance for the line. This is so because this impedance is affected by the soil resistivity, which may be variable under the whole line route, and it is also dependent on weather conditions.
- Inaccurate compensation for the mutual effects on the zero-sequence components. This takes place if the current required for compensating for the mutual coupling is for some reasons unavailable.
- Insufficient accuracy of the line model, i.e., if untransposed lines are represented as being transposed, and line shunt capacitance is not considered.
- Presence of shunt reactors and capacitors or series capacitor compensating devices.
- Load unbalance.
- Errors of current and voltage instrument transformers and unfaithful reproduction of the primary signals due to their limited bandwidth.
- Insufficient sampling frequency and bit resolution of A/D system.

To improve the fault-location estimation, it is important to eliminate, or at least to reduce possible errors associated with the used technique.

## 1.4 Motivation

Due to their importance, fault-location research studies have recently attracted widespread attention among researchers in power system technology. Fast and accurate fault location on a power network can expedite repair of faulted components, speed-up power restoration and thus enhance power system reliability and availability. Rapid restoration of service could reduce customer complaints, outage time, loss of revenue and crew repair expense. This also enables the blackouts to be minimized.

At present, PMUs have come out of their academic infancy with commercial viability. There are now about 24 commercial manufacturers of PMUs and pertinent industry standards have made possible the interoperability of units from different manufacturers [5]. A PMU has the potential to revolutionize the monitoring and control of electric power systems. This device has the ability to measure current, voltage, and calculate the angle between the two. Phase angles from buses around the system can then be calculated in real time. This is possible because of two important advantages over traditional measurement; time stamping and synchronization. With the satellite GPS availability, digital measurements at different line terminals can be performed synchronously to the accuracy of one micro-second. The ability of GPS to provide a time reference signal, synchronized at widely separated locations has been widely recognized as having many applications in power-systems including the application for fault location. PMU-based fault location algorithms are highly accurate and, therefore, needed to cope with the modern power system requirements.

When power system operates normally, over-current occurs in the transmission line because of the fault of the other part in the system. The over-current will change the

sag of the line which will change the parameters of the line. On the other hand, the surrounding environments such as the humidity and temperature make the impedance and admittance of the line being different from the parameters provided by the power utility. Moreover, the system's impedance provided by the power utility is not constant and it changes with the loading conditions. Uncertainty about the line parameters and system's impedance is one of the most severe factors that could impact on the fault location accuracy. In order to enhance the accuracy of the fault-location algorithm, the effect of parameter uncertainty shall be reduced or eliminated. Synchronized phasor measurements obtained from PMUs can be utilized for online determination of such parameters and hence calculate the fault location adaptively.

The majority of published PMU-based fault location algorithms are conventional impedance-based that require both line parameters and system Thevenin's equivalents to be provided by the electric utility. Adaptive PMU-based fault location algorithms reported in the literature are very few and they require the system Thevenin's equivalent to be provided by the electric utility. The biggest stimulus in this research work is to propose PMU-based adaptive fault location algorithms that depend only on PMU measurements to determine the fault location and do not require any data to be provided by the electric utility. This shall improve the fault location accuracy since data provided by the electric utility is ideal and does not reflect the practical operating conditions of the system. In addition, no adaptive PMU-based fault location algorithm has been proposed in the literature for series compensated lines to the best knowledge of the author and this thesis attempts to address this subject.



## 1.5 Thesis objectives

The work under this thesis is concerned with utilizing the synchronized phasor measurements obtained from optimally-allocated PMUs to locate, in an adaptive manner, faults that may occur in electrical networks. The specific objectives are as follows:

- Developing a novel formulation for the optimal PMU placement (OPP) problem in electrical networks and solving it using a population-based optimization technique prior to utilizing the synchronized phasor measurements obtained by the optimally-allocated PMUs in fault location studies.
- Proposing novel approaches for adaptive fault location in two-terminal, three-terminal and series-compensated transmission networks which utilize only the synchronized fundamental-frequency currents and voltages measured by the installed PMUs to determine the fault location.
- Performing the fault-location accuracy evaluation of the proposed adaptive fault location approaches taking into account various factors that are commonly considered as changeable during the evaluation analysis. These factors include, but not limited to, fault position, fault type, fault resistance, fault inception angle and pre-fault loading.
- Building and testing a prototype of a PMU-based adaptive fault locator using real time digital simulator (RTDS) to validate the proposed adaptive fault location algorithm.

## 1.6 Contributions

The main contributions of the work carried out under this thesis can be summarized as follows:

- Development of a novel formulation of the OPP problem that considers not only the new PMUs to be installed but also the existing PMUs to be retained or relocated. In addition, the new formulation considers some practical constraints and limitations such as the set of power system buses at which PMUs must be installed, the set of buses at which PMU installation should be avoided and the set of zero-injection buses.
- Development of an OPP problem solver based on Differential Evolution optimization algorithm to achieve full network observability at the minimum PMU installation/relocation cost and, at the same time, the maximum PMU measurement redundancy.
- Proposal of novel and very accurate algorithms for adaptive fault location in two-terminal, three-terminal and series-compensated electrical networks that determine the required system parameters online and thus consider the system's practical operating conditions during the fault. These algorithms utilize only the synchronized phasor measurements obtained by the PMUs and do not require any data to be provided by the electric utility.
- Development of an adaptive PMU-based fault locator prototype using RTDS. The said fault locator prototype will help enhance power system availability and reliability and hence utilize electrical networks in a more efficient way. The developed prototype system will help in building research capacity in the area of

application of synchronized phasor measurements for adaptive fault location in electrical networks.

## **1.7 Organization of the thesis**

The material of this thesis is organized in twelve chapters. It starts, after this introductory chapter, with an extensive literature review addressing the subject of fault location based on synchronized phasor measurements in Chapter 2. Chapter, 3, is dedicated to the synchronized phasor measurements and their applications in power systems. The OPP problem is formulated in Chapter 4. Differential evolution (DE) for solving OPP problem is presented in Chapter 5. The issue of transmission line parameter identification using PMU synchronized measurements is addressed in Chapter 6. Chapter 7 is included to describe the use of synchronized phasor measurements for online determination of system's Thevenin's equivalent at a particular node. PMU-based adaptive fault location algorithms in two-terminal-, three-terminal and series-compensated- transmission networks are proposed in Chapter 8, Chapter 9 and Chapter 10 respectively. RTDS implementation of the proposed PMU-based fault locator is described in Chapter 11. Finally, Chapter 12 highlights some conclusions and future work in the area of adaptive fault location using synchronized phasor measurements.

## CHAPTER 2

### Literature Review

This chapter presents a comprehensive survey on fault location based on synchronized phasor measurements. Varieties of fault-location algorithms have been developed and presented in literature. The majority of them are based on an impedance principle, making use of the fundamental frequency voltages and currents. Fault-location algorithms based on traveling-wave phenomenon, high-frequency components of currents and voltages generated by faults and artificial intelligence such as fuzzy neural network [6] have also been developed. Depending on the availability of the fault-locator input signals, fault location algorithms can be categorized as one-end, two-end and multi-end. This survey is concerned with the two-end and multi-end algorithms utilizing synchronized measurements. A Fault location algorithm based on aforesaid measurements prove to be robust under power swing and out-of-step conditions [7] and has been proposed [8] as part of a strategy aimed at preventing or mitigating the

cascading blackouts that involve relay misoperations or inadequate local diagnostic support.

In this chapter, the issue of fault location utilizing two-end synchronized measurements is addressed in the next section. Fault location on three-terminal and multi-terminal lines is then presented in Section 2.2. A special attention shall be paid while developing a fault location algorithm for a series-compensated transmission line in order to locate any fault accurately. Therefore, Section 2.3 is devoted to discuss this matter. In order to overcome the limitations of the conventional fault location algorithms, some work has been carried out to locate power system faults in an adaptive manner and this subject is reported in Section 2.4. In comparison with the work pertaining to fault location on transmission lines, there is a quite limited published work related to fault location on power system networks. This work is highlighted in Section 2.5 along with a short review of the non-standard high-frequency-related fault location techniques based on wavelet transform.

## **2.1 Fault location utilizing two-end synchronized measurements**

As mentioned in Chapter 1, a PMU has the ability to measure current, voltage, and calculate the angle between the two. Phase angles from buses around the system can then be calculated in real time. This is possible because of two important advantages over traditional measurement; time stamping and synchronization. With the satellite GPS availability, digital measurements at different line terminals can be performed synchronously. A synchronized measurement system requires that the measurements taken at different substations include, in addition to magnitude, the phase-angle data with

respect to an arbitrary but common reference. Phase information is obtained from knowledge of the absolute time at which the measurements were obtained (time tagging). The time for all measurements must be synchronized with a time reference that must be the same for all local systems. This time reference is obtained from the GPS. [9]

The potential uses of the sub-second GPS-synchronized phasor data collected from various locations within an electric power system promise endless benefits for the applications targeting reliable operation of electric power system [10]. Various PMU applications in power systems including fault location [5, 11-16] have been reported. Merging of time correlated information from PMU, SCADA and non-operational data has also been suggested [17] to improve the effectiveness of alarm processing, accuracy of fault location and ability to detect cascades.

Two-end fault location algorithms have been proposed with the aim of overcoming the limitations of the one-end fault location techniques and improving fault-location accuracy. A schematic diagram for two-end synchronized fault-location arrangement using PMUs is shown in Figure 2.1. Fault location algorithms based on two-end synchronized measurements have been developed using either complete or incomplete two-end measurements. With the use of complete two-end measurements the three-phase voltages and currents from both line ends are utilized. In case of incomplete two end measurements, the following options are of interest [2]:

- Three-phase voltages from both line ends with three-phase current from only one end
- Three-phase currents from both line ends with three-phase voltage from only one end
- Three-phase voltages from both line ends

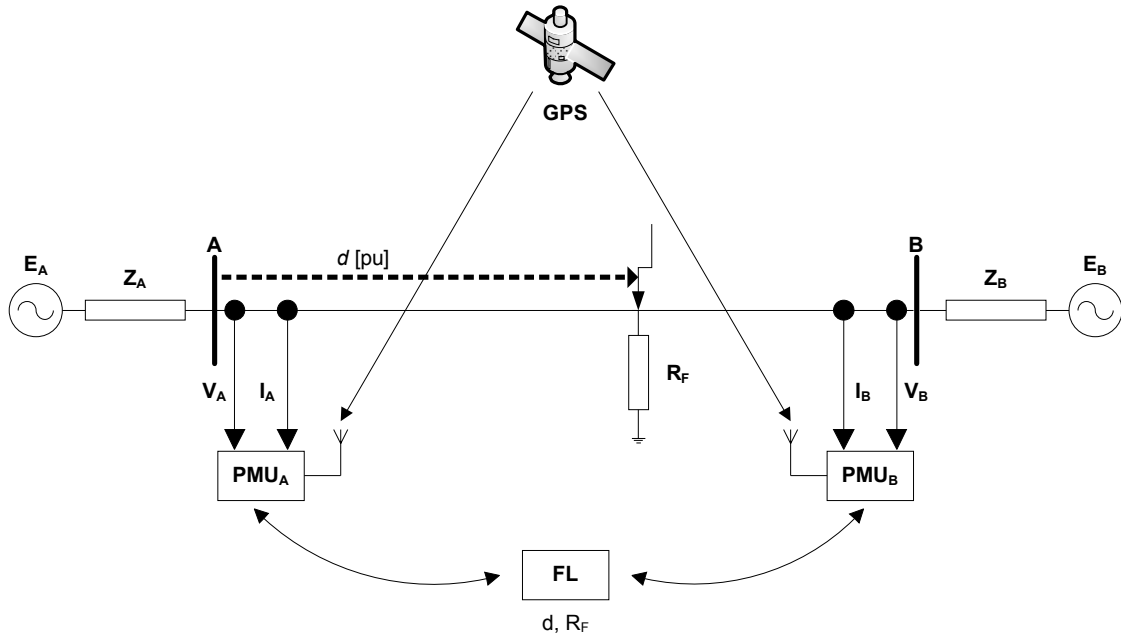


Figure 2.1: Two-end synchronized fault-location arrangement using PMUs

Various fault location algorithms utilizing complete two-end synchronized measurements [3, 18-39] have been developed. Both iterative [18] and non-iterative [25, 27] methods have been proposed to locate faults on a single transmission line. In the non-iterative method, an analytical synchronization of the unsynchronized voltage and current measurements from two ends of a line is performed with use of the determined synchronization operator. Then, the distance to fault is calculated as for the synchronized measurements. Simultaneous usage of two kinds of symmetrical components for determining the synchronization operator makes the calculations simple and highly accurate.

Fault location taking into account the arc faults has been addressed in [22, 26, 30-33, 36]. The proposed fault detection/location technique [22, 36] for both arcing and permanent faults is achieved by a combination of a fault detection index and a fault location index which are obtained by processing synchronized fundamental phasors. In

order to discriminate between arcing and permanent faults, the proposed technique estimates the amplitude of arc voltage by least error squares method through the measured synchronized harmonic phasors caused by the nonlinear arc behavior. The discrimination is then achieved by comparing the estimated amplitude of arc voltage to a given threshold value. In order to eliminate the error caused by exponentially decaying dc offset on the computations of fundamental and harmonic phasors, an extended discrete Fourier transform (DFT) algorithm is also proposed. In [26, 30, 31, 33], the electric arc is considered as a source of higher harmonics and included in the complete fault model accordingly. The developed algorithm can determine both the arc and the fault resistance. In [32], the fault location algorithm is derived in the time domain. The faulted phase voltage is modeled as a serial connection of fault resistance and arc voltage. The algorithm does not require the line zero sequence resistance as an input datum. The influences of remote infeed, fault resistance, higher order harmonics, network topology are investigated.

For short and medium-length lines using the lumped model is usually sufficient. In order to improve fault-location accuracy, especially in the case of long-length lines, the distributed nature of overhead-line parameters has to be considered [2]. Algorithms presented in [21, 34, 38, 39] take such requirement into account by representing long lines with distributed parameters where shunt capacitance is included in the line model.

Transmission systems may sometimes consist of an overhead line in combination with an underground power cable. The fault location scheme developed in [23, 37] for such systems requires synchronized phasor measurement data at one end of the



transmission line and the most far end of the power cable. The algorithm is derived using distributed line model, modal transformation theory and DFT.

The fault location algorithm presented in [35] takes the three-phase unbalance into consideration. The algorithm models the line with its distributed parameters and uses the theory of mode transformation. In [40], a fault location algorithm in joint parallel lines is proposed using six-sequence fault components in fault location. Although the algorithm is not influenced by factors such as the load current, the operating mode of the power system or the fault resistance, the associated percentage error can reach up to 2%. A fault detection/location algorithm on transmission line based on linear state estimation is presented in [41] where fault location and voltage of fault point are added as the new state variables in a linear state estimator based on PMU data.

Fault location algorithms based on incomplete two-end synchronized measurements utilizing only three-phase voltages from both line ends [42-45] have also been developed. Algorithm proposed in [43] can be applied for both transposed and untransposed lines and algorithms presented in [44, 45] suit single or double transmission lines. However, algorithm suggested in [44] utilizes, in addition to the synchronized voltage measurements at both ends of the faulted line, the synchronized voltages at neighboring nodes. Although the method is highly accurate, the number of utilized PMUs is not optimal. Fault location algorithms utilizing only synchronized measurements of two-end voltages have the advantage of being immune to CT saturation as they completely reject the currents from the input signals.

## 2.2 Fault location on three-terminal and multi-terminal lines

Use is made of multi-terminal and tapped lines for economical or environmental-protection reasons. Lines having three or more terminals with substantial generation behind each are named multi-terminal lines. Tapped lines are those having three or more terminals with substantial power generation behind, at a maximum at two of them. The taps themselves feed only loads, which means that they are terminated by the passive networks, while at the remaining terminals there are active networks. [2]

Various fault location algorithms on three-terminal lines are presented in [46-52]. In [46], a fault location method is developed based on synchronized measurements of three-phase current from all three terminals and additionally three-phase voltage from the terminal at which a fault locator is installed. The delivered fault-location algorithm consists of three subroutines designated for locating faults within particular line sections and a procedure for indicating the faulted line section. An approach for fault location on EHV teed feeders [47] utilizes synchronized voltages and currents at all three ends of a teed feeder. Measurements are then digitally filtered to accurately extract the power frequency phasors. In this approach, use is made of superimposed modal components of signals so as to minimize errors arising in accuracy due to line loading or source impedances. Algorithms presented in [48, 49] use synchronized voltage and current data from two terminals only. They are not influenced by fault resistance, fault location, pre-fault loading conditions, source impedance and fault types.

Algorithms discussed in [53-59] are related to multi-terminal lines. The iterative method presented in [53] uses synchronized voltage and current measurements from all terminals. Current measurements, however, were avoided in [54] to overcome current-

transformer errors in the current measurements that can be as high as 10%. In [56], a universal non-iterative fault location technique for N-terminal transmission lines based on two-terminal fault location technique is presented. The method discussed in [57] is also non-iterative and it is based on distributed line model and synchronized positive sequence voltage and current phasors. In [55], a fault location algorithm for transmission line with tapped legs is developed. The algorithm only uses the synchronized phasors measured on two terminals of the original line to calculate the fault location. The algorithm does not need the model of tapped leg and, therefore, can be applied to any type of tapped leg such as generators, loads or combined system.

## 2.3 Fault location on series-compensated lines

The one-line diagrams of a series-compensated transmission line (SCL) with Series Capacitors (SCs) and MOVs installed at midpoint and at both ends of the line are shown respectively in Figure 2.2 and Figure 2.3. MOVs are installed to protect SCs against over-voltages.

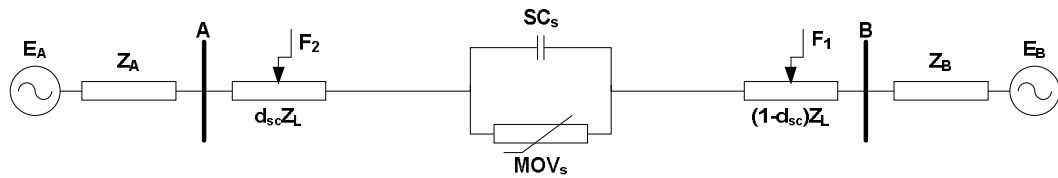


Figure 2.2: Transmission line compensated with SCs and MOVs installed at midpoint

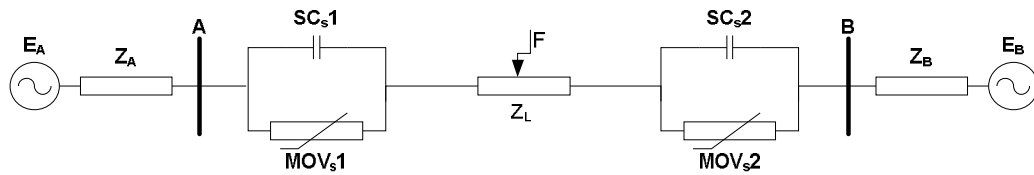


Figure 2.3: Transmission line compensated with SCs and MOVs installed at both ends

Various fault location algorithms on SCLs are presented in [60-65]. A fault location algorithm, presented in [60-62] does not need the series device model and information of the protection function of series device to predict the voltage drop. Instead, two iteration steps, pre-location step and correction step are used to calculate the voltage drop and fault location. The algorithm can be applied to any series FACTS system with a very high accuracy.

Use of instantaneous values for fault location of SCLs while avoiding the accuracy limitation caused by the operation of MOV is discussed in [63]. The method requires only a short duration of fault measurement data to estimate the location and can be applied with minimum filtering of high frequencies. It is independent of the fault type and does not require the fault to be pure resistive. However, it requires knowledge of the source impedance at both ends of the line.

In [64], a fault location algorithm based on distributed time domain line model for a transmission line with a FACTS device connected in series is presented. The algorithm can be applied to any series FACTS compensated line since the series device model and knowledge of the operating mode of the compensating device are not utilized to compute the voltage drop across the series device during the fault period. Filtering of DC and other frequency components is not needed. The algorithm is not sensitive to fault resistance and fault inception angle and does not require knowledge of source impedance.

## **2.4 Adaptive fault location**

The prime aim of adaptive fault location algorithms is to achieve a better fault location accuracy. The idea of adaptive fault location on transmission lines boils down to proper

estimation of line parameters and system impedance. The surrounding environment and operation history such as overcurrent and overload change the sag of the transmission line. Increasing the current causes the conductor temperature to increase and, consequently, the conductors to elongate and sag. The line resistance changes with the change in the temperature of the line. The reactance is related with the distance between the phase lines that is changed when the sag of the line is changed. Uncertainty about the line parameters is one of the most severe factors that could impact on the fault location accuracy. The effect of parameters uncertainty on fault location accuracy can reach up to 6.7 % if the parameters used in fault location vary 20 % of the practical parameters. The line parameters will vary not only with the environmental conditions but also with the system operation situations. It is difficult to precisely presage what will happen to the line parameters with the transmission line in service. The parameters provided by the power utility are very ideal and do not reflect the operation history of the line. [66]

When a power system operates normally, PMU monitors the voltage of the two ends and current of the line. The measured pre-fault phase and amplitude of the voltages and currents can be employed to calculate the parameters of the line. Four methods are presented in [67] to identify transmission line impedance parameters from synchronized measurements.

Algorithms discussed in [66, 68-81] are related to adaptive fault location on transmission lines. All adaptive fault location algorithms presented in above-mentioned references utilize synchronized voltage and current measurements at both ends of a transmission line. Adaptive fault location for aged power cables is presented in [70, 79]. The algorithm is incorporated with distributed line model, modal transformation theory

and DFT. It solves the problem of cable changing parameters especially the change of the relative permittivity over its age and, thus, for the operating positive, negative and zero-sequence capacitance changes.

Algorithm presented in [71] utilizes synchronized measurements for on-line estimation of line parameters. A fault location index in terms of Clarke components of the synchronized voltage and current phasors is proposed to calculate the fault location. Also, a DFT-based algorithm is proposed to eliminate system noise and measurement errors. This work has been extended in [76, 77] by adding a fault detection index to the algorithm. A similar adaptive relaying scheme has been developed in [74, 75].

An adaptive fault protection scheme for transmission lines is discussed in [68, 69]. The work includes fault detection, direction discrimination, classification and location. Both fault detection and fault location indices are derived by using two-terminal synchronized measurements incorporated with distributed line model and modal transformation theory. The fault detection index is composed of two complex phasors and the angle difference between the two phasors determines whether the fault is internal or external to the protected zone. The fault types can be classified by the modal fault detection index. The proposed scheme also combines on-line parameter estimation to assure protection scheme performance and to achieve adaptive protection. Simulation studies show that fault location accuracy is high under various system and fault conditions.

An adaptive protection scheme is presented in [72, 73] for both transposed and untransposed parallel transmission lines based on the distributed line model. The fault detection and location indices are derived using the eigenvalue/eigenvector theory to

decouple the mutual coupling effects between parallel lines. The two proposed indices are used in coordination such that the internal and external fault events can be distinguished. By on-line estimating of line parameters under the actual system conditions, the proposed scheme responds more accurately to power system faults.

In [80], an adaptive fault location algorithm for transmission line tapped with a source of generation using the concept of superimposed voltage and current phasors is discussed. A discrimination index is proposed to identify the faulted section while taking the effects caused by tapped lines into account. The equivalent source impedance outside the considered transmission lines is estimated on-line.

Adaptive fault location for single, double and teed transmission lines is addressed in [66]. In the proposed algorithm, line parameters are calculated online. In addition, suddenly changed voltage and current are utilized to obtain suddenly changed positive voltage and current components to solve the system's impedance at the fault time that exactly reflects the generation mode of the power system. The subject of adaptive fault location for double-circuit transmission lines has also been discussed in [81] where a six-sequence fault component method is employed to implement fault location. Line parameters are estimated online and the line is represented with its distributed parameters.

## **2.5 Fault location in power system networks**

Fault location in distribution networks creates new problems compared with the same task in HV and EHV transmission lines. In HV and EHV networks each transmission line may be equipped with a dedicated fault locator (FL). In such a case, the FL algorithm is a

numerical procedure that converts voltage and current into a single number being a distance to fault. The distribution networks, in contrast to the transmission lines, are usually non-homogeneous with branches and loads along the line which make the fault location difficult. [2]

Various fault location algorithms in power system networks are presented in [82-96]. A method for location of single phase to ground faults in distribution network based on wide-area synchronizing information is discussed in [82]. Network lines are modeled with their distributed parameters and a fault location function is constructed according to the relations between fault current and fault distance. The transverse fault current corresponding to the hypothetical fault distance is obtained using synchronized voltage and currents from two ends of a line. The maximum transverse fault current is obtained using the interactive search algorithm on the whole line and the distance corresponding to the maximum of the transverse fault current is the fault distance.

In [84], a fault location algorithm for urban distribution system with distributed generation is presented. The method uses only currents and thus avoids the need for installation of voltage transformers. A differential current ratio (DCR) contains the differential current information to describe the feature of the faulted segment and differential current information of normal one. The faulted segment would have a DCR of a value less than one while the normal one would have a DCR greater than one. The largest fault current would be sensed by one feeder terminal unit (FTU) in the faulted segment.

Fault-location observability with minimum installation of PMUs in a power system network is an optimization problem that has been solved by different methods such as



GA [88], branch and bound [89] and tabu search [94]. The aim here is to utilize synchronized measurements of optimally-installed PMUs in a suitable algorithm to locate faults that occur anywhere in the network.

Some attempts to use discriminant analysis theory of multivariate statistical analysis theory [90], cluster analysis theory [91], power flow fingerprint [92], depth first search of graph theory [93], neural networks [86, 96] and structural analysis [95] have also been reported for fault location in power system networks.

In addition to above-mentioned standard nominal-frequency-related fault location techniques, some non-standard high-frequency-related techniques based on wavelet transform (WT) have been reported in the literature. The idea of the WT-based fault location method is illustrated in Figure 2.4. Measurement of arriving times of waves at the terminal buses, together with knowing the velocity of these waves, allows determination of a distance to fault. Thus, the problem in fact boils down to proper detection of arriving waves, to distinguish the type of these waves (direct waves or reflected waves) and to capture times of their arriving at terminal buses. All these tasks can be directly realized by using WTs (time location of wave) combined with artificial neural network (ANN) (distinguishing kinds of wave). [2]

Various fault location algorithms using WT are presented in [85, 97-102]. A fault-location scheme for multi-end aged cable system utilizing synchronized measurements at the two terminals of each cable is presented in [98]. The developed scheme is applied on the modal coordinates instead of the phase coordinates. It can eliminate the impact of the change in the propagation velocity of the travelling waves on the fault-location

calculations. This solves the problem of cable changing parameters especially the change of the relative permittivity of the cable with age.

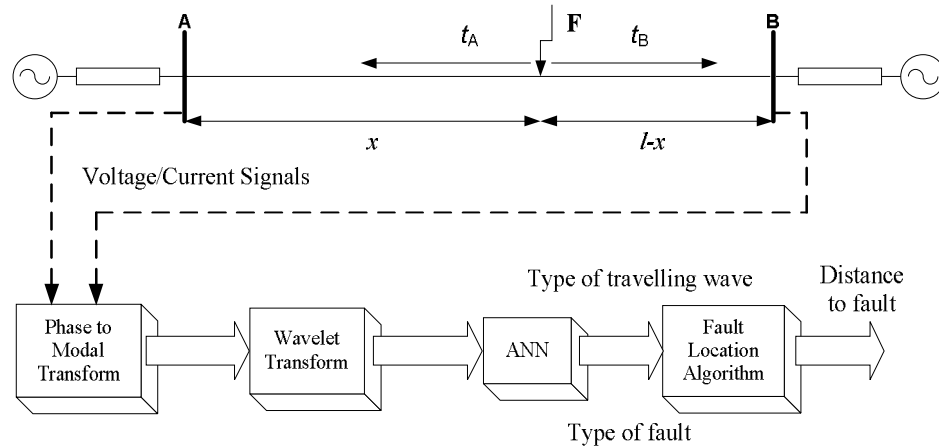


Figure 2.4: Illustration of a distorted voltage analysis using wavelet transform

The application of Discrete Wavelet Transform (DWT) for fault location on power distribution lines with tapped loads is investigated in [99]. When a fault occurs, a transient wave travels from the fault point to substation busbars and load terminals. The time taken for the fault generated transient wave to arrive at busbars or load terminals depends on the distance traveled and the velocity of the travelling wave. Fault transient detectors are installed at substation busbars and load terminals to capture the time taken for the transient to arrive and be synchronized with a GPS clock. From the recorded time and the topological structure of the network, fault location is deduced.

Fault location for teed circuits with mutually coupled lines and SCs is proposed in [101], based on DWT, by processing of travelling waves to extract the arrival times of fault initiated waves reflected from the discontinuities. The method is not influenced by series compensation rate and its location, fault resistance, fault type and any existing mutual coupling between the lines.

Fault location for three-terminal transmission lines is addressed in [100, 102] where WT is used to analyze high and low frequency components generated by a fault. The proposed fault location scheme is based on travelling waves and on calculation of the fundamental frequency component. The method is independent of fault impedance, fault type, fault inception angle, fault position and mutual coupling effects.

## **CHAPTER 3**

# **Synchronized Phasor Measurements and Their Applications**

The introduction of PMUs in power systems greatly improves the possibilities of power system monitoring and analyzing of its dynamics. PMUs can directly measure phase angles between corresponding phasors in different locations within the power system. With PMU improved monitoring and remedial action capabilities, network operators can utilize the existing power system in a more efficient way. Synchronized measurements not only allow fast and reliable emergency actions but also make it possible to reduce the need for relatively high transmission margins required by potential power system disturbances.

Synchronized phasor measurements are no longer an academic curiosity as they presently provide solutions that otherwise would have been too expensive or too complicated to implement with traditional approaches. This chapter provides a brief

introduction to the PMU and wide-area measurement system (WAMS) technology and discusses the uses of these measurements in power systems.

### **3.1 Historical overview**

The PMU has the potential to revolutionize the way electric power systems are monitored and controlled. This device has the ability to measure current, voltage, and calculate the angle between the two. Phase angles from buses around the system can then be calculated in real time. This is possible because of two important advantages over traditional meters; time stamping and synchronization. The algorithms behind phasor measurement date back to the development of symmetrical component distance relays (SCDR) in the 1970's. The major breakthrough of SCDR was its ability to calculate symmetric positive sequence voltage and current using a recursive DFT. The recursive algorithm continually updates the sample data array by including the newest sample and removing the oldest sample to produce a constant phasor. The advent of the GPS in the 1980's was the second breakthrough that enabled the modern PMU. Researchers at Virginia Tech's Power Systems Laboratory in the mid-1980's were able to use the pulses from the GPS satellites to time stamp and synchronize the phasor data with an accuracy of 1.0  $\mu$ s. With the addition of effective communication and data collection systems, voltage and current phasors from different locations could be compared in real-time. Prototype PMUs produced by Virginia Tech were supplied to American Electric Power (AEP) and the Bonneville Power administration (BPA). These units were tested and used by these utilities for several years before the first commercial unit, the Macrodyne 1690, was introduced in 1991. Using the original PMUs, AEP and BPA built phasor measurement

systems that only provided recorded data for analysis with basic plotting tools. BPA redesigned the measurement system in 1997 into a true real-time, wide-area measurement system using commercial PMUs and a custom phasor data concentrator (PDC). [9, 103]

At present, PMUs have come out of their academic infancy with commercial viability. They are now commercially produced by all major IED providers in the power industry. Many more PMU models have become available with a range of options. Several variations of PDC units have been produced, and many applications are available for analysis of recorded phasor data as well as real-time display and alarming. To aid the maturing of the industry, an important standard has been developed by the IEEE. The IEEE synchrophasor standard, C37.118-2005, was developed from an earlier version, the IEEE 1344-1995. It ensures that PMUs from different manufacturers operate well together. [9, 103]

### 3.2 Classical definition of a phasor

A phasor is simply a unique complex number used to represent a pure sinusoidal waveform. Considering a sinusoidal signal given by

$$x(t) = X_m \cos(\omega t + \varphi) \quad (3.1)$$

The phasor representation of this sinusoid is given by

$$X = \frac{X_m}{\sqrt{2}} e^{j\varphi} = \frac{X_m}{\sqrt{2}} (\cos\varphi + j\sin\varphi) \quad (3.2)$$

Note that the signal frequency is not explicitly stated in (3.2). The magnitude of the phasor is the rms value of the sinusoid ( $X_m/\sqrt{2}$ ) and its phase angle is  $\varphi$ , the phase angle of the signal in (3.1). Positive phase angles are measured in a counter-clockwise direction

from the real axis. Since the frequency of the sinusoid is implicit in the phasor definition, it is clear that all phasors that are included in a single phasor diagram must have the same frequency. Phasor representation of the sinusoid implies that the signal remains stationary at all times, leading to a constant phasor representation. [104]

### 3.3 Phasor measurement concepts

Although a constant phasor implies a stationary sinusoidal waveform, it is necessary in practice to deal with phasor measurements which consider the input signal over a finite data window. In many PMUs the data window in use is one period of the fundamental frequency of the input signal. To shed some light on phasor measurement, let us consider the steady-state waveform of a nominal power frequency signal as shown in Figure 3.1. If the waveform observation starts at the instant  $t = 0$ , the steady-state waveform may be represented, as highlighted earlier, by a complex number with a magnitude equal to the *rms* value of the signal and with a phase angle equal to the angle  $a$

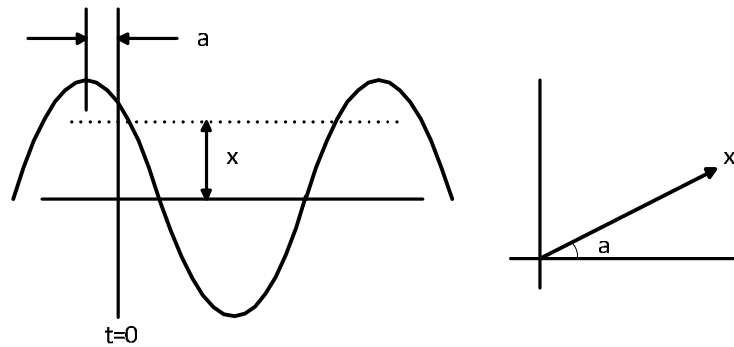


Figure 3.1: Phasor representation of a sinusoidal waveform

In a digital measuring system, samples of the waveform for one (nominal) period are collected, starting at  $t = 0$ , and then the fundamental frequency component of the DFT is calculated according to the relation:

$$X = (\sqrt{2}/N_s) \sum_{k=1}^{N_s} x[k] e^{-j2\pi k/N_s} \quad (3.3)$$

where  $N_s$  is the total number of samples in one period,  $X$  is the phasor, and  $x[k]$  is the waveform samples. This definition of the phasor has the merit that it uses a number of samples  $N_s$  of the waveform, and is the correct representation of the fundamental frequency component, when other transient components are present. The DFT phasor estimation technique produces an accurate and very usable phasor value for most system conditions if a sufficient sample rate and accurate synchronization with coordinated universal time (UTC) is maintained. Once the phasors ( $X_a, X_b$  and  $X_c$ ) for the three phases are computed, a positive, negative and zero sequence phasors ( $X_1, X_2$  and  $X_0$ ) are computed using the following transformation [20, 104-109]:

$$\begin{bmatrix} X_1 \\ X_2 \\ X_0 \end{bmatrix} = \frac{1}{3} \begin{bmatrix} 1 & \alpha & \alpha^2 \\ 1 & \alpha^2 & \alpha \\ 1 & 1 & 1 \end{bmatrix} \cdot \begin{bmatrix} X_a \\ X_b \\ X_c \end{bmatrix} \quad (3.4)$$

with  $\alpha = e^{j2\pi/3}$

### 3.4 Synchrophasor definition and measurements

Synchrophasor is a term used to describe a phasor that has been estimated at an instant known as the time tag of the synchrophasor. To obtain simultaneous measurement of phasors across a wide area of the power system, it is necessary to synchronize these time tags, so that all phasor measurements which belong to the same time tag are truly simultaneous. Consider the marker  $t = 0$  in Figure 3.1 is the time tag of the measurement. The PMU must then provide the phasor given by (3.2) using the sampled data of the input signal. Since sampled data are used to represent the input signal, it is



essential that anti-aliasing filters be applied to the signal before data samples are taken. The anti-aliasing filters are analog devices that limit the bandwidth of the bass band to less than half the data sampling frequency as per Nyquist criterion. The anti-aliasing filters produce a phase delay depending upon the filter characteristic. Moreover, this delay will be a function of the signal frequency. The task of the PMU is to compensate for this delay because the sampled data are taken after the anti-aliasing delay is introduced by the filter. [104]

The synchronization is achieved by using a sampling clock which is phase-locked to the one-pulse-per-second signal provided by a GPS receiver. The receiver may be built in the PMU or may be installed in the substation and the synchronizing pulse distributed to the PMU and to any other device which requires it. [104]

The time tags are at intervals that are multiples of a period of the nominal power system frequency. It should also be noted that the normal output of the PMU is the positive sequence voltage and current phasors. In many instances the PMUs are also able to provide phasors for individual phase voltages and currents. [104]

### **3.5 A generic PMU**

The PMUs manufactured by different manufacturers differ from each other in many important aspects. Therefore, it is difficult to discuss the PMU hardware configuration in a universally-applicable way. It is, however, possible to discuss a generic PMU [5, 108-109] capturing the major PMU components. Figure 3.2 illustrates the block logic diagram of a modern PMU [5]. Recalling that PMUs evolved out of the development of the SCDR, the structure shown in Figure 3.2 parallels that of a computer relay. The analog

inputs are voltages and currents obtained from the secondary windings of the voltage and current transformers. All three phase voltages and currents are used so that positive-sequence measurement can be carried out. A PMU, in contrast to a relay, may have currents in several feeders originating in the substation and voltages belonging to various buses in the substation.

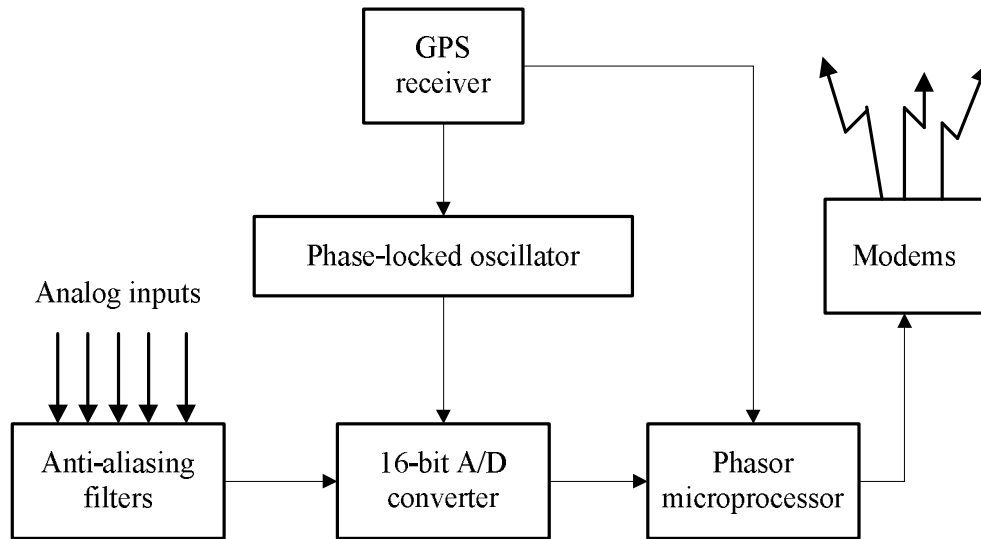


Figure 3.2: PMU block logic diagram

The current and voltage signals are converted to voltages with appropriate shunts or instrument transformers (typically within the range of  $\pm 10$  volts) so that they are matched with the requirements of the analog-to-digital converters. The sampling rate selected for the sampling process dictates the frequency response of the anti-aliasing filters. In most cases these are analog-type filters with a cut-off frequency less than half the sampling frequency in order to satisfy the Nyquist criterion. As in many relay designs one may use a high sampling rate (called oversampling) with corresponding high cut-off frequency of the analog anti-aliasing filters. This step is then followed by a digital ‘decimation filter’ which converts the sampled data to a lower sampling rate, thus

providing a ‘digital anti-aliasing filter’ concatenated with the analog anti-aliasing filters. The advantage of such a scheme is that the effective anti-aliasing filters made up of an analog front end and a digital decimation filter are far more stable as far as aging and temperature variations are concerned. This ensures that all the analog signals have the same phase shift and attenuation, thus assuring that the phase angle differences and relative magnitudes of the different signals are unchanged. As an added benefit of the oversampling technique, if there is a possibility of storing raw data from samples of the analog signals, they can be of great utility as high-bandwidth “digital fault recorders”. [5]

The sampling clock is phase-locked with the GPS clock pulse. Sampling rates have been going up steadily over the years starting, in the first PMUs, with a rate of 12 samples per cycle of the nominal power frequency to as high as 96 or 128 samples per cycle in more modern devices as faster analog-to-digital converters and microprocessors have become commonplace. Even higher sampling rates are certainly likely in the future leading to more accurate phasor estimates since an improved estimation accuracy is achieved with higher sampling rates. [5]

The microprocessor calculates positive-sequence estimates of all the current and voltage signals. Certain other estimates of interest are frequency and rate of change of frequency measured locally, and these also are included in the output of the PMU. The time-stamp is created from two of the signals derived from the GPS receiver. The time-stamp identifies the identity of the UTC second and the instant defining the boundary of one of the power frequency periods as defined in the IEEE standard. Finally, the principal output of the PMU is the time-stamped measurement to be transferred over the communication links through suitable modems to a higher level in the measurement

system hierarchy. It is the specification of these output file structures which is the subject of the industry standard for PMUs. [5]

### **3.6 Global positioning system (GPS)**

When several voltages and currents in a power system are measured and converted to phasors, they are on a common reference if they are sampled at precisely the same instant. This is easy to achieve in a substation, where the common sampling clock pulses can be distributed to all the measuring systems. However, to measure common-reference phasors in substations separated from each other by long distances, the task of synchronizing the sampling clocks is not a trivial one. Over the years, recognizing the importance of phasors and phase angle difference measurements between remote points of a system, many attempts have been made to synchronize the phasor measurements. None of these early attempts were too successful, as the technology of the earlier era is very limited on what could be accomplished. It is only in recent years, with the advent of the GPS satellite transmissions, that the technology has reached a stage whereby we can synchronize the sampling processes in distant substations economically and with an error of less than 1 microsecond. This error corresponds to  $0.021^\circ$  for a 60 Hz system and  $0.081^\circ$  for a 50 Hz system and is certainly more accurate than any presently conceived application would demand. [107, 110]

The GPS was initiated in 1978 with the launch of the first Block I satellites by US Department of Defense. The complete constellation of 24 modern satellites was put in place in 1994. These are arranged in six orbital planes displaced from each other by  $60^\circ$  and having an inclination of about  $55^\circ$  with respect to the equatorial plane. The satellites

have an orbital radius of 16,500 miles and go around the earth twice a day. They are arranged so that at least six satellites are visible at most locations on earth and often as many as 10 satellites may be available for viewing. The most common use of the GPS system is in determining the coordinates of the receiver. For the PMUs, however, the signal which is most important is the one pulse per second. This pulse as received by any receiver on earth is coincident with all other received pulses to within 1 microsecond. In practice much better accuracies of synchronization, of the order of a few hundred nanoseconds, have been realized. [5]

The GPS satellites keep accurate clocks which provide the one pulse per second signal. The time they keep is known as the GPS time which does not take into consideration the earth's rotation. Corrections to the GPS time are made in the GPS receivers to account for this difference (leap-second correction) so that the receivers provide UTC clock time. The identity of the pulse is defined by the number of seconds since the time that the clocks began to count on January 6, 1980. It should be noted that the PMU standard uses UNIX time base with a "second-of-century" counter which began counting at midnight on January 1, 1970. Presently, there are a number of GPS-like systems being deployed by other nations, with similar goals. However, it is expected that the GPS system will remain the principal source of synchronization for PMUs for the foreseeable future. [5]

### **3.7 Phasor measurement systems**

The PMUs are installed in power system substations. The selection of substations where these installations take place depends upon the intended PMU application. The phasor

data could be recorded locally or sent to a remote location in real time. Local recording systems have been used successfully but can't take full advantage of the information since it is only available after the fact. In most applications, the phasor data is used at locations remote from the PMUs. In order to realize the full benefit of the PMU measurement system, an architecture involving PMUs, communication links, and data concentrators must exist. Since utility communications have evolved around centralized control centers, the simplest solution has been to deploy PMUs at substations and send the data to a concentrator at the control center. Figure 3.3 shows a generally accepted architecture of such a system. [5, 105, 109]

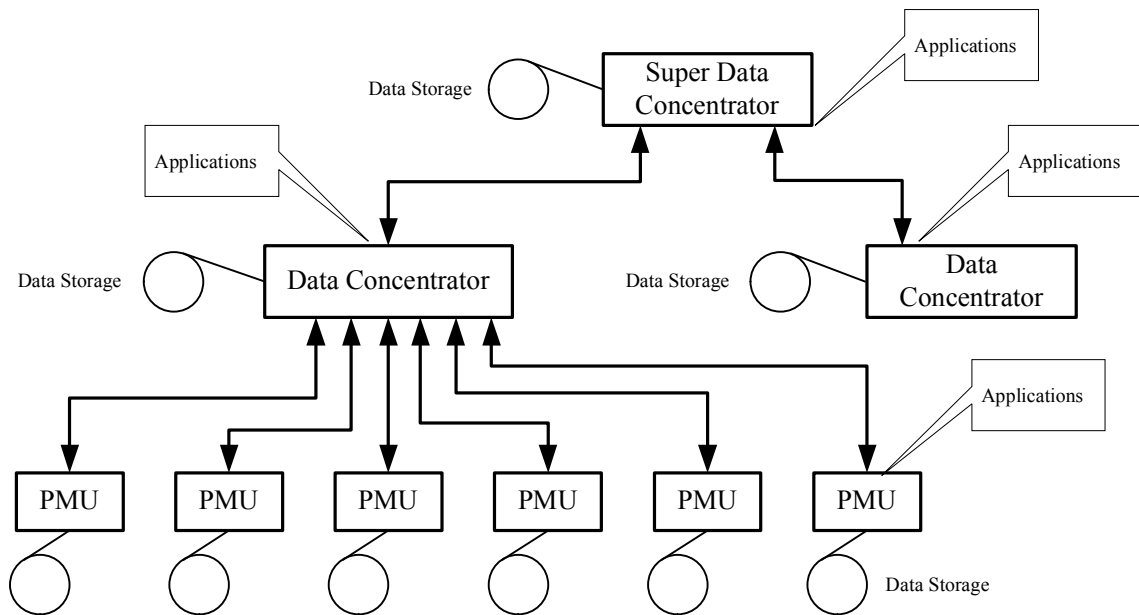


Figure 3.3: Hierarchy of the phasor measurement systems and levels of phasor data concentrators

In Figure 3.3 the PMUs are located in power system substations and provide measurements of time-stamped positive-sequence voltages and currents of all monitored buses and feeders. The measurements are stored in local data storage devices that can be

accessed remotely for post-mortem or diagnostic purposes. The local storage capacity is limited. In addition, the phasor data is available for real time applications in a steady stream as soon as the measurements are made. There may be some local application tasks requiring PMU data where it can be made available locally for such tasks. The main use of the real-time data is, however, at a higher level where data from several PMUs is available. [5]

Due to differences in distances and communication technologies, data measured at the same moment in time from remote devices arrives to its destination at different times and each device will have a variable time delay for data transmission. In order for this data to be used effectively it must be sorted together, by time stamp, waiting long enough for the slowest moving measurement to arrive. Even so, because the data move typically at speeds of 30 times per second, this wait time cannot be very long, and the nature of some applications of this data will be extremely time sensitive. This process of waiting for and sorting measurements is known as “data concentration”. In the context of phasor measurements, it is “phasor data concentration” performed by a PDC. Typical function of the PDCs is to gather data from several PMUs, reject bad data, align the time-stamps, and create a coherent record of simultaneously recorded data from a wider part of the power system. There are local storage facilities in the PDCs and application functions which need the PMU data available at the PDC. This can be made available by the PDCs to the local applications in real time. [5, 105]

One may view the first hierarchical level of PDCs as being regional in their data-gathering capability. On a system-wide scale, one must contemplate another level of the hierarchy (Super Data Concentrator in Figure 3.3). The functions at this level are similar

to those at the PDC levels in the sense that there is facility for data storage of data aligned with time-tags (at a somewhat increased data latency), as well as a steady stream of near real time data for applications which require data over the entire system. [5]

Figure 3.3 shows the communication links to be bidirectional. Indeed, most of the data flow is upward in the hierarchy, although there are some tasks which require communication capability in the reverse direction. Usually these are commands for configuring the downstream components, requesting data in a particular form, etc. In general, the capacity for downward communication is not as demanding as one in the upward direction. [5]

### 3.8 Application of phasor measurements

Phasor measurements obtained from PMUs have a wide variety of applications in support of maintaining and improving power system reliability. According to the North American Synchrophasor Initiative (NASPI)'s synchrophasor applications table [111-112] given in Appendix-A, actual and potential phasor data application areas include reliability operations, market operation, planning, and others. Among all, PMU application for state estimation, power system protection [113-114], power system stability [115-116], model validation and event identification and fault location are considered to be of a great significance.

PMUs have been installed in many countries [103, 117] for different applications. All installations are reaching for a hierarchical WAMS so that the measurement obtained from various substations on the system can be collected at central locations from which



various monitoring, protection and control applications can be developed. PMU deployment in different parts of the world [117] is shown in Table 3.1.

TABLE 3.1 : PMU DEPLOYMENT IN DIFFERENT PARTS OF THE WORLD

<i>PMU Applications</i>	<i>North America</i>	<i>Europe</i>	<i>China</i>	<i>India</i>	<i>Brazil</i>	<i>Russia</i>
Post-disturbance analysis	✓	✓	✓	P	T	✓
Stability monitoring	✓	✓	✓	P	P	✓
Thermal overload monitoring	✓	✓	✓	P	P	✓
Power system restoration	✓	✓	✓	P	P	P
Model validation	✓	✓	✓	P	T	✓
State Estimation	P	P	P	P	P	P
Real-time control	T	T	T	P	P	P
Adaptive protection	P	P	P	P	P	P
Wide area stabilizer	T	T	T	P	P	P

T (Testing Phase), P (Planning Phase)

Modern PMUs are now able to obtain measurements synchronously and thus are more accurate than traditional SCADA systems. As a result, PMUs improve the performance of state estimation dramatically. Given PMU data can be reported at rates as high as 60 times a second, a truly dynamic estimate would be available which can provide better input to contingency analysis and other downstream energy management system (EMS) functions. Moreover, monitoring of angles to detect possible instabilities and taking discrete switching controls in an attempt to militate against these events is a form of control made possible only with PMU. One of the early applications of PMU data is the detection and location of faults. A typical PMU-based fault detection and location algorithm contains two steps: first identify the faulted section and then locate the fault on this section. These techniques make use of local fault messages (synchronized voltages and currents at two terminals of a transmission line) to estimate fault location. [104, 111, 118, 119]

## CHAPTER 4

### Optimal PMU Placement (OPP) Problem Formulation

It is neither economical nor necessary to install a PMU at each bus of a wide-area power network. To achieve the fault-location observability over the entire network, it is important to examine minimal PMU placement considering the installation cost of PMUs in the PMU-based fault-location scheme. The optimal PMU placement (OPP) problem concerns with where and how many PMUs should be installed in a power system to achieve full observability at minimum number of PMUs. [111, 120]

When a PMU is placed at a bus in a power system, the voltage phasor at that bus and current phasors in all branches that are incident on that bus can be obtained. A bus is said to be observable if the voltage phasor at that bus is known and the power system is said to be completely observable when all the buses are observable. Clearly, installation of a PMU at a bus makes that bus observable. Since all branch currents at such a bus are

also known, the voltage phasors at buses adjacent to this PMU bus can be calculated from knowledge of the line parameters. Therefore, a PMU placed at a bus makes that bus and all buses adjacent to it observable. [121-124]

Being an area of a great research interest, different techniques have been used to solve OPP problem as summarized in [125]. References [121, 126-128] propose an integer linear programming formulation to solve OPP problem. In [126] OPP problem is solved under different cases of redundant PMU placement, full observability and incomplete observability. The proposed formulation takes the situations with and without zero injection measurements into consideration. In [127], OPP problem is solved considering not only the base case operating conditions but also the contingency cases. The proposed method makes use of a voltage stability based contingency ranking method and a graph theoretic approach to modify the constraints under contingency. Reference [128] proposes a procedure for multistage scheduling of PMU placement in a given time horizon taking into account the zero injection constraints. In [121], the problem of joint OPP and conventional measurements to ensure full network observability is addressed. The problem is first formulated as a nonlinear integer programming problem and then recast into an equivalent integer linear programming problem by introducing auxiliary variables and constraints. The branch and bound optimization method is adopted in [129] to solve OPP problem considering secondary voltage control. Constraint functions considering adjacent zero-injection buses are constructed using a novel hybrid topology transformation nonlinear constraint method. References [130, 131] propose solution methods to OPP problem based on particle swarm (PSO) optimization. The objective in [130] is to solve OPP problem using the minimum number of PMUs while maximizing

the measurement redundancy at the power system buses. In [131], the performance of the proposed PSO algorithm is compared with that of adaptive GA, CLONALG and adaptive CLONALG. An integer quadratic programming approach is used in [132] to solve OPP problem by minimizing the total number of PMUs required and, at the same time, maximizing the measurement redundancy at the power system buses. The proposed formulation considers the existing conventional measurements, outage of a single transmission line or a single PMU. The binary search method, proposed in [133], accounts also for single branch outages and seeks to maximize the measurement redundancy with minimum number of PMUs. An evolutionary-based approach is proposed in [134] to solve OPP problem for a power system such that a minimum mean square error (MSE) for state estimation is gained in normal operating conditions. The proposed approach employs differential evolution (DE) algorithm to do a state estimation for a power system, calculate the corresponding MSE and then determine the minimum number of PMU needed to make a minimum MSE for the system. Convex relaxation method is proposed in [135] to solve the OPP problem. Different OPP problem formulations considering probabilistic cost/benefit analysis [136], a defined number of PMUs [137] and existing smart meters [138] have also been proposed.

This chapter proposes a new formulation for OPP problem to achieve full network observability while incorporating real-life practical constraints and limitations. It first describes the OPP problem as a constrained minimization problem with a single objective to achieve full network observability using a minimum number of PMUs. Such formulation is then extended by considering the presence of zero-injection buses and having another objective to maximize the PMU measurement redundancy at the power

system buses. This chapter also details several topological observability rules which are applied to assess the electric network observability.

## 4.1 Introduction

A general constrained minimization problem [139] can be described as

$$\text{Min } y = f(x) \quad (4.1)$$

subject to

$$g(x) \leq 0 \quad (4.2)$$

where  $x = \{x_i\}, (i = 1, 2, \dots, n)$ , is the vector of variables where an optimal value is to be calculated to minimize  $y; f(x) = \{f_j(x)\}, (j = 1, 2, \dots, m_1)$ , is the vector of objective functions, and  $g(x) = \{g_k(x)\}, (k = 1, 2, \dots, m_2)$ , is the vector of equality and inequality constraints. Let  $m = m_1 + m_2$  and assume that  $x$  is represented as a vector of floating numbers. This minimization problem can be further represented as

$$\text{Min } F(x) \quad (4.3)$$

where  $F(x)$  incorporates the objective function  $f(x)$  and the constraint function  $g(x)$ . There are different ways to convert (4.1)–(4.2) into (4.3), among which weighted sum is a popular approach as shown in (4.4) with the weighting factors  $w_i > 0$

$$F(x) = \sum_{j=1}^n w_j f_j(x) + \sum_{k=1}^m w_k g_k(x) \quad (4.4)$$

For (4.3) and (4.4), the local and global minima can be calculated if the region of realizability of  $x$  is convex. For power system problems, the optimization problem may not always be convex and therefore requires heuristic (intelligent optimization) algorithms to solve it.

## 4.2 OPP problem formulation

The OPP problem concerns with where and how many PMUs should be installed in a power system to have it fully observable with minimum number of PMUs. Therefore, the objective function of this optimization problem is to minimize the number of PMUs subject to the constraint of achieving full network observability. To meet ever-increasing growth in the load demand, power systems are expanded in a continuous manner by implementing more and more generation power plants, transmission line and substation projects. Power system's network topology changes when such projects are introduced. If a power system is equipped with some PMUs and its topology changes by introducing new expansion projects, then the OPP optimization problem for the expanded system shall take the existing PMUs into account. An existing PMU may either be retained in its location or relocated to some other location based on the optimal solution obtained. The new OPP problem formulation being presented in this chapter takes into account the existing PMUs and the associated removal and relocation cost.

While formulating the OPP problem, one might require PMUs to be installed at particular buses due to their specific importance or to better suit a certain PMU application. The two ends of a tie line connecting two areas of a power network represent an example falling under the set of "must place" buses. Moreover, we may sometimes need to prohibit PMU installation at some buses to meet the problem constraints. Power system buses lacking communication facilities and virtual buses that are nonexistent in reality represent some examples falling under the set of "do not place" buses. Based on the above, the OPP problem is treated as a constrained minimization problem and it is mathematically formulated as shown in (4.5).

$$\text{Min } F(x)$$

$$F(x) = \sum_{k=1}^{N_b} C_i n_{ki} + \sum_{k=1}^{N_b} C_r n_{kr} + \sum_{k=1}^{N_b} W_k U_k \quad (4.5)$$

$$\text{such that } S \in S_{MP}, S \notin S_{DP}$$

where

$N_b$  : Number of buses

$C_i$  : Installation cost of a new PMU

$C_r$  : Removal and relocation cost of an existing PMU

$n_{ki}$  : A binary number to indicate PMU installation at bus 'k'. It is set to 1 if a new PMU is installed at bus 'k' and 0 otherwise

$n_{kr}$  : A binary number to indicate PMU removal from bus 'k'. It is set to 1 if a new PMU is removed from bus 'k' and 0 otherwise

$W_k$  : Penalty factor for bus unobservability. Since the aim is to place PMUs to have a completely observable system,  $W_k$  is set to be high

$U_k$  : A binary number to indicate unobservability of bus 'k'. It is set to 0 if bus 'k' is observable and 1 otherwise

$S_{MP}$  : A set of "must place" buses, if any, at which PMUs must be placed

$S_{DP}$  : A set of "do not place" buses, if any, at which installation of PMUs shall be avoided

$S$  : A candidate solution represented by a set of binary numbers indicating PMU installation at system buses. Mathematically, it can be represented as follows

$$S = \{x_1 \ x_2 \ x_3 \ \dots \ \dots \ x_{N_b}\}$$

such that  $x_i = 1$  if  $i \in S_{MP}$  and  $x_i = 0$  if  $i \in S_{DP}$

### 4.3 Extended OPP problem formulation

Traditionally, OPP problem is formulated with a single objective to find the minimum number of PMUs, and their respective locations, required to have the power system fully observable. A natural extension of such formulation is to combine two or more objectives. In this section, OPP problem is formulated to achieve dual objectives; to minimize the required number of PMUs and to maximize the PMU measurement redundancy at the power system buses. Moreover, we consider in this formulation the existence of zero-injection buses which are defined as neither generation nor load buses. To assess the power network observability, we apply the following topological observability rules as depicted in Figure 4.1 [140-143]:

1. A PMU placed at a bus makes that bus and all buses adjacent to it observable
2. When buses incident to an observable zero-injection bus are all observable except one, then the unobservable bus will also be identified as observable by applying the KCL at zero-injection bus
3. When buses incident to an unobservable zero-injection bus are all observable, then the zero-injection bus will also be identified as observable by applying the KCL at zero-injection bus

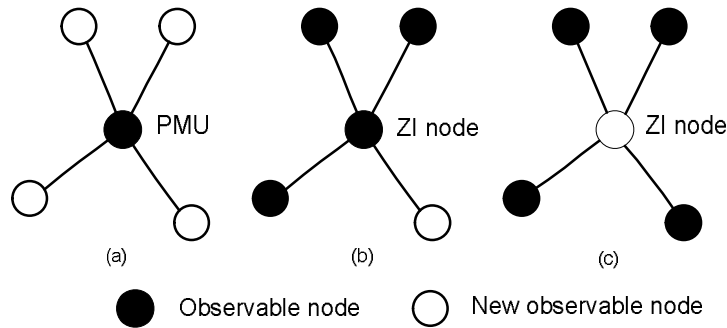


Figure 4.1: Topological observability rules



Based on the above, extended OPP problem is mathematically formulated as shown below in (4.6)

$$\begin{aligned}
 & \text{Min } F(x) \\
 & F(x) = \sum_{k=1}^{N_b} C_i n_{ki} + \sum_{k=1}^{N_b} C_r n_{kr} + \sum_{k=1}^{N_b} W_k U_k + \sum_{k=1}^{N_b} W_1 R_k \quad (4.6) \\
 & \text{such that } S \in S_{MP}, S \notin S_{DP}
 \end{aligned}$$

where

$W_1$  : A design factor to maximize PMU measurement redundancy

$R_k$  : An integer number to indicate bus 'k' observability redundancy index. If  $N_k$  indicates number of times bus 'k' is observed, then:

$$R_k = \begin{cases} N_k - 1 & \text{if } N_k \geq 2 \\ 0 & \text{Otherwise} \end{cases}$$

#### 4.4 Justifying OPP problem for fault location application

As this thesis addresses the subject of adaptive fault location application in power system networks based on PMU measurements, we may justify the need to solve OPP problem for such application as follows:

1. Depending on the intended system application, a power system planner may plan PMU installation for limited local purposes instead of comprehensive wide area measurements. Some applications such as postmortem analysis, congestion management, system restoration and separation do not rely on full network observability and, therefore, do not require OPP problem to be solved. For fault

location application, however, it is pre-requisite to achieve full network observability from PMU measurements so that the fault can be located over the entire network and, hence, solving OPP problem to satisfy the constraint of full network observability becomes mandatory for such application.

2. PMU placement at all substations allows direct measurement of the state of the network. However, PMU placement on each bus of a system is not needed for fault location application. As a consequence of Ohm's Law, when a PMU is placed at a bus, neighboring buses also become observable (rule # 1). This implies that the system can be made fully observable with a lesser number of PMUs than the number of buses and, hence, justifies the need to solve OPP problem to know the minimum number of PMUs and their corresponding locations needed to have the system fully observable.
3. PMU placement on each bus of a system for fault location application is practically difficult to achieve due to cost factor. The cost of a phasor measurement system includes the communication infrastructure costs, unit cost, installation cost and testing and commissioning costs of PMUs, phasor data concentrators and super data concentrators. Since the total cost of a phasor measurement system depends on the number of PMUs to be installed, it becomes therefore mandatory to solve OPP problem for fault location application in order to minimize the required number of PMUs and hence the cost of the associated phasor measurement system.
4. In addition to the cost factor, PMU placement on each bus of a system for fault location application is practically not possible due to nonexistence of communication

facilities in some substations. Therefore, OPP problem shall be solved for fault location application considering such a practical constraint.

## **CHAPTER 5**

### **Differential Evolution (DE) Algorithm for Solving OPP Problem**

As we discussed in chapter 4, several algorithms have been introduced to solve OPP problem with the aim of achieving the full observability of a power system with a minimum number of PMUs. In this thesis work, we elect to solve OPP problem using differential evolution (DE) algorithm due to many advantages that will be pointed out in due course.

This chapter provides an overview of DE algorithm and presents its fundamentals and key operators. It also details DE application to OPP problem where MATLAB simulation results are presented for IEEE 14-, 30-, 39- and 57-bus test systems and compared to the published results obtained using other optimization techniques. Moreover, it details DE application to the extended formulation of OPP problem in a similar fashion. DE application to OPP problem for a real-life 115 kV transmission

system is then presented. Next, the issue of reducing the search space is highlighted in relation with the application of virtual buses reduction rules and selection of “don’t place” and “must place” buses. Finally, DE performance is analyzed with respect to the design of its scaling factor, mutation scheme, population size and crossover rate.

## **5.1 DE optimization algorithm**

DE is a relatively new population-based optimization technique as it was first proposed by Storn and Price at Berkeley over 1994–1996. Since then, DE has been attracting increasing attention for a wide variety of engineering applications including power engineering. Unlike the conventional evolutionary algorithms (EAs) that depend on pre-defined probability distribution function for mutation process, DE uses the differences of randomly sampled pairs of objective vectors for its mutation process. As a result, the object vectors’ differences will pass the objective functions topographical information toward the optimization process and therefore provide more efficient global optimization capability. DE is a stochastic direct search optimization method. In general, it is considered to be simple, accurate, reasonably fast and robust. It is easy to use in solving optimization problems that require a minimization process with real-valued and multimodal objective functions. DE uses a non-uniform crossover that makes use of child vector parameters to guide through the minimization process. In comparison with GAs, the mutation operation with DE is performed by arithmetical combinations of individuals rather than perturbing the genes in individuals with small probability. Another main advantage of DE over many basic EAs is its ability to search with floating point representation instead of binary representation. [134, 139, 144, 145]

### 5.1.1 DE fundamentals

The most significant feature of DE is that it uses the differences of randomly sampled pairs of object vectors to guide the mutation operation instead of using probability distribution functions as other EAs. The distribution of the differences between randomly sampled object vectors is determined by the distribution of these object vectors. Since the distribution of the object vectors is mainly determined by the corresponding objective function's topography, the biases where DE tries to optimize the problem match those of the function to be optimized. This enables DE to function robustly and more as a generic global optimizer than other EAs. According to [139, 146], the main advantages of a DE include:

- Fast and simple for application and modification
- Effective global optimization capability
- Parallel processing nature
- Operating on floating point format with high precision
- Efficient algorithm without sorting or matrix multiplication
- Self-referential mutation operation
- Effective on integer, discrete and mixed parameter optimization
- Ability to handle non-differentiable, noisy, and/or time-dependent objective functions
- Operates on flat surfaces
- Ability to provide multiple solutions in a single run and effective in non-linear constraint optimization problems with penalty functions

Being a member of the EA family, DE also depends on the initial population generation, mutation, recombination and selection through repeated generations until the stopping criteria is met. DE uses a population of  $NP$  parameter vectors for each generation. At generation  $G$ , the population  $P^G$  is composed of  $x_i^G, i = 1, 2, \dots, NP$ . If there is nothing known about the problem to be optimized, the initial population  $P^{G0}$  can be chosen randomly under uniform probability distribution. Otherwise, the preliminary solution can be included to the initial population by adding normally distributed random deviations to the nominal solution. [139, 146]

The key characteristic of a DE is the way it generates trial parameter vectors throughout the generations. A weighted difference vector between two individuals is added to a third individual to form a new parameter vector. The newly generated vector will be evaluated by the objective function. The value of the corresponding objective function will be compared with a pre-determined individual. If the newly generated parameter vector has lower objective function value, it will replace the pre-determined parameter vector. The best parameter vector is evaluated for every generation in order to track the progress made throughout the minimization process. The random deviations of DE are generated by the search distance and direction information from the population. This adaptive approach is associated with the normally fast convergence properties of a DE. [139, 146]

DE generates, for each parent parameter vector, a candidate child vector based on the distance of two other parameter vectors. For each dimension  $\in [1, d]$ , this process is shown in (5.1):

$$x' = x_{r3}^G + F * (x_{r1}^G - x_{r2}^G) \quad (5.1)$$

where the random integers  $r1 \neq r2 \neq r3 \neq i$  are used as indices to index the current parent object vector.  $F$  is a real constant positive scaling factor, normally  $F \in (0, 1 +)$ , that controls the scale of the differential variation  $(x_{r1}^G - x_{r2}^G)$ . Selection of this newly generated vector is based on comparison with another control variable, the crossover constant  $CR \in [0, 1]$ , to ensure the search diversity. Some of the newly generated vectors will be used as child vector for the next generation and others will remain unchanged. The selection process of DE follows the typical EA process. Each new vector  $x'$  is compared with  $x_i$ . The new vector  $x'$  replaces  $x_i$  as a member of the next generation if it produces a better solution than  $x_i$ . [139, 146]

### 5.1.2 DE key operators

In this section, some specific operators of DE are analyzed in more details to achieve better understanding and application of the technique. These include mutation, crossover and other operators. The objective of *mutation* is to enable search diversity in the parameter space and to direct the existing object vectors with suitable amount of parameter variation in a way that will lead to better results at a suitable time. It keeps the search robust and explores new areas in the search domain. In DE, the mutation vectors are generated by adaptively scaling and correlating the output of pre-defined, multivariate probability distribution. The DE mutation of a vector is achieved by adding the weighted difference of two randomly selected vectors [139, 146, 147] as in (5.2):

$$x_i'^{G+1} = x_i^G + f_1 * (x_{r1}^G - x_{r2}^G) \quad (5.2)$$



where  $G$  represents the  $G^{\text{th}}$  generation;  $r1 \neq r2 \neq i$ , and  $r1, r2$  are randomly selected integers within the population size  $NP$ , that is,  $r1, r2 \in \{1, 2, \dots, NP\}$ . Instead of employing a single difference vector as in (5.2), the mutation process can also begin, as proposed in [134, 148-150], by randomly selecting four population vectors which are then combined to form the sum of two difference vectors as shown in (5.3):

$$x_i'^{G+1} = x_i^G + f_1 * [(x_{r1}^G - x_{r2}^G) + (x_{r3}^G - x_{r4}^G)] \quad (5.3)$$

*Crossover* or recombination is the main operator for GAs and a complementary process for DE. It aims at reinforcing prior successes by generating child individuals out of existing individuals or object vector parameters. The basic recombination process is a discrete recombination. The crossover constant  $CR$  is used to determine if the newly generated individual is to be recombined.

Among other operators, *population size* and *selection operation* are considered to be the most important. DE usually employs fixed population size throughout the search process. Selection of the population size  $NP$  involves conflicting objectives. The population size should be as small as possible to achieve fast computational speed. However, too small  $NP$  may lead to premature convergence or stagnation. DE adopts a very simple selection operator. A newly generated child individual  $x_i'$  is selected to replace the parent individual  $x_i^G$  only if its corresponding objective function is of a lower value. This ensures that the cost of the individual and the overall population will not increase throughout the search process. Figure 5.1 shows the flow chart of a typical DE optimization process. [139, 146, 151]

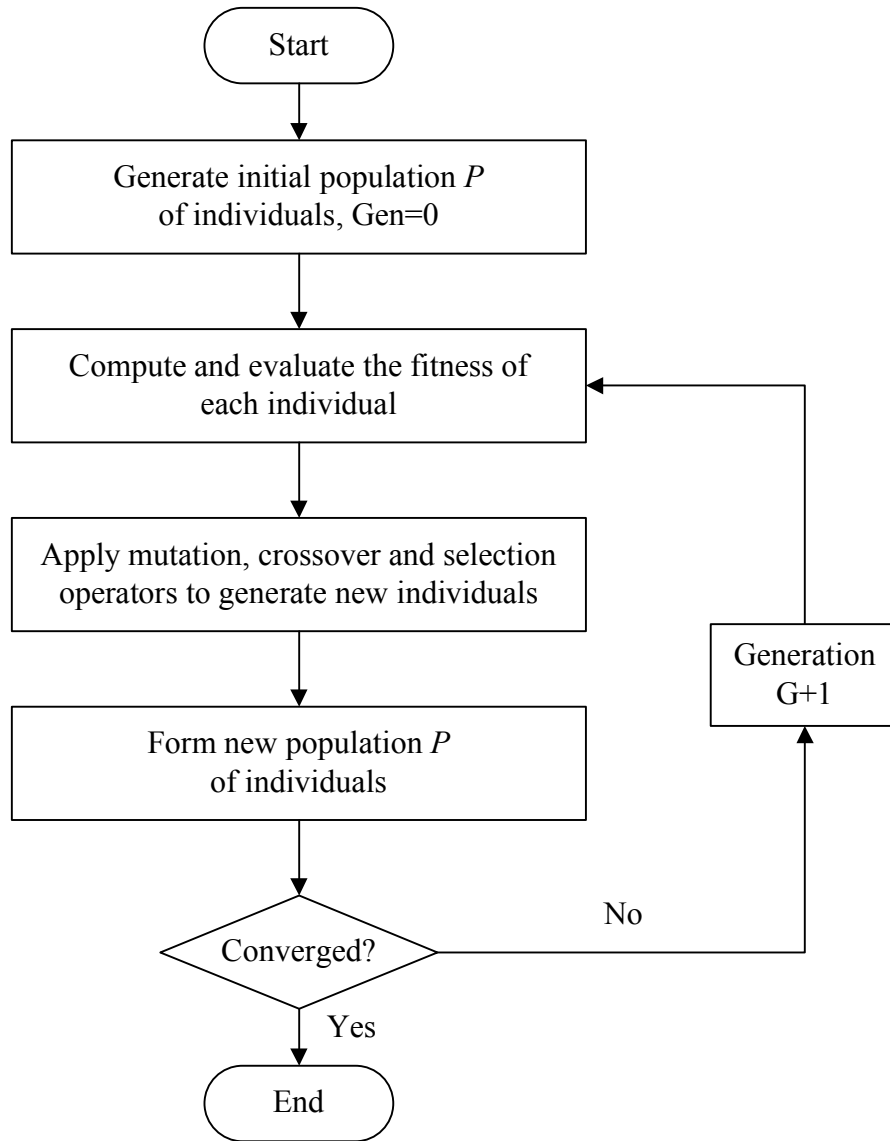


Figure 5.1: Flow chart of a typical DE optimization process

## 5.2 DE application to OPP problem

A MATLAB program is developed to simulate a DE-based algorithm to solve the OPP problem formulated as described in (4.5). The program is used to solve the OPP problem by finding the minimum number of PMUs, required to have the system completely observable, and their respective locations. The proposed solution method is applied to

IEEE 14-bus, 30-bus, 39-bus and 57-bus test systems. Appendix-B shows the one line diagrams of aforesaid systems. We shall now present the results obtained and compare them with those obtained and published using some other optimization techniques.

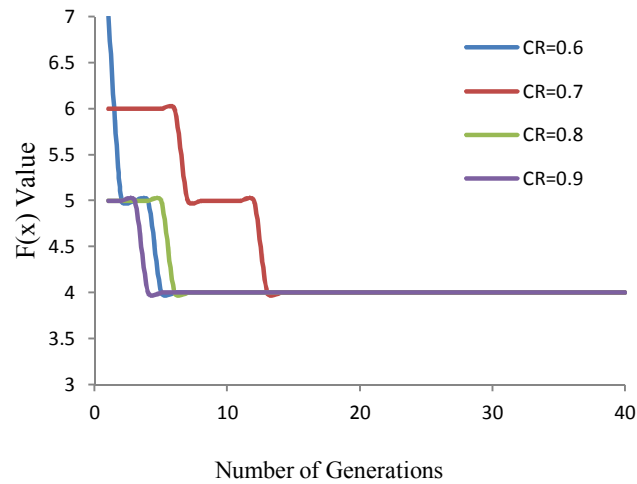
### 5.2.1 Application to IEEE 14-bus test system

Table 5.1 summarizes the simulation results obtained for the IEEE 14-bus test system. Three different values of scaling factor  $F$ , namely 0.9, 0.8 and 0.7 are considered. For each value of  $F$ , the crossover constant  $CR$  is varied from 0.4 to 0.9 with an increment of 0.1. The population size is fixed throughout the search process and it is selected as 30. The table also displays the number of generations required before DE algorithm convergence is reached  $NG$  for each combination of  $F$  and  $CR$ . It also displays number of PMUs  $N_{PMU}$  in the optimal solution. A minimum of 4 and a maximum of 24 generations are required by DE algorithm to converge depending on the selection of  $F$  and  $CR$  values.

Simulation results reveal that the IEEE 14-bus test system can be observed completely by installing a minimum of 4 PMUs. However, the solution is not unique as far as PMU locations are concerned in accordance with Table 5.1. Out of the 4 candidate PMU locations, only bus-2 is found common in all the optimal solutions obtained. The optimal solutions listed, although different in PMU locations, are considered to be the same since the OPP problem is formulated considering a single objective to minimize the number of PMUs needed to have the system completely observable.  $ORI$  is an index that shall be defined and discussed later. Figures 5.2-5.4 display DE algorithm convergence for each scaling factor  $F$  with different crossover constants  $CR$ . Although not a rule of thumb, we may generally state based on these figures that DE algorithm converges faster with higher crossover rates from 0.7 to 0.9.

TABLE 5.1 : OPP OF IEEE 14-BUS TEST SYSTEM

<i>CR</i>	<i>F</i>	<i>NG</i>	<i>Best solution</i>		
			<i>N<sub>PMU</sub></i>	<i>Locations</i>	<i>ORI</i>
0.4	0.9	6	4	2,6,7,9	5
0.5	0.9	7		2,7,11,13	2
0.6	0.9	5		2,6,7,9	5
0.7	0.9	13		2,6,7,9	5
0.8	0.9	6		2,7,10,13	2
0.9	0.9	4		2,8,10,13	0
0.4	0.8	14		2,7,10,13	2
0.5	0.8	14		2,7,10,13	2
0.6	0.8	16		2,7,10,13	2
0.7	0.8	10		2,6,8,9	3
0.8	0.8	12		2,7,10,13	2
0.9	0.8	9		2,6,7,9	5
0.4	0.7	24		2,7,11,13	2
0.5	0.7	18		2,7,11,13	2
0.6	0.7	12		2,7,10,13	2
0.7	0.7	5		2,6,8,9	3
0.8	0.7	13		2,7,10,13	2
0.9	0.7	8		2,6,7,9	5

Figure 5.2: IEEE 14-bus: DE algorithm convergence for  $F=0.9$  and different values of  $CR$

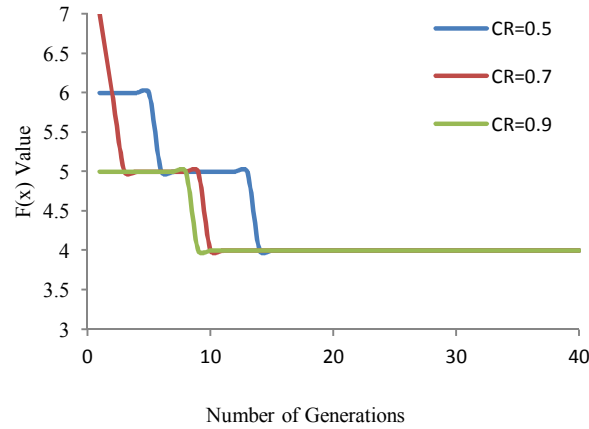


Figure 5.3: IEEE 14-bus: DE algorithm convergence for  $F=0.8$  and different values of  $CR$

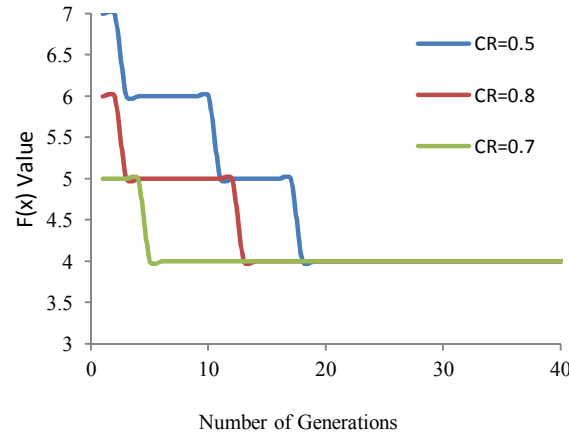


Figure 5.4: IEEE 14-bus: DE algorithm convergence for  $F=0.7$  and different values of  $CR$

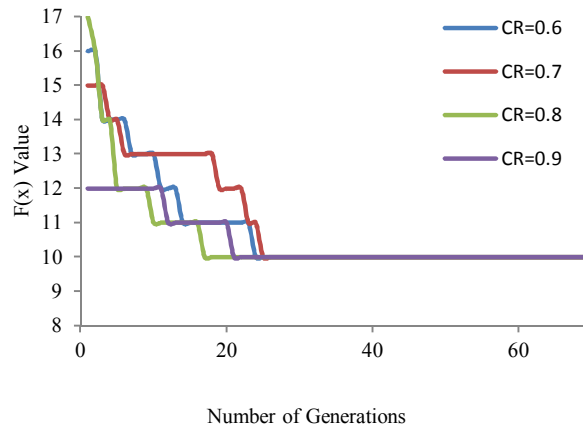
### 5.2.2 Application to IEEE 30-bus test system

Table 5.2 displays the simulation results obtained for the IEEE 30-bus test system. The population size is selected as 60. Selection of a smaller size yields pre-mature convergence. With such a selection, a minimum of 17 and a maximum of 62 generations are required by DE algorithm to converge depending on the selection of  $F$  and  $CR$  values. Simulation results reveal that this test system can be observed completely by installing a minimum of 10 PMUs. However, the solution is again not unique. Out of the 10

candidate PMU locations, only bus-10 and bus-12 are found common in all the optimal solutions obtained. Figures 5.5-5.7 display DE algorithm convergence for each scaling factor  $F$  with different crossover constants  $CR$ .

TABLE 5.2 : OPP OF IEEE 30-BUS TEST SYSTEM

$CR$	$F$	$NG$	<i>Best solution</i>		
			$N_{PMU}$	<i>Locations</i>	$ORI$
0.4	0.9	49	10	1,5,8,10,11,12,19,23,26,29	5
0.5	0.9	39		1,5,10,11,12,19,23,25,27,28	10
0.6	0.9	29		1,6,7,10,11,12,18,23,26,30	10
0.7	0.9	40		1,7,10,11,12,19,24,26,28,30	7
0.8	0.9	29		1,5,9,10,12,19,23,26,27,28	10
0.9	0.9	27		2,3,6,9,10,12,18,23,25,29	16
0.4	0.8	62		1,5,8,10,11,12,19,23,26,29	5
0.5	0.8	51		1,7,10,11,12,18,24,25,28,30	9
0.6	0.8	24		3,5,9,10,12,19,24,25,27,28	13
0.7	0.8	25		3,5,8,10,11,12,18,23,26,29	5
0.8	0.8	17		3,5,10,11,12,15,18,25,27,28	12
0.9	0.8	21		1,5,9,10,12,19,24,26,27,28	11
0.4	0.7	45		1,5,8,9,10,12,18,24,26,30	8
0.5	0.7	60		1,7,10,11,12,15,20,25,27,28	12
0.6	0.7	39		1,5,8,9,10,12,15,20,25,29	11
0.7	0.7	27		1,5,6,10,11,12,18,24,26,27	13
0.8	0.7	26		1,5,8,9,10,12,19,24,25,27	12
0.9	0.7	25		1,5,6,9,10,12,18,24,25,27	17

Figure 5.5: IEEE 30-bus: DE algorithm convergence for  $F=0.9$  and different values of  $CR$

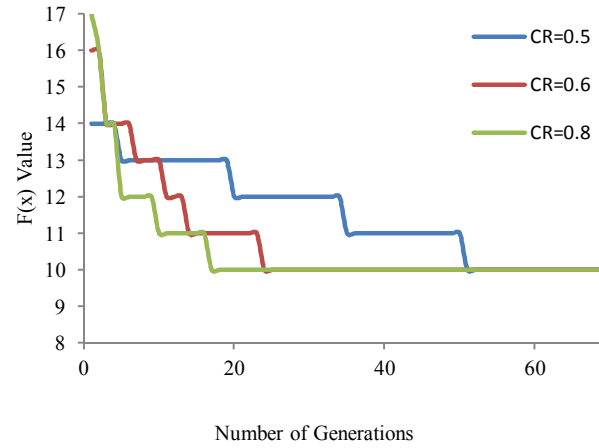


Figure 5.6: IEEE 30-bus: DE algorithm convergence for  $F=0.8$  and different values of  $CR$

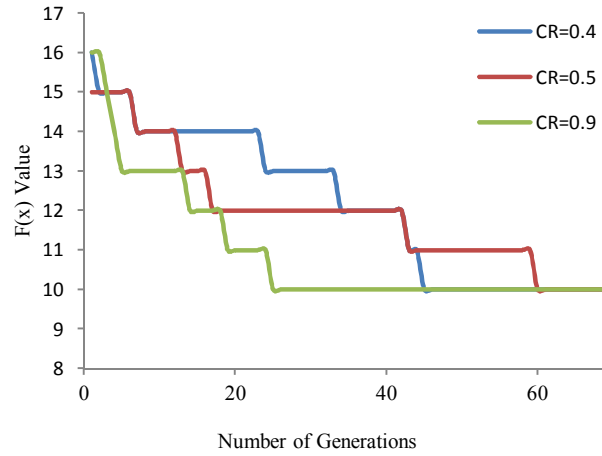


Figure 5.7: IEEE 30-bus: DE algorithm convergence for  $F=0.7$  and different values of  $CR$

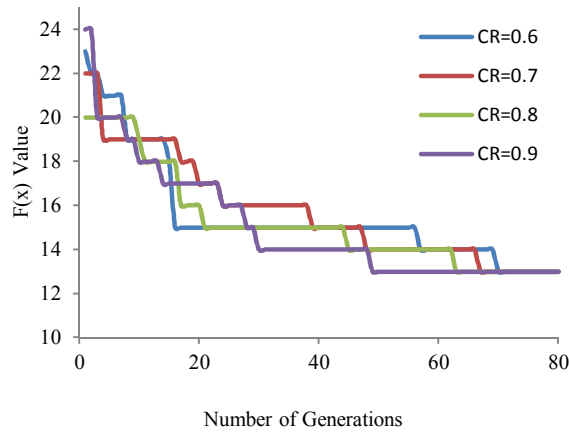
### 5.2.3 Application to IEEE 39-bus test system

Table 5.3 displays the simulation results obtained for the IEEE 39-bus test system. The population size is selected as 100. Selection of a smaller size yields pre-mature convergence. With such a selection, a minimum of 49 and a maximum of 80 generations are required by DE algorithm to converge depending on the selection of  $F$  and  $CR$  values. Simulation results reveal that this test system can be observed completely by installing a minimum of 13 PMUs. However, the solution is again not unique. Out of the 13

candidate PMU locations, only bus-2, bus-6, bus-9, bus-14, bus-17, bus-22, bus-23 and bus-29 are found common in all the optimal solutions obtained. Figures 5.8-5.10 display DE algorithm convergence for each scaling factor  $F$  with different  $CR$ .

TABLE 5.3 : OPP OF IEEE 39-BUS TEST SYSTEM

$CR$	$F$	$NG$	<i>Best solution</i>		
			$N_{PMU}$	<i>Locations</i>	$ORI$
0.4	0.9	66	15	2,3,6,9,10,13,16,19,20,24,26,35,36,37,38	15
0.5	0.9	80	13	2,6,9,12,14,17,22,23,25,29,32,33,34	7
0.6	0.9	70	13	2,6,9,12,14,17,22,23,29,32,33,34,37	5
0.7	0.9	67	13	2,6,9,10,11,14,17,22,23,29,33,34,37	8
0.8	0.9	63	13	2,6,9,11,14,17,19,22,23,29,32,34,37	8
0.9	0.9	49	13	2,6,9,10,12,14,17,22,23,25,29,33,34	9
0.4	0.8	74	14	2,6,9,10,13,14,16,17,19,20,22,23,29,37	17
0.5	0.8	59	14	2,6,9,10,13,14,17,22,23,24,25,29,33,34	13
0.6	0.8	57	13	2,6,9,12,14,17,19,22,23,25,29,32,34	9
0.7	0.8	75	13	2,6,9,12,14,17,20,22,23,25,29,32,33	8
0.8	0.8	64	13	2,6,9,10,12,14,17,20,22,23,25,29,33	10
0.9	0.8	56	13	2,6,9,10,11,14,17,19,22,23,25,29,34	12
0.4	0.7	71	14	2,5,6,13,15,17,20,22,23,25,29,32,33,39	12
0.5	0.7	66	14	2,5,6,9,10,13,16,17,20,29,33,35,36,37	11
0.6	0.7	68	13	2,6,9,12,14,17,22,23,25,29,32,33,34	7
0.7	0.7	65	13	2,6,9,10,12,14,17,19,22,23,25,29,34	11
0.8	0.7	66	13	2,6,9,13,14,17,19,20,22,23,29,32,37	9
0.9	0.7	51	13	2,6,9,11,14,17,19,22,23,25,29,32,34	10

Figure 5.8: IEEE 39-bus: DE algorithm convergence for  $F=0.9$  and different values of  $CR$



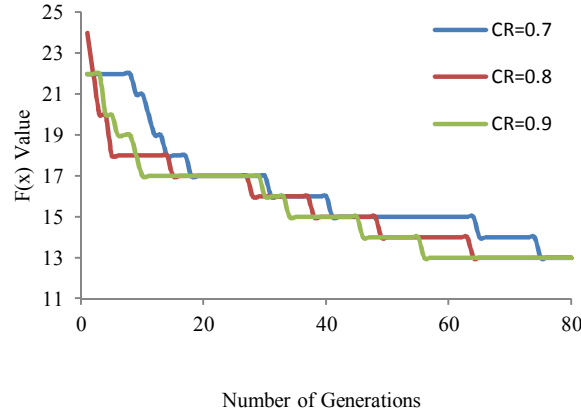


Figure 5.9: IEEE 39-bus: DE algorithm convergence for  $F=0.8$  and different values of  $CR$

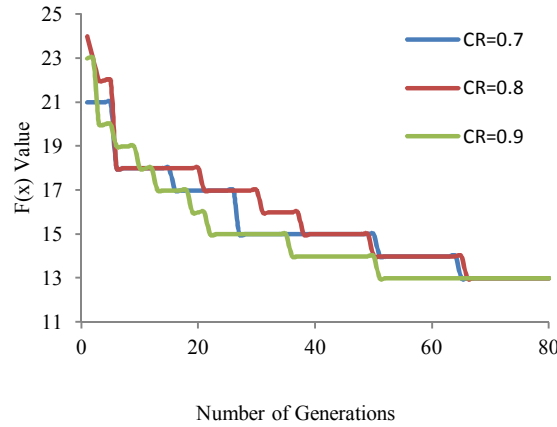


Figure 5.10: IEEE 39-bus: DE algorithm convergence for  $F=0.7$  and different values of  $CR$

#### 5.2.4 Application to IEEE 57-bus test system

Table 5.4 displays the simulation results obtained for the IEEE 57-bus test system. The population size is selected as 170. Selection of a smaller size yields pre-mature convergence. With such a selection, a minimum of 99 and a maximum of 142 generations are required by DE algorithm to converge depending on the selection of  $F$  and  $CR$  values. Simulation results reveal that this test system can be observed completely by installing a minimum of 17 PMUs. However, the solution is again not unique. Out of the 17 candidate PMU locations, only bus-32, bus-36 and bus-41 are found common. Figures

5.11-5.13 display DE convergence for each scaling factor  $F$  with different crossover constants  $CR$ .

TABLE 5.4 : OPP OF IEEE 57-BUS TEST SYSTEM

$CR$	$F$	$NG$	<i>Best solution</i>		
			$N_{PMU}$	<i>Locations</i>	$ORI$
0.4	0.9	149	19	3,4,6,12,15,20,24,28,30,33,34,38,39, 40,41,47,51,52,54	16
0.5	0.9	116	18	1,4,9,14,20,23,25,27,29,32,35,37,43,44,48,50,54,56	12
0.6	0.9	142	17	2,6,12,13,19,22,25,27,32,36,39,41,44, 47,50,52,54	8
0.7	0.9	126	18	2,6,12,14,18,21,24,26,29,30,32,36,39, 41,45,48,51,54	10
0.8	0.9	99	17	1,4,9,19,22,25,27,29,32,36,41,45,46, 49,51,53,57	10
0.9	0.9	101	17	1,4,7,9,15,20,23,27,30,32,36,38,41,46,51,53,57	13
0.4	0.8	146	19	1,6,15,17,18,20,24,28,31,32,36,38,41, 47,49,51,52,55,57	17
0.5	0.8	116	18	1,4,9,14,20,23,25,27,29,32,35,37,43,44,48,50,54,56	12
0.6	0.8	142	17	2,6,12,13,19,22,25,27,32,36,39,41,44, 47,50,52,54	8
0.7	0.8	124	17	1,4,8,9,20,24,25,28,32,36,38,39,41,45,46,51,53	11
0.8	0.8	131	17	1,4,7,9,13,19,22,25,27,32,36,41,44,47,51,53,57	12
0.9	0.8	101	17	1,4,7,9,15,20,23,27,30,32,36,38,41,46,51,53,57	13
0.4	0.7	137	18	1,4,9,13,20,23,26,29,30,32,36,41,44, 47,49,50,53,57	16
0.5	0.7	137	17	1,4,9,13,19,22,25,26,29,32,36,39,41, 44,47,51,53	12
0.6	0.7	138	18	1,4,7,9,14,19,22,25,27,32,36,41,44,46,48,50,53,57	13
0.7	0.7	112	18	1,4,7,13,18,21,24,27,30,32,36,39,41, 44,47,51,53,54	11
0.8	0.7	99	17	1,4,9,19,22,25,27,29,32,36,41,45,46, 49,51,53,57	10
0.9	0.7	101	17	1,4,7,9,15,20,23,27,30,32,36,38,41,46,51,53,57	13

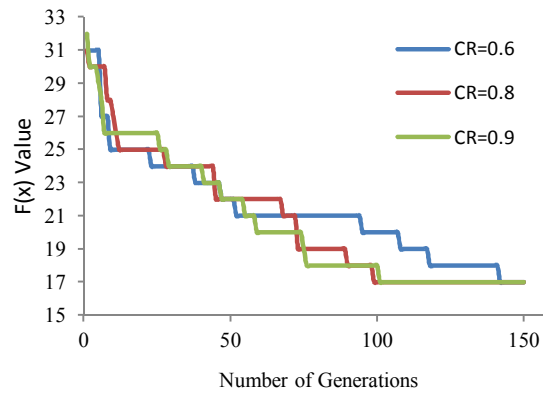


Figure 5.11: IEEE 57-bus: DE algorithm convergence for  $F=0.9$  and different values of  $CR$

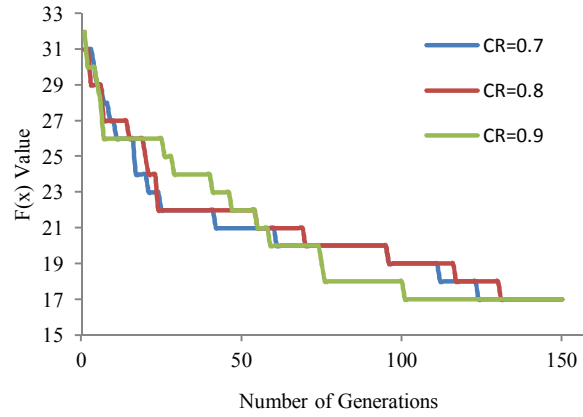


Figure 5.12: IEEE 57-bus: DE algorithm convergence for  $F=0.8$  and different values of  $CR$

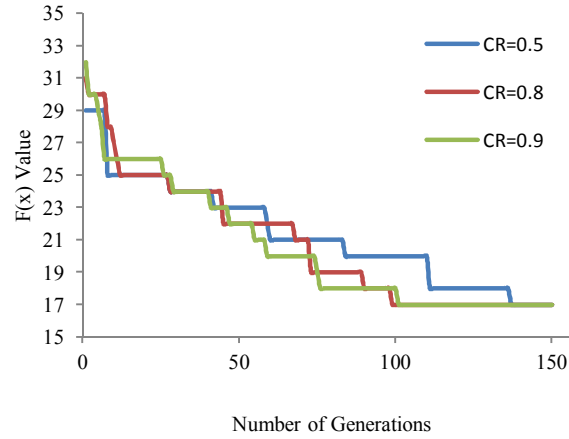


Figure 5.13: IEEE 57-bus: DE algorithm convergence for  $F=0.7$  and different values of  $CR$

### 5.2.5 Comparison with other optimization techniques

To validate the results obtained using DE algorithm, a comparison is made with the published results obtained using other optimization techniques, namely Branch and Bound (B&B), Binary Particle Swarm Optimization (BPSO), Integer Quadratic Programming (IQP), Binary Search Algorithm (BSA), Integer Linear Programming (ILP) and Genetic Algorithm (GA). Table 5.5 shows an acceptable performance of DE algorithm when compared to these optimization techniques. It may also be noted that reference [129] reported a minimum of 16 PMUs to be installed to fully observe the IEEE

57-bus system. However, with the reported PMU locations, it was found that bus-26 can't be observed and hence the system is not fully observable.

TABLE 5.5: NUMBER AND LOCATIONS OF PMUs FROM DE AND OTHER OPTIMIZATION ALGORITHMS (WITHOUT CONSIDERING ZI BUSES)

<i>Algorithm</i>		<i>14-Bus</i>	<i>30-Bus</i>	<i>39-Bus</i>	<i>57-Bus</i>
DE	No.	4	10	13	17
	Loc.	As per Table 5.1	As per Table 5.2	As per Table 5.3	As per Table 5.4
ILP [126]	No.	4	10	--	17
	Loc.	Not reported	Not reported	--	Not reported
ILP [121, 128]	No.	4	--	--	17
	Loc.	2,6,7,9	--	--	1,4,9,10,19,22, 25,26,29,32,36,39, 41,44,46,49,53
B&B [129]	No.	--	10	13	16
	Loc.	--	1,5,6,9,10, 12,15,19,25,29	2,6,9,10,13,14,17, 19,22,23,25,29,34	1,6,9,15,19,22, 25,28,32,36,38,41, 47,51,53,57
BPSO [130]	No.	4	10	--	--
	Loc.	2,7,10,13	1,5,6,9,10, 12,15,19,25,27	--	--
BPSO [131]	No.	4	--	--	17
	Loc.	2,7,11,13	--	--	2,4,7,12,15,20, 24,27,30,32,36,38, 39,41,46,50,54
IQP [132]	No.	4	10	--	17
	Loc.	2,7,10,13	2,4,6,9,10, 12,15,19,25,27	--	1,4,6,9,15,20, 24,25,28,32,36,38, 41,47,50,53,57
BSA [133]	No.	4	10	13	--
	Loc.	2,6,7,9	1,2,6,9,10, 12,15,19,25,27	2,6,9,10,11,14,17, 19,20,22,23,25,29	--
				2,6,9,10,13,14,17, 19,20,22,23,25,29	
GA [152]	No.	4	10	--	--
	Loc.	2,6,7,9	2,4,6,9,10, 12,15,19,25,27	--	--

### 5.3 DE application to the extended OPP problem

A MATLAB program is developed to simulate a DE-based algorithm to solve OPP problem formulated as described in (4.6). The proposed solution method is applied to IEEE 14-, 30-, 39- and 57-bus test systems. The program is used to solve OPP problem by finding the minimum number of PMUs, required to have the system completely observable, and their respective locations for the following four cases:

- Case-I: With no consideration of the zero-injection buses and without maximizing PMU measurement redundancy
- Case-II: With no consideration of the zero-injection buses and with maximizing PMU measurement redundancy
- Case-III: With consideration of the zero-injection buses and without maximizing PMU measurement redundancy
- Case-IV: With consideration of the zero-injection buses and with maximizing PMU measurement redundancy

#### 5.3.1 Application to IEEE 14-bus test system

Table 5.6 summarizes the simulation results of Case-I obtained for the IEEE 14-bus test system. Three different values of scaling factor  $F$ , namely 0.9, 0.8 and 0.7 are considered. For each value of  $F$ ,  $CR$  is varied from 0.4 to 0.9 with an increment of 0.1. The population size is fixed throughout the search process and it is selected as 30 for Case-I, Case-II and 50 for Case-III and Case-IV. The table displays the number of generations required before DE algorithm convergence is reached  $NG$  for each combination of  $F$  and  $CR$ . A minimum of 8 and a maximum of 24 generations are required by DE algorithm to

converge depending on the selection of  $F$  and  $CR$  values. Simulation results reveal that the IEEE 14-bus test system can be observed completely by installing a minimum of 4 PMUs at buses 2, 8, 10 and 13. The Observability Redundancy Index  $ORI$  of the system is the sum of all bus observability redundancy indices as shown in (5.4):

$$ORI = \sum_{k=1}^{N_b} R_k \quad (5.4)$$

For this case,  $ORI$  of the optimal solution equals zero meaning that every bus is observed only once either by direct PMU measurement or by calculation. This sounds reasonable because the OPP solution sought for this case is not meant to maximize the PMU measurement redundancy.

Table 5.7 summarizes the simulation results of Case-II obtained for this test system. Simulation results reveal that the IEEE 14-bus test system can be observed completely by installing a minimum of 4 PMUs at buses 2, 6, 7 and 9. For this case,  $ORI$  of the optimal solution equals 5 meaning that some buses are observed more than once because the OPP solution sought for this case is meant to maximize the PMU measurement redundancy. Effect of the maximization of PMU measurement redundancy is shown in Table 5.8. The IEEE 14-bus test system has only one zero injection bus which is bus-7. Table 5.9 and Table 5.10 summarize the test results for Case-III and Case-IV respectively. As expected, an optimal solution with less number of PMUs (3 for Case-III and IV instead of 4 for Case-I and II) is obtained when network observability rules are applied considering the zero-injection buses. The same solution is obtained for Case-III and Case-IV since it is the only possible solution where this system can be completely observed using 3 PMUs.

TABLE 5.6 : CASE I OPP OF IEEE 14-BUS TEST SYSTEM

<i>CR</i>	<i>F</i>	<i>NG</i>	<i>Best solution</i>		
			<i>N<sub>PMU</sub></i>	<i>Locations</i>	<i>ORI</i>
0.4	0.9	18	4	2,8,10,13	0
0.5	0.9	18			
0.6	0.9	14			
0.7	0.9	10			
0.8	0.9	19			
0.9	0.9	17			
0.4	0.8	24			
0.5	0.8	13			
0.6	0.8	15			
0.7	0.8	20			
0.8	0.8	17			
0.9	0.8	17			
0.4	0.7	24			
0.5	0.7	24			
0.6	0.7	21			
0.7	0.7	8			
0.8	0.7	14			
0.9	0.7	8			

TABLE 5.7 : CASE II OPP OF IEEE 14-BUS TEST SYSTEM

<i>CR</i>	<i>F</i>	<i>NG</i>	<i>Best solution</i>		
			<i>N<sub>PMU</sub></i>	<i>Locations</i>	<i>ORI</i>
0.4	0.9	21	4	2,6,7,9	5
0.5	0.9	29			
0.6	0.9	17			
0.7	0.9	13			
0.8	0.9	12			
0.9	0.9	20			
0.4	0.8	37			
0.5	0.8	31			
0.6	0.8	15			
0.7	0.8	19			
0.8	0.8	14			
0.9	0.8	6			
0.4	0.7	17			
0.5	0.7	23			
0.6	0.7	17			
0.7	0.7	13			
0.8	0.7	12			
0.9	0.7	17			

TABLE 5.8 : EFFECT OF THE MAXIMIZATION OF PMU MEASUREMENT REDUNDANCY (CASE-I AND CASE-II OPP)

<i>PMU locations</i>	<i>N<sub>k</sub></i>
2,8,10,13	1,1,1,1,1,1,1,1,1,1,1,1
2,6,7,9	1,1,1,3,2,1,2,1,2,1,1,1,1

TABLE 5.9 : CASE III OPP OF IEEE 14-BUS TEST SYSTEM

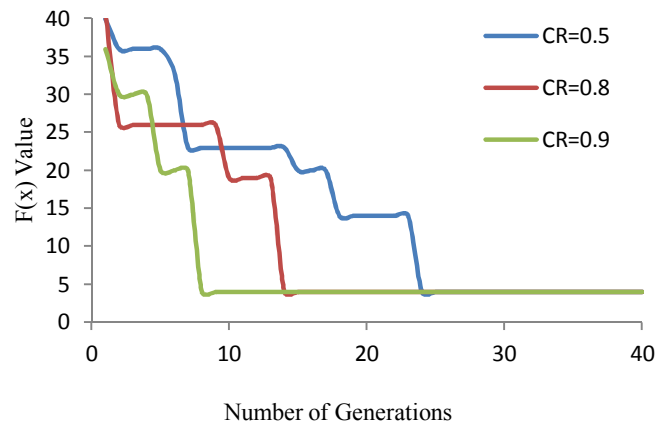
<i>CR</i>	<i>F</i>	<i>NG</i>	<i>Best solution</i>		
			<i>N<sub>PMU</sub></i>	<i>Locations</i>	<i>ORI</i>
0.4	0.9	13	3	2,6,9	2
0.5	0.9	9			
0.6	0.9	20			
0.7	0.9	28			
0.8	0.9	16			
0.9	0.9	21			
0.4	0.8	31			
0.5	0.8	21			
0.6	0.8	11			
0.7	0.8	19			
0.8	0.8	13			
0.9	0.8	11			
0.4	0.7	34			
0.5	0.7	19			
0.6	0.7	15			
0.7	0.7	21			
0.8	0.7	20			
0.9	0.7	15			



TABLE 5.10 : CASE IV OPP OF IEEE 14-BUS TEST SYSTEM

$CR$	$F$	$NG$	<i>Best solution</i>		
			$N_{PMU}$	<i>Locations</i>	$ORI$
0.4	0.9	34	3	2,6,9	2
0.5	0.9	20			
0.6	0.9	30			
0.7	0.9	27			
0.8	0.9	23			
0.9	0.9	24			
0.4	0.8	27			
0.5	0.8	27			
0.6	0.8	15			
0.7	0.8	24			
0.8	0.8	13			
0.9	0.8	12			
0.4	0.7	7			
0.5	0.7	30			
0.6	0.7	20			
0.7	0.7	16			
0.8	0.7	16			
0.9	0.7	15			

Figures 5.14 to 5.17 display DE algorithm convergence for Case-I to Case-IV respectively considering a scaling factor of 0.7 with different crossover constants  $CR$ . Although not a rule of thumb, we may generally state based on these figures that DE algorithm converges faster with higher crossover rates from 0.7 to 0.9.

Figure 5.14: DEA Convergence for  $F=0.7$  and Different values of  $CR$  (IEEE 14-bus, Case-I)

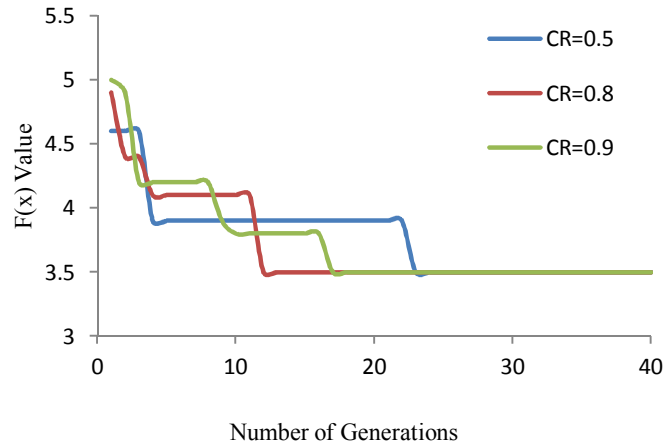


Figure 5.15: DEA Convergence for  $F=0.7$  and Different values of  $CR$  (IEEE 14-bus, Case-II)

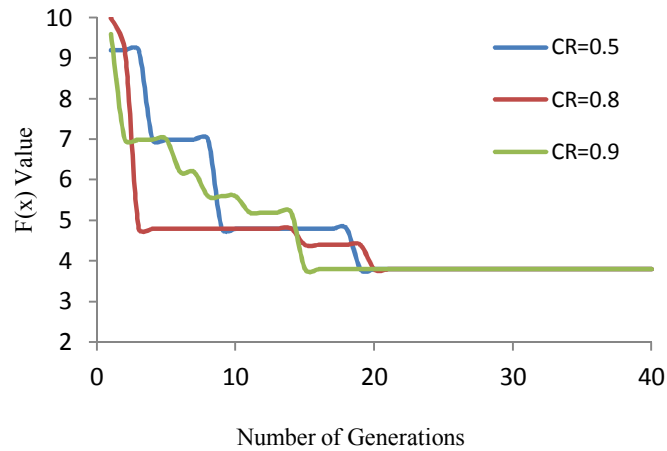


Figure 5.16: DEA Convergence for  $F=0.7$  and Different values of  $CR$  (IEEE 14-bus, Case-III)

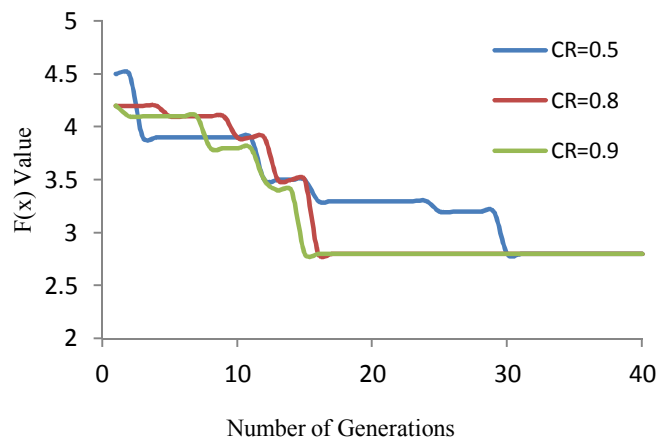


Figure 5.17: DEA Convergence for  $F=0.7$  and Different values of  $CR$  (IEEE 14-bus, Case-IV)

### 5.3.2 Application to IEEE 30-bus test system

Table 5.11 summarizes the simulation results of Case-I obtained for the IEEE 30-bus test system. Three different values of scaling factor  $F$ , namely 0.9, 0.8 and 0.7 are considered. For each value of  $F$ , the crossover constant  $CR$  is varied from 0.4 to 0.9 with an increment of 0.1. The population size is fixed throughout the search process and it is selected as 60 for Case-I to Case-IV. The table displays the number of generations required before DE algorithm convergence is reached  $NG$  for each combination of  $F$  and  $CR$ . A minimum of 22 and a maximum of 81 generations are required by DE algorithm to converge depending on the selection of  $F$  and  $CR$  values. Simulation results reveal that the IEEE 30-bus test system can be observed completely by installing a minimum of 10 PMUs at different buses. For this case,  $ORI$  of the optimal solution ranges from 5 to 7.

Table 5.12 summarizes the simulation results of Case-II obtained for this test system. Simulation results reveal that the IEEE 30-bus test system can be observed completely by installing a minimum of 10 PMUs at different buses. For this case,  $ORI$  of the optimal solution ranges from 19 to 22. This sounds reasonable because the OPP solution sought for this case is meant to maximize the PMU measurement redundancy.

The IEEE 30-bus test system has a total of six zero injection buses given by  $ZI_{bus} = \{6, 9, 22, 25, 27, 28\}$ . Table 5.13 and Table 5.14 summarize the test results for Case-III and Case-IV respectively. As expected, an optimal solution with less number of PMUs (7 for Case-III and IV instead of 10 for Case-I and II) is obtained when network observability rules are applied considering the zero-injection buses. In addition,  $ORI$  of the best solution in Case-IV has increased to 6 instead of an  $ORI$  of 3 for the best solution in Case-III.

TABLE 5.11 : CASE I OPP OF IEEE 30-BUS TEST SYSTEM

<i>CR</i>	<i>F</i>	<i>NG</i>	<i>Best solution</i>		
			<i>N<sub>PMU</sub></i>	<i>Locations</i>	<i>ORI</i>
0.4	0.9	61	10	1,7,8,10,11,12,19,23,25,30	7
0.5	0.9	52		1,7,8,10,11,12,19,23,26,29	5
0.6	0.9	46		3,5,8,10,11,12,19,23,26,29	5
0.7	0.9	38		1,5,8,10,11,12,18,23,26,29	5
0.8	0.9	34		1,5,8,10,11,12,19,23,26,30	5
0.9	0.9	33		3,5,8,10,11,12,19,23,26,30	5
0.4	0.8	63		3,5,10,11,12,19,23,26,28,29	6
0.5	0.8	42		1,5,8,10,11,12,19,23,26,29	5
0.6	0.8	50		1,5,8,10,11,12,19,23,26,30	5
0.7	0.8	64		3,5,8,10,11,12,18,23,26,29	5
0.8	0.8	23		3,5,8,10,11,12,18,23,26,29	5
0.9	0.8	22		3,5,8,10,11,12,19,23,26,29	5
0.4	0.7	81		1,7,8,10,11,12,19,23,26,29	5
0.5	0.7	41		1,5,8,10,11,12,19,23,26,30	5
0.6	0.7	53		1,7,8,10,11,12,18,23,26,29	5
0.7	0.7	44		3,5,8,10,11,12,18,23,26,30	5
0.8	0.7	26		1,7,8,10,11,12,18,23,26,30	5
0.9	0.7	33		3,5,8,10,11,12,19,23,26,30	5

TABLE 5.12 : CASE II OPP OF IEEE 30-BUS TEST SYSTEM

<i>CR</i>	<i>F</i>	<i>NG</i>	<i>Best solution</i>		
			<i>N<sub>PMU</sub></i>	<i>Locations</i>	<i>ORI</i>
0.4	0.9	50	10	2,4,6,9,10,12,18,24,25,29	19
0.5	0.9	69		2,4,6,9,10,12,18,23,25,27	20
0.6	0.9	49		1,2,6,9,10,12,15,18,25,27	20
0.7	0.9	51		2,4,6,9,10,12,15,20,25,29	20
0.8	0.9	53		2,4,6,10,11,12,15,19,25,27	20
0.9	0.9	39		1,2,6,9,10,12,15,19,25,27	20
0.4	0.8	52		1,2,6,9,10,12,15,18,25,27	20
0.5	0.8	63		2,4,6,9,10,12,15,19,25,27	22
0.6	0.8	44		2,4,6,9,10,12,18,24,25,27	21
0.7	0.8	40		2,4,6,10,11,12,15,20,25,27	20
0.8	0.8	38		2,3,6,9,10,12,15,19,25,27	20
0.9	0.8	41		2,4,6,9,10,12,19,24,25,27	21
0.4	0.7	52		1,2,6,9,10,12,15,18,25,27	20
0.5	0.7	63		2,4,6,9,10,12,15,19,25,27	22
0.6	0.7	44		2,4,6,9,10,12,18,24,25,27	21
0.7	0.7	40		2,4,6,10,11,12,15,20,25,27	20
0.8	0.7	41		2,4,6,9,10,12,19,24,25,27	21
0.9	0.7	44		2,4,6,9,10,12,19,24,25,27	21

TABLE 5.13 : CASE III OPP OF IEEE 30-BUS TEST SYSTEM

<i>CR</i>	<i>F</i>	<i>NG</i>	<i>Best solution</i>		
			<i>N<sub>PMU</sub></i>	<i>Locations</i>	<i>ORI</i>
0.4	0.9	64	7	3,5,10,12,19,23,27	3
0.5	0.9	62	7	1,5,10,12,18,23,27	3
0.6	0.9	16	7	1,7,10,12,18,24,29	3
0.7	0.9	37	7	1,7,10,12,18,23,27	3
0.8	0.9	39	7	3,5,10,12,18,24,30	3
0.9	0.9	48	8	1,5,9,12,17,19,24,27	4
0.4	0.8	55	7	3,5,10,12,18,23,27	3
0.5	0.8	62	7	1,5,10,12,18,23,27	3
0.6	0.8	60	7	3,5,10,12,19,23,27	3
0.7	0.8	47	7	3,5,10,12,18,23,27	3
0.8	0.8	52	7	3,5,10,12,18,24,29	3
0.9	0.8	11	7	3,5,10,12,19,24,29	3
0.4	0.7	59	7	1,7,10,12,18,24,30	3
0.5	0.7	57	7	1,5,10,12,19,23,27	3
0.6	0.7	55	7	1,7,10,12,18,24,30	3
0.7	0.7	28	7	1,7,10,12,18,24,30	3
0.8	0.7	32	7	1,7,10,12,18,24,29	3
0.9	0.7	32	7	1,7,10,12,18,23,27	3

TABLE 5.14 : CASE IV OPP OF IEEE 30-BUS TEST SYSTEM

<i>CR</i>	<i>F</i>	<i>NG</i>	<i>Best solution</i>		
			<i>N<sub>PMU</sub></i>	<i>Locations</i>	<i>ORI</i>
0.4	0.9	61	7	1,7,10,12,19,23,27	3
0.5	0.9	52		3,5,10,12,19,24,30	3
0.6	0.9	45		1,7,10,12,18,24,29	3
0.7	0.9	36		1,5,10,12,15,20,27	6
0.8	0.9	42		1,5,10,12,19,23,27	3
0.9	0.9	40		1,5,10,12,15,20,27	6
0.4	0.8	42		3,5,10,12,15,20,27	6
0.5	0.8	50		1,5,10,12,18,23,27	3
0.6	0.8	55		1,7,10,12,15,18,27	6
0.7	0.8	34		3,5,10,12,19,24,29	3
0.8	0.8	48		3,5,10,12,15,20,27	6
0.9	0.8	46		3,5,10,12,18,24,30	3
0.4	0.7	63		1,5,10,12,15,18,27	6
0.5	0.7	59		1,7,10,12,18,23,27	3
0.6	0.7	24		1,5,10,12,19,24,27	4
0.7	0.7	31		1,7,10,12,15,18,27	6
0.8	0.7	51		3,5,10,12,15,20,27	6
0.9	0.7	32		3,5,10,12,18,24,29	3

Figures 5.18 to 5.21 display DE algorithm convergence for Case-I to Case-IV respectively considering a scaling factor of 0.7 with different crossover constants  $CR$ . Although not a rule of thumb, we may generally state based on these figures that DE algorithm converges faster with higher crossover rates from 0.7 to 0.9.

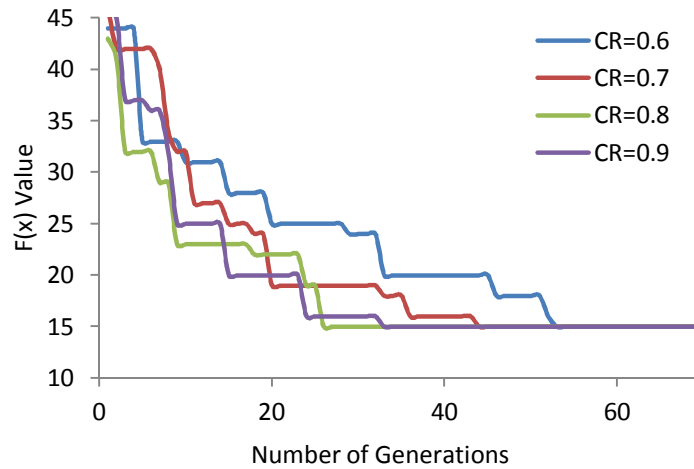


Figure 5.18: DEA Convergence for  $F=0.7$  and Different values of  $CR$  (IEEE 30-bus, Case-I)

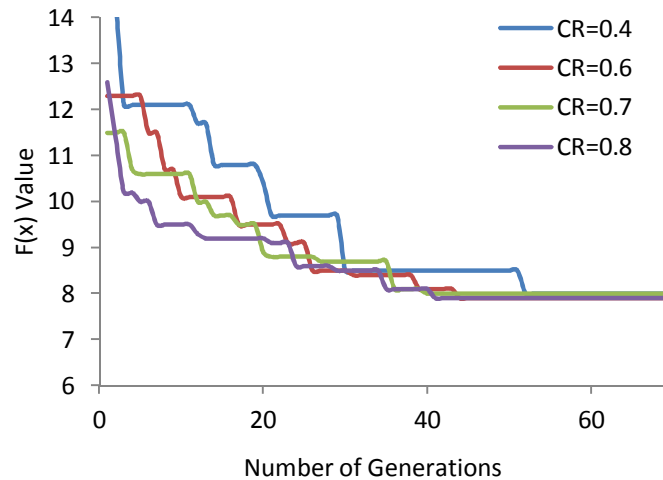


Figure 5.19: DEA Convergence for  $F=0.7$  and Different values of  $CR$  (IEEE 30-bus, Case-II)

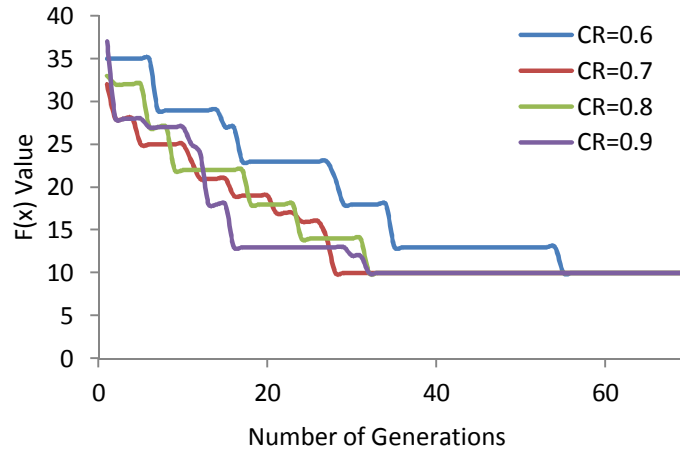


Figure 5.20: DEA Convergence for  $F=0.7$  and Different values of  $CR$  (IEEE 30-bus, Case-III)

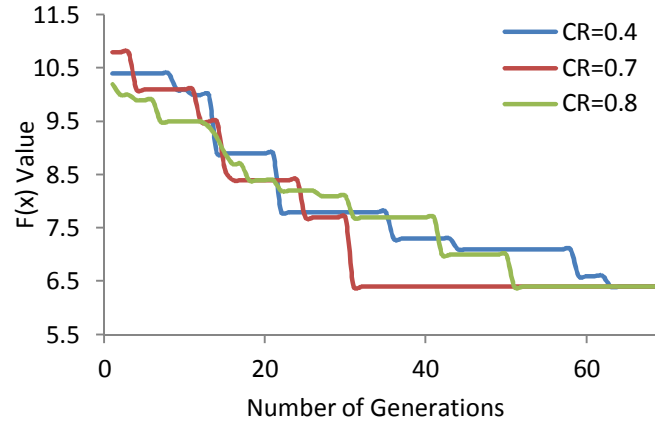


Figure 5.21: DEA Convergence for  $F=0.7$  and Different values of  $CR$  (IEEE 30-bus, Case-IV)

### 5.3.3 Application to IEEE 39-bus test system

Table 5.15 summarizes the simulation results of Case-I obtained for the IEEE 39-bus test system. Three different values of scaling factor  $F$ , namely 0.9, 0.8 and 0.7 are considered. For each value of  $F$ , the crossover constant  $CR$  is varied from 0.4 to 0.9 with an increment of 0.1. The population size is fixed throughout the search process and it is selected as 100 for Case-I & Case-II and 120 for Case-III & Case-IV. The table displays the number of generations required before DE algorithm convergence is reached  $NG$  for each combination of  $F$  and  $CR$ . A minimum of 27 and a maximum of 80 generations are

required by DE algorithm to converge depending on the selection of  $F$  and  $CR$  values. Simulation results reveal that the IEEE 39-bus test system can be observed completely by installing a minimum of 13 PMUs at different buses. For this case,  $ORI$  of the optimal solution ranges from 5 to 7. Table 5.16 summarizes the simulation results of Case-II obtained for this test system. Simulation results reveal that the IEEE 39-bus test system can be observed completely by installing a minimum of 13 PMUs at different buses. For this case,  $ORI$  of the optimal solution ranges from 9 to 13 as this case is meant to maximize the PMU measurement redundancy.

TABLE 5.15 : CASE I OPP OF IEEE 39-BUS TEST SYSTEM

$CR$	$F$	$NG$	<i>Best solution</i>		
			$N_{PMU}$	<i>Locations</i>	$ORI$
0.4	0.9	80	15	2,6,9,13,14,17,20,22,23,29,31,32,33,34,37	11
0.5	0.9	75	13	2,6,9,13,14,17,22,23,29,32,33,34,37	6
0.6	0.9	69	13	2,6,9,12,14,17,22,23,25,29,32,33,34	7
0.7	0.9	57	13	2,6,9,12,14,17,22,23,29,32,33,34,37	5
0.8	0.9	27	13	2,6,9,13,14,17,22,23,29,32,33,34,37	6
0.9	0.9	72	13	2,6,9,10,12,14,17,22,23,29,33,34,37	7
0.4	0.8	76	14	1,2,6,9,12,14,17,20,22,23,29,32,33,37	9
0.5	0.8	69	13	2,6,9,13,14,17,20,22,23,29,32,33,37	7
0.6	0.8	65	13	2,6,9,12,14,17,22,23,29,32,33,34,37	5
0.7	0.8	57	13	2,6,9,12,14,17,22,23,29,32,33,34,37	5
0.8	0.8	49	13	2,6,9,12,14,17,22,23,29,32,33,34,37	5
0.9	0.8	59	13	2,6,9,11,14,17,22,23,29,32,33,34,37	6
0.4	0.7	72	15	1,3,6,9,10,13,16,25,27,29,30,33,34,35,36	11
0.5	0.7	66	14	2,3,6,9,13,16,20,27,29,32,33,35,36,37	8
0.6	0.7	78	13	2,6,9,13,14,17,20,22,23,29,32,33,37	7
0.7	0.7	59	13	2,6,9,12,14,17,22,23,29,32,33,34,37	5
0.8	0.7	69	13	2,6,9,12,14,17,22,23,29,32,33,34,37	5
0.9	0.7	51	13	2,6,9,13,14,17,20,22,23,29,32,33,37	7



TABLE 5.16 : CASE II OPP OF IEEE 39-BUS TEST SYSTEM

<i>CR</i>	<i>F</i>	<i>NG</i>	<i>Best solution</i>		
			<i>N<sub>PMU</sub></i>	<i>Locations</i>	<i>ORI</i>
0.4	0.9	79	15	2,3,6,9,10,13,15,18,19,20,22,23,25,26,29	20
0.5	0.9	79	13	2,6,9,10,13,14,17,19,20,22,23,25,29	13
0.6	0.9	79	13	2,6,9,10,11,14,17,19,20,22,23,25,29	13
0.7	0.9	73	13	2,6,9,10,13,14,17,19,22,23,25,29,34	12
0.8	0.9	62	13	2,6,9,10,13,14,17,19,22,23,29,34,37	10
0.9	0.9	34	13	2,6,9,13,14,17,20,22,23,25,29,32,33	9
0.4	0.8	73	15	2,5,6,10,13,16,18,19,20,23,25,26,29,35,39	21
0.5	0.8	80	13	2,6,9,10,11,14,17,20,22,23,25,29,33	10
0.6	0.8	66	13	2,6,9,10,12,14,17,19,20,22,23,25,29	12
0.7	0.8	65	13	2,6,9,10,13,14,17,20,22,23,25,29,33	11
0.8	0.8	78	13	2,6,9,10,12,14,17,19,20,22,23,25,29	12
0.9	0.8	66	13	2,6,9,10,11,14,17,19,20,22,23,25,29	13
0.4	0.7	75	15	2,6,9,10,13,14,17,18,19,20,22,23,25,27,29	19
0.5	0.7	71	14	2,6,9,10,11,14,17,19,20,22,23,26,37,38	14
0.6	0.7	64	13	2,6,9,10,13,14,17,19,20,22,23,29,37	11
0.7	0.7	76	13	2,6,9,10,13,14,17,19,20,22,23,25,29	13
0.8	0.7	66	13	2,6,9,10,11,14,17,19,20,22,23,25,29	13
0.9	0.7	70	13	2,6,9,10,11,14,17,19,20,22,23,25,29	13

The IEEE 39-bus test system has a total of twelve zero injection buses given by  $ZI_{bus} = \{1,2,5,6,9,10,11,13,14,17,19,22\}$ . Table 5.17 and Table 5.18 summarize the test results for Case-III and Case-IV respectively. As expected, an optimal solution with less number of PMUs (8 for Case-III and IV instead of 13 for Case-I and II) is obtained when network observability rules are applied considering the zero-injection buses. For this system, *ORIs* of the best solution obtained in Case-III and Case-IV are equal to 4. Figures 5.22 to 5.25 display DE algorithm convergence for Case-I to Case-IV respectively considering a scaling factor of 0.7 with different crossover constants *CR*. Although not a rule of thumb, we may generally state based on these figures that DE algorithm converges faster with higher crossover rates from 0.7 to 0.9.

TABLE 5.17 : CASE III OPP OF IEEE 39-BUS TEST SYSTEM

<i>CR</i>	<i>F</i>	<i>NG</i>	<i>Best solution</i>		
			<i>N<sub>PMU</sub></i>	<i>Locations</i>	<i>ORI</i>
0.4	0.9	99	9	3,8,13,16,23,29,34,37,39	2
0.5	0.9	99	8	3,8,11,16,23,25,29,34	3
0.6	0.9	92	9	3,8,11,12,16,23,29,34,37	3
0.7	0.9	68	8	8,13,16,18,23,25,29,34	3
0.8	0.9	94	8	3,8,10,16,20,23,29,37	2
0.9	0.9	71	8	3,8,10,16,23,29,34,37	1
0.4	0.8	98	9	2,7,10,16,23,25,26,29,34	8
0.5	0.8	71	9	3,8,12,16,19,23,25,29,34	6
0.6	0.8	86	9	6,9,10,18,20,21,23,25,29	3
0.7	0.8	99	8	3,8,11,16,20,23,29,37	2
0.8	0.8	68	8	3,8,13,16,20,23,25,29	4
0.9	0.8	78	8	3,8,11,16,23,29,34,37	1
0.4	0.7	90	10	3,6,11,16,21,29,34,36,37,39	4
0.5	0.7	100	9	3,8,10,16,23,29,30,34,37	2
0.6	0.7	87	9	1,6,13,16,18,23,29,34,37	2
0.7	0.7	88	8	8,13,16,18,23,25,29,34	3
0.8	0.7	83	8	8,11,16,18,23,25,29,34	3
0.9	0.7	69	8	3,8,11,16,23,29,34,37	1

TABLE 5.18 : CASE IV OPP OF IEEE 39-BUS TEST SYSTEM

<i>CR</i>	<i>F</i>	<i>NG</i>	<i>Best solution</i>		
			<i>N<sub>PMU</sub></i>	<i>Locations</i>	<i>ORI</i>
0.4	0.9	98	9	4,8,12,16,23,25,26,34,38	5
0.5	0.9	95	9	8,10,13,16,18,20,23,25,29	6
0.6	0.9	85	9	1,6,10,16,18,20,23,25,29	6
0.7	0.9	87	9	8,13,15,16,18,20,23,25,29	7
0.8	0.9	98	8	3,8,13,16,20,23,25,29	4
0.9	0.9	80	8	3,8,10,16,20,23,25,29	4
0.4	0.8	96	10	2,7,13,16,20,23,25,26,29,32	10
0.5	0.8	93	9	2,3,6,10,16,20,23,25,29	8
0.6	0.8	99	9	3,8,11,16,20,22,23,25,29	7
0.7	0.8	83	8	8,13,16,18,20,23,25,29	4
0.8	0.8	98	8	3,8,12,16,20,23,25,29	4
0.9	0.8	67	8	3,8,11,16,20,23,25,29	4
0.4	0.7	98	10	2,4,8,11,17,20,21,23,29,37	5
0.5	0.7	96	9	3,8,12,20,21,23,25,26,29	7
0.6	0.7	81	9	3,8,12,16,23,25,26,29,34	7
0.7	0.7	84	8	8,11,16,18,20,23,25,29	4
0.8	0.7	96	8	3,8,11,16,20,23,25,29	4
0.9	0.7	80	8	3,8,13,16,20,23,25,29	4

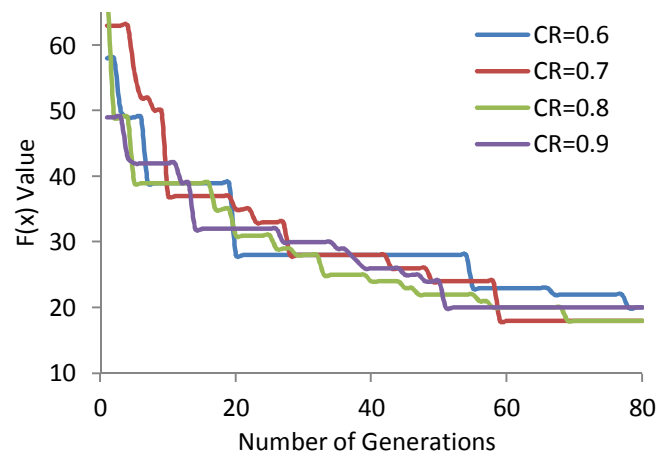


Figure 5.22: DEA Convergence for  $F=0.7$  and Different values of  $CR$  (IEEE 39-bus, Case-I)

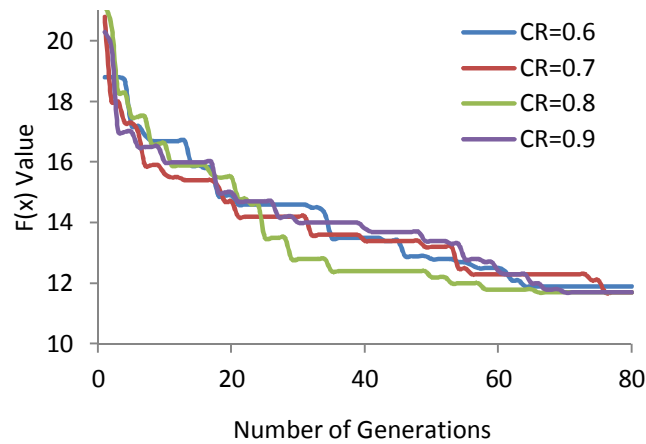


Figure 5.23: DEA Convergence for  $F=0.7$  and Different values of  $CR$  (IEEE 39-bus, Case-II)

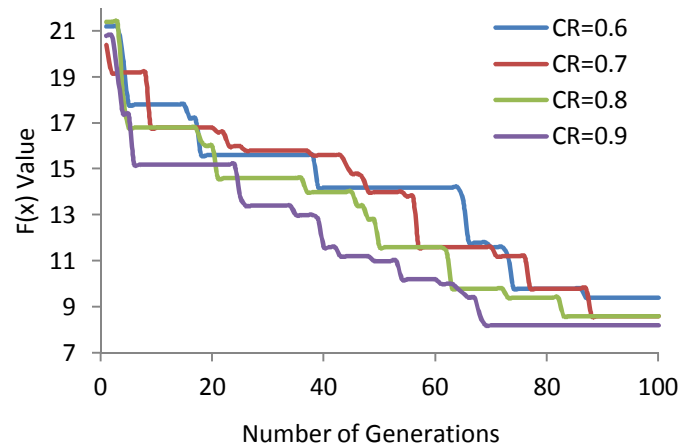


Figure 5.24: DEA Convergence for  $F=0.7$  and Different values of  $CR$  (IEEE 39-bus, Case-III)

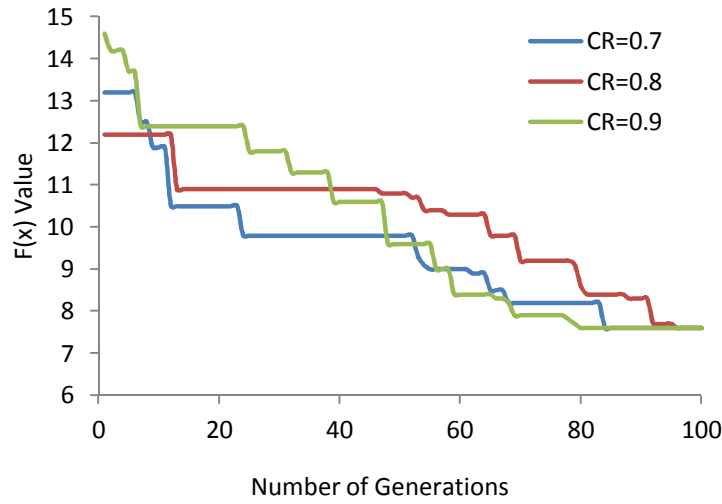


Figure 5.25: DEA Convergence for  $F=0.7$  and Different values of  $CR$  (IEEE 39-bus, Case-IV)

### 5.3.4 Application to IEEE 57-bus test system

Table 5.19 summarizes the simulation results of Case-I obtained for the IEEE 39-bus test system. The population size is fixed throughout the search process and it is selected as 170 for Case-I & Case-II and 190 for Case-III & Case-IV. A minimum of 114 and a maximum of 149 generations are required by DE algorithm to converge depending on the selection of  $F$  and  $CR$  values. Simulation results reveal that the IEEE 39-bus test system can be observed completely by installing a minimum of 17 PMUs at different buses. For this case,  $ORI$  of the optimal solution ranges from 6 to 8. Table 5.20 summarizes the simulation results of Case-II obtained for this test system. Simulation results reveal that the IEEE 39-bus test system can be observed completely by installing a minimum of 17 PMUs at different buses. For this case,  $ORI$  of the optimal solution ranges from 10 to 15 as this case is meant to maximize the PMU measurement redundancy.

TABLE 5.19 : CASE I OPP OF IEEE 57-BUS TEST SYSTEM

<i>CR</i>	<i>F</i>	<i>NG</i>	<i>Best solution</i>		
			<i>N<sub>PMU</sub></i>	<i>Locations</i>	<i>ORI</i>
0.4	0.9	139	18	1,4,8,13,20,22,25,27,32,33,36,39,41,44,47,51,52,55	10
0.5	0.9	149	19	2,6,12,19,22,26,29,30,33,34,35,37,43,45,46,49,50,54,56	11
0.6	0.9	129	18	1,4,8,10,20,23,25,26,29,32,36,37,43,44,46,49,54,56	11
0.7	0.9	145	17	1,4,8,13,20,23,25,26,29,32,36,41,44,47,51,54,57	8
0.8	0.9	114	17	2,6,12,14,19,22,25,27,32,36,39,41,44,48,50,52,55	6
0.9	0.9	120	17	1,4,7,13,20,22,25,27,32,36,39,41,44,47,51,52,55	8
0.4	0.8	141	19	1,4,7,9,18,20,23,25,27,32,36,39,41,45,46,48,50,53,55	14
0.5	0.8	139	18	1,4,8,13,20,22,25,27,32,33,36,39,41,44,47,51,52,55	10
0.6	0.8	129	18	1,4,8,10,20,23,25,26,29,32,36,37,43,44,46,49,54,56	11
0.7	0.8	145	17	1,4,8,13,20,23,25,26,29,32,36,41,44,47,51,54,57	8
0.8	0.8	114	17	2,6,12,14,19,22,25,27,32,36,39,41,44,48,50,52,55	6
0.9	0.8	120	17	1,4,7,13,20,22,25,27,32,36,39,41,44,47,51,52,55	8
0.4	0.7	117	19	1,4,6,12,20,24,25,28,29,32,36,38,39,42,43,45,46,51,54	16
0.5	0.7	137	19	1,4,7,14,17,20,23,27,30,33,35,36,39,41,44,48,51,53,55	9
0.6	0.7	142	18	2,4,7,12,14,20,23,25,27,32,36,41,44,47,50,52,54,57	8
0.7	0.7	118	18	1,4,9,19,22,25,27,29,32,34,37,43,44,46,47,50,53,56	11
0.8	0.7	114	17	2,6,12,14,19,22,25,27,32,36,39,41,44,48,50,52,55	6
0.9	0.7	120	17	1,4,7,13,20,22,25,27,32,36,39,41,44,47,51,52,55	8

TABLE 5.20 : CASE II OPP OF IEEE 57-BUS TEST SYSTEM

<i>CR</i>	<i>F</i>	<i>NG</i>	<i>Best solution</i>		
			<i>N<sub>PMU</sub></i>	<i>Locations</i>	<i>ORI</i>
0.4	0.9	147	19	2,6,11,12,15,18,21,24,28,29,30,32,36,42,44,47,50,54,57	14
0.5	0.9	150	18	1,4,9,11,14,20,23,25,27,29,32,36,39,41,45,48,50,54	14
0.6	0.9	142	17	1,6,7,9,15,19,22,25,27,32,36,38,39,41,46,50,53	14
0.7	0.9	127	17	1,6,9,15,19,22,25,27,29,32,36,38,41,47,51,53,57	14
0.8	0.9	125	17	1,4,7,9,13,19,22,25,27,32,36,39,41,45,47,51,53	12
0.9	0.9	107	17	1,4,9,15,20,23,27,29,30,32,36,38,41,47,51,54,57	13
0.4	0.8	148	19	1,4,9,10,13,15,20,24,27,29,31,32,36,38,39,41,47,49,53	27
0.5	0.8	148	17	1,6,9,15,18,21,24,28,31,32,36,38,41,47,50,53,57	13
0.6	0.8	144	17	2,6,12,15,19,22,25,26,29,32,36,38,39,41,46,50,54	11
0.7	0.8	145	17	1,4,6,9,15,20,24,28,31,32,36,38,41,47,51,53,57	15
0.8	0.8	106	17	1,4,7,9,19,22,25,27,32,36,38,39,41,45,46,50,53	11
0.9	0.8	101	17	1,4,9,20,23,26,29,30,32,36,38,39,41,44,46,50,54	10
0.4	0.7	147	19	2,6,11,12,15,18,21,24,28,29,30,32,36,42,44,47,50,54,57	14
0.5	0.7	150	18	1,4,9,11,14,20,23,25,27,29,32,36,39,41,45,48,50,54	14
0.6	0.7	137	18	1,4,9,11,19,22,26,29,30,32,36,38,39,42,44,46,50,54	14
0.7	0.7	147	17	1,6,7,9,15,19,22,25,27,32,36,41,45,47,50,53,57	11
0.8	0.7	103	17	1,6,9,15,18,20,24,28,30,32,36,38,41,47,51,53,57	13
0.9	0.7	129	17	1,4,9,15,20,24,25,26,29,32,36,38,39,41,46,51,54	14

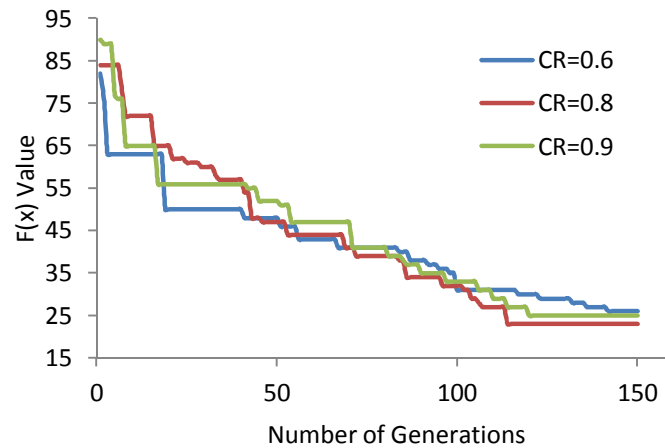
The IEEE 57-bus test system has a total of fifteen zero injection buses given by  $ZI_{bus} = \{4,7,11,21,22,24,26,34,36,37,39,40,45,46,48\}$ . Table 5.21 and Table 5.22 summarize the test results for Case-III and Case-IV respectively. As expected, an optimal solution with less number of PMUs (11 for Case-III and Case-IV instead of 17 for Case-I and II) is obtained when network observability rules are applied considering the zero-injection buses. For this system, *ORIs* of the best solution obtained in Case-III and Case-IV are equal to 3. Figures 5.26 to 5.29 display DE algorithm convergence for Case-I to Case-IV respectively considering a scaling factor of 0.7 with different crossover constants *CR*. Although not a rule of thumb, we may generally state based on these figures that DE algorithm converges faster with higher crossover rates from 0.7 to 0.9.

TABLE 5.21 : CASE III OPP OF IEEE 57-BUS TEST SYSTEM

<i>CR</i>	<i>F</i>	<i>NG</i>	<i>Best solution</i>		
			$N_{PM}$ <i>U</i>	<i>Locations</i>	<i>ORI</i>
0.4	0.9	193	16	1,3,8,12,19,27,30,32,37,41,44,46,50,52,55,57	20
0.5	0.9	194	14	3,4,14,16,17,19,25,29,32,35,38,41,51,54	7
0.6	0.9	189	13	1,9,15,18,22,25,29,31,33,47,50,53,56	6
0.7	0.9	179	12	1,6,13,19,25,27,32,38,51,52,55,56	3
0.8	0.9	138	12	1,6,9,19,27,30,33,44,47,50,53,56	1
0.9	0.9	132	11	1,6,13,19,25,29,32,38,51,54,56	3
0.4	0.8	199	14	3,5,12,15,20,25,29,32,36,41,48,49,51,54	10
0.5	0.8	186	13	1,6,13,19,27,30,33,38,44,51,53,55,56	6
0.6	0.8	200	12	1,6,9,14,19,25,28,32,38,50,53,56	4
0.7	0.8	184	12	1,5,13,16,19,25,29,32,38,42,51,54	5
0.8	0.8	169	12	1,6,10,19,25,29,32,38,41,46,50,54	3
0.9	0.8	159	12	1,4,10,20,25,29,32,38,41,46,50,54	2
0.4	0.7	199	14	3,5,12,15,20,25,29,32,36,41,48,49,51,54	10
0.5	0.7	188	13	1,3,9,18,21,25,29,32,38,47,50,54,56	7
0.6	0.7	185	13	1,4,9,19,27,29,30,33,38,46,50,54,56	4
0.7	0.7	177	12	1,6,9,19,25,28,32,38,46,50,53,56	2
0.8	0.7	169	12	1,6,10,19,25,29,32,38,41,46,50,54	3
0.9	0.7	159	12	1,4,10,20,25,29,32,38,41,46,50,54	2

TABLE 5.22 : CASE IV OPP OF IEEE 57-BUS TEST SYSTEM

$CR$	$F$	$NG$	<i>Best solution</i>		
			$N_{PMU}$	<i>Locations</i>	$ORI$
0.4	0.9	182	15	1,4,7,9,15,18,23,25,29,30,32,38,41,50,53	18
0.5	0.9	188	13	1,3,9,15,18,23,29,30,33,48,51,53,56	9
0.6	0.9	186	12	1,9,10,15,18,21,25,29,32,49,54,56	8
0.7	0.9	188	12	2,4,12,13,20,25,29,32,38,42,51,54	6
0.8	0.9	153	12	1,6,9,15,19,28,30,32,38,41,50,53	7
0.9	0.9	183	11	1,4,13,19,25,29,32,38,42,51,54	3
0.4	0.8	182	15	1,4,7,9,15,18,23,25,29,30,32,38,41,50,53	18
0.5	0.8	195	12	1,4,13,19,25,29,32,38,49,51,54,56	8
0.6	0.8	189	13	1,4,9,13,15,20,25,29,32,48,51,54,56	13
0.7	0.8	197	12	1,6,9,13,19,27,30,32,38,50,53,56	9
0.8	0.8	198	12	1,9,15,18,21,25,29,32,38,51,54,56	6
0.9	0.8	183	11	1,4,13,19,25,29,32,38,42,51,54	3
0.4	0.7	178	14	1,4,6,9,19,26,27,30,32,38,41,46,50,53	10
0.5	0.7	193	14	1,6,9,13,15,20,28,30,33,46,47,51,53,56	14
0.6	0.7	193	13	1,4,9,13,14,20,25,28,32,38,41,51,53	11
0.7	0.7	188	12	2,4,12,13,20,25,29,32,38,42,51,54	6
0.8	0.7	153	12	1,6,9,15,19,28,30,32,38,41,50,53	7
0.9	0.7	183	11	1,4,13,19,25,29,32,38,42,51,54	3

Figure 5.26: DEA Convergence for  $F=0.7$  and Different values of  $CR$  (IEEE 57-bus, Case-I)

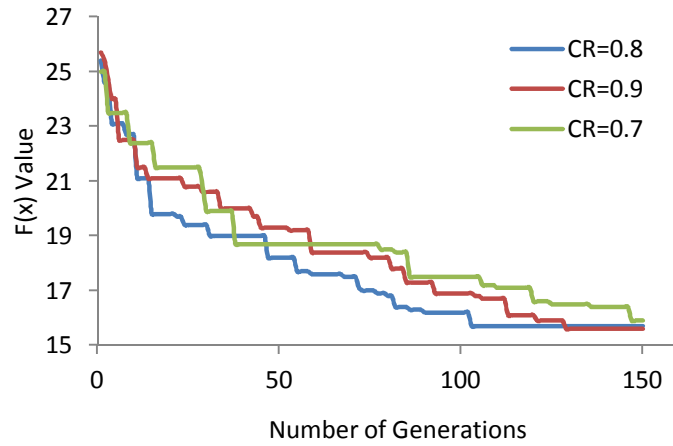


Figure 5.27: DEA Convergence for  $F=0.7$  and Different values of  $CR$  (IEEE 57-bus, Case-II)

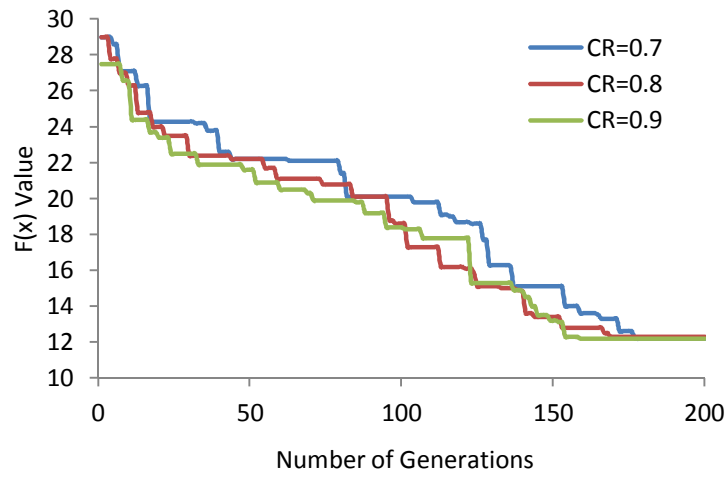


Figure 5.28: DEA Convergence for  $F=0.7$  and Different values of  $CR$  (IEEE 57-bus, Case-III)

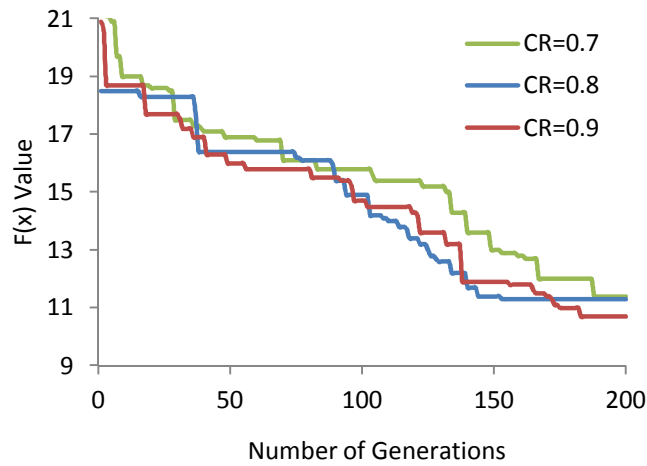


Figure 5.29: DEA Convergence for  $F=0.7$  and Different values of  $CR$  (IEEE 57-bus, Case-IV)



### 5.3.5 Comparison with other optimization techniques

To validate the results obtained using DE algorithm, a comparison is made with the published results obtained using other optimization techniques, namely B&B, BPSO, BSA, ILP, GA, Modified Binary Particle Swarm Optimization (MPSO) and Immunity Genetic Algorithm (IGA). Table 5.23 shows the superiority of the proposed DE algorithm when the zero-injection buses are considered.

5.23: NUMBER AND LOCATIONS OF PMUs FROM DE AND OTHER OPTIMIZATION ALGORITHMS  
(WITH CONSIDERATION OF ZI BUSES)

<i>Algorithm</i>		<i>14-Bus</i>	<i>30-Bus</i>	<i>39-Bus</i>	<i>57-Bus</i>
DE	No.	3	7	8	11
	Loc.	As per Table 5.10	As per Table 5.14	As per Table 5.18	As per Table 5.22
ILP [121, 128]	No.	3	--	--	14
	Loc.	2,6,9	--	--	1,4,9,20,24,25,28, 32,37,44,46,50,53,56
IGA [122]	No.	3	7	--	11
	Loc.	2,6,9	1,5,10,12,18,24,30	--	1,6,13,19,25,29, 32,38,51,54,56
ILP [126]	No.	3	7	--	11
	Loc.	Not Reported	Not Reported	--	Not Reported
B&B [129]	No.	--	7	9	12
	Loc.	--	3,5,10,12,19,24,27	3,9,12,16,23, 29,31,34,37	1,5,9,14,15,20, 25,28,32,50,53,56
BSA [133]	No.	3	7	8	--
	Loc.	2,6,9	1,2,10,12,15,19,27 1,2,10,12,15,20,27	3,8,10,16,20,23,25,29	--
				3,8,12,16,20,23,25,29	
				3,8,13,16,20,23,25,29	
				8,13,16,18,20,23,25,29	
ILP [140]	No.	3	7	8	11
	Loc.	2,6,9	3,5,10,12,18,24,27	3,8,11,16,20,23,25,29	1,4,13,20,25,29, 32,38,51,54,56
BPSO [141]	No.	3	--	8	--
	Loc.	2,6,9	--	3,8,13,16,23,29,34,37	--
				3,8,10,16,20,23,25,29	
MPSO [142, 153]	No.	3	7	--	11
	Loc.	2,6,9	2,3,10,12,18,24,27	--	1,5,13,19,25,29, 32,38,41,51,54
GA [152]	No.	3	7	--	--
	Loc.	2,6,9	Not Reported Correctly	--	--

## **5.4 Application to a 115 kV system from SEC transmission network**

An interconnected 115 kV system is selected from the Saudi Electricity Company (SEC) network. The system's base MVA and base voltage are considered as 100 MVA and 115 kV respectively. Figure 5.30 shows the one line diagram of this system. The system consists of 38 substations and 39, 115 kV transmission lines with an approximate total length of 500 kilometers. Out of the 38 substations, there are four (4) central substations called "Bulk Supply Point" or BSP numbered as bus-1, 17, 21 and 38. It shall be noted that these buses are fed directly from the existing generation power plants and are, therefore, considered as generation buses.

Each substation is treated as a 115 kV bus. The majority of the substations in this system are outdoor-type where the high side 115 kV equipment are installed in an open-to-sky switchyard, and thus designed to withstand severe environmental conditions, while the low side (34.5 kV or 13.8 kV) equipment are installed indoor, inside air-conditioned buildings. In this system, there are few substations that are indoor GIS-type, where GIS stands for Gas Insulated Switchgear. In these substations both the high and low side equipment (except for power transformers) are installed indoor.

The transmission lines in this system are all overhead with a maximum line length of about 35 kilometers. The old lines in this system were constructed using wooden monopoles while the new ones are constructed using steel monopoles. Porcelain and glass insulators were used in the majority of the lines, however, composite rubber-silicon insulators have replaced these two types of insulators in the newly constructed transmission lines.

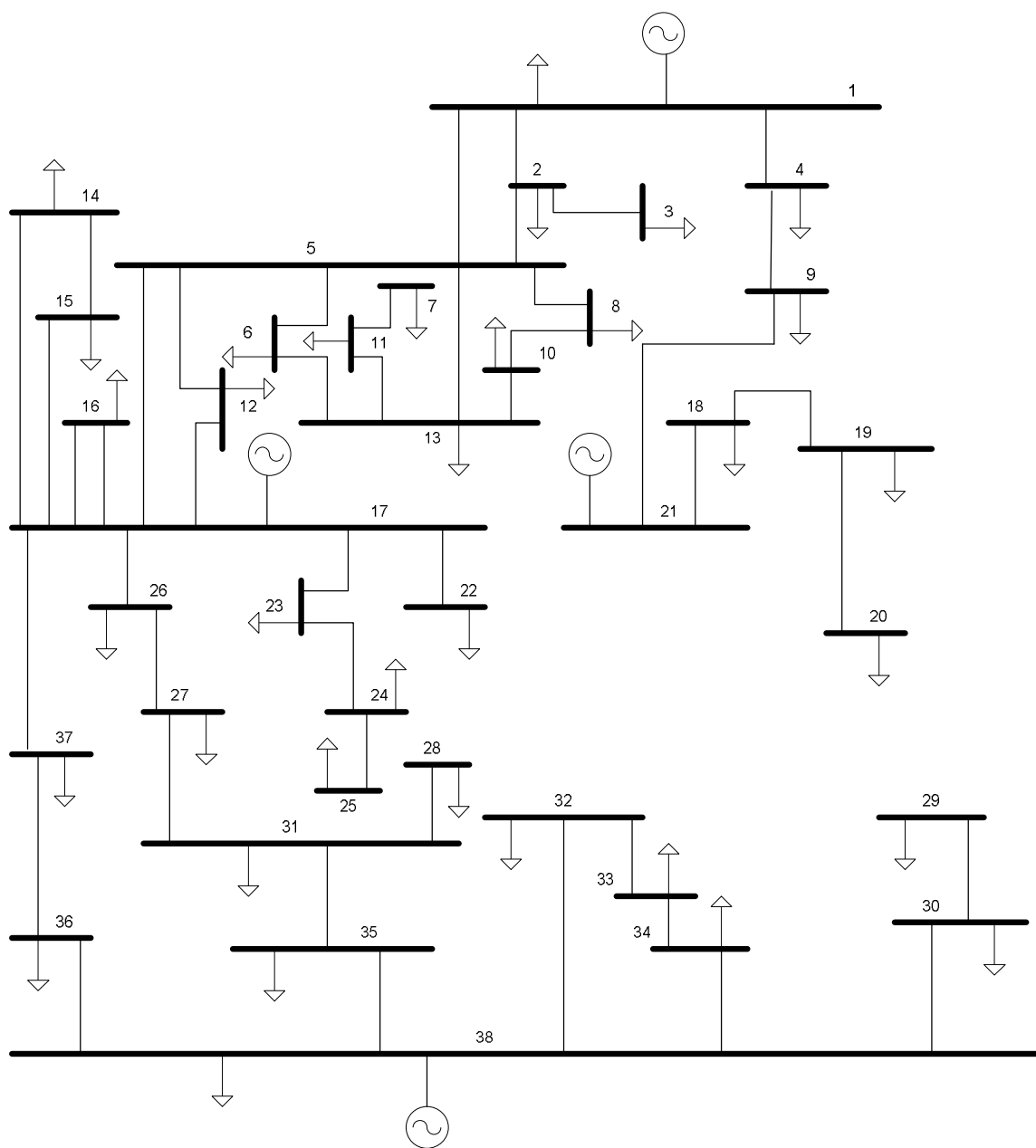


Figure 5.30: One line diagram of SEC 115 kV system

This system has only one zero-injection bus which is bus-5. Also, bus-23 is not equipped with any communication facility and it is, therefore, specified in the OPP problem formulation as a “don’t place” bus. Table 5.24 summarizes the simulation results obtained for Case-I. The population size is fixed throughout the search process and it is selected as 100 for Case-I & Case-II and 120 for Case-III & Case-IV. The table displays the number of generations required before DE algorithm convergence is reached  $NG$  for each combination of  $F$  and  $CR$ . A minimum of 46 and a maximum of 80 generations are required by DE algorithm to converge depending on the selection of  $F$  and  $CR$  values. Simulation results reveal that SEC 115 kV system can be observed completely by installing a minimum of 12 PMUs at different buses. For this case,  $ORI$  of the optimal solution ranges from 5 to 15. Table 5.25 summarizes the simulation results of Case-II with an optimal number of 12 PMUs as well. For this case,  $ORI$  of the optimal solution ranges from 12 to 17 as this case is meant to maximize the PMU measurement redundancy. Table 5.26 and Table 5.27 summarize the test results for Case-III and Case-IV respectively. As expected, an optimal solution with less number of PMUs (11 for Case-III and IV instead of 12 for Case-I and II) is obtained when network observability rules are applied considering the zero-injection buses. We may notice here that a reduction of only one PMU has been achieved since there is only one zero-injection bus. For this system,  $ORIs$  of the best solution obtained in Case-III and Case-IV are equal to 9 and 10 respectively. Figures 5.31 to 5.34 display DE algorithm convergence for Case-I to Case-IV considering a scaling factor of 0.7 with different crossover constants  $CR$ . Although not a rule of thumb, we may generally state based on these figures that DE algorithm converges faster with higher crossover rates from 0.7 to 0.9.

TABLE 5.24 : CASE I OPP OF SEC 115 kV SYSTEM

<i>CR</i>	<i>F</i>	<i>NG</i>	<i>Best solution</i>		
			<i>N<sub>PMU</sub></i>	<i>Locations</i>	<i>ORI</i>
0.4	0.9	46	13	1,3,5,7,13,17,19,21,25,29,31,33,36	13
0.5	0.9	72	12	2,6,7,9,10,17,19,24,29,31,33,38	8
0.6	0.9	52	12	2,10,11,12,14,18,20,25,31,32,33,38	12
0.7	0.9	50	12	3,5,9,10,11,17,19,24,30,31,33,38	13
0.8	0.9	51	12	2,5,7,9,10,17,19,24,30,31,33,36	11
0.9	0.9	51	12	2,6,8,9,11,17,19,25,30,31,32,38	9
0.4	0.8	70	13	1,3,5,8,11,17,20,21,24,29,31,33,38	15
0.5	0.8	80	12	2,5,7,9,13,17,19,25,30,31,33,37	12
0.6	0.8	70	12	2,9,10,11,13,17,19,25,30,31,33,36	8
0.7	0.8	63	12	2,7,8,9,13,17,19,25,30,31,33,36	7
0.8	0.8	64	12	3,5,8,9,11,17,19,24,29,31,32,38	12
0.9	0.8	46	12	2,5,8,9,11,17,19,24,30,31,32,38	15
0.4	0.7	70	13	2,5,7,9,13,17,19,23,25,30,31,33,38	18
0.5	0.7	61	12	3,5,9,10,11,17,19,24,29,31,33,36	9
0.6	0.7	62	12	2,5,9,10,11,17,19,25,30,31,33,36	11
0.7	0.7	57	12	2,6,7,8,9,17,19,24,29,31,33,36	5
0.8	0.7	62	12	2,6,7,8,9,17,19,24,30,31,33,36	6
0.9	0.7	46	12	2,5,9,11,13,17,19,25,29,31,33,36	12

TABLE 5.25 : CASE II OPP OF SEC 115 kV SYSTEM

<i>CR</i>	<i>F</i>	<i>NG</i>	<i>Best solution</i>		
			<i>N<sub>PMU</sub></i>	<i>Locations</i>	<i>ORI</i>
0.4	0.9	68	13	2,5,9,10,11,17,20,21,24,30,31,32,38	17
0.5	0.9	79	13	3,5,9,11,13,15,17,19,25,30,31,32,38	17
0.6	0.9	73	12	3,5,8,9,11,17,19,24,29,31,33,38	12
0.7	0.9	71	12	2,5,9,10,11,17,19,24,30,31,34,38	15
0.8	0.9	68	12	2,5,8,9,11,17,19,24,30,31,32,38	15
0.9	0.9	56	12	2,5,9,11,13,17,19,24,30,31,34,38	17
0.4	0.8	75	12	2,5,8,9,11,17,19,24,30,31,33,36	12
0.5	0.8	74	12	2,5,9,11,13,17,19,25,29,31,32,38	15
0.6	0.8	80	12	2,5,8,9,11,17,19,25,30,31,33,38	14
0.7	0.8	70	12	3,5,9,10,11,17,19,24,30,31,32,38	13
0.8	0.8	71	12	2,5,9,10,11,17,19,25,30,31,33,36	11
0.9	0.8	73	12	2,5,9,10,11,17,19,24,30,31,33,38	15
0.4	0.7	66	13	2,4,5,7,8,17,20,21,25,30,31,33,37	12
0.5	0.7	75	12	2,6,7,9,10,17,19,24,30,31,34,38	9
0.6	0.7	77	12	2,5,9,11,13,17,19,25,30,31,32,38	16
0.7	0.7	80	12	2,5,9,11,13,17,19,24,30,31,33,38	17
0.8	0.7	55	12	2,5,9,11,13,17,19,24,30,31,33,36	14
0.9	0.7	78	12	2,5,9,11,13,17,19,24,29,31,34,38	16

TABLE 5.26 : CASE III OPP OF SEC 115 kV SYSTEM

<i>CR</i>	<i>F</i>	<i>NG</i>	<i>Best solution</i>		
			<i>N<sub>PMU</sub></i>	<i>Locations</i>	<i>ORI</i>
0.4	0.9	100	11	2,8,9,11,17,19,25,29,31,34,38	5
0.5	0.9	68	11	2,8,9,11,17,19,24,29,31,32,38	7
0.6	0.9	73	11	2,9,10,11,17,19,25,30,31,32,38	7
0.7	0.9	70	11	2,8,9,11,17,19,25,29,31,34,38	6
0.8	0.9	81	11	2,7,9,10,17,19,25,30,31,33,38	6
0.9	0.9	64	11	2,7,9,13,17,19,24,29,31,33,38	8
0.4	0.8	65	12	1,3,8,11,17,20,21,24,30,31,33,36	6
0.5	0.8	78	11	2,9,11,13,17,19,25,29,31,33,36	5
0.6	0.8	100	11	2,7,9,13,17,19,25,29,31,32,38	7
0.7	0.8	73	11	2,7,9,10,17,19,24,30,31,33,36	4
0.8	0.8	75	11	2,9,11,13,17,19,24,29,31,34,38	9
0.9	0.8	45	11	2,7,9,10,17,19,24,30,31,34,38	7
0.4	0.7	98	11	2,9,10,11,17,19,25,29,31,33,36	3
0.5	0.7	85	11	2,9,10,11,17,19,24,29,31,32,38	7
0.6	0.7	72	11	2,9,11,13,17,19,24,29,31,34,38	9
0.7	0.7	66	11	2,9,10,11,17,19,24,29,31,33,36	4
0.8	0.7	72	11	2,8,9,11,17,19,25,30,31,33,36	4
0.9	0.7	76	11	2,9,11,13,17,19,25,30,31,33,37	6

TABLE 5.27 : CASE IV OPP OF SEC 115 kV SYSTEM

<i>CR</i>	<i>F</i>	<i>NG</i>	<i>Best solution</i>		
			<i>N<sub>PMU</sub></i>	<i>Locations</i>	<i>ORI</i>
0.4	0.9	100	11	2,7,9,13,17,19,25,29,31,33,38	7
0.5	0.9	98	11	2,9,11,13,17,19,24,30,31,32,38	10
0.6	0.9	97	11	2,7,9,13,17,19,25,30,31,32,38	8
0.7	0.9	100	11	2,7,9,13,17,19,24,30,31,33,38	9
0.8	0.9	72	11	2,9,10,11,17,19,24,30,31,34,38	8
0.9	0.9	60	11	2,9,11,13,17,19,24,30,31,32,38	10
0.4	0.8	99	12	2,5,8,9,11,17,19,24,29,31,32,38	14
0.5	0.8	86	11	2,9,11,13,17,19,24,29,31,32,38	9
0.6	0.8	83	11	2,7,9,13,17,19,24,30,31,34,38	9
0.7	0.8	88	11	2,9,11,13,17,19,24,30,31,32,38	10
0.8	0.8	61	11	2,9,11,13,17,19,24,30,31,32,38	10
0.9	0.8	50	11	2,9,11,13,17,19,24,30,31,34,38	10
0.4	0.7	95	12	2,9,11,13,17,19,21,24,30,31,33,38	13
0.5	0.7	96	11	2,9,11,13,17,19,24,30,31,33,38	10
0.6	0.7	99	11	2,9,11,13,17,19,24,30,31,34,38	10
0.7	0.7	73	11	2,9,11,13,17,19,24,30,31,34,38	10
0.8	0.7	71	11	2,9,11,13,17,19,24,30,31,34,38	10
0.9	0.7	69	11	2,9,11,13,17,19,24,30,31,34,38	10

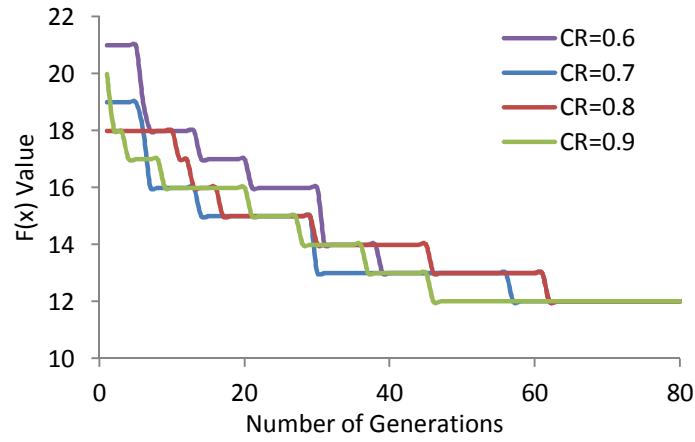


Figure 5.31: DEA Convergence for  $F=0.7$  and Different values of  $CR$  (SEC system, Case-I)

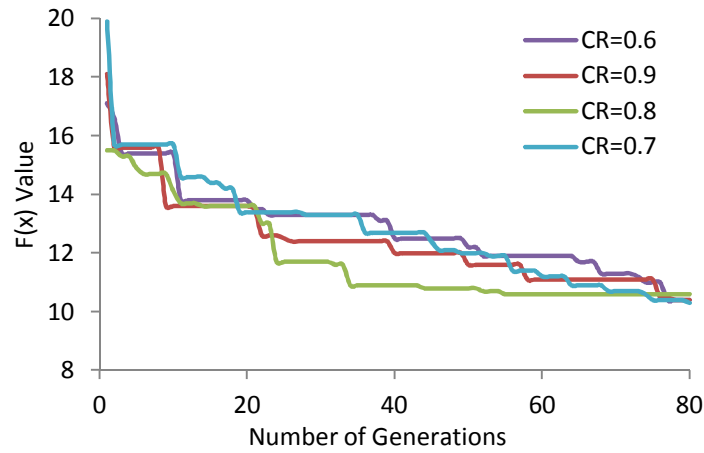


Figure 5.32: DEA Convergence for  $F=0.7$  and Different values of  $CR$  (SEC system, Case-II)

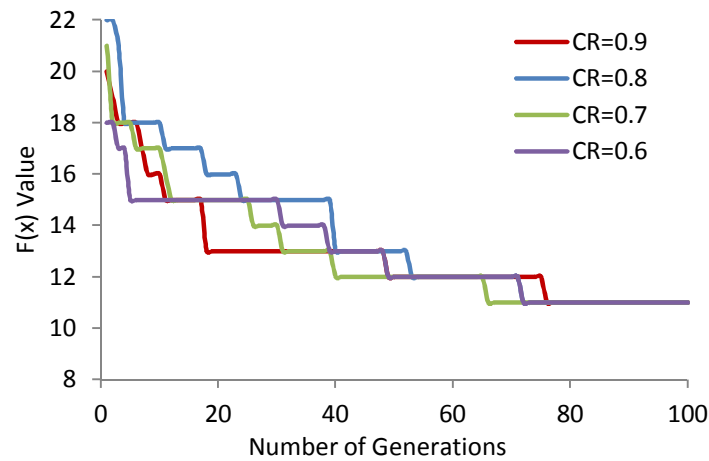


Figure 5.33: DEA Convergence for  $F=0.7$  and Different values of  $CR$  (SEC system, Case-III)

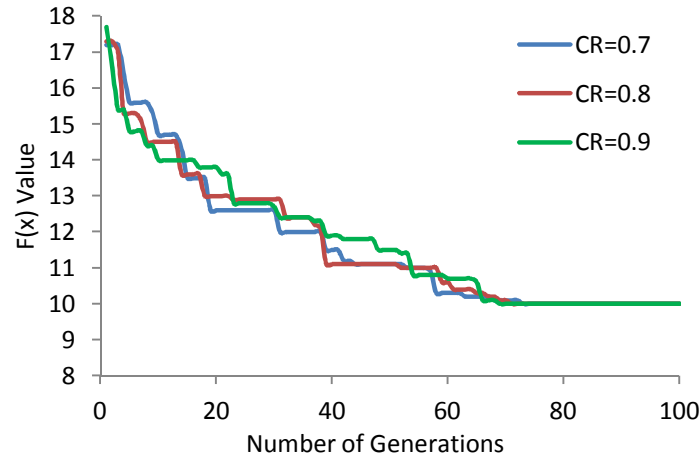


Figure 5.34: DEA Convergence for  $F=0.7$  and Different values of  $CR$  (SEC system, Case-IV)

## 5.5 Reducing DE search space

The trend in recent years is the steady increase of PMU installations worldwide for various power system applications. Different algorithms used to solve OPP problem perform an optimization process by considering all system buses. In real systems, however, some buses may be selected for mandatory PMU installations and some others can be selected as not desirable for PMU installations considering different practical reasons. In other words, a group of buses may be identified beforehand for the optimal placement. By identifying those buses with “known status”, the computational efforts associated with solving OPP problem could be significantly reduced. [154]

For system study and modeling purposes, the system models used by the electric utilities typically include virtual buses which either do not exist physically or are not practical locations to install PMUs. Examples of such virtual buses include tapped line buses and series capacitor nodes. If these virtual buses are included in the system model of the placement study, it is quite possible that some PMUs will be assigned to these



nonexistent and non-practical virtual buses. Therefore, methods to exclude these buses shall be incorporated in the placement process. In addition, the existence of large numbers of virtual buses increases the scale of the system and the dimension of optimization problem and, hence, it is necessary to eliminate the virtual buses before searching an optimal solution of the OPP problem. [154]

This section aims at providing some hints that help in reducing the search space and achieving high-quality solutions to OPP problem. It first starts by highlighting some virtual buses reduction rules that can be applied to reduce the dimension of the optimization problem prior to implementing a certain optimization method. Three different cases are then discussed to help make proper decisions on the buses that may be selected in the set of “must place” or “don’t place” buses to reduce the search space of the optimization problem.

### **5.5.1 Virtual buses reduction rules**

M. Zhou et al. introduce in [154] a preprocessing methodology to reduce the scale of a PMU placement study beforehand, so as to significantly reduce the computation effort. The reduction of system size is both beneficial and necessary especially for a large power system. Different rules applied in virtual bus reduction depend upon the type of virtual bus. In the PMU placement study presented in [154], virtual buses were categorized into five different types with the assumption that all local physical line currents are monitored by any PMU placed in the system. The categories and the corresponding bus reduction rules applied to each type are listed hereunder:

1. Tapped lines create a bus in the middle of a branch where there are no physical measurement facilities to monitor the signals at the tap. For a virtual bus at a

tapped line, the bus created by the tapped line and the branches connecting the tap point to the system are removed and equivalent injection is added to the adjoining buses.

2. Some power system generators may be grouped together to present an equivalent generator connected to the system by a virtual bus. Virtual buses connecting equivalent generators are removed and replaced by an equivalent injection on the actual bus.
3. For the convenience of analysis, a shunt circuit is modeled with its own virtual bus which physically is the same as the connecting bus. If a virtual bus connects to a shunt, the virtual bus and the shunt element are removed and replaced by a corresponding injection.
4. Series capacitors are modeled with a virtual bus which physically does not exist. If a virtual bus connects to a series capacitor (regardless of the capacitor line location) the bus and the two connecting branches are removed and replaced by an equivalent branch.
5. Three winding transformers are modeled as three 2-winding transformers with one side in common. In per unit, the three buses represent the same voltage and if needed could be monitored by a single PMU. If a virtual bus is the middle point of 3 winding transformers, the corresponding three winding transformer is replaced by a single bus. This bus is connected to the buses originally connecting the middle and high voltage windings.

Optimization results from the studies on the reduced system, obtained after applying aforesaid rules, will be practical and no PMU will be placed on virtual buses. The

observability of the reduced system also ensures the observability of the original system since virtual buses reduction only reduces the scale of optimization problem under study, but keeps the valid system topology intact.

### 5.5.2 Base case

Prior to studying the effect of various design-related decisions one might make while developing a DE-based algorithm to solve OPP problem, we first consider a base case to serve as a reference against which the algorithm's performance is checked when a particular decision is adopted. Simulation results given in Tables 5.10, 5.14, 5.18 and 5.22 are considered to be the base case for OPP problem pertaining to IEEE 14-, 30-, 39- and 57-bus systems respectively. In the base case, topological observability rules considering the zero-injection buses are taken into account and the algorithm design considers dual objectives to minimize the number of PMUs to have the system completely observable and, at the same time, maximize the PMU measurement redundancy. The DE algorithm for the base case is designed with a real constant positive scaling factor which assumes a fixed value (0.7, 0.8 or 0.9) throughout the search process and the crossover constant is selected to vary from 0.4 to 0.9 with an increment of 0.1. The DE algorithm's mutation scheme is designed according to (5.1) where three independent vectors are used in generating a new candidate child vector. As highlighted earlier, the population size is kept constant and selected as 50, 60, 120 and 190 for IEEE 14-, 30-, 39- and 57-bus systems respectively. The DE algorithm is designed to stop after a certain number of generations and this design parameter is selected as 40, 70, 100 and 200 for IEEE 14-, 30-, 39- and 57-bus systems respectively. For this case, no buses are selected to be either in the set of "must place" or in the set of "don't place" buses.

### 5.5.3 Selection of “don’t place” buses (Case I and II)

For Case I, we simulate the IEEE systems keeping the same design parameters of the base case but we introduce one change only by selecting the zero-injection buses of each system to be in the set of “don’t place” buses. The idea behind avoiding PMU placement at the zero-injection buses is to limit the search space. Simulation results for this case are shown in Tables 5.28-5.31. Comparing the simulation results for this case to those presented earlier for the base case, one may note the following:

1. For the IEEE 14-bus system, the same optimal solution is obtained where the system can be fully observed by installing 3 PMUs at buses 2, 6 and 9. However, the DE algorithm converges faster for this case. The average number of generations for this case to converge is 5.39 compared to 21.11 for the base case.
2. For the IEEE 30-bus system, a better optimal solution has been obtained for this case in comparison with the base case. The optimal number of PMUs equals 7 as in the base case but with a best *ORI* value of 8 compared to a best *ORI* value of 6 in the base case. The average cost of optimal solutions obtained here is 6.37 compared to 6.55 for the base case. Also, the DE algorithm converges faster. The average number of generations for the algorithm to converge is 40.28 compared to 45.05 for the base case.
3. For the IEEE 39-bus system, the optimal solution of 8 PMUs and an *ORI* value of 4 has been obtained for all combinations of *CR* and *F* while it was obtained only for some combinations of *CR* and *F* in the base case. The average cost of optimal solutions obtained here is 7.60 compared to 8.11 for the base case. Also, the DE

algorithm converges faster. The average number of generations for the algorithm to converge is 55.72 compared to 89.67 for the base case.

4. For the IEEE 57-bus system, the optimal solution of 11 PMUs has been obtained for all combinations of  $CR$  and  $F$  while it was obtained only for some combinations of  $CR$  and  $F$  in the base case. Moreover, with this number of PMUs the best  $ORI$  value increased to 4 compared to a best  $ORI$  value of 3 in the base case. The average cost of optimal solutions obtained here is 10.63 compared to 11.67 for the base case. Also, the DE algorithm converges faster. The average number of generations for the algorithm to converge is 131.05 compared to 184 for the base case.

TABLE 5.28: IEEE 14-BUS SYSTEM - CASE-I

$CR$	$F$	$NP$	$NG$	<i>Best solution</i>		
				$N_{PMU}$	<i>Locations</i>	$ORI$
0.4	0.9	50	14	3	2,6,9	2
0.5	0.9		12			
0.6	0.9		6			
0.7	0.9		4			
0.8	0.9		5			
0.9	0.9		6			
0.4	0.8		8			
0.5	0.8		4			
0.6	0.8		3			
0.7	0.8		2			
0.8	0.8		3			
0.9	0.8		2			
0.4	0.7		2			
0.5	0.7		6			
0.6	0.7		4			
0.7	0.7		5			
0.8	0.7		6			
0.9	0.7		5			

TABLE 5.29: IEEE 30-BUS SYSTEM - CASE-I

<i>CR</i>	<i>F</i>	<i>NP</i>	<i>NG</i>	<i>Best solution</i>		
				<i>N<sub>PMU</sub></i>	<i>Locations</i>	<i>ORI</i>
0.4	0.9	60	58	7	1,2,10,12,18,24,30	6
0.5	0.9		51		3,7,10,12,18,24,29	4
0.6	0.9		37		3,7,10,12,19,24,29	4
0.7	0.9		28		1,2,10,12,18,24,30	6
0.8	0.9		36		1,7,10,12,19,24,30	3
0.9	0.9		32		2,4,10,12,18,24,30	8
0.4	0.8		63		2,4,10,12,19,24,29	8
0.5	0.8		42		1,2,10,12,18,24,29	6
0.6	0.8		30		1,2,10,12,18,24,30	6
0.7	0.8		40		2,3,10,12,19,24,29	6
0.8	0.8		35		1,2,10,12,18,24,29	6
0.9	0.8		40		2,3,10,12,19,24,29	6
0.4	0.7		55		2,4,10,12,18,24,29	8
0.5	0.7		31		2,4,10,12,18,24,29	8
0.6	0.7		50		2,4,10,12,18,24,30	8
0.7	0.7		30		1,2,10,12,19,24,30	6
0.8	0.7		40		2,3,10,12,19,24,30	6
0.9	0.7		27		2,4,10,12,19,24,30	8

TABLE 5.30: IEEE 39-BUS SYSTEM - CASE-I

<i>CR</i>	<i>F</i>	<i>NP</i>	<i>NG</i>	<i>Best solution</i>		
				<i>N<sub>PMU</sub></i>	<i>Locations</i>	<i>ORI</i>
0.4	0.9	120	92	8	3,8,12,16,20,23,25,29	4
0.5	0.9		65			
0.6	0.9		64			
0.7	0.9		60			
0.8	0.9		48			
0.9	0.9		42			
0.4	0.8		68			
0.5	0.8		60			
0.6	0.8		57			
0.7	0.8		46			
0.8	0.8		44			
0.9	0.8		43			
0.4	0.7		66			
0.5	0.7		56			
0.6	0.7		52			
0.7	0.7		61			
0.8	0.7		39			
0.9	0.7		40			

TABLE 5.31: IEEE 57-BUS SYSTEM - CASE-I

<i>CR</i>	<i>F</i>	<i>NP</i>	<i>NG</i>	<i>Best solution</i>		
				<i>N<sub>PMU</sub></i>	<i>Locations</i>	<i>ORI</i>
0.4	0.9	190	163	11	1,6,13,19,25,29,32,38,41,51,54	4
0.5	0.9		151		1,6,13,19,25,29,32,38,41,51,54	4
0.6	0.9		174		1,6,13,19,25,29,32,38,41,51,54	4
0.7	0.9		127		1,6,13,19,25,29,32,38,41,51,54	4
0.8	0.9		97		1,6,13,19,25,29,32,38,41,51,54	4
0.9	0.9		107		1,6,13,19,25,29,32,38,42,51,54	3
0.4	0.8		194		1,6,13,19,25,29,32,38,51,54,56	3
0.5	0.8		151		1,6,13,19,25,29,32,38,41,51,54	4
0.6	0.8		106		1,6,13,19,25,29,32,38,41,51,54	4
0.7	0.8		115		1,6,13,19,25,29,32,38,41,51,54	4
0.8	0.8		97		1,6,13,19,25,29,32,38,41,51,54	4
0.9	0.8		107		1,6,13,19,25,29,32,38,42,51,54	3
0.4	0.7		194		1,6,13,19,25,29,32,38,51,54,56	3
0.5	0.7		151		1,6,13,19,25,29,32,38,41,51,54	4
0.6	0.7		106		1,6,13,19,25,29,32,38,41,51,54	4
0.7	0.7		115		1,6,13,19,25,29,32,38,41,51,54	4
0.8	0.7		97		1,6,13,19,25,29,32,38,41,51,54	4
0.9	0.7		107		1,6,13,19,25,29,32,38,42,51,54	3

Based on the above, we may conclude that designing a DE-based algorithm to solve the OPP problem with a constraint to avoid PMU installation at the zero-injection buses not only helps produce an optimal solution of a higher quality but also leads to a faster convergence of the algorithm.

To reduce the search space further, we simulate in Case II the IEEE systems keeping the same design parameters of the base case but we introduce one change by selecting the zero-injection buses and buses that have only one incident line of each system to be in the set of “don’t place” buses. Simulation results for this case are shown in Tables 5.32-5.35. Comparing the simulation results for this case to those presented earlier for the base case, one may note the following:

1. For the IEEE 14-bus system, the same optimal solution is obtained where the system can be fully observed by installing 3 PMUs at buses 2, 6 and 9. However, the DE algorithm converges faster for this case. The average number of generations for this case to converge is 5.28 compared to 21.11 for the base case.
2. For the IEEE 30-bus system, a better optimal solution has been obtained for this case in comparison with the base case. The optimal number of PMUs equals 7 as in the base case but with a best *ORI* value of 8 compared to a best *ORI* value of 6 in the base case. The average cost of optimal solutions obtained here is 6.33 compared to 6.55 for the base case. Also, the DE algorithm converges faster. The average number of generations for the algorithm to converge is 30.89 compared to 45.05 for the base case.
3. For the IEEE 39-bus system, the optimal solution of 8 PMUs and an *ORI* value of 4 has been obtained for all combinations of *CR* and *F* while it was obtained only for some combinations of *CR* and *F* in the base case. The average cost of optimal solutions obtained here is 7.60 compared to 8.11 for the base case. Also, the DE algorithm converges faster. The average number of generations for the algorithm to converge is 23.11 compared to 89.67 for the base case.
4. For the IEEE 57-bus system, the optimal solution of 11 PMUs has been obtained for 13 out of 18 combinations of *CR* and *F* while it was obtained only for 3 combinations of *CR* and *F* in the base case. Furthermore, with this number of PMUs the best *ORI* value increased to 4 compared to a best *ORI* value of 3 in the base case. The average cost of optimal solutions obtained here is 10.75 compared to 11.67 for the base case. Also, the DE algorithm converges faster. The average



number of generations for the algorithm to converge is 145.89 compared to 184 for the base case.

In light of the above, we may conclude that designing a DE-based algorithm to solve the OPP problem with a constraint to avoid PMU installation at the zero-injection buses and buses that have only one incident line helps produce an optimal solution of a higher quality and leads to a faster convergence of the algorithm. Comparing the calculated average number of generations to reach algorithm's convergence in each system for this case to those calculated for Case-I, one can easily find that this case converged faster for the IEEE 14-, 30- and 39-bus system. Case-I, however, converged faster for the IEEE 57-bus system.

TABLE 5.32: IEEE 14-BUS SYSTEM - CASE-II

<i>CR</i>	<i>F</i>	<i>NP</i>	<i>NG</i>	<i>Best solution</i>		
				<i>N<sub>PMU</sub></i>	<i>Locations</i>	<i>ORI</i>
0.4	0.9	50	8	3	2,6,9	2
0.5	0.9		5			
0.6	0.9		5			
0.7	0.9		5			
0.8	0.9		4			
0.9	0.9		3			
0.4	0.8		6			
0.5	0.8		7			
0.6	0.8		6			
0.7	0.8		4			
0.8	0.8		3			
0.9	0.8		5			
0.4	0.7		11			
0.5	0.7		6			
0.6	0.7		4			
0.7	0.7		4			
0.8	0.7		5			
0.9	0.7		4			

TABLE 5.33: IEEE 30-BUS SYSTEM - CASE-II

<i>CR</i>	<i>F</i>	<i>NP</i>	<i>NG</i>	<i>Best solution</i>		
				<i>N<sub>PMU</sub></i>	<i>Locations</i>	<i>ORI</i>
0.4	0.9	60	39	7	2,4,10,12,18,24,29	8
0.5	0.9		41		3,7,10,12,19,24,29	4
0.6	0.9		29		1,2,10,12,18,24,30	6
0.7	0.9		35		2,4,10,12,18,24,29	8
0.8	0.9		22		1,5,10,12,19,24,29	3
0.9	0.9		28		2,3,10,12,18,24,29	6
0.4	0.8		31		2,3,10,12,19,24,30	6
0.5	0.8		35		2,4,10,12,18,24,29	8
0.6	0.8		38		2,4,10,12,18,24,29	8
0.7	0.8		35		3,7,10,12,19,24,30	4
0.8	0.8		28		2,3,10,12,18,24,30	6
0.9	0.8		16		2,3,10,12,18,24,29	6
0.4	0.7		61		2,4,10,12,18,24,30	8
0.5	0.7		14		2,4,10,12,19,24,30	8
0.6	0.7		30		1,2,10,12,19,24,29	6
0.7	0.7		17		2,4,10,12,19,24,29	8
0.8	0.7		27		2,4,10,12,19,24,29	8
0.9	0.7		30		2,4,10,12,18,24,29	8

TABLE 5.34: IEEE 39-BUS SYSTEM - CASE-II

<i>CR</i>	<i>F</i>	<i>NP</i>	<i>NG</i>	<i>Best solution</i>		
				<i>N<sub>PMU</sub></i>	<i>Locations</i>	<i>ORI</i>
0.4	0.9	120	55	8	3,8,12,16,20,23,25,29	4
0.5	0.9		32			
0.6	0.9		18			
0.7	0.9		16			
0.8	0.9		12			
0.9	0.9		13			
0.4	0.8		34			
0.5	0.8		33			
0.6	0.8		29			
0.7	0.8		17			
0.8	0.8		13			
0.9	0.8		16			
0.4	0.7		29			
0.5	0.7		24			
0.6	0.7		22			
0.7	0.7		17			
0.8	0.7		20			
0.9	0.7		16			

TABLE 5.35: IEEE 57-BUS SYSTEM - CASE-II

<i>CR</i>	<i>F</i>	<i>NP</i>	<i>NG</i>	<i>Best solution</i>		
				<i>N<sub>PMU</sub></i>	<i>Locations</i>	<i>ORI</i>
0.4	0.9	190	193	12	1,5,9,15,19,25,28,32,49,51,53,56	6
0.5	0.9		187	11	1,5,13,19,25,29,32,38,42,51,54	3
0.6	0.9		167	11	1,5,13,19,25,29,32,38,42,51,54	3
0.7	0.9		143	11	1,6,13,19,25,29,32,38,41,51,54	4
0.8	0.9		89	11	1,6,13,19,25,29,32,38,41,51,54	4
0.9	0.9		118	11	1,6,13,19,25,29,32,38,41,51,54	4
0.4	0.8		170	12	1,5,12,13,19,25,29,32,38,41,51,54	9
0.5	0.8		181	11	1,6,13,19,25,29,32,38,41,51,54	4
0.6	0.8		167	11	1,5,13,19,25,29,32,38,42,51,54	3
0.7	0.8		143	11	1,6,13,19,25,29,32,38,41,51,54	4
0.8	0.8		89	11	1,6,13,19,25,29,32,38,41,51,54	4
0.9	0.8		118	11	1,6,13,19,25,29,32,38,41,51,54	4
0.4	0.7		179	12	1,6,9,13,18,27,30,32,38,41,50,53	11
0.5	0.7		200	12	1,6,9,13,18,25,28,32,38,41,51,53	10
0.6	0.7		114	11	1,6,13,19,25,29,32,38,51,54,56	3
0.7	0.7		143	11	1,6,13,19,25,29,32,38,41,51,54	4
0.8	0.7		135	11	1,6,13,19,25,29,32,38,41,51,54	4
0.9	0.7		90	12	1,6,9,13,19,25,29,32,38,50,53,56	10

#### 5.5.4 Selection of “must place” buses (Case III)

In real life, some buses are intentionally selected as candidate locations for PMU installation because of their importance in the network or due to some practical necessity. One might think, however, that it is a good choice to select beforehand the buses having the highest number of incident lines as candidate locations for PMU installation to reduce the search space and achieve a high-quality optimal solution. In this case, we simulate the IEEE systems keeping the same design parameters of the base case but we introduce one change by selecting the buses that have the highest number of incident lines to be in the set of “must place” buses. Simulation results for this case are shown in Tables 5.36-5.39. Comparing the simulation results for this case to those presented earlier for the base case, one may note the following:

1. For the IEEE 14-bus system, bus-4 has the highest number of 5 incident lines and it is selected as a candidate location for PMU installation. In this case, an optimal solution of a lower quality is obtained where the system can be fully observed by installing 4 PMUs instead of 3 PMUs in the base case. The average number of generations for this case to converge is 17.17 compared to 21.11 for the base case. However, this faster convergence is of no value considering that the optimal solution obtained is of a lower quality.
2. For the IEEE 30-bus system, bus-6 has the highest number of 7 incident lines and it is selected as a candidate location for PMU installation. In this case, an optimal solution of a lower quality is obtained where the system can be fully observed by installing 8 PMUs instead of 7 PMUs in the base case. Also, the DE algorithm needs more generations to converge. The average number of generations for this case to converge is 48.17 compared to 45.05 for the base case.
3. For the IEEE 39-bus system, bus-16 has the highest number of 5 incident lines and it is selected as a candidate location for PMU installation. We may note here that bus-16 appears in the optimal solution for the base case unlike the buses selected previously for IEEE 14- and 30-bus system that do not appear in the optimal solution of the respective base cases. Due to this, an optimal solution of 8 PMUs has been obtained, in this case, for 14 out of 18 combinations of  $CR$  and  $F$  while it was obtained only for 8 combinations of  $CR$  and  $F$  in the base case. The average cost of optimal solutions obtained here is 7.86 compared to 8.11 for the base case. The average number of generations for the algorithm to converge is 89.67 which equals to that for the base case.

4. For the IEEE 57-bus system, bus-9 and bus-13 have the highest number of 6 incident lines and they are selected as candidate locations for PMU installation. We may note here that bus-9 and bus-13 do not appear together in the optimal solution for the base case. In this case, the average cost of optimal solutions obtained here is 11.50 compared to 11.67 for the base case. Also, the DE algorithm converges faster. The average number of generations for this case to converge is 173.17 compared to 184 for the base case.

Therefore, we may conclude that designing a DE-based algorithm to solve the OPP problem with a constraint to have PMUs installed at buses having the highest number of incident lines may sometimes lead to optimal solutions of a lower quality. In some other times, this may not be the case depending on the system topology.

TABLE 5.36: IEEE 14-BUS SYSTEM - CASE-III

<i>CR</i>	<i>F</i>	<i>NP</i>	<i>NG</i>	<i>Best solution</i>		
				<i>N<sub>PMU</sub></i>	<i>Locations</i>	<i>ORI</i>
0.4	0.9	50	31	4	4,5,6,9	8
0.5	0.9		21		2,4,6,9	
0.6	0.9		18		4,5,6,9	
0.7	0.9		11		2,4,6,9	
0.8	0.9		13		4,5,6,9	
0.9	0.9		13		2,4,6,9	
0.4	0.8		18		2,4,6,9	
0.5	0.8		3		2,4,6,9	
0.6	0.8		30		4,5,6,9	
0.7	0.8		17		4,5,6,9	
0.8	0.8		8		2,4,6,9	
0.9	0.8		11		4,5,6,9	
0.4	0.7		29		4,5,6,9	
0.5	0.7		21		4,5,6,9	
0.6	0.7		24		2,4,6,9	
0.7	0.7		18		2,4,6,9	
0.8	0.7		21		2,4,6,9	
0.9	0.7		2		4,5,6,9	

TABLE 5.37: IEEE 30-BUS SYSTEM - CASE-III

<i>CR</i>	<i>F</i>	<i>NP</i>	<i>NG</i>	<i>Best solution</i>		
				<i>N<sub>PMU</sub></i>	<i>Locations</i>	<i>ORI</i>
0.4	0.9	60	70	8	1,2,6,10,12,15,19,30	14
0.5	0.9		54		2,3,6,10,12,15,20,30	14
0.6	0.9		37		2,4,6,10,12,15,20,29	16
0.7	0.9		48		2,4,6,10,12,15,18,29	16
0.8	0.9		44		1,6,7,10,12,18,23,27	10
0.9	0.9		53		1,2,6,10,12,15,18,27	15
0.4	0.8		70		2,3,6,10,12,19,23,30	11
0.5	0.8		63		2,3,6,10,12,15,20,29	14
0.6	0.8		56		1,2,6,10,12,15,20,29	14
0.7	0.8		46		3,5,6,12,17,19,24,27	8
0.8	0.8		37		1,5,6,10,12,18,23,29	9
0.9	0.8		37		2,4,6,10,12,15,19,27	17
0.4	0.7		54		2,4,6,12,17,19,24,29	10
0.5	0.7		55		2,3,6,10,12,15,18,27	15
0.6	0.7		34		1,6,7,10,12,15,20,29	12
0.7	0.7		42		1,2,6,10,12,15,19,29	14
0.8	0.7		31		2,4,6,10,12,19,24,27	15
0.9	0.7		36		1,5,6,10,12,15,19,30	12

TABLE 5.38: IEEE 39-BUS SYSTEM - CASE-III

<i>CR</i>	<i>F</i>	<i>NP</i>	<i>NG</i>	<i>Best solution</i>		
				<i>N<sub>PMU</sub></i>	<i>Locations</i>	<i>ORI</i>
0.4	0.9	120	99	8	3,8,12,16,20,23,25,29	4
0.5	0.9		98	9	3,8,10,16,20,21,23,25,29	7
0.6	0.9		95	8	8,11,16,18,20,23,25,29	4
0.7	0.9		94	8	3,8,10,16,20,23,25,29	4
0.8	0.9		82	8	3,8,10,16,20,23,25,29	4
0.9	0.9		79	8	3,8,11,16,20,23,25,29	4
0.4	0.8		100	10	2,8,11,16,20,21,23,26,37,38	8
0.5	0.8		88	9	2,6,10,16,18,20,23,25,29	8
0.6	0.8		91	8	3,8,12,16,20,23,25,29	4
0.7	0.8		78	8	3,8,10,16,20,23,25,29	4
0.8	0.8		93	8	3,8,10,16,23,29,34,37	1
0.9	0.8		82	8	3,8,11,16,20,23,25,29	4
0.4	0.7		78	9	2,8,11,16,20,23,27,29,37	5
0.5	0.7		89	8	3,8,10,16,23,29,34,37	1
0.6	0.7		93	8	3,8,11,16,20,23,25,29	4
0.7	0.7		98	8	3,8,13,16,23,29,34,37	1
0.8	0.7		86	8	8,11,16,18,20,23,25,29	4
0.9	0.7		91	8	3,8,11,16,20,23,25,29	4

TABLE 5.39: IEEE 57-BUS SYSTEM - CASE-III

<i>CR</i>	<i>F</i>	<i>NP</i>	<i>NG</i>	<i>Best solution</i>		
				<i>N<sub>PMU</sub></i>	<i>Locations</i>	<i>ORI</i>
0.4	0.9	190	188	13	1,4,9,13,20,25,29,32,38,48,51,53,56	11
0.5	0.9		198	14	1,6,9,13,14,15,17,20,27,30,33,51,53,56	17
0.6	0.9		189	12	1,3,9,13,19,25,29,32,38,50,53,56	10
0.7	0.9		189	12	1,4,9,13,18,25,28,32,38,41,51,53	10
0.8	0.9		173	12	1,6,9,13,18,25,28,32,38,41,50,53	10
0.9	0.9		115	12	1,6,9,13,19,25,29,32,38,41,50,54	11
0.4	0.8		188	13	1,4,9,13,20,25,29,32,38,48,51,53,56	11
0.5	0.8		190	13	1,4,9,13,19,23,29,30,32,38,41,51,54	12
0.6	0.8		199	13	1,6,7,9,12,19,25,29,32,38,51,53,56	14
0.7	0.8		189	13	1,9,13,14,15,18,21,25,29,32,50,53,56	14
0.8	0.8		152	13	1,3,9,13,19,25,29,32,38,41,49,51,53	16
0.9	0.8		115	12	1,6,9,13,19,25,29,32,38,41,50,54	11
0.4	0.7		200	14	2,9,12,13,15,18,23,25,29,32,48,51,53,56	17
0.5	0.7		192	14	1,9,13,15,18,22,27,29,31,32,38,42,51,54	17
0.6	0.7		194	13	1,3,9,13,18,25,28,29,32,38,41,50,54	14
0.7	0.7		116	12	1,6,9,13,19,27,31,32,38,41,51,53	11
0.8	0.7		165	13	2,9,12,13,18,26,29,30,32,38,41,51,53	13
0.9	0.7		165	12	1,6,9,13,19,27,31,32,38,51,53,56	10

## 5.6 DE performance analysis

In this section, we analyze the DE-based algorithm's performance considering different design aspects in some of its key operators. In particular, two cases are discussed considering a DE algorithm design with a variable scaling factor and a modified mutation scheme. Finally, few words are stated on proper selection of the DE algorithm population size and crossover constant to suit OPP problem.

### 5.6.1 DE design with a variable scaling factor (Case IV)

The DE-based optimization algorithm of the base case is designed assuming a real constant positive scaling factor. In this case, we simulate the IEEE systems keeping the same design parameters of the base case but we introduce one change by designing the

DE algorithm with a variable scaling factor. Simulation results for this case are shown in Tables 5.40-5.43. Comparing the simulation results for this case to the base case results, one may note the following:

1. For the IEEE 14-bus system, the same optimal solution is obtained where the system can be fully observed by installing 3 PMUs at buses 2, 6 and 9. However, the DE algorithm converges faster for this case. The average number of generations for this case to converge is 10.67 compared to 21.11 for the base case.
2. For the IEEE 30-bus system, a better optimal solution has been obtained for this case in comparison with the base case. The optimal number of PMUs equals 7 as in the base case but with a best *ORI* value of 11 compared to a best *ORI* value of 6 in the base case. The average cost of optimal solutions obtained here is 5.93 compared to 6.55 for the base case. However, the DE algorithm needs few more generations to converge. The average number of generations for the algorithm to converge is 54.33 compared to 45.05 for the base case.
3. For the IEEE 39-bus system, the optimal solution of 8 PMUs and an *ORI* value of 4 has been obtained for this case as obtained for the base case. In addition, the average number of generations for the algorithm to converge and the average cost of optimal solutions obtained here are almost the same as those obtained in the base case.
4. For the IEEE 57-bus system, the optimal solution of 11 PMUs and an *ORI* value of 3 has been obtained for this case as obtained for the base case. The average cost of optimal solutions obtained here is 11.38 compared to 11.67 for the base



case. Also, the DE algorithm converges faster. The average number of generations for the algorithm to converge is 172.17 compared to 184 for the base case.

TABLE 5.40: IEEE 14-BUS SYSTEM - CASE-IV

<i>CR</i>	<i>F</i>	<i>NP</i>	<i>NG</i>	<i>Best solution</i>		
				<i>N<sub>PMU</sub></i>	<i>Locations</i>	<i>ORI</i>
0.4	Variable	50	14	3	2,6,9	2
0.5			7			
0.6			12			
0.7			14			
0.8			10			
0.9			7			

TABLE 5.41: IEEE 30-BUS SYSTEM - CASE-IV

<i>CR</i>	<i>F</i>	<i>NP</i>	<i>NG</i>	<i>Best solution</i>		
				<i>N<sub>PMU</sub></i>	<i>Locations</i>	<i>ORI</i>
0.4	Variable	60	57	7	2,4,10,12,18,24,27	9
0.5			53		2,4,10,12,15,18,27	11
0.6			62		2,4,10,12,15,18,27	11
0.7			53		2,4,10,12,15,19,27	11
0.8			48		2,4,10,12,15,19,27	11
0.9			53		2,4,10,12,15,18,27	11

TABLE 5.42: IEEE 39-BUS SYSTEM - CASE-IV

<i>CR</i>	<i>F</i>	<i>NP</i>	<i>NG</i>	<i>Best solution</i>		
				<i>N<sub>PMU</sub></i>	<i>Locations</i>	<i>ORI</i>
0.4	Variable	120	100	9	3,8,13,16,20,23,25,29,30	5
0.5			94	9	2,7,10,16,18,23,25,29,34	6
0.6			97	9	2,6,12,16,23,25,26,29,34	9
0.7			93	8	8,11,16,18,23,25,29,34	3
0.8			89	8	3,8,11,16,20,23,29,37	2
0.9			75	8	8,11,16,18,20,23,25,29	4

TABLE 5.43: IEEE 57-BUS SYSTEM - CASE-IV

<i>CR</i>	<i>F</i>	<i>NP</i>	<i>NG</i>	<i>Best solution</i>		
				<i>N<sub>PMU</sub></i>	<i>Locations</i>	<i>ORI</i>
0.4	Variable	190	199	15	1,6,9,14,15,18,21,22,24,27,31,32,50,53,56	14
0.5			200	11	1,4,13,20,25,29,32,38,51,54,56	2
0.6			183	12	1,6,9,13,19,28,30,32,38,42,50,53	9
0.7			194	12	1,4,12,13,19,25,29,32,38,41,51,54	10
0.8			145	12	1,6,9,15,20,27,31,32,49,51,53,56	9
0.9			112	11	1,5,13,19,25,29,32,38,42,51,54	3

We may, therefore, conclude that designing a DE-based algorithm to solve the OPP problem with a variable scaling factor can sometimes enhance the quality of the optimal solution as demonstrated clearly in the case of IEEE 30-bus system. Moreover, such a design can also lead to faster convergence.

### 5.6.2 DE design with another mutation scheme (Case V)

The objective of mutation is to enable search diversity in the parameter space and to direct the existing object vectors with suitable amount of parameter variation in a way that will lead to better results at a suitable time. It keeps the search robust and explores new areas in the search domain. In the design of a DE-based optimization algorithm, there are many mutation schemes that can be implemented. Some of these schemes can be found in [139]. In the base case, the DE mutation operation is designed according to (5.1) where three independent vectors are used to generate a new candidate child vector. For this case, we simulate the IEEE systems keeping the same design parameters of the base case but we introduce one change only by designing the mutation operation of the DE algorithm according to the following equation:

$$x' = x_{r5}^G + F * [(x_{r1}^G - x_{r2}^G) + (x_{r3}^G - x_{r4}^G)] \quad (5.6)$$

With this mutation scheme, five independent vectors are needed to generate a new candidate vector. Simulation results for this case are shown in Tables 5.44-6.47. Comparing the simulation results for this case to those presented earlier for the base case, one may note the following:

1. For the IEEE 14-bus system, the same optimal solution is obtained where the system can be fully observed by installing 3 PMUs at buses 2, 6 and 9. However, the DE algorithm converges faster for this case. The average number of generations for this case to converge is 16.72 compared to 21.11 for the base case.
2. For the IEEE 30-bus system, the optimal number of PMUs equals 7 as in the base case but with a best *ORI* value of 9 compared to a best *ORI* value of 6 in the base case. However, the average cost of optimal solutions obtained here is 6.72 compared to 6.55 for the base case. Also, the DE algorithm here needs more generations to converge. The average number of generations for the algorithm to converge is 58.17 compared to 45.05 for the base case.
3. For the IEEE 39-bus system, the base case optimal solution of 8 PMUs and an *ORI* value of 4 could not be obtained with the new mutation scheme for all *CR* and *F* combinations. The average cost of optimal solutions obtained here is 10.44 compared to 8.11 for the base case. The average number of generations for this case to converge is 73.11 compared to 89.67 for the base case. However, this faster convergence is of no value considering that the optimal solution obtained is of a lower quality.
4. For the IEEE 57-bus system, the base case optimal solution of 11 PMUs with a best *ORI* value of 3 has not been obtained here for all combinations of *CR* and *F*.

Instead, we obtain an optimal solution of 18 PMUs with a best *ORI* value of 22. The average cost of optimal solutions is 16.29 compared to 11.67 for the base case. Also, the DE algorithm converges faster. The average number of generations for the algorithm to converge is 145.22 compared to 184 for the base case. However, this faster convergence is of no value considering that the optimal solution obtained is more costly.

Considering the above, one might conclude that a DE algorithm designed with mutation scheme according to (5.1) performed, most of the time, better than the DE algorithm designed with mutation scheme according to (5.6) with the population size and stopping criterion selected as mentioned earlier. In any case, however, there is no rule of thumb on the mutation scheme that has always the best performance.

TABLE 5.44: IEEE 14-BUS SYSTEM - CASE-V

<i>CR</i>	<i>F</i>	<i>NP</i>	<i>NG</i>	<i>Best solution</i>		
				<i>N<sub>PMU</sub></i>	<i>Locations</i>	<i>ORI</i>
0.4	0.9	50	33	3	2,6,9	2
0.5	0.9		15			
0.6	0.9		24			
0.7	0.9		20			
0.8	0.9		18			
0.9	0.9		13			
0.4	0.8		16			
0.5	0.8		17			
0.6	0.8		17			
0.7	0.8		7			
0.8	0.8		15			
0.9	0.8		12			
0.4	0.7		10			
0.5	0.7		20			
0.6	0.7		19			
0.7	0.7		15			
0.8	0.7		16			
0.9	0.7		14			

TABLE 5.45: IEEE 30-BUS SYSTEM - CASE-V

<i>CR</i>	<i>F</i>	<i>NP</i>	<i>NG</i>	<i>Best solution</i>		
				<i>N<sub>PMU</sub></i>	<i>Locations</i>	<i>ORI</i>
0.4	0.9	60	61	8	3,5,10,12,15,18,28,30	8
0.5	0.9		59	8	3,7,10,12,15,19,27,29	10
0.6	0.9		64	8	2,4,10,12,19,24,27,29	12
0.7	0.9		59	7	3,5,10,12,19,23,27	3
0.8	0.9		68	7	2,3,10,12,19,24,29	4
0.9	0.9		55	7	2,3,10,12,19,23,27	6
0.4	0.8		65	8	1,5,6,10,12,15,20,30	12
0.5	0.8		32	8	1,2,10,12,14,19,23,27	9
0.6	0.8		63	8	1,2,8,10,12,15,19,29	10
0.7	0.8		43	7	2,4,10,12,19,24,27	9
0.8	0.8		70	7	3,7,10,12,19,24,27	5
0.9	0.8		67	7	1,7,10,12,19,23,27	3
0.4	0.7		61	7	1,7,10,12,19,23,27	3
0.5	0.7		46	8	2,3,10,12,18,23,25,30	8
0.6	0.7		62	7	3,5,10,12,18,24,30	3
0.7	0.7		70	7	2,3,10,12,19,24,30	6
0.8	0.7		67	7	3,5,10,12,15,20,27	6
0.9	0.7		35	7	1,7,10,12,18,24,27	4

TABLE 5.46: IEEE 39-BUS SYSTEM - CASE-V

<i>CR</i>	<i>F</i>	<i>NP</i>	<i>NG</i>	<i>Best solution</i>		
				<i>N<sub>PMU</sub></i>	<i>Locations</i>	<i>ORI</i>
0.4	0.9	120	21	12	3,4,10,11,12,16,23,29,31,34,37,39	9
0.5	0.9		23	12	2,4,6,10,11,16,20,22,23,26,29,37	16
0.6	0.9		45	11	1,7,11,14,16,18,23,26,29,34,37	8
0.7	0.9		94	11	8,10,14,18,20,21,23,25,29,30,33	5
0.8	0.9		94	11	1,2,7,13,16,19,20,23,25,26,29	14
0.9	0.9		88	11	6,8,11,16,18,19,20,23,25,29,35	12
0.4	0.8		81	12	8,13,16,18,20,21,25,29,35,36,38,39	9
0.5	0.8		83	12	6,9,13,17,20,22,23,25,28,30,38,39	7
0.6	0.8		45	11	2,4,6,20,21,23,27,28,32,37,38	6
0.7	0.8		100	11	4,8,12,17,18,20,23,24,25,29,35	9
0.8	0.8		86	11	2,7,12,14,16,18,20,22,23,25,29	12
0.9	0.8		36	11	3,4,8,13,14,16,22,29,34,36,37	10
0.4	0.7		80	12	1,4,7,10,18,20,22,23,24,26,37,38	7
0.5	0.7		85	12	4,6,7,8,18,20,21,23,25,29,32,33	10
0.6	0.7		86	12	3,5,7,8,11,16,23,24,29,34,37,39	12
0.7	0.7		92	11	1,3,8,11,16,23,24,29,33,34,37	6
0.8	0.7		82	11	3,6,10,14,16,20,21,23,29,30,37	10
0.9	0.7		95	11	6,13,16,17,18,20,23,25,29,30,32	9

TABLE 5.47: IEEE 57-BUS SYSTEM - CASE-V

<i>CR</i>	<i>F</i>	<i>NP</i>	<i>NG</i>	<i>Best solution</i>		
				<i>N<sub>PMU</sub></i>	<i>Locations</i>	<i>ORI</i>
0.4	0.9	190	165	18	2,4,6,7,9,12,14,19,22,27,30,33,35,42, 45,50,53,57	16
0.5	0.9		33	19	1,3,4,5,9,15,18,23,24,25,29,32,35,37, 41,48,51,53,56	26
0.6	0.9		151	18	3,8,14,15,16,17,18,22,24,29,30,33,36, 41,47,50,51,54	15
0.7	0.9		200	18	3,6,8,12,17,19,25,28,29,32,37,40,41,43, 47,51,54	17
0.8	0.9		198	18	1,6,13,15,18,25,26,27,28,30,33,34,38, 42,49,51,53,54	22
0.9	0.9		200	19	1,3,4,9,11,13,18,19,21,26,29,30,32,38, 40,49,51,53,56	30
0.4	0.8		122	20	3,8,12,13,17,19,22,23,25,26,28,29,31, 33,38,49,51,52,55,56	29
0.5	0.8		136	20	2,5,12,13,20,23,26,29,31,33,34,38,39,4 6,49,50,54,56,57	30
0.6	0.8		37	20	1,3,6,7,9,10,11,13,14,15,19,20,28,30,32 49,51,52,55,56	39
0.7	0.8		182	19	1,3,4,6,7,9,13,19,25,29,31,33,38,39,41, 47,50,54,57	30
0.8	0.8		180	19	1,5,9,10,11,13,14,15,17,20,25,27,28,32, 39,41,50,53,56	32
0.9	0.8		149	19	1,4,9,10,11,13,19,23,29,30,31,33,38,40, 45,49,54,56,57	29
0.4	0.7		165	18	2,4,6,7,9,12,14,19,22,27,30,33,35,42, 45,50,53,57	16
0.5	0.7		197	19	1,5,7,9,18,20,28,30,33,36,37,38,41,44,4 7,48,49,50,53	23
0.6	0.7		100	19	1,6,9,10,15,17,18,20,22,27,31,32,38,42, 44,47,48,50,53	27
0.7	0.7		70	19	1,5,9,10,13,14,17,19,23,25,27,29,32,45, 46,50,53,54,56	25
0.8	0.7		180	19	1,5,9,10,11,13,14,15,17,20,25,27,28,32, 39,41,50,53,56	32
0.9	0.7		149	19	1,4,9,10,11,13,19,23,29,30,31,33,38,40, 45,49,54,56,57	29

### 5.6.3 Selection of population size and crossover rate

DE usually employs fixed population size throughout the search process. Variable population size can also be an option with proper size control algorithms to suit different

objectives of DE applications [139]. Selection of the population size involves conflicting objectives. In order to achieve fast computational speed, the population size should be as small as possible. However, too small population size may lead to premature convergence or stagnation. For the OPP problem, a population size of two to three times the number of buses of the power system under study will usually generate satisfactory results.

With regard to the crossover rate selection, one might conclude based on all the simulation results presented here that designing a DE optimization algorithm to solve the OPP problem with crossover rates in the range 0.7-0.9 produces, most of the time, solutions of a higher quality compared to the solutions obtained using smaller crossover rates in the range 0.4-0.6.

Having a power system fully observable using optimally allocated PMUs as presented in this chapter opens the door for a variety of significant applications in power systems as pointed out earlier. In the remaining part of this thesis, we shall discuss one of these applications where power system faults are located in an adaptive manner using synchronized phasor measurements obtained from optimally allocated PMUs. Implementation of a PMU-based adaptive fault location algorithm requires first the line parameters and system impedance to be properly estimated and this issue is addressed in Chapter 6 and 7. The subsequent three chapters present, in details, various adaptive fault location algorithms for two-terminal-, three-terminal and series-compensated transmission networks.

## **CHAPTER 6**

### **Transmission Line Parameter Identification Using PMU Synchronized Measurements**

There are some limitations and shortcomings associated with the traditional way being used by the electric utilities for line parameter estimation. This source of error affects the accuracy of impedance-based fault location algorithms which depend on the line impedance value provided by the electric utility. In the context of adaptive fault location aiming at achieving very high fault location accuracy, such source of error is removed by having the line parameters calculated online.

This chapter describes how the synchronized voltage and current measurements, obtained by PMUs, are utilized for online determination of transmission line parameters including line resistance, line reactance and shunt admittance. Depending on how many independent sets of synchronized phasor measurements are available, three PMU-based parameter identification methods designated as single measurement method, double measurement method and multiple measurement method using linear regression are



presented. In real life, voltage and current measurements are not noise-free. Therefore, the accuracy and robustness of aforesaid methods are quantified and verified using PSCAD/EMTDC and MATLAB simulations not only in the case of noise-free measurements but also in the cases where random noise and biased errors are present.

## 6.1 Introduction

Accurate determination of power system parameters, including the transmission line parameters, is the foundation to form a reliable power system model that is essential for state estimation, network losses analysis, power flow and contingency analysis, stability analysis and protective relay setting calculation. Traditionally, electric utilities calculate sequence impedances of transmission lines based on the geometric and electrical characteristics of the conductors. This method, however, can give considerable errors which will translate into incorrect settings on distance relays, fault locators, etc. Part of the data utilized for the calculations of positive sequence impedance are the permeability constants of the conductor and the environment since the conductor material is assumed to be fully paramagnetic. Even when using ferromagnetic conductors, as in the case of ACSR conductors, the approximation is utilized since the permeability variation is considered small. Moreover, the calculations involve the resistance of the conductor and a series of geometric parameters such as radius and distance between conductors to obtain the GMR and the GMD and the line length. [16]

If the line includes ground wires, the calculations require the resistance and the geometric arrangement of such wires. The value of conductor resistance varies with the temperature and the power flow. Some lines include sections with a different conductor

type having different resistance per unit length. Therefore, using a single resistance value in the impedance calculation program is a source of errors. With regard to the geometric parameters, the conductor arrangement can differ from section to section due to different tower configurations. However, the calculations are usually done with an average value and this is another source of errors. [16]

In addition to the parameters above, zero sequence impedance calculations require the distance from the conductors to ground (geometric parameter also taken as an average), and the ground resistance (evaluated from empirical results by Carson, as a function of the frequency). Also is needed the ground resistivity, a piece of information hard to estimate accurately due to the non-homogenous return path. Ground resistivity is affected by the soil composition, which changes along the line, by the humidity and the temperature. Ground conditions are also dependent on the weather. On another aspect, ground composition studies do not take into account buried metallic objects, such as pipes, cables, etc. [16]. Some classical approaches used to determine the transmission line parameters are described in [155-157].

Nowadays, PMUs enable a number of different applications to improve the efficiency in power systems and one of such applications is their use to determine the transmission line parameters. Calculations of sequence impedances based on synchronized readings from two PMUs, one at each end of the line, allow for a simple method to obtain accurate results. Positive sequence impedance can be obtained anytime, derived from positive sequence currents and voltages at both ends of the line. Zero sequence impedance requires zero sequence currents and voltages; therefore it can only be obtained when there is a zero sequence flow. Such flow will be present during ground

faults or serial faults (one or two open phases, impedance unbalances, etc.). In case of parallel circuits, zero sequence voltages and currents from both lines allow to derive the zero sequence mutual impedance. [16]

Several methods have been developed in the past by researchers to calculate the impedance parameters of the transmission line based on synchronized phasor measurements. Wilson et al. [158] proposed to use the synchronized voltage and current measurements from both ends of a transmission line to determine the ABCD chain parameters of the line from which the impedance parameters can then be obtained. Knowing the voltage, current and power measurements at the two ends of the line, the transmission line parameters are determined iteratively in [159] using the Newton-Raphson method. The method considers the distributed nature of the line parameters and determines the per-meter line parameters from the equivalent- $\pi$  network. The least-square approach is employed in [160] to find the line parameters in an iterative manner using the voltage and current measurements during the fault. The fault location and synchronization angle are also determined.

The non-linear optimal estimation theory is harnessed in [161-164] to determine the series resistance, series reactance and shunt susceptance per unit length of a transmission line modeled with its distributed parameters. In [161], different sub-networks including single, double, teed and series-compensated lines are all considered. Four different PMU-based methods, three of which are not iterative, utilizing single, double and multiple measurements are described in [67] to determine the transmission line parameters. The effect of biased and unbiased noise on the performance of these methods is also discussed.

The least square method is adopted in [165, 166] to identify the transmission line parameters. In [165], two methods based on least squares utilizing both synchronized and unsynchronized voltage and current phasor measurements are developed for estimating positive-sequence line parameters of series-compensated lines. To account for measurement inaccuracy, measurements at different moments are taken.

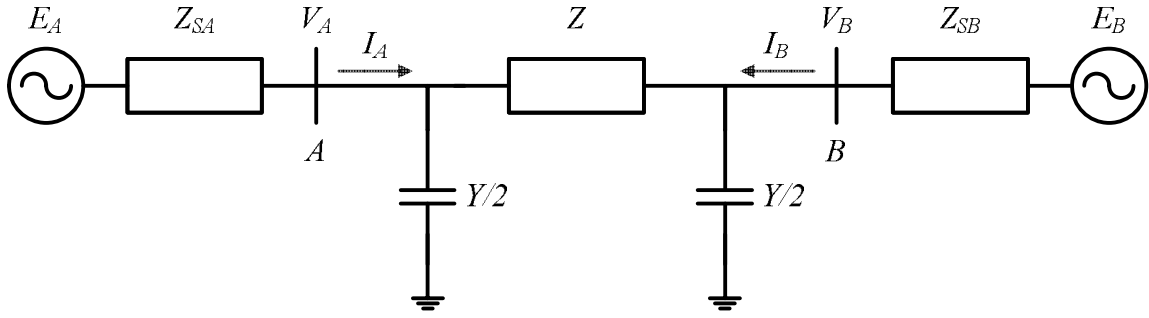
The fault location algorithm proposed in [167] utilizes only the fault data to determine the location of unsymmetrical faults. As a byproduct, positive-sequence line parameters are estimated. The effect of measurement errors on both fault location and parameter determination is studied. The iterative fault location algorithm proposed in [168] estimates the line parameters within the algorithm itself. A simultaneous state and parameter estimation algorithm is applied in [106] to an artificial system to find the parameters of the line or a transformer.

## **6.2 Transmission line parameter identification methods**

This section presents three different methods based on [67] for identification of transmission line parameters utilizing synchronized voltage and current phasor measurements at both ends of the line.

### **6.2.1 Single measurement method**

The measured steady state phase and amplitude of the voltages and currents are employed to calculate the parameters of the line. Representing a single line with its  $\pi$ -type equivalent circuit as shown in Figure 6.1 below:

Figure 6.1:  $\pi$ -type equivalent circuit of a single line

where

$E_A, E_B$  : Equivalent source voltage at terminal A, B

$Z_{SA}, Z_{SB}$  : Equivalent source impedance at terminal A, B

$Z$  : Line impedance

$Y$  : Line admittance

$V_A$  : Phase voltages at bus A during normal operation

$V_B$  : Phase voltages at bus B during normal operation

$I_A$  : Phase currents at bus A during normal operation

$I_B$  : Phase currents at bus B during normal operation

We may calculate the line parameters as shown below:

$$Y = \frac{2(I_A + I_B)}{V_A + V_B} \quad (6.1)$$

$$Z = \frac{V_A^2 - V_B^2}{V_B I_A - V_A I_B} \quad (6.2)$$

For parallel lines, positive sequence impedance and admittance are calculated respectively for each circuit as per above equations, then averaged values are considered as parameters for parallel (double-circuit) line.  $V_A, I_A, V_B, I_B$  are influenced by mutual

inductance between lines and phases, mutual inductance factor has been considered when the positive parameters are calculated.

### 6.2.2 Double measurement method

Two-port ABCD parameters are used to represent the transmission line in the most general form. The following two equations can be derived based on Figure 6.1:

$$V_A = A \cdot V_B + B \cdot I_B \quad (6.3)$$

$$I_A = C \cdot V_B + D \cdot I_B \quad (6.4)$$

If the PMUs at the two terminals of the line generate two different sets of measurements for different load conditions, the ABCD chain parameters can be determined by the following equations:

$$V_{A1} = A \cdot V_{B1} + B \cdot I_{B1} \quad (6.5)$$

$$I_{A1} = C \cdot V_{B1} + D \cdot I_{B1} \quad (6.6)$$

$$V_{A2} = A \cdot V_{B2} + B \cdot I_{B2} \quad (6.7)$$

$$I_{A2} = C \cdot V_{B2} + D \cdot I_{B2} \quad (6.8)$$

where

$V_{A1}, V_{B1}, I_{A1}, I_{B1}$  are voltage and current phasors from measurement 1

$V_{A2}, V_{B2}, I_{A2}, I_{B2}$  are voltage and current phasors from measurement 2

Solving complex equations (6.5) to (6.8) in four unknown parameters using Cramer's Rule gives:

$$A = \frac{I_{B1} \cdot V_{A2} - I_{B2} \cdot V_{A1}}{I_{B1} \cdot V_{B2} - I_{B2} \cdot V_{B1}} \quad (6.9)$$

$$B = \frac{V_{B2} \cdot V_{A1} - V_{B1} \cdot V_{A2}}{I_{B1} \cdot V_{B2} - I_{B2} \cdot V_{B1}} \quad (6.10)$$

$$C = \frac{I_{B1} \cdot I_{A2} - I_{B2} \cdot I_{A1}}{I_{B1} \cdot V_{B2} - I_{B2} \cdot V_{B1}} \quad (6.11)$$

$$D = \frac{I_{A1} \cdot V_{B2} - I_{A2} \cdot V_{B1}}{I_{B1} \cdot V_{B2} - I_{B2} \cdot V_{B1}} \quad (6.12)$$

Once the ABCD parameters are found, the impedance parameters are directly calculated using the following relationships:

$$A = 1 + \frac{YZ}{2} \quad (6.13)$$

$$B = Z \quad (6.14)$$

$$C = Y \cdot \left(1 + \frac{YZ}{4}\right) \quad (6.15)$$

$$D = 1 + \frac{YZ}{2} \quad (6.16)$$

Since we only have two unknowns, there are two redundant equations. Combining equations (6.13) and (6.14) we get:

$$Z = B \quad (6.17)$$

$$Y = \frac{2 \cdot (A - 1)}{B} \quad (6.18)$$

### 6.2.3 Multiple measurement method using linear regression

Equations (6.3) and (6.4) are two complex equations with eight complex variables.

Expanding them into four real equations we get:

$$Re[V_A] = Re[A] \cdot Re[V_B] - Im[A] \cdot Im[V_B] + Re[B] \cdot Re[I_B] - Im[B] \cdot Im[I_B] \quad (6.19)$$

$$Im[V_A] = Re[A] \cdot Im[V_B] + Im[A] \cdot Re[V_B] + Re[B] \cdot Im[I_B] + Im[B] \cdot Re[I_B] \quad (6.20)$$

$$Re[I_A] = Re[C] \cdot Re[V_B] - Im[C] \cdot Im[V_B] + Re[D] \cdot Re[I_B] - Im[D] \cdot Im[I_B] \quad (6.21)$$

$$Im[I_A] = Re[C] \cdot Im[V_B] + Im[C] \cdot Re[V_B] + Re[D] \cdot Im[I_B] + Im[D] \cdot Re[I_B] \quad (6.22)$$

We collectively write equations (6.19) to (6.22) into the matrix format and get:

$$\begin{bmatrix} Re[V_A] \\ Im[V_A] \end{bmatrix} = \begin{bmatrix} Re[V_B] & -Im[V_B] & Re[I_B] & -Im[I_B] \\ Im[V_B] & Re[V_B] & Im[I_B] & Re[I_B] \end{bmatrix} \cdot \begin{bmatrix} Re[A] \\ Im[A] \\ Re[B] \\ Im[B] \end{bmatrix} \quad (6.23)$$

$$\begin{bmatrix} Re[I_A] \\ Im[I_A] \end{bmatrix} = \begin{bmatrix} Re[V_B] & -Im[V_B] & Re[I_B] & -Im[I_B] \\ Im[V_B] & Re[V_B] & Im[I_B] & Re[I_B] \end{bmatrix} \cdot \begin{bmatrix} Re[C] \\ Im[C] \\ Re[D] \\ Im[D] \end{bmatrix} \quad (6.24)$$

If  $K$  measurements have been collected from the PMUs, we define the following:

$$E = \begin{bmatrix} Re[V_{A1}] \\ Im[V_{A1}] \\ Re[V_{A2}] \\ Im[V_{A2}] \\ \vdots \end{bmatrix} \quad (6.25)$$

$$H = \begin{bmatrix} Re[V_{B1}] & -Im[V_{B1}] & Re[I_{B1}] & -Im[I_{B1}] \\ Im[V_{B1}] & Re[V_{B1}] & Im[I_{B1}] & Re[I_{B1}] \\ \vdots & \vdots & \vdots & \vdots \\ Re[V_{BK}] & -Im[V_{BK}] & Re[I_{BK}] & -Im[I_{BK}] \\ Im[V_{BK}] & Re[V_{BK}] & Im[I_{BK}] & Re[I_{BK}] \end{bmatrix} \quad (6.26)$$

$$F = \begin{bmatrix} Re[A] \\ Im[A] \\ Re[B] \\ Im[B] \end{bmatrix} \quad (6.27)$$



Using the unbiased least square estimator, the best estimation of the chain parameters A and B are found to be:

$$F = (H^T H)^{-1} H^T E \quad (6.28)$$

Similarly, best estimated values of C and D can be found. The impedance parameters are calculated using equations (6.17) and (6.18).

### 6.3 Simulation results

A 38-bus 115 kV SEC system as depicted in Figure 5.30 is modeled in PSCAD/EMTDC under this study. In particular, the line connecting bus-38 (sending end) and bus-30 (receiving end) is selected for parameter identification. The selected line is a short one with a length of only 26 km and is modeled by the nominal- $\pi$  circuit. The actual parameters of this transmission line are shown in Table 6.1. In the PSCAD/EMTDC simulation, two sets of simulated PTs and CTs are placed at both ends of the selected line to sample the voltages and currents simultaneously. In this simulation, the output of the CTs and PTs are real-time data, which are further processed by a DFT to obtain the phasor components. Since we desire the positive sequence impedance parameters of the transmission line, these phasor components are further processed to obtain the sequence components. As method # 2 and method # 3 require two and multiple measurements respectively, it has been ensured that each set of measurement represents a different loading condition. We shall now present the simulation results obtained assuming noise-free measurements and the results obtained with the presence of both random noise and bias errors.

TABLE 6.1: ACTUAL LINE PARAMETERS

<i>Parameter</i>	<i>Actual Value</i>
$r$	1.9044
$x$	9.852625
$B_C$	9.103969754e-5

### 6.3.1 Results with noise-free measurements

Table 6.2 summarizes the MATLAB simulation results obtained for each method. The line resistance  $r$ , reactance  $x$  and shunt susceptance  $B_C$  where  $Y = jB_C$  are all calculated. The line parameter estimation accuracy is measured by the percentage error evaluated as shown below:

$$\text{error (\%)} = \frac{|\text{Actual value} - \text{Calculated value}|}{\text{Actual value}} \times 100 \quad (6.29)$$

As Table 6.3 indicates, all methods work well with noise-free measurements and the results obtained are highly accurate.

TABLE 6.2: CALCULATED LINE PARAMETERS

<i>Method #</i>	<i>Calculated Parameter</i>		
	$r$	$x$	$B_C$
1	1.90440435	9.85284554	9.104156930e-5
2	1.90441128	9.85288077	9.104818567e-5
3	1.90441146	9.85288163	9.104834949e-5

TABLE 6.3: PERCENTAGE ERROR IN THE CALCULATED LINE PARAMETERS

<i>Method #</i>	<i>Error (%) in</i>		
	$r$	$x$	$B_C$
1	2.28585e-4	0.00223845	0.00205598
2	5.92651e-4	0.00259600	0.00932355
3	6.01799e-4	0.00260477	0.00950349

### 6.3.2 Results with biased and non-biased noise

In reality, noise is present in all measurements. Although PMU measurements have greater accuracy than other measurements, this potential performance is not achieved in an actual field installation due to errors from instrumentation channels, errors from data conversion, CT saturation, system imbalances or communication device abnormalities. For short transmission lines, such as the one selected, the noise in the measurements is more problematic than in the case of long transmission lines. [67, 162, 169, 170]

Two types of measurement noise are considered; the random noise and bias errors. Bias errors are the measurements that are constantly and consistently in error by a fixed amount. The bias error is assumed in our simulation to have a magnitude of 1 % of the mean value of the current or voltage experienced over a 24 hour cycle. Random noise is random in nature as the name implies and in our simulation is normally distributed with zero mean and 1 % deviation. Figure 6.2 depicts phase-A, phase-B and phase-C voltages at bus-38 and the associated random noise considered in the simulation. There exist three places where noise can be injected as mentioned below:

- Case-1: Noise added to the time domain samples from the PSCAD/EMTDC simulation
- Case-2: Noise added to the phasor values obtained from the DFT
- Case-3: Noise added to the sequence components we obtain from symmetrical component transformation

Both random noise and bias errors were added to the noise-free PMU voltage and current measurements to test the performance of each method under noise conditions.

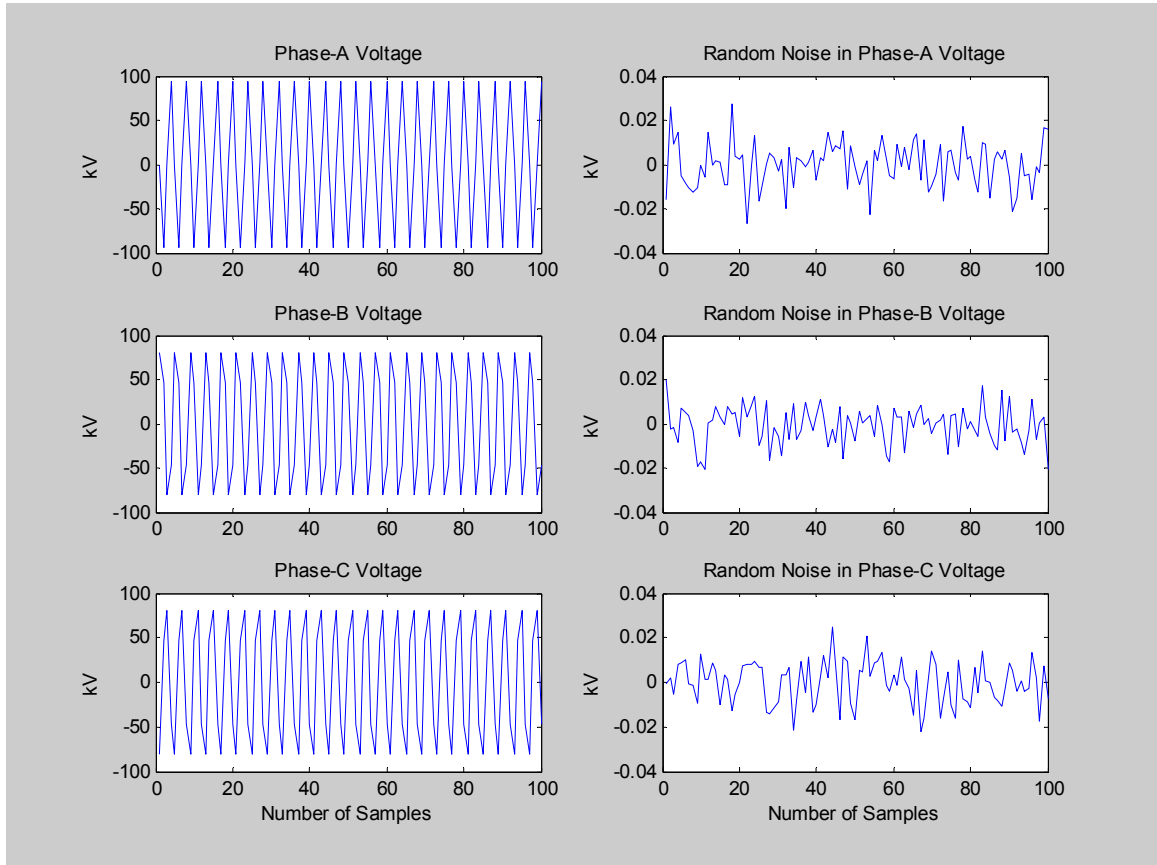


Figure 6.2: Phasor voltages at bus-38 and associated random noise

Results obtained are shown in Table 6.4 for all the cases highlighted above. Instead of giving absolute numbers, the results are given in the form of “A” for acceptable and “U” for unacceptable. The estimated parameter is determined to be acceptable if the parameter is within a reasonable band (i.e.  $\pm 10\%$  for  $x$  and  $B_C$  and  $\pm 20\%$  for  $r$ ). Otherwise, the result is considered unacceptable. A close look to the simulation results reveals the following:

1. Some parameter estimates are acceptable for certain types of noise and unacceptable for other types. For instance, in row # 1 & 5 of Table 6.4 for Case-1, with noise added to the measurements of sending end voltage, the series resistance and reactance calculated are unacceptable while the shunt susceptance is acceptable.

This indicates that the series resistance and reactance are very sensitive to random noise and bias errors in the sending end voltage while the shunt susceptance is not.

One can make similar observations for the other rows in the table.

2. Method # 2 works much better than Method # 1 for bias errors although it is still very sensitive to the random noise. This suggests that redundancy in the measurements may improve the parameter estimation.
3. For Method # 2, the random noise and bias errors introduced in the sending end current measurements does not affect our calculations since equations (6.9) and (6.10) are not functions of such measurements.
4. As far as random noise is concerned and considering all the three cases, Method # 3 outperforms both Method # 1 and Method # 2. This means that accurate impedance parameters can be obtained even when there is a random noise in the PMU measurements.
5. Method # 3 has acceptable performance when calculating the series resistance and reactance from phasor measurements in the presence of random noise and bias errors. However, the shunt susceptance calculated is still sensitive to the random noise and bias errors.

TABLE 6.4: METHODS PERFORMANCE WHEN NOISE AND BIAS ERRORS APPEAR IN THE MEASUREMENTS

Method #	Type of Noise		Calculated Parameter								
			Case-1			Case-2			Case-3		
			R	X	B <sub>C</sub>	R	X	B <sub>C</sub>	R	X	B <sub>C</sub>
1	Bias Error in	V <sub>A</sub>	U	U	A	U	U	A	U	U	A
		V <sub>B</sub>	U	U	A	U	U	A	U	U	A
		I <sub>A</sub>	A	A	U	A	A	U	A	A	U
		I <sub>B</sub>	A	A	U	A	A	U	A	A	U
	Random Noise in	V <sub>A</sub>	U	U	A	U	U	A	U	U	A
		V <sub>B</sub>	U	U	A	U	U	A	U	U	A
		I <sub>A</sub>	A	A	A	A	A	A	A	A	A
		I <sub>B</sub>	A	A	A	A	A	A	A	A	A
2	Bias Error in	V <sub>A</sub>	A	A	U	A	A	U	A	A	U
		V <sub>B</sub>	A	A	U	A	A	U	A	A	U
		I <sub>A</sub>	A	A	A	A	A	A	A	A	A
		I <sub>B</sub>	A	A	A	A	A	A	A	A	A
	Random Noise in	V <sub>A</sub>	U	U	U	A	A	U	A	A	U
		V <sub>B</sub>	U	U	U	A	A	U	A	A	U
		I <sub>A</sub>	A	A	A	A	A	A	A	A	A
		I <sub>B</sub>	U	U	U	A	A	A	A	A	A
3	Bias Error in	V <sub>A</sub>	A	A	U	A	A	U	A	A	U
		V <sub>B</sub>	A	A	U	A	A	U	A	A	U
		I <sub>A</sub>	A	A	A	A	A	A	A	A	A
		I <sub>B</sub>	A	A	A	A	A	A	A	A	A
	Random Noise in	V <sub>A</sub>	A	A	U	A	A	U	A	A	U
		V <sub>B</sub>	U	U	U	A	A	U	A	A	U
		I <sub>A</sub>	A	A	A	A	A	A	A	A	A
		I <sub>B</sub>	A	A	U	A	A	A	A	A	A

A : Acceptable    U : Unacceptable

## **CHAPTER 7**

### **Determination of Thevenin's Equivalent (TE) Using PMU Measurements**

A Thevenin's equivalent (TE) provided by the electric utility at a certain node is usually different from practical parameters and does not reflect the actual operating conditions of the power system. This source of error affects the accuracy of impedance-based fault location algorithms which depend on the TEs provided by the electric utility at both terminals of the line under study. In the context of adaptive fault location aiming at achieving very high fault location accuracy, such source of error is removed by having the said TEs calculated online.

Determination of a TE for a system at one of its ports opens the door to many interesting possibilities. The quality and reliability of results obtained using TE is, however, determined by the accuracy of the TE itself. For a linear system, the TE represents a perfect equivalent at the port it is determined for over the entire range of

variations which may take place in voltage and/or current provided that the rest of the system is kept unchanged. In a real power system, the transmission network itself is linear, but node specifications, power injections and/or voltages, are not. Node specifications are either P, Q at load nodes or P, V at generation nodes. Hence, voltage/current relationships at the system nodes experience the nonlinearities of the specified injections. Therefore, the problem lies mainly in the nonlinearity of the load/generation injections. Methods based on power flow solution may not suit the purpose of online TE determination as data of the whole system have to be processed each time. In addition, the rate of updating these data is determined by the SCADA system which is too slow. On the other hand, local measurements using PMUs provide voltage and current phasors at rates as high as 1 measurement/cycle and, therefore, are more useful for online TE determination. [171]

This chapter presents, in details, a method for the determination of TE based on PMU measurements followed by simulation results.

## 7.1 Algorithm description

In this section, we shall highlight the basics of the PMU-based algorithm used to determine TE at a given node followed by the calculation procedure [171]. Equation 7.1 gives the node voltage using TE model.

$$V = E_{th} + Z_{th} \cdot I \quad (7.1)$$

Once accurate values of  $E_{th}$  and  $Z_{th}$  are available, all the required variables at that node can be reliably estimated without the need of detailed system representation.



Determination of TE parameters using local PMU measurements require at least two different  $(V, I)$  pairs measured at different time instants.  $V$  and  $I$  phasors for the different time instants must be measured to the same reference. However, the measurement reference (MR) rotates at the slip frequency between the system and the PMU because of variations in system frequency. The result is that the phase angles of  $V$  and  $I$  at subsequent time steps will be measured for different references. Figure 7.1 and Figure 7.2 show the phasor diagrams for two different measurements. The effect of the PMU phase drift is to rotate all phasors by the same angle while the relative angles between individual phasors remain unchanged.

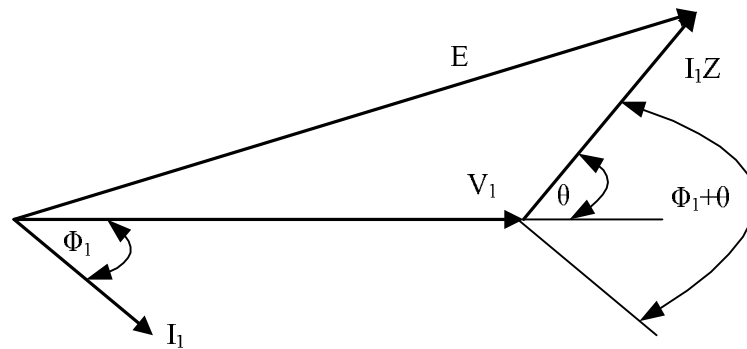


Figure 7.1: Phasor diagram for the first set of measurements

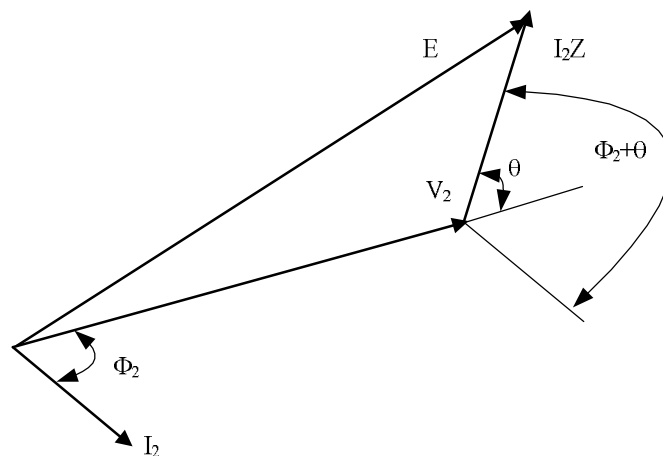


Figure 7.2: Phasor diagram for the second set of measurements

Since  $E$  is the Thevenin voltage, it has to be the same in the two cases. However,  $E$  in case b is shifted by an angle equal to the phase drift but its magnitude is still the same.

For the first set of PMU measurements, case a, the equation for  $E$  can be written as

$$E^2 = V_1^2 + I_1^2 Z^2 + 2V_1 I_1 Z \cos(\theta + \varphi) \quad (7.2)$$

Expanding  $\cos(\theta + \varphi)$ , equation (7.2) can be rewritten as

$$E^2 = V_1^2 + I_1^2 Z^2 + 2P_1 r_{th} - 2Q_1 x_{th} \quad (7.3)$$

$r_{th}$  and  $x_{th}$  are the resistance and the reactance of the Thevenin impedance  $Z$ .  $P_1$  and  $Q_1$  are respectively the real and reactive powers for the first set of measurements. Similarly, for the second set of PMU measurements we can write

$$E^2 = V_2^2 + I_2^2 Z^2 + 2P_2 r_{th} - 2Q_2 x_{th} \quad (7.4)$$

Subtracting (7.4) from (7.3) we get

$$V_1^2 - V_2^2 + (I_1^2 - I_2^2) Z^2 + 2(P_1 - P_2) r_{th} - 2(Q_1 - Q_2) x_{th} = 0 \quad (7.5)$$

Equation (7.5) can be arranged and written as follows

$$\left( r_{th} + \frac{P_1 - P_2}{I_1^2 - I_2^2} \right)^2 + \left( x_{th} - \frac{Q_1 - Q_2}{I_1^2 - I_2^2} \right)^2 = \frac{V_2^2 - V_1^2}{I_1^2 - I_2^2} + \left( \frac{P_1 - P_2}{I_1^2 - I_2^2} \right)^2 + \left( \frac{Q_1 - Q_2}{I_1^2 - I_2^2} \right)^2 \quad (7.6)$$

This is the equation of a circle in the impedance plane defining the locus for Thevenin impedance that satisfies the two measurements but it does not define a specific value for  $Z$ . Therefore, a third measurement is required which can be used with either the first or the second set of PMU measurements in the same way as above to produce another locus for  $Z$ , another circle. The equivalent Thevenin impedance is determined by the intersection of the two circles. The coordinates of the intersection point in the  $Z$ -plane define the values of the resistance and reactance of the Thevenin impedance.

Based on the above, the TE calculation procedure can be summarized by the following simple steps [171]:

- At a given instant of time, the most recent voltage and current measurements from the PMU along with the two preceding measurements are used to form two circle equations as defined by (7.6).
- Intersection points of the two circles are determined defining two values for  $Z$ , namely  $Z_1$  and  $Z_2$ .
- Thevenin voltage,  $E$ , is determined for each value of  $Z$  using (7.1). Having two values of  $Z$ , two corresponding values of  $E$  will be obtained; the higher one that is near to the system voltage is taken to be  $E_{th}$  and the corresponding  $Z$  is  $Z_{th}$ .
- The phase drift caused by the PMU can be determined by determining  $E_{th}$  using the three measurements one at a time. The angle difference between  $E_{th}$  determined using the first set of PMU measurements and that determined by the second set of PMU measurements determines the drift that took place between these two measurements and so on.

## 7.2 Simulation results

The 115 kV SEC system, discussed in chapter 5, is used as a test system for online TE determination using the PMU measurements. With an aim to determine TE equivalents at bus 30 and bus 38, three different loading cases are simulated using PSCAD/EMTDC. The three sets of PMU voltage and current phasor measurements at aforesaid buses are then sampled as shown in Figure 7.3 to 7.5 and recorded for further processing to obtain the corresponding rms values. The three sets of PMU measurements are generated by

varying the load at bus 30 and bus 38 while representing all the generators as voltage sources with their voltage and phase angles are set equal to its values at the base case. This is a reasonable assumption for online application where measurements are taken at small intervals, usually one measurement per cycle. All other loads are kept unchanged. Load at bus 30 and 38 are changed until no convergence obtained.

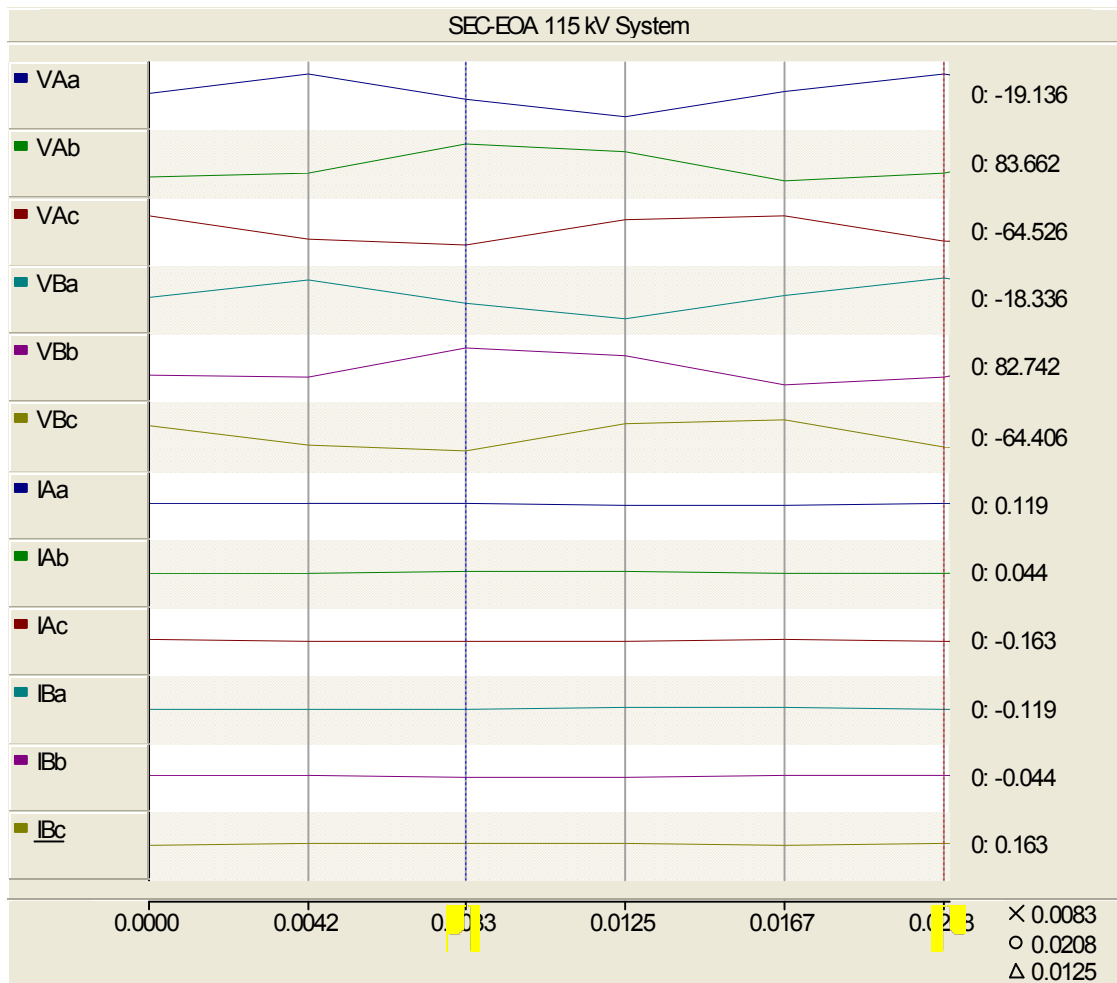


Figure 7.3: Sampling of 1<sup>st</sup> set of PMU phasor measurements at bus 30 & bus 38

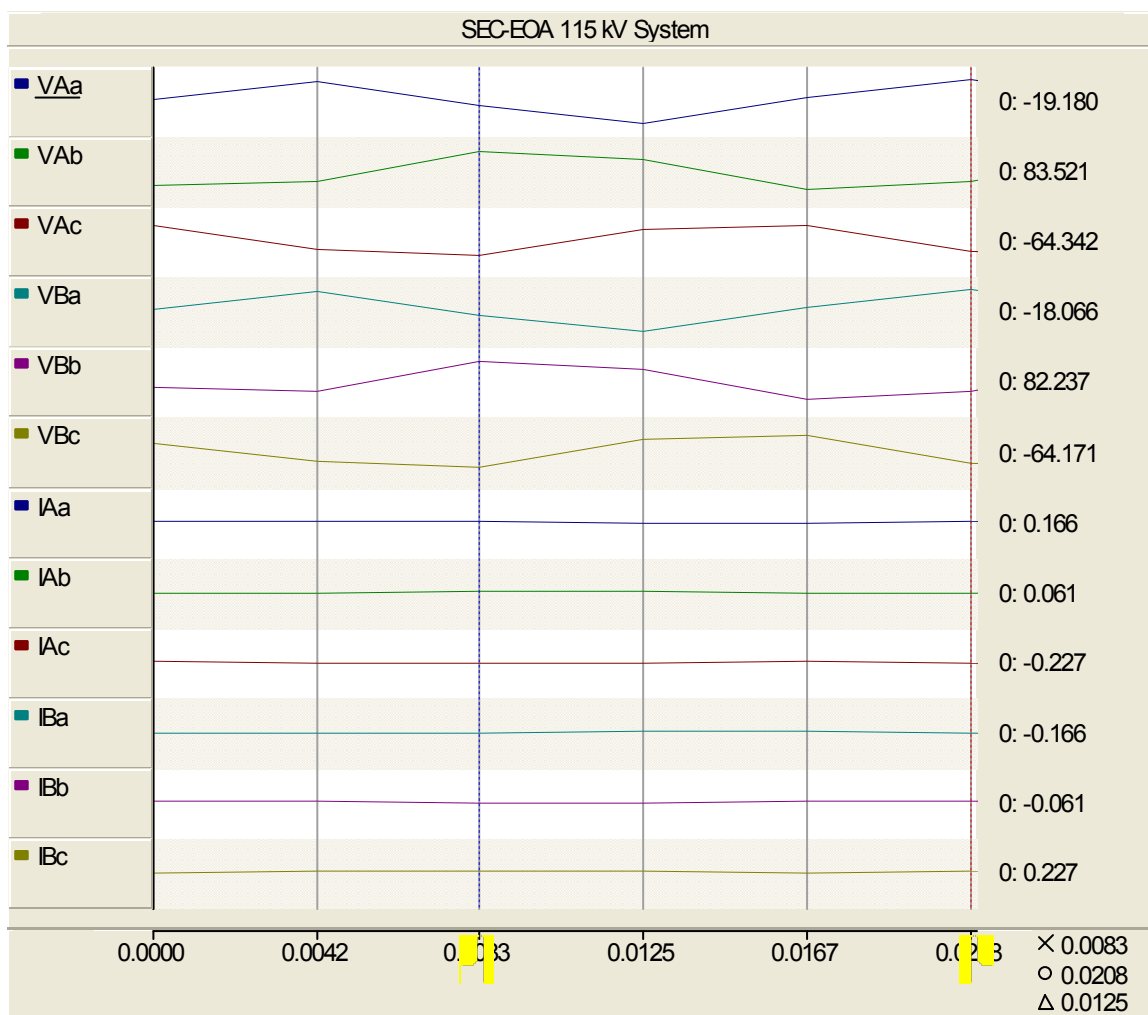


Figure 7.4: Sampling of 2<sup>nd</sup> set of PMU phasor measurements at bus 30 & bus 38

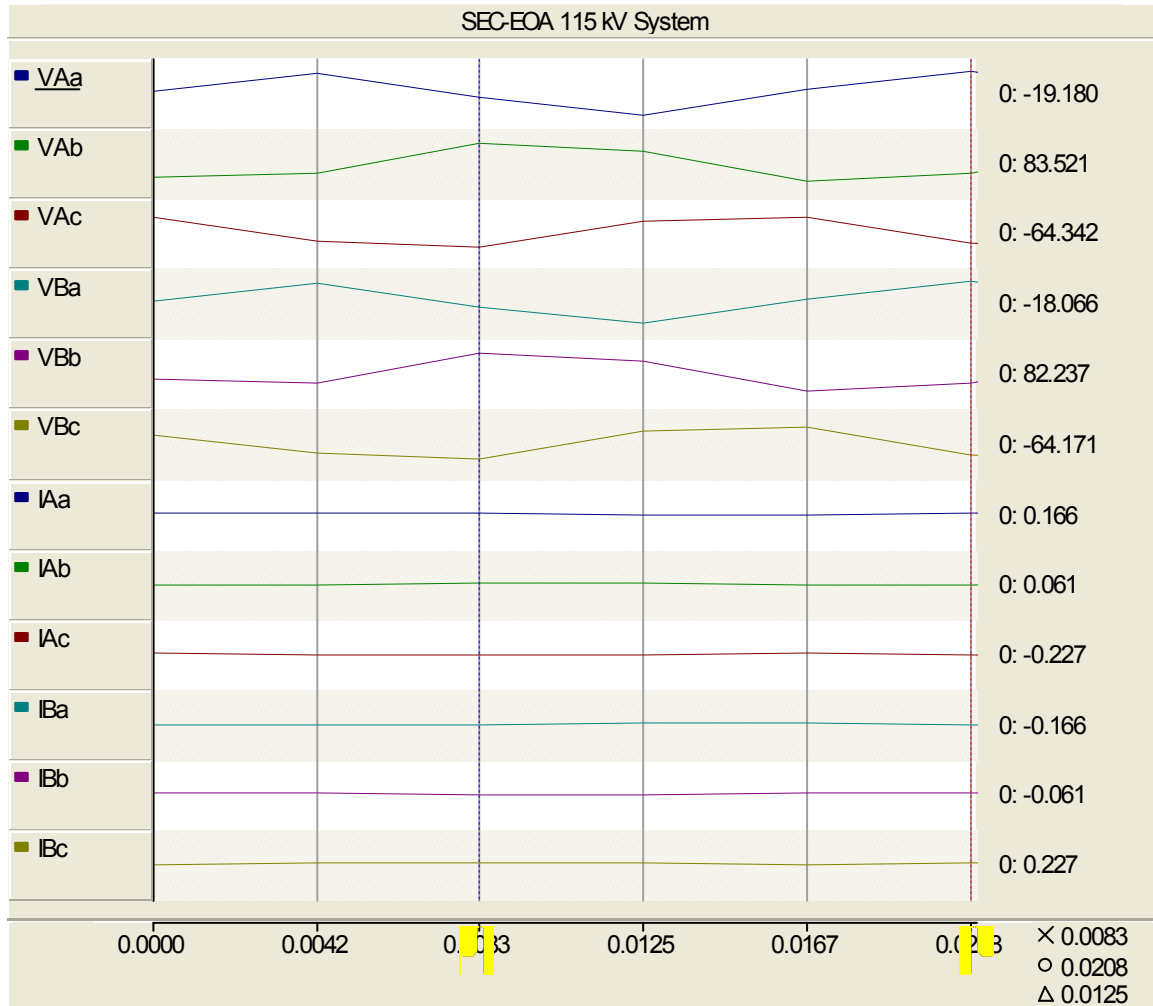


Figure 7.5: Sampling of 3<sup>rd</sup> set of PMU phasor measurements at bus 30 & bus 38

Figure 7.6 and 7.7 show the  $Z$  circles in the impedance plane formed using different combinations of the three set of measurements recorded at bus 30 and bus 38 respectively. It is clear that all the circles intersect at the same point corresponding to  $Z_{th}$  at each bus. To determine the  $Z_{th}$  value, however, only two circles are needed. Figure 7.8 and Figure 7.9 display  $Z_{th}$  determination at bus 30 and bus 38 which exactly coincide with the intersection point.

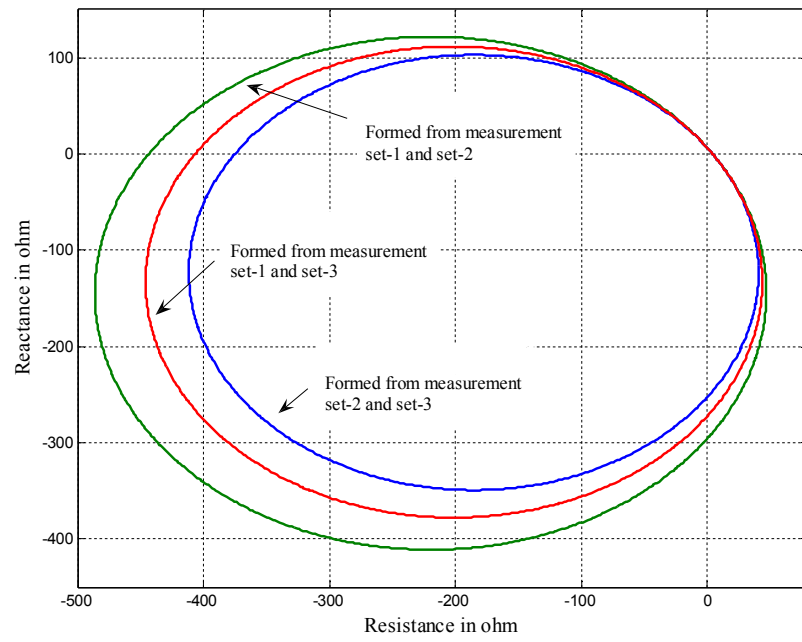


Figure 7.6: Z circles at bus 30

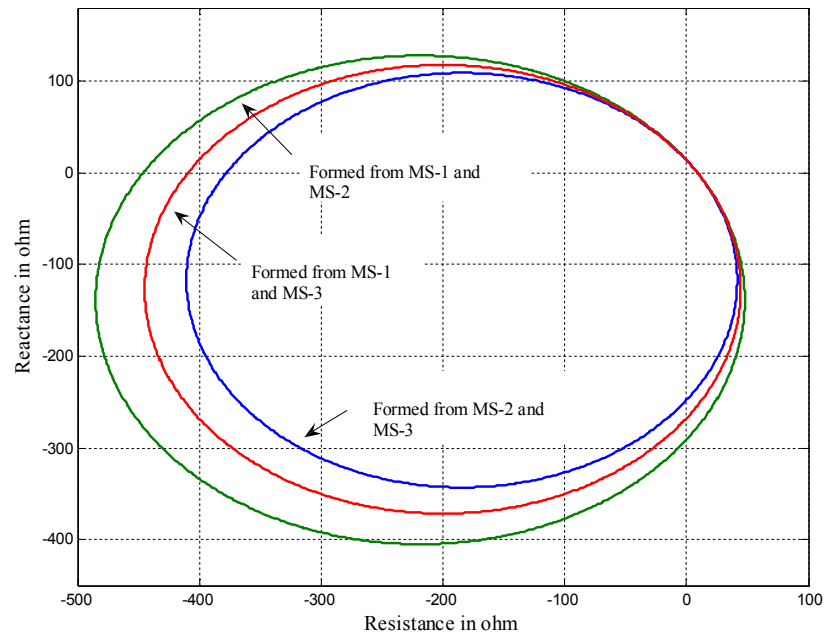
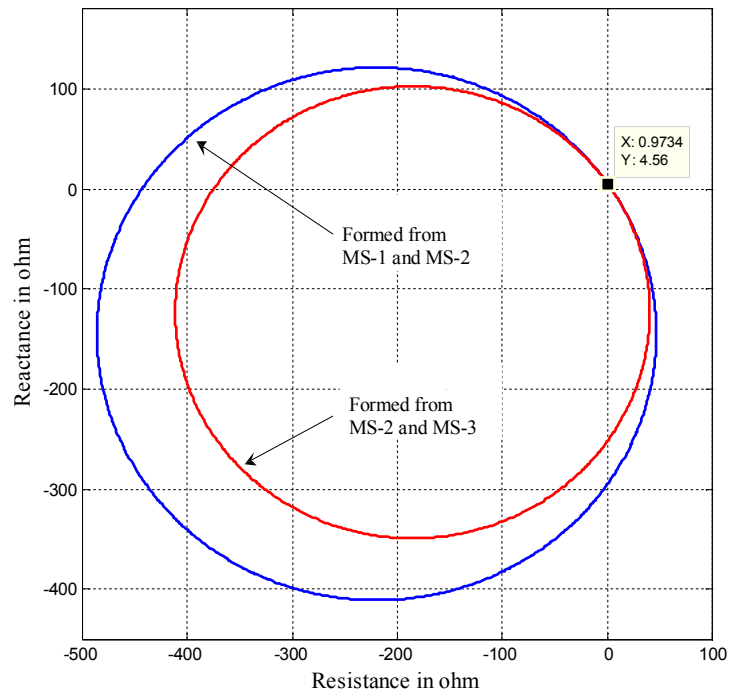
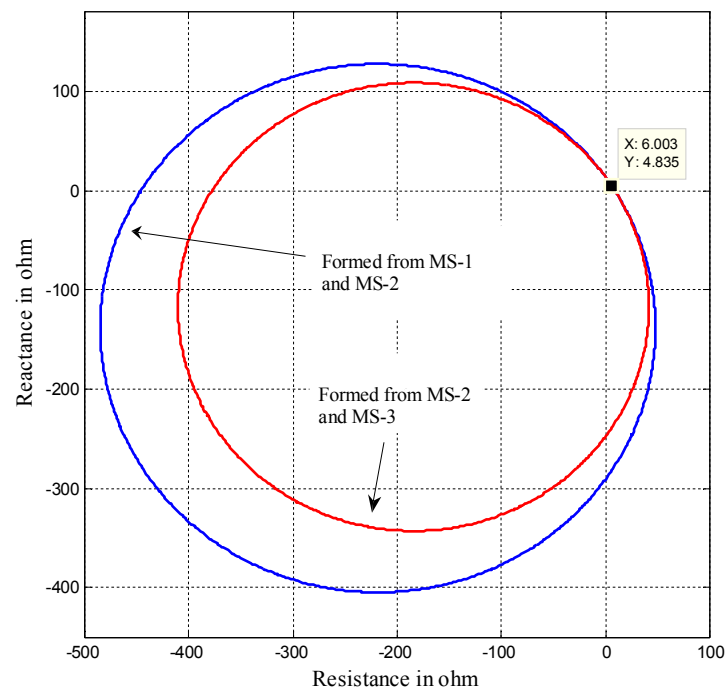


Figure 7.7: Z circles at bus 38

Figure 7.8: Determination of  $Z_{th}$  at bus 30Figure 7.9: Determination of  $Z_{th}$  at bus 38



## **CHAPTER 8**

### **Adaptive PMU-based Fault Location Algorithms for Two-terminal Lines**

This chapter aims at providing two PMU-based adaptive fault location algorithms for two terminal lines. After an introductory section, the two adaptive fault location algorithms are described where detailed mathematical formulation and simulation results based on PSCAD/EMTDC and MATLAB are presented. In both algorithms, the two-terminal line is represented with its distributed parameters. In order to verify the algorithms' robustness, the effect of some factors, which are usually considered in fault location studies, on the algorithms' accuracy is then discussed.

#### **8.1 Introduction**

Accurate and swift fault location on a power network can expedite repair of faulted components, speed-up power restoration and thus enhance power system reliability and

availability. Rapid restoration of service could reduce customer complaints, outage time, loss of revenue and crew repair expense. [41, 64, 70, 83, 87-89, 172-174]

PMUs using synchronization signals from the GPS satellite system have recently evolved into mature tools and are now being utilized in the field of fault location. Recognizing the importance of the fault location function for electric power utilities, several PMU-based fault location algorithms have been proposed in the past literature. Some of them are based on using both synchronized current and voltage phasors at the two ends of a line [41, 83, 87-89, 172, 175]. Other algorithms are developed based on utilizing only voltage phasor measurements [50, 176-178] to avoid the consequences of inappropriate operation of current transformers due to overvoltage and transient state of power network during fault period. A fault detection/location algorithm that considers arcing faults is proposed in [179, 180]. Fault location schemes for aged power cables [70], two and three-terminal transmission lines [50], double-circuit transmission lines [40, 181], overhead line combined with an underground power cable [173] and transposed/untransposed transmission lines [174] are reported. To determine the fault location, these classical algorithms need the line impedance parameters to be known. Such parameters are assumed to be constant as provided by the electric utility regardless of the system's operating conditions at the time when the fault occurs. To improve the fault location accuracy of the classical PMU-based fault location algorithms, various adaptive fault location algorithms have been developed [66, 76, 77, 81, 110, 160, 162, 167, 174, 182]. These algorithms either utilize voltage and current phasor measurements at both ends of a line for online calculation of the transmission line parameters or do not

require the line parameters at all. In [183], PMU measurements are utilized for fault location based on principal component analysis.

In this chapter, two adaptive fault location algorithms are proposed for two-terminal lines as an extension to the work presented in [50] and [66]. In both algorithms, three different sets of pre-fault voltage and current phasor measurements at both terminals of the faulty line are obtained through PMUs. Local PMU measurements at each terminal are then used for online calculation of the respective TE instead of having this piece of information provided by electric power utility which may not be accurate. Aforesaid measurements are also utilized, using the method of multiple measurements with linear regression, for online calculation of the transmission line parameters to obtain the practical operating parameters when fault occurs. This solves the problem that parameters provided by electric power utility are different from the practical parameters due to the running environment and the operation history. In the first proposed algorithm, voltage and current measurements at both terminals prior to and during the fault are needed. Also, applying the principle of superposition, the suddenly changed voltages and currents are utilized to obtain suddenly changed positive voltage and current components to solve the system's impedance at the fault time. The second proposed algorithm differs from the first in the sense that it is independent of the current measurements during the fault to avoid any possible CT saturation.

## **8.2 Proposed adaptive fault location algorithm # 1 (AFLA-1)**

The prime aim of adaptive fault location algorithms is to achieve a better fault location accuracy. The idea of adaptive fault location on transmission lines boils down to proper

estimation of line parameters and system impedance. The surrounding environment and operation history such as overcurrent and overload change the sag of the transmission line. Increasing the current causes the conductor temperature to increase and, consequently, the conductors to elongate and sag. The line resistance changes with the change in the temperature of the line. The reactance is related with the distance between the phase lines that is changed when the sag of the line is changed. [66]

Uncertainty about the line parameters is one of the most severe factors that could impact on the fault location accuracy. The effect of parameters uncertainty on fault location accuracy can reach up to 6.7 % if the parameters used in fault location vary 20 % of the practical parameters. The line parameters will vary not only with the environmental conditions but also with the system operation situations. It is difficult to precisely presage what will happen to the line parameters with the transmission line in service. The parameters provided by the power utility are very ideal and do not reflect the operation history of the line. [66]

In the proposed AFLA-1, the principle of superposition in the linear network theory is applied to separate a post-fault network into a pre-fault network and the superimposed network. Out of the three sets of pre-fault PMU measurements of voltages and currents at both line terminals, the pre-fault network represented by the most recent set of measurements is considered. Superimposed electrical measurements are utilized in the fault location method to reduce the effect of pre-fault load current on fault location accuracy. The superimposed phase network is transformed into sequence electrical measurement network as shown in Figure 8.1.

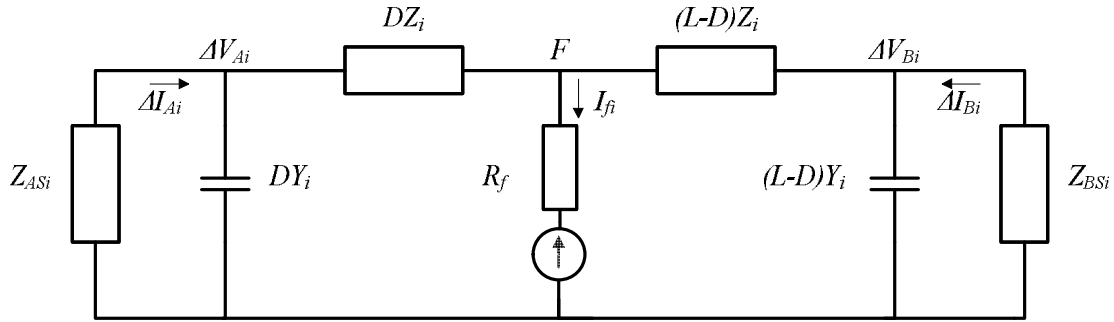


Figure 8.1: Superimposed network of a transmission line

where

- $i$  : The  $i^{\text{th}}$  sequence,  $i=0,1,2$ , namely zero, positive and negative sequence
- $\Delta V_{Ai}$  : The  $i^{\text{th}}$  sequence of superimposed voltage at terminal A
- $\Delta V_{Bi}$  : The  $i^{\text{th}}$  sequence of superimposed voltage at terminal B
- $\Delta I_{Ai}$  : The  $i^{\text{th}}$  sequence of superimposed current at terminal A
- $\Delta I_{Bi}$  : The  $i^{\text{th}}$  sequence of superimposed current at terminal B
- $Z_i$  : The  $i^{\text{th}}$  sequence impedance of the line between terminals A and B
- $Y_i$  : The  $i^{\text{th}}$  sequence admittance of the line between terminals A and B
- $R_f$  : Fault resistance
- $I_{fi}$  : The  $i^{\text{th}}$  sequence of fault current
- $Z_{ASi}$  : The  $i^{\text{th}}$  sequence of terminal A equivalent source impedance
- $Z_{BSi}$  : The  $i^{\text{th}}$  sequence of terminal B equivalent source impedance
- $L$  : The total length of the line
- $D$  : Distance between bus A and fault point F

Assuming that  $dV_{Aj}, dI_{Aj}, dV_{Bj}, dI_{Bj}$  ( $j$  indicates the phase a, b, c) are the superimposed phase measurements, then symmetrical components are obtained using symmetrical components method:

$$\Delta V_{Ai} = M^{-1} \times dV_{Aj} \quad (8.1)$$

$$\Delta I_{Ai} = M^{-1} \times dI_{Aj} \quad (8.2)$$

$$\Delta V_{Bi} = M^{-1} \times dV_{Bj} \quad (8.3)$$

$$\Delta I_{Bi} = M^{-1} \times dI_{Bj} \quad (8.4)$$

where

$$M^{-1} = \frac{1}{3} \begin{bmatrix} 1 & 1 & 1 \\ 1 & e^{j120^\circ} & e^{j240^\circ} \\ 1 & e^{j240^\circ} & e^{j120^\circ} \end{bmatrix} \quad (8.5)$$

The equivalent source impedances are changed according to the change of generation mode of the system. In this fault location algorithm the source impedances are calculated online so that the electrical measurements used in the fault location equation can reflect the practical operation mode. From Figure 8.1, the source impedances are calculated as shown below:

$$Z_{ASi} = \Delta V_{Ai} / \Delta I_{Ai} \quad (8.6)$$

$$Z_{BSi} = \Delta V_{Bi} / \Delta I_{Bi} \quad (8.7)$$

The sequence voltage at the fault resistance can be solved from the suddenly changed sequence voltages at bus A, B and the currents flowing in the transmission from bus A, B respectively as shown below:

$$V_{AFi} = (\Delta I_{Ai} - \Delta V_{Ai} D Y_i) \times \left( \left( Z_{ASi} \parallel \frac{1}{D Y_i} \right) + D Z_i \right) \quad (8.8)$$

$$V_{BFi} = (\Delta I_{Bi} - \Delta V_{Bi} (L - D) Y_i) \times \left( \left( Z_{BSi} \parallel \frac{1}{(L - D) Y_i} \right) + (L - D) Z_i \right) \quad (8.9)$$

Plotting  $|V_{AFi}|$  and  $|V_{BFi}|$  along the entire length of the line, the point of intersection gives the fault distance D. This is depicted in Figures 8.2-8.13 considering all

types of faults occurring on a 200 km long, 230 kV test system. The flow chart of the adaptive fault location algorithm is shown in Figure 8.14.

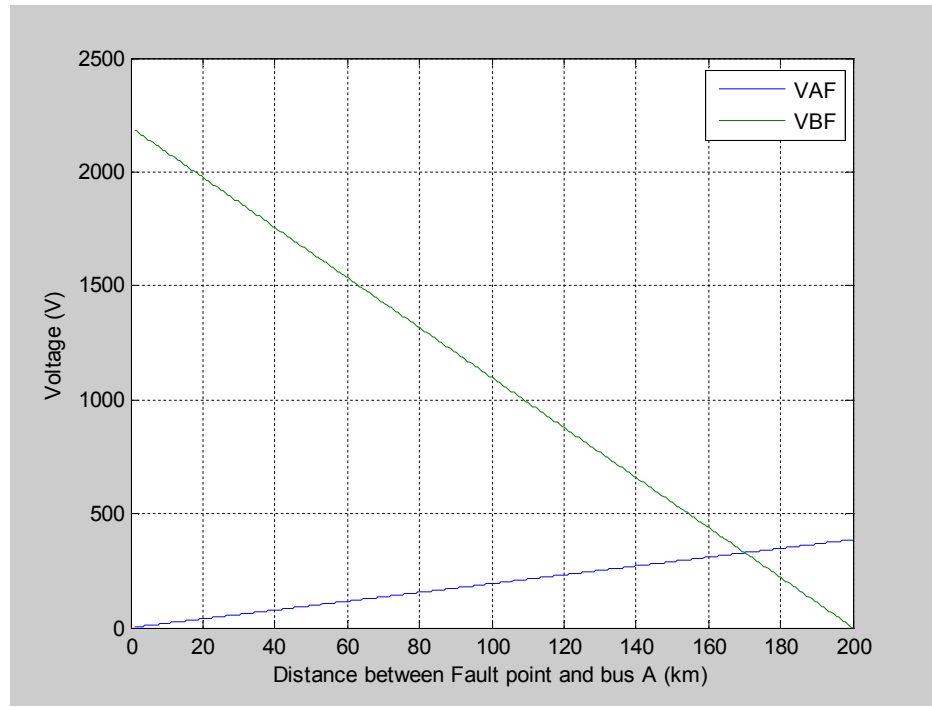


Figure 8.2: Curve of voltage for AG fault at 170 km from bus A

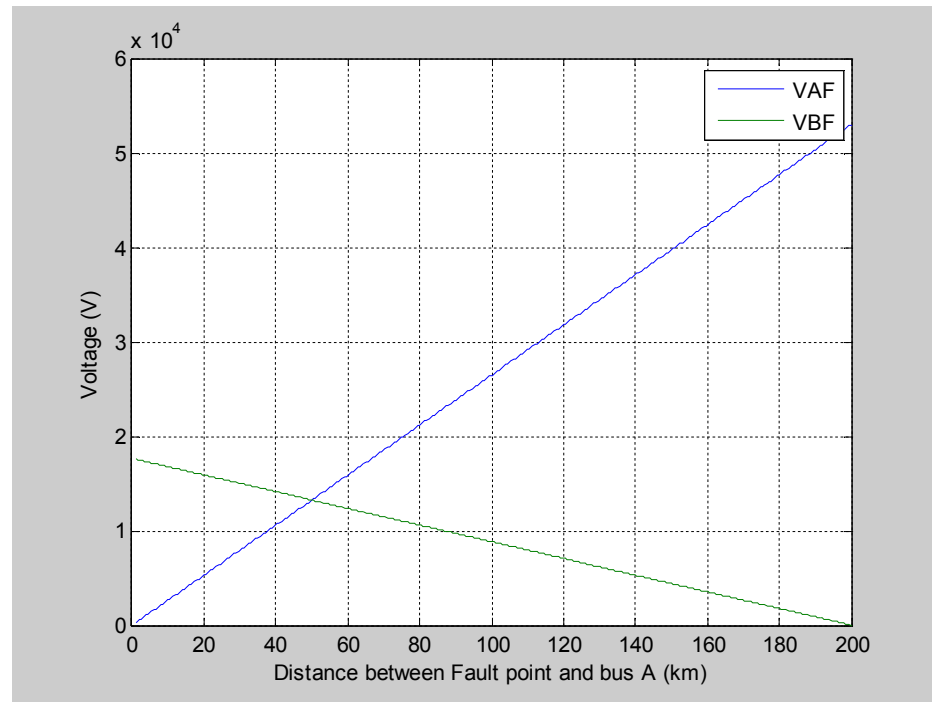


Figure 8.3: Curve of voltage for BG fault at 50 km from bus A

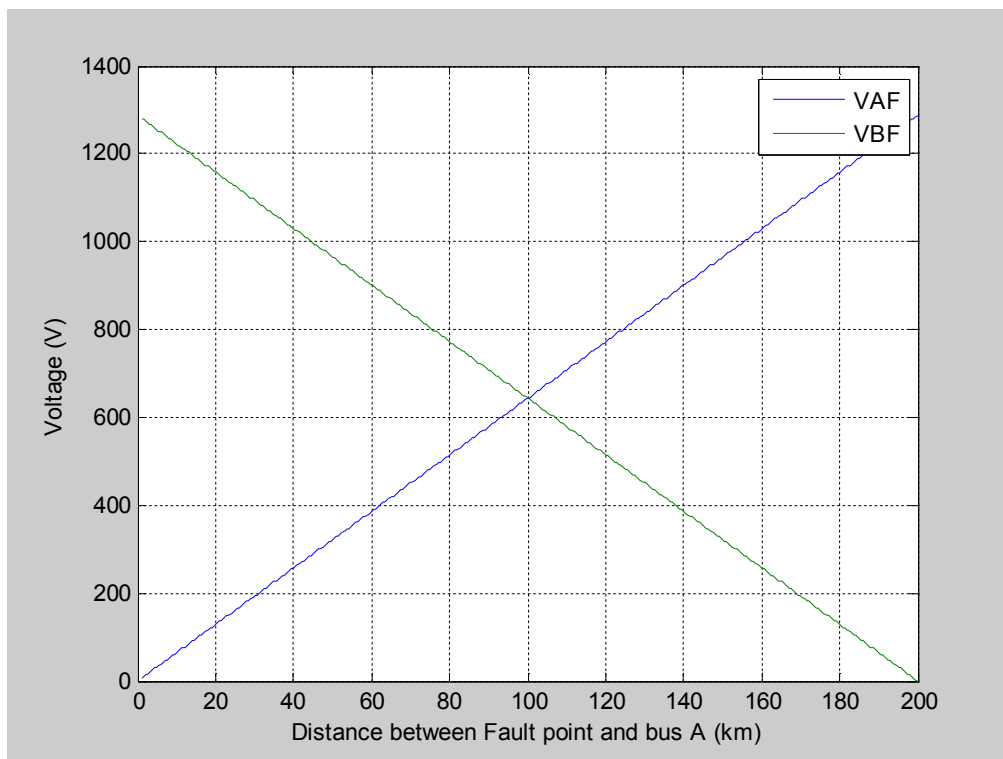


Figure 8.4: Curve of voltage for CG fault at 100 km from bus A

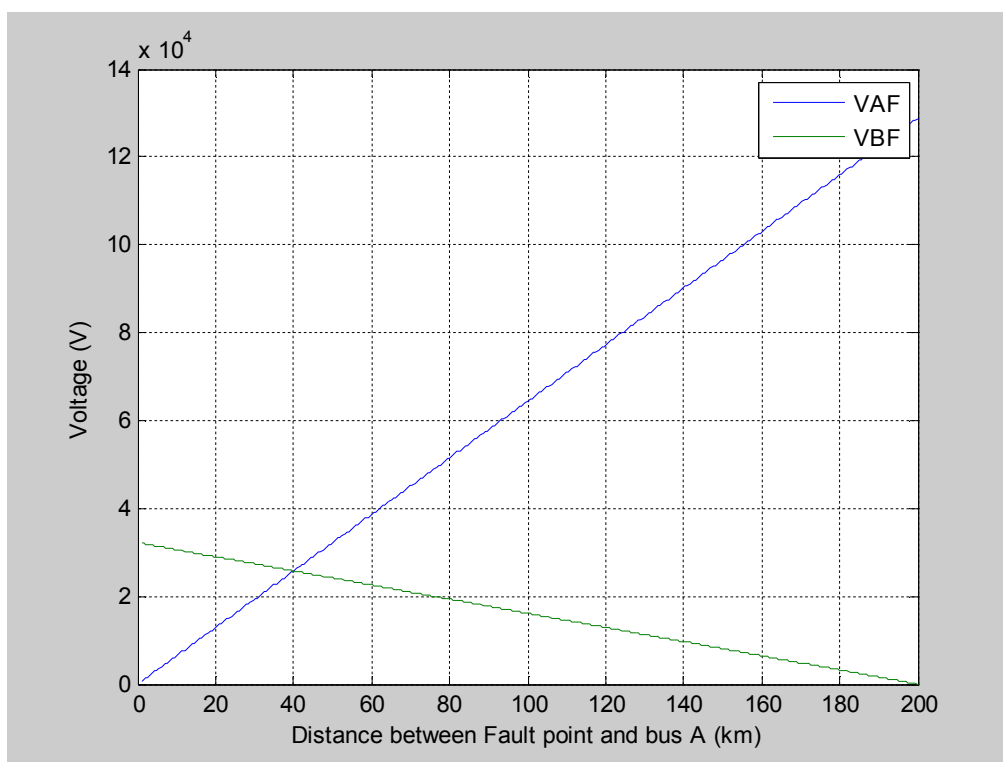


Figure 8.5: Curve of voltage for ABC fault at 40 km from bus A



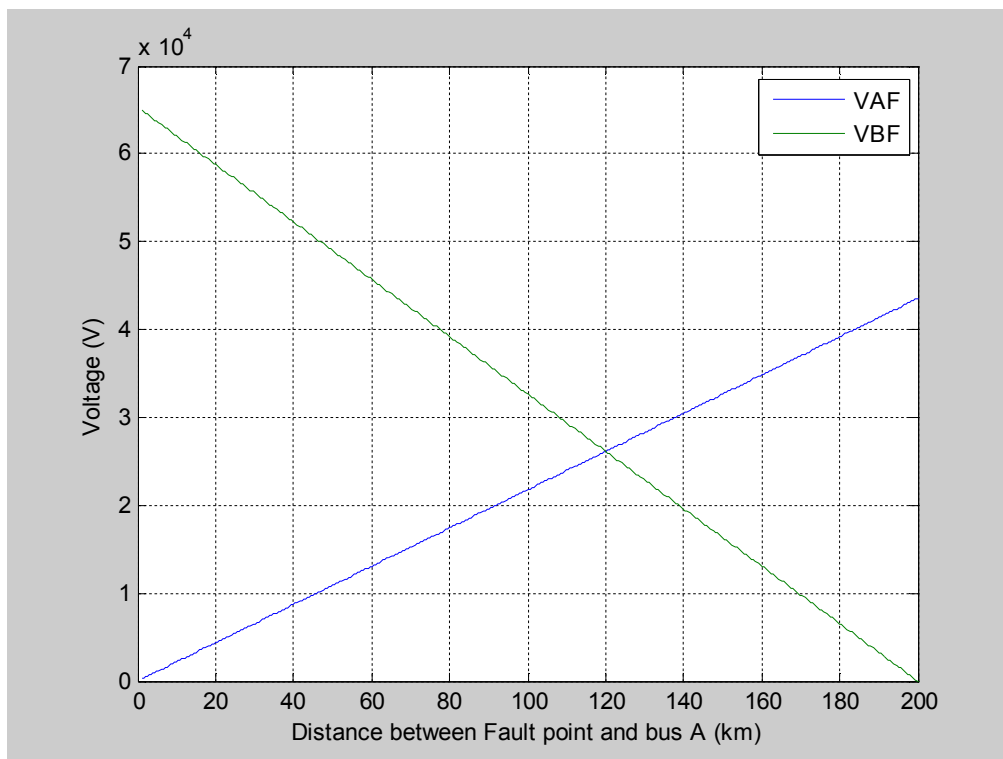


Figure 8.6: Curve of voltage for ABC fault at 120 km from bus A

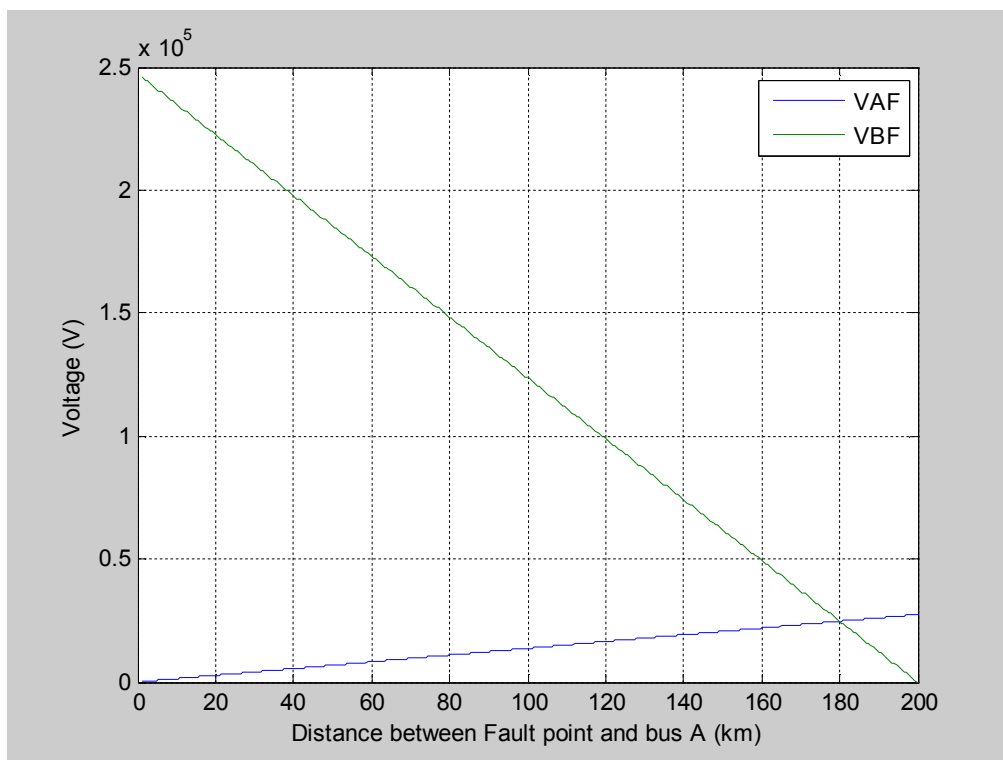


Figure 8.7: Curve of voltage for ABC fault at 180 km from bus A

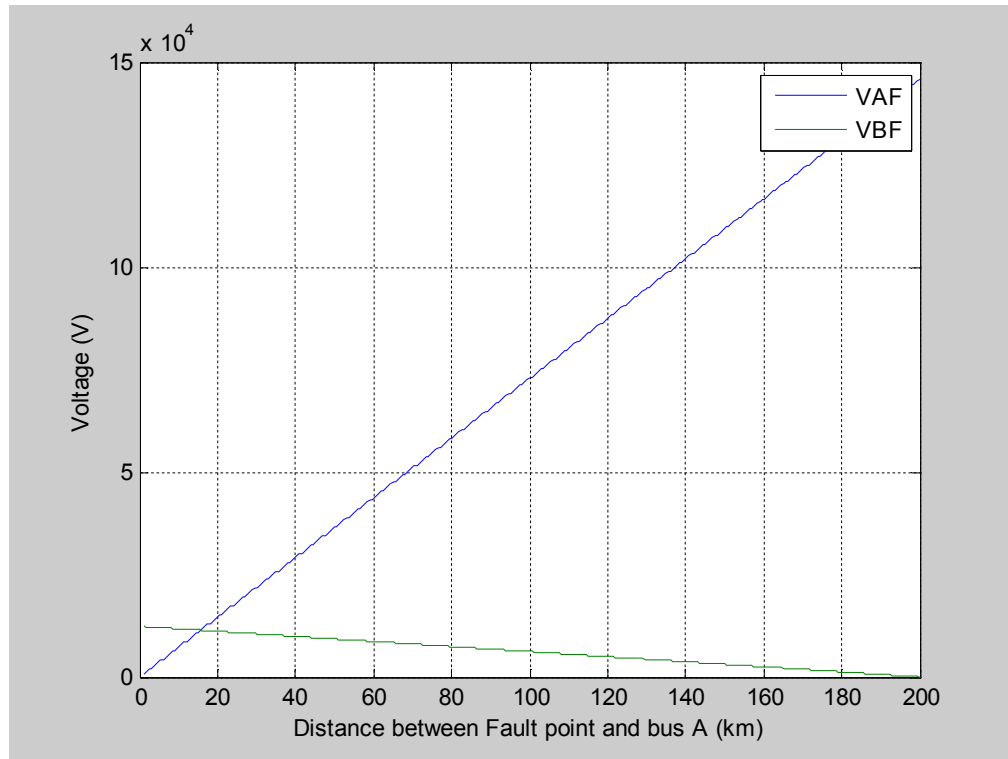


Figure 8.8: Curve of voltage for AC fault at 15 km from bus A

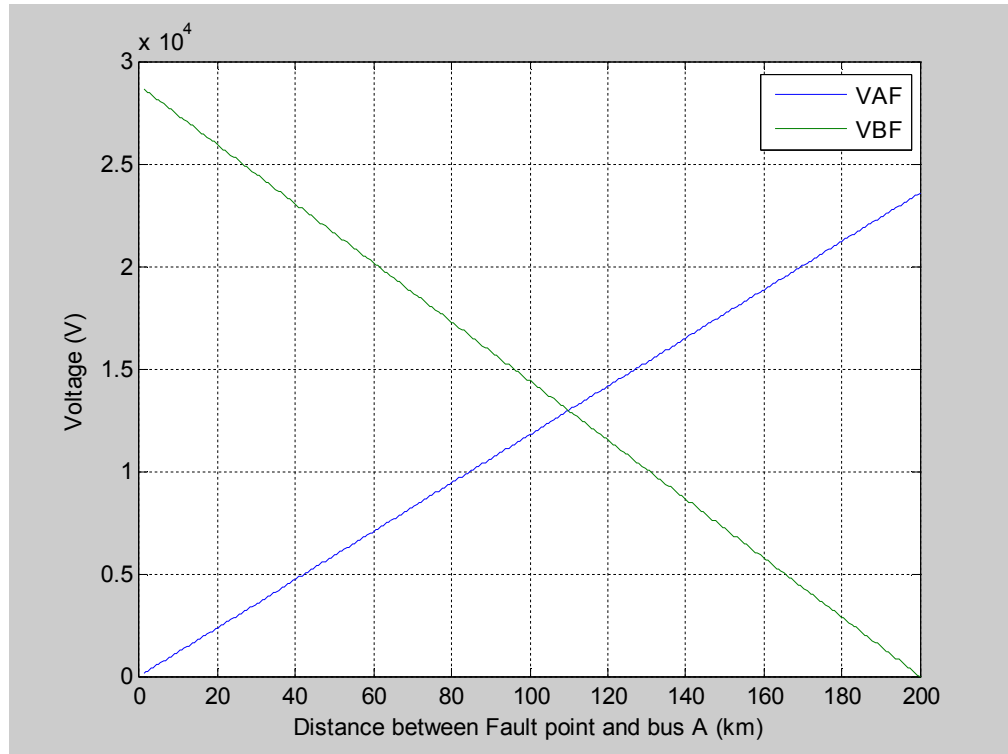


Figure 8.9: Curve of voltage for AB fault at 110 km from bus A

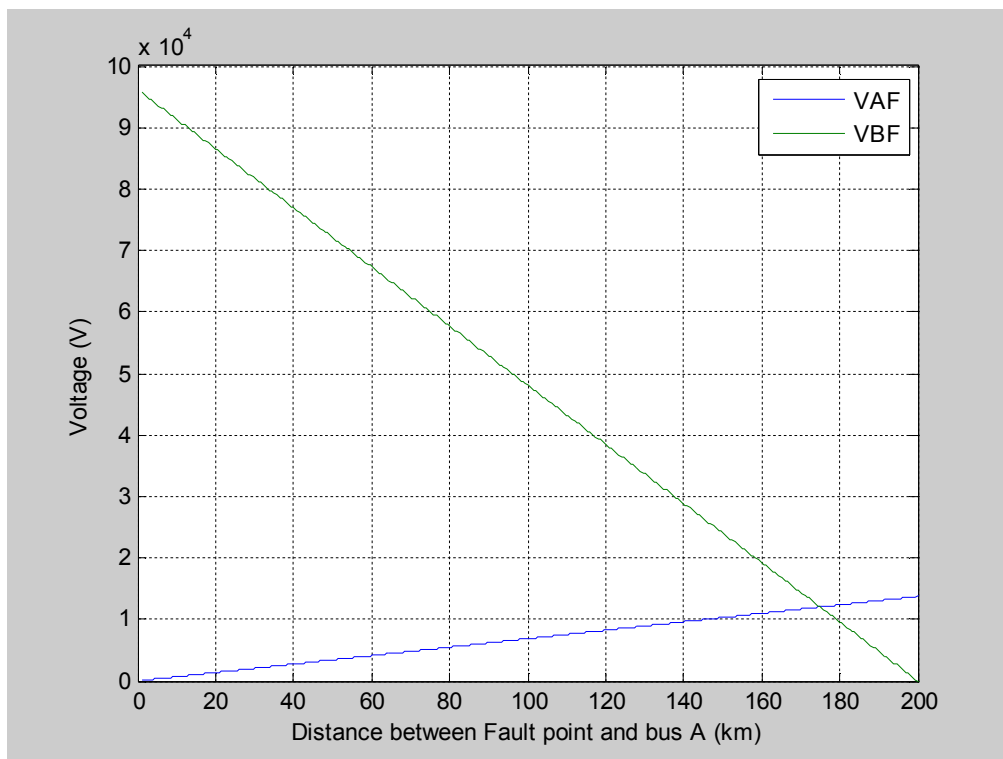


Figure 8.10: Curve of voltage for BC fault at 175 km from bus A

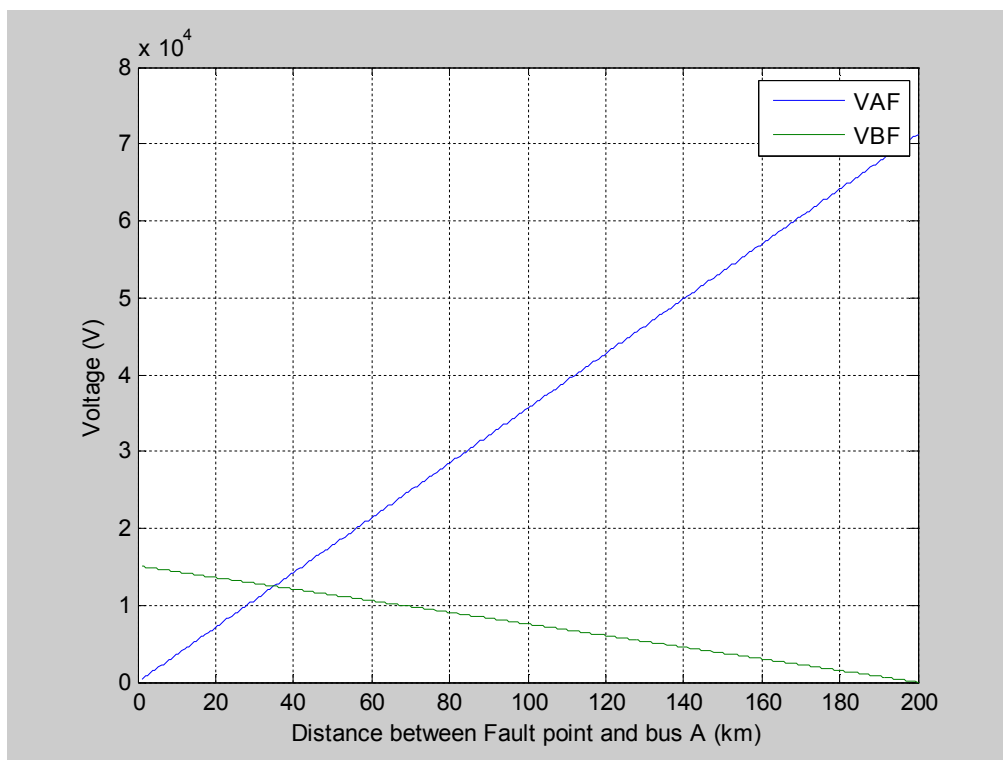


Figure 8.11: Curve of voltage for BCG fault at 35 km from bus A

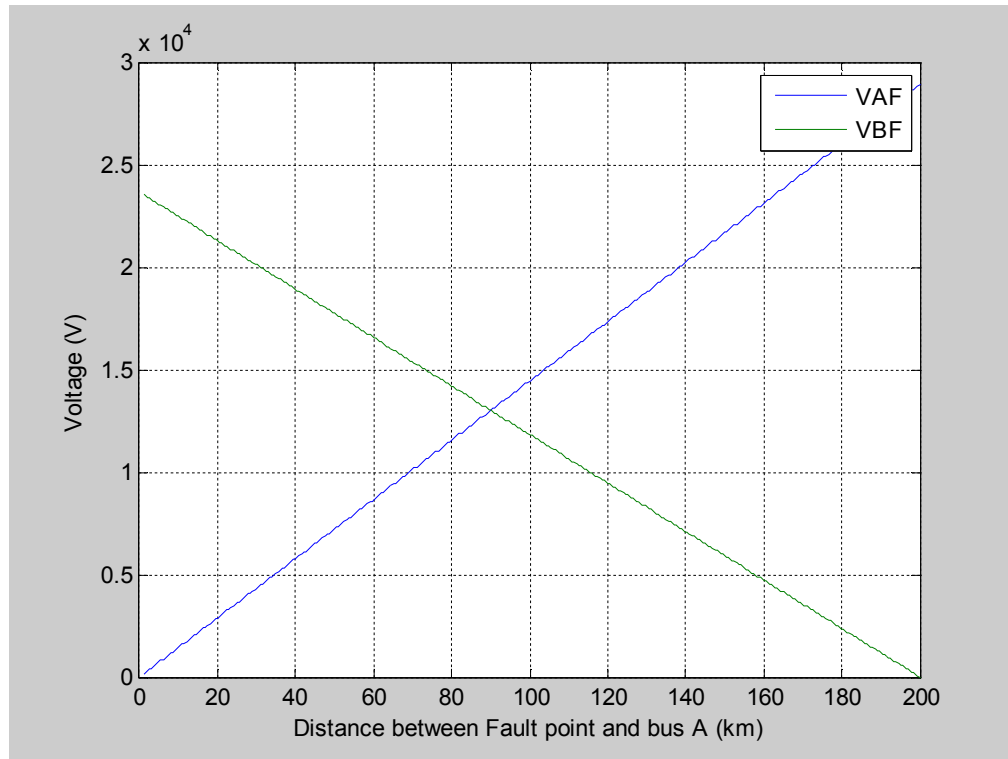


Figure 8.12: Curve of voltage for ABG fault at 90 km from bus A

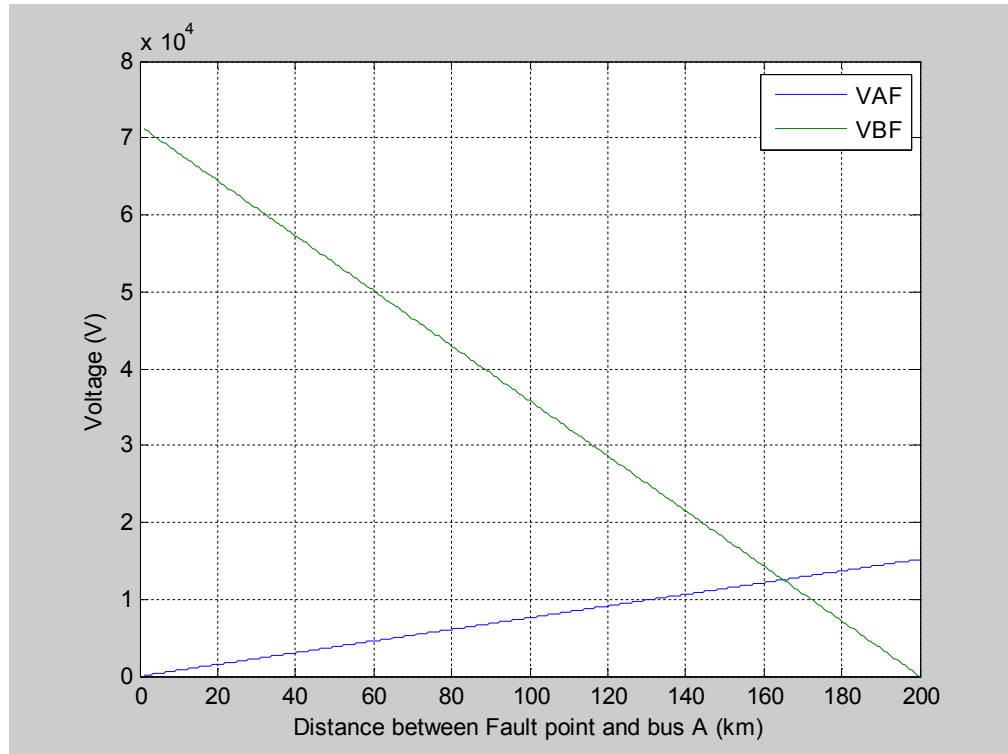


Figure 8.13: Curve of voltage for ACG fault at 165 km from bus A

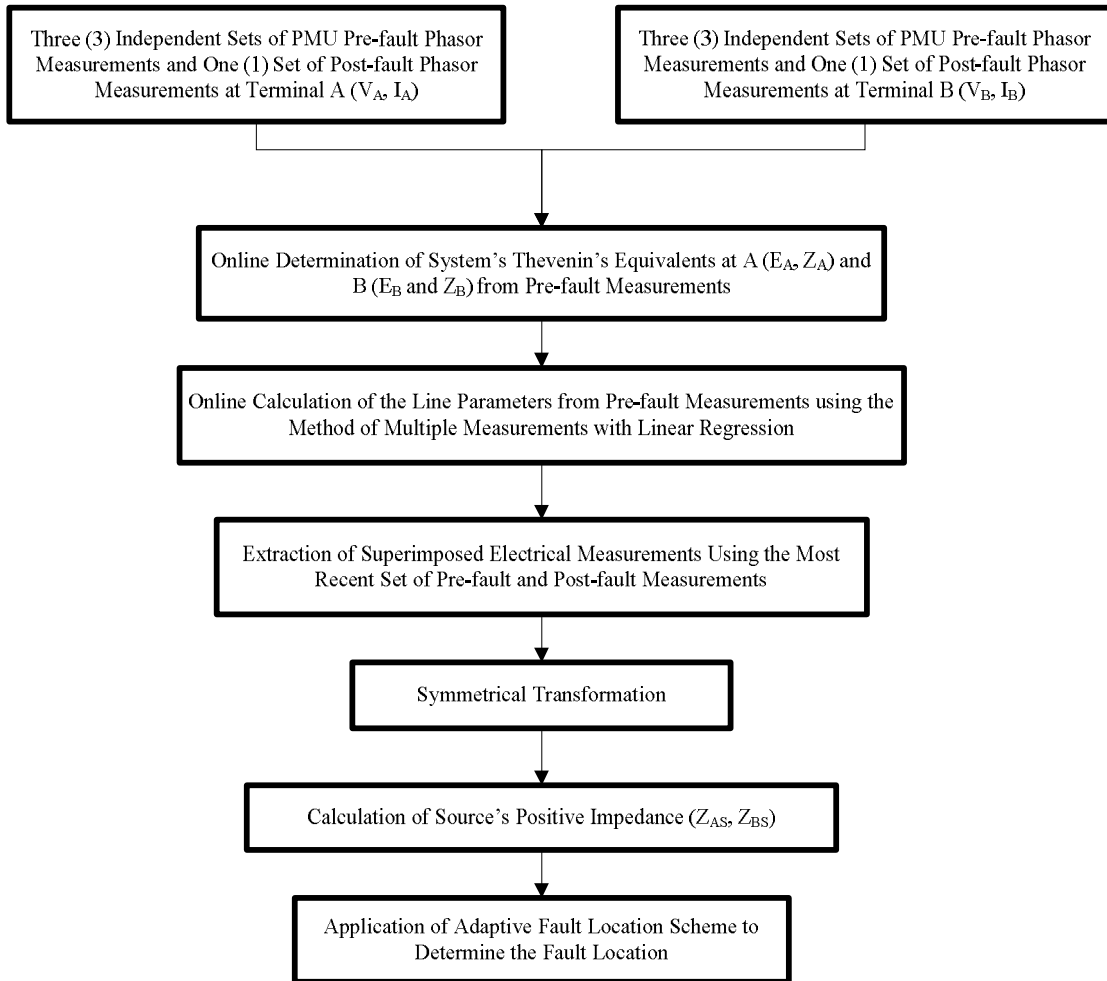


Figure 8.14: Flow chart of AFLA-1

### 8.3 Simulation results of AFLA-1

This section presents the simulation results of AFLA-1 when applied to the 115 kV SEC system and discusses the effect of various factors on the algorithms accuracy.

#### 8.3.1 Data generation and conditioning

The 115 kV SEC system, discussed in chapter 5, is considered under this study. The presented fault location algorithm has been evaluated using pre-fault and post-fault data obtained from reliable PSCAD/EMTDC simulations of faults assumed to occur on the

line connecting bus-38 (A) and bus-30 (B). The line is modeled by the nominal- $\pi$  circuit and its parameters are as shown in Table 8.1. System's Thevenin's impedances at A and B are determined as described in chapter 7 and shown in Figure 7.8 and Figure 7.9 respectively. TE voltages are calculated using (7.1) and shown in Table 8.1. In order to show the errors of the presented algorithm itself, the CTs and VTs located at each line terminal are intentionally assumed as ideal devices. The three-phase voltage and current signals are sampled, as shown in Figure 7.3-7.5, at a frequency of 240 Hz which corresponds to 4 samples per cycle and are stored for post-processing. The DFT given by (3.3) is applied to extract the voltage and current phasors. The proposed algorithm is implemented in MATLAB. In this study, the percentage error used to measure the accuracy of fault location algorithm is expressed as

$$\%Error = \frac{|Actual\ location - Estimated\ location|}{Total\ line\ length} \times 100 \quad (8.10)$$

TABLE 8.1: PARAMETERS OF THE 115 kV, 60 Hz SEC NETWORK

<i>Parameter</i>	<i>Value</i>
$L$	26 km
$Z$	0.014400+j0.07500 p.u. in 100 MVA Base
$Y$	0.012040 p.u. in 100 MVA Base
$E_A$	112.28 kV
$E_B$	112.4 kV

### 8.3.2 Accuracy analysis

To test the accuracy of the proposed algorithm, different type of faults with different fault locations and fault resistances have been simulated. Tables 8.2-8.5 present the fault

location estimates obtained for the single line to ground (LG) faults, line to line (LL) faults, line to line to ground (LLG) faults and three phase (LLL) faults. The fault type, fault resistance and actual fault location are given in the first, second and third column respectively. The estimated distance to fault and the estimation errors resulting from the proposed algorithm are respectively displayed in the fourth and fifth column. From the results obtained, it is observed that the proposed algorithm is very accurate as the maximum error is less than 0.6% for all type of faults.

TABLE 8.2  
AFLA-1: FAULT-LOCATION ESTIMATES FOR SINGLE-LINE-TO-GROUND FAULTS

<i><b>Fault Type</b></i>	<i><b>Fault Res. (<math>\Omega</math>)</b></i>	<i><b>Actual FL (p. u)</b></i>	<i><b>Estimated FL (p. u)</b></i>	<i><b>Error of Estimated FL (%)</b></i>
AG	10	0.2	0.2007	0.3430
		0.4	0.3990	0.2427
		0.6	0.5974	0.4345
		0.8	0.7958	0.5260
	100	0.2	0.2007	0.3419
		0.4	0.3990	0.2430
		0.6	0.5974	0.4345
		0.8	0.7958	0.5259
BG	10	0.2	0.2007	0.3440
		0.4	0.3990	0.2425
		0.6	0.5974	0.4345
		0.8	0.7958	0.5261
	100	0.2	0.2007	0.3520
		0.4	0.3990	0.2410
		0.6	0.5974	0.4354
		0.8	0.7958	0.5283
CG	10	0.2	0.2007	0.3451
		0.4	0.3990	0.2422
		0.6	0.5974	0.4346
		0.8	0.7958	0.5263
	100	0.2	0.2007	0.3616
		0.4	0.3990	0.2395
		0.6	0.5974	0.4365
		0.8	0.7958	0.5305

TABLE 8.3  
AFLA-1: FAULT-LOCATION ESTIMATES FOR LINE-TO-LINE FAULTS

<i><b>Fault Type</b></i>	<i><b>Fault Res. (<math>\Omega</math>)</b></i>	<i><b>Actual FL (p. u)</b></i>	<i><b>Estimated FL (p. u)</b></i>	<i><b>Error of Estimated FL (%)</b></i>
AB	1	0.2	0.2007	0.3429
		0.4	0.3990	0.2427
		0.6	0.5974	0.4344
		0.8	0.7958	0.5258
	10	0.2	0.2007	0.3430
		0.4	0.3990	0.2427
		0.6	0.5974	0.4344
		0.8	0.7958	0.5259
BC	1	0.2	0.2007	0.3433
		0.4	0.3990	0.2425
		0.6	0.5974	0.4344
		0.8	0.7958	0.5258
	10	0.2	0.2007	0.3441
		0.4	0.3990	0.2424
		0.6	0.5974	0.4345
		0.8	0.7958	0.5260
CA	1	0.2	0.2007	0.3434
		0.4	0.3990	0.2426
		0.6	0.5974	0.4345
		0.8	0.7958	0.5260
	10	0.2	0.2007	0.3436
		0.4	0.3990	0.2426
		0.6	0.5974	0.4345
		0.8	0.7958	0.5261



TABLE 8.4  
AFLA-1: FAULT-LOCATION ESTIMATES FOR LINE-TO-LINE-TO-GROUND FAULTS

<i><b>Fault Type</b></i>	<i><b>Fault Res. (<math>\Omega</math>)</b></i>	<i><b>Actual FL (p. u)</b></i>	<i><b>Estimated FL (p. u)</b></i>	<i><b>Error of Estimated FL (%)</b></i>
ABG	5	0.2	0.2007	0.3429
		0.4	0.3990	0.2427
		0.6	0.5974	0.4344
		0.8	0.7958	0.5259
	50	0.2	0.2007	0.3429
		0.4	0.3990	0.2427
		0.6	0.5974	0.4344
		0.8	0.7958	0.5259
BCG	5	0.2	0.2007	0.3433
		0.4	0.3990	0.2426
		0.6	0.5974	0.4344
		0.8	0.7958	0.5258
	50	0.2	0.2007	0.3433
		0.4	0.3990	0.2426
		0.6	0.5974	0.4344
		0.8	0.7958	0.5258
CAG	5	0.2	0.2007	0.3433
		0.4	0.3990	0.2426
		0.6	0.5974	0.4345
		0.8	0.7958	0.5260
	50	0.2	0.2007	0.3433
		0.4	0.3990	0.2426
		0.6	0.5974	0.4345
		0.8	0.7958	0.5260

TABLE 8.5  
AFLA-1: FAULT-LOCATION ESTIMATES FOR THREE-PHASE FAULTS

<i><b>Fault Type</b></i>	<i><b>Fault Res. (<math>\Omega</math>)</b></i>	<i><b>Actual FL (p. u)</b></i>	<i><b>Estimated FL (p. u)</b></i>	<i><b>Error of Estimated FL (%)</b></i>
ABC	1	0.2	0.2007	0.3432
		0.4	0.3990	0.2426
		0.6	0.5974	0.4344
		0.8	0.7958	0.5259
	10	0.2	0.2007	0.3440
		0.4	0.3990	0.2425
		0.6	0.5974	0.4345
		0.8	0.7958	0.5261

### 8.3.3 Influence of the fault resistance

The effect of the variation of the fault resistance in the algorithm's accuracy for all types of LG, LL, LLG and LLL faults are shown respectively in Table 8.6-8.9 assuming that the fault occurs at a distance of 0.8 p. u. from bus-38. Faults involving ground have been investigated for fault resistance values varying from 0 to 500  $\Omega$ . This captures low- and high-resistance faults. Faults not involving ground have been investigated for resistance values ranging between 0 to 30  $\Omega$ . In all cases the local and remote source impedances are set equal to the system values. It can be easily seen that the fault location estimates are highly accurate and virtually independent of the fault resistance.

TABLE 8.6  
AFLA-1: INFLUENCE OF THE FAULT RESISTANCE ON THE ALGORITHM'S ACCURACY FOR  
SINGLE-LINE-TO-GROUND FAULTS (ACTUAL FL: 0.8 P.U.)

<i>Fault Res.</i> ( $\Omega$ )	<i>Fault Type</i>					
	<i>AG</i>		<i>BG</i>		<i>CG</i>	
	<i>Estim. FL</i> (p. u)	<i>Error of Estim. FL</i> (%)	<i>Estim. FL</i> (p. u)	<i>Error of Estim. FL</i> (%)	<i>Estim. FL</i> (p. u)	<i>Error of Estim. FL</i> (%)
0	0.7958	0.5260	0.7958	0.5258	0.7958	0.5258
1	0.7958	0.5260	0.7958	0.5258	0.7958	0.5259
5	0.7958	0.5260	0.7958	0.5259	0.7958	0.5261
10	0.7958	0.5260	0.7958	0.5261	0.7958	0.5263
20	0.7958	0.5260	0.7958	0.5264	0.7958	0.5268
50	0.7958	0.5259	0.7958	0.5271	0.7958	0.5282
100	0.7958	0.5259	0.7958	0.5283	0.7958	0.5305
200	0.7958	0.5258	0.7958	0.5307	0.7957	0.5352
400	0.7958	0.5257	0.7957	0.5356	0.7956	0.5446
500	0.7958	0.5256	0.7957	0.5380	0.7956	0.5493

TABLE 8.7

AFLA-1: INFLUENCE OF THE FAULT RESISTANCE ON THE ALGORITHM'S ACCURACY FOR LINE-TO-LINE FAULTS (ACTUAL FL: 0.8 P.U.)

<i>Fault Res. (<math>\Omega</math>)</i>	<i>Fault Type</i>					
	<i>AB</i>		<i>BC</i>		<i>CA</i>	
	<i>Estim. FL (p. u)</i>	<i>Error of Estim. FL (%)</i>	<i>Estim. FL (p. u)</i>	<i>Error of Estim. FL (%)</i>	<i>Estim. FL (p. u)</i>	<i>Error of Estim. FL (%)</i>
0	0.7958	0.5259	0.7958	0.5257	0.7958	0.5260
0.5	0.7958	0.5259	0.7958	0.5258	0.7958	0.5260
1	0.7958	0.5258	0.7958	0.5258	0.7958	0.5260
2.5	0.7958	0.5258	0.7958	0.5259	0.7958	0.5260
5	0.7958	0.5259	0.7958	0.5259	0.7958	0.5260
7.5	0.7958	0.5259	0.7958	0.5260	0.7958	0.5261
10	0.7958	0.5259	0.7958	0.5260	0.7958	0.5261
15	0.7958	0.5259	0.7958	0.5262	0.7958	0.5261
20	0.7958	0.5259	0.7958	0.5263	0.7958	0.5262
30	0.7958	0.5259	0.7958	0.5265	0.7958	0.5263

TABLE 8.8

AFLA-1: INFLUENCE OF THE FAULT RESISTANCE ON THE ALGORITHM'S ACCURACY FOR LINE-TO-LINE-TO-GROUND FAULTS (ACTUAL FL: 0.8 P.U.)

<i>Fault Res. (<math>\Omega</math>)</i>	<i>Fault Type</i>					
	<i>ABG</i>		<i>BCG</i>		<i>CAG</i>	
	<i>Estim. FL (p. u)</i>	<i>Error of Estim. FL (%)</i>	<i>Estim. FL (p. u)</i>	<i>Error of Estim. FL (%)</i>	<i>Estim. FL (p. u)</i>	<i>Error of Estim. FL (%)</i>
0	0.7958	0.5258	0.7958	0.5258	0.7958	0.5260
1	0.7958	0.5259	0.7958	0.5259	0.7958	0.5260
5	0.7958	0.5259	0.7958	0.5259	0.7958	0.5260
10	0.7958	0.5259	0.7958	0.5259	0.7958	0.5260
25	0.7958	0.5259	0.7958	0.5259	0.7958	0.5260
50	0.7958	0.5259	0.7958	0.5259	0.7958	0.5260
100	0.7958	0.5259	0.7958	0.5259	0.7958	0.5260
150	0.7958	0.5259	0.7958	0.5259	0.7958	0.5260
200	0.7958	0.5259	0.7958	0.5259	0.7958	0.5260
250	0.7958	0.5259	0.7958	0.5259	0.7958	0.5260

TABLE 8.9  
AFLA-1: INFLUENCE OF THE FAULT RESISTANCE ON THE ALGORITHM'S ACCURACY FOR THREE-  
PHASE FAULTS (ACTUAL FL: 0.8 p.u.)

<i><b>Fault Res. (<math>\Omega</math>)</b></i>	<i><b>Estimated FL (p. u)</b></i>	<i><b>Error of Estimated FL (%)</b></i>
0	0.7958	0.5259
0.5	0.7958	0.5259
1	0.7958	0.5259
2.5	0.7958	0.5259
5	0.7958	0.5259
7.5	0.7958	0.5259
10	0.7958	0.5260
15	0.7958	0.5260
20	0.7958	0.5260
30	0.7958	0.5261

### 8.3.4 Influence of the fault inception angle

The effect of the variation of the fault inception angle on the algorithm's accuracy for AG, BC and CAG faults is shown in Table 8.10 assuming that the fault occurs at a distance of 0.6 p. u. from terminal A. Fault inception angle is varied from 0 to 150°. Considering all the cases simulated and presented in aforesaid tables, it is observed that the proposed algorithm is highly accurate and virtually independent of the fault inception angle with an average error of 0.384%, 0.163% and 0.256% for AG, BC and CAG faults respectively. Figure 8.15 depicts the effect of the variation of the fault inception angle on the algorithm's accuracy for aforementioned types of faults occurred at 0.6 p.u. from terminal A.

TABLE 8.10  
AFLA-1: INFLUENCE OF THE FAULT INCEPTION ANGLE ON THE ALGORITHM'S ACCURACY  
(ACTUAL FL: 0.6 P.U.)

<i>Fault Inception Angle (°)</i>	<i>Fault Type</i>					
	<i>AG</i>		<i>BC</i>		<i>CAG</i>	
	<i>Estim. FL (p. u)</i>	<i>Error of Estim. FL (%)</i>	<i>Estim. FL (p. u)</i>	<i>Error of Estim. FL (%)</i>	<i>Estim. FL (p. u)</i>	<i>Error of Estim. FL (%)</i>
0	0.6023	0.3805	0.6011	0.1851	0.6016	0.2669
30	0.6023	0.3784	0.6011	0.1873	0.6016	0.2667
45	0.6022	0.3743	0.6011	0.1890	0.6016	0.2641
60	0.6022	0.3669	0.6011	0.1876	0.6015	0.2570
90	0.6021	0.3547	0.6010	0.1679	0.6014	0.2352
120	0.6023	0.3752	0.6008	0.1330	0.6014	0.2303
135	0.6024	0.4020	0.6007	0.1218	0.6015	0.2476
150	0.6026	0.4399	0.6008	0.1294	0.6017	0.2839

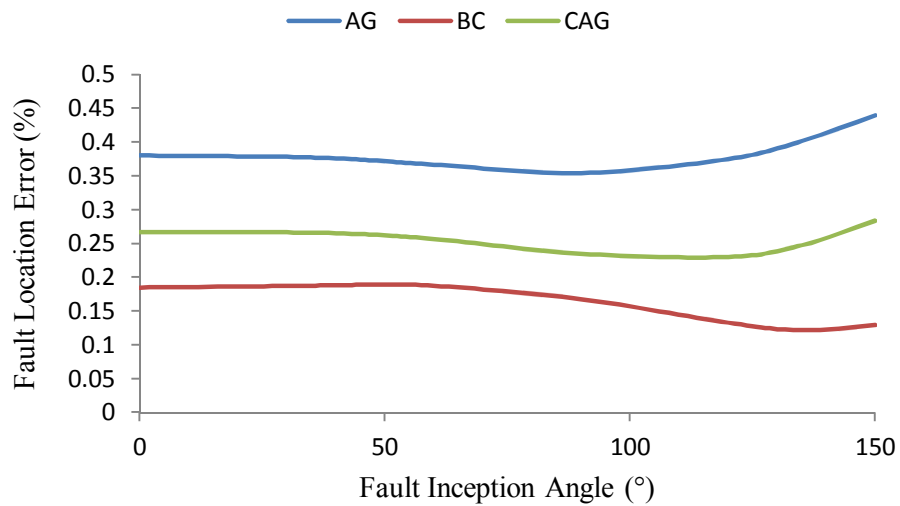


Figure 8.15: AFLA-1: Effect of fault inception angle on FL accuracy (Actual FL: 0.6 p.u.)

### 8.3.5 Influence of the pre-fault loading

Table 8.11 shows the influence of the pre-fault loading on the algorithm's accuracy for AG, BC and CAG faults assuming that these faults occur at 0.6 p.u. distance from terminal A. The pre-fault loading is varied from 0.5 to 3 times its original value.

Considering all the cases simulated and presented in aforesaid tables, it is observed that the proposed algorithm is highly accurate with an average error of 0.492%, 0.296% and 0.378% for AG, BC and CAG faults respectively. Figure 8.15 depicts the effect of the variation of the pre-fault loading on the algorithm's accuracy for aforementioned types of faults.

TABLE 8.11  
AFLA-1: INFLUENCE OF THE PRE-FAULT LOADING AT TERMINAL-A ON THE ALGORITHM'S ACCURACY (ACTUAL FL: 0.6 P.U.)

<i>Variation of Pre-fault Loading (%)</i>	<i>Fault Type</i>					
	<i>AG</i>		<i>BC</i>		<i>CAG</i>	
	<i>Estim. FL (p. u)</i>	<i>Error of Estim. FL (%)</i>	<i>Estim. FL (p. u)</i>	<i>Error of Estim. FL (%)</i>	<i>Estim. FL (p. u)</i>	<i>Error of Estim. FL (%)</i>
-50	0.6016	0.2691	0.6004	0.0735	0.6009	0.1554
-20	0.6020	0.3359	0.6008	0.1404	0.6013	0.2223
20	0.6025	0.4250	0.6014	0.2297	0.6019	0.3115
50	0.6030	0.4918	0.6018	0.2966	0.6023	0.3784
100	0.6036	0.6029	0.6024	0.4080	0.6029	0.4897
200	0.6049	0.8250	0.6038	0.6306	0.6043	0.7120

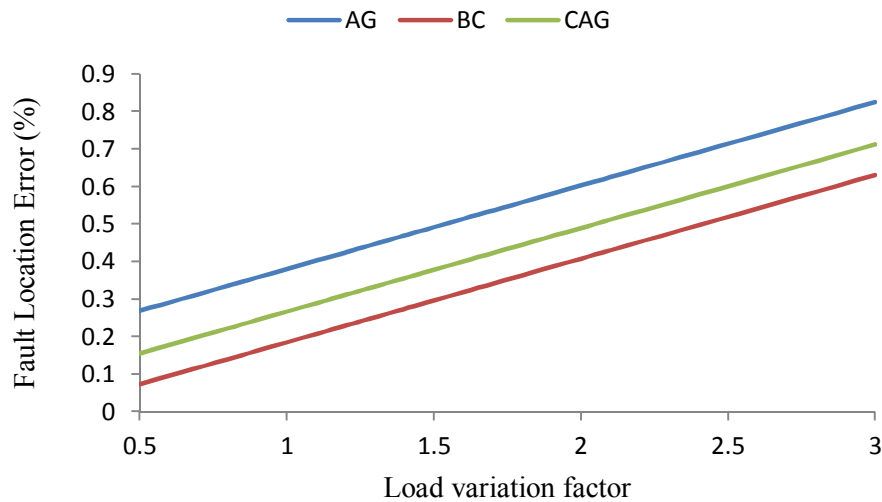


Figure 8.16: AFLA-1: Effect of pre-fault loading on FL accuracy (Actual FL: 0.6 p.u.)

### 8.3.6 Error analysis

Since both CTs and VTs may introduce errors in practice, we elect to carry out error analysis to study the impacts of measurement errors on the proposed algorithm. In this study, error of 2% for magnitude and 2° for angle are added to the voltages and currents measured at the line ends. Errors on fault location estimates are then investigated for all types of LG faults.

TABLE 8.12  
AFLA-1: INFLUENCE OF 2% VOLTAGE MAGNITUDE ERROR ON FAULT-LOCATION ESTIMATES  
FOR SINGLE-LINE-TO-GROUND FAULTS

<i><b>Fault Type</b></i>	<i><b>Fault Res. (<math>\Omega</math>)</b></i>	<i><b>Actual FL (p. u)</b></i>	<i><b>Estimated FL (p. u)</b></i>	<i><b>Error of Estimated FL (%)</b></i>
AG	10	0.2	0.2007	0.3421
		0.4	0.3990	0.2430
		0.6	0.5974	0.4344
		0.8	0.7958	0.5257
	100	0.2	0.2007	0.3411
		0.4	0.3990	0.2433
		0.6	0.5974	0.4345
		0.8	0.7958	0.5256
BG	10	0.2	0.2007	0.3431
		0.4	0.3990	0.2427
		0.6	0.5974	0.4345
		0.8	0.7958	0.5258
	100	0.2	0.2007	0.3511
		0.4	0.3990	0.2413
		0.6	0.5974	0.4353
		0.8	0.7958	0.5280
CG	10	0.2	0.2007	0.3442
		0.4	0.3990	0.2425
		0.6	0.5974	0.4346
		0.8	0.7958	0.5260
	100	0.2	0.2007	0.3608
		0.4	0.3990	0.2397
		0.6	0.5974	0.4364
		0.8	0.7958	0.5302

Table 8.12 and 8.13 present the results for a 2% error in the magnitude of the voltage and current measurements at both ends of the line respectively. Table 8.14 and 8.15 present the results for a 2° error in the angle of the voltage and current measurements at both ends of the line respectively. It can be seen that measurement errors within the range specified above had almost no impact on the fault location accuracy.

TABLE 8.13  
AFLA-1: INFLUENCE OF 2° VOLTAGE ANGLE ERROR ON FAULT-LOCATION ESTIMATES FOR  
SINGLE-LINE-TO-GROUND FAULTS

<i><b>Fault Type</b></i>	<i><b>Fault Res. (Ω)</b></i>	<i><b>Actual FL (p. u)</b></i>	<i><b>Estimated FL (p. u)</b></i>	<i><b>Error of Estimated FL (%)</b></i>
AG	10	0.2	0.2007	0.3429
		0.4	0.3990	0.2428
		0.6	0.5974	0.4345
		0.8	0.7958	0.5260
	100	0.2	0.2007	0.3419
		0.4	0.3990	0.2430
		0.6	0.5974	0.4345
		0.8	0.7958	0.5259
BG	10	0.2	0.2007	0.3439
		0.4	0.3990	0.2425
		0.6	0.5974	0.4345
		0.8	0.7958	0.5261
	100	0.2	0.2007	0.3519
		0.4	0.3990	0.2411
		0.6	0.5974	0.4354
		0.8	0.7958	0.5283
CG	10	0.2	0.2007	0.3450
		0.4	0.3990	0.2422
		0.6	0.5974	0.4346
		0.8	0.7958	0.5263
	100	0.2	0.2007	0.3616
		0.4	0.3990	0.2395
		0.6	0.5974	0.4365
		0.8	0.7958	0.5305



TABLE 8.14  
AFLA-1: INFLUENCE OF 2% CURRENT MAGNITUDE ERROR ON FAULT-LOCATION ESTIMATES  
FOR SINGLE-LINE-TO-GROUND FAULTS

<i><b>Fault Type</b></i>	<i><b>Fault Res. (<math>\Omega</math>)</b></i>	<i><b>Actual FL (p. u)</b></i>	<i><b>Estimated FL (p. u)</b></i>	<i><b>Error of Estimated FL (%)</b></i>
AG	10	0.2	0.2007	0.3438
		0.4	0.3990	0.2425
		0.6	0.5974	0.4345
		0.8	0.7958	0.5262
	100	0.2	0.2007	0.3428
		0.4	0.3990	0.2428
		0.6	0.5974	0.4346
		0.8	0.7958	0.5262
BG	10	0.2	0.2007	0.3448
		0.4	0.3990	0.2422
		0.6	0.5974	0.4346
		0.8	0.7958	0.5263
	100	0.2	0.2007	0.3528
		0.4	0.3990	0.2408
		0.6	0.5974	0.4354
		0.8	0.7958	0.5285
CG	10	0.2	0.2007	0.3459
		0.4	0.3990	0.2420
		0.6	0.5974	0.4347
		0.8	0.7958	0.5266
	100	0.2	0.2007	0.3625
		0.4	0.3990	0.2392
		0.6	0.5974	0.4365
		0.8	0.7958	0.5308

TABLE 8.15  
AFLA-1: INFLUENCE OF 2° CURRENT ANGLE ERROR ON FAULT-LOCATION ESTIMATES FOR  
SINGLE-LINE-TO-GROUND FAULTS

<i><b>Fault Type</b></i>	<i><b>Fault Res. (<math>\Omega</math>)</b></i>	<i><b>Actual FL (p. u)</b></i>	<i><b>Estimated FL (p. u)</b></i>	<i><b>Error of Estimated FL (%)</b></i>
AG	10	0.2	0.2007	0.3430
		0.4	0.3990	0.2427
		0.6	0.5974	0.4344
		0.8	0.7958	0.5259
	100	0.2	0.2007	0.3420
		0.4	0.3990	0.2430
		0.6	0.5974	0.4345
		0.8	0.7958	0.5259
BG	10	0.2	0.2007	0.3440
		0.4	0.3990	0.2424
		0.6	0.5974	0.4345
		0.8	0.7958	0.5261
	100	0.2	0.2007	0.3521
		0.4	0.3990	0.2410
		0.6	0.5974	0.4354
		0.8	0.7958	0.5282
CG	10	0.2	0.2007	0.3452
		0.4	0.3990	0.2422
		0.6	0.5974	0.4346
		0.8	0.7958	0.5263
	100	0.2	0.2007	0.3617
		0.4	0.3990	0.2394
		0.6	0.5974	0.4364
		0.8	0.7958	0.5305

#### 8.4 Proposed adaptive fault location algorithm # 2 (AFLA-2)

As pointed out earlier, this algorithm is proposed to be independent of current measurements during the fault in order to avoid possible errors resulting from CT saturation. Figure 8.17 displays a single line diagram of a faulted two-terminal transmission line represented with its  $\pi$ -equivalent model. If the line has a length  $L$  and assuming that an unknown fault is occurred at a distance of  $D_1$  from the sending end (A) and  $D_2$  from the receiving end (B) of the line, then we may model the pre-fault circuit as

shown earlier in Figure 8.1 and post-fault circuit as depicted in Figure 8.18 with all parameters in the three phase form (abc). [50]

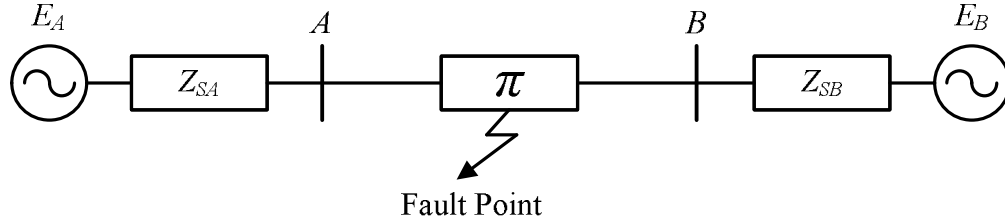


Figure 8.17: A faulted power system

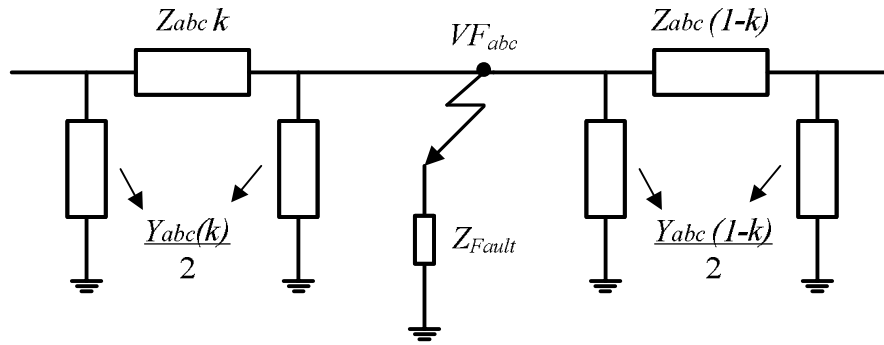


Figure 8.18: Transmission line model in post-fault

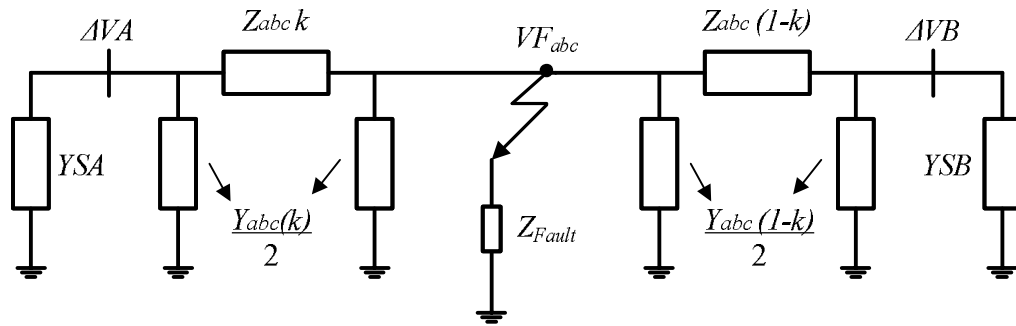


Figure 8.19: Thevenin equivalent model of the faulted system

Considering the post fault conditions, the transmission line is separated into two parts with distances of  $D_1$  and  $D_2$  from each end of the line, we define thereby:

$$k = \frac{D_1}{L}, \quad (1 - k) = \frac{D_2}{L} \quad (8.11)$$

The Thevenin's equivalent model of the faulted system is shown in Figure 8.19 where  $YSA$  and  $YSB$  represent the Thevenin's admittance of bus A and B respectively. Bus voltages at the line terminals A and B vary between pre-fault and post-fault system conditions and they are equal to post-fault voltages minus pre-fault voltages. Knowing the voltage variations at bus A ( $\Delta VA$ ) and bus B ( $\Delta VB$ ), the system equations can be written as:

$$IA_{abc} = \begin{bmatrix} IA_a \\ IA_b \\ IA_c \end{bmatrix}, \quad IB_{abc} = \begin{bmatrix} IB_a \\ IB_b \\ IB_c \end{bmatrix} \quad (8.12)$$

$$IA_{abc} = \left[ YSA_{abc} + \frac{Y_{abc}}{2} k \right] \Delta VA_{abc} \quad (8.13)$$

$$IB_{abc} = \left[ YSB_{abc} + \frac{Y_{abc}}{2} (1 - k) \right] \Delta VB_{abc}$$

Using (3.4), the phasor currents given by (8.13) can then be transformed into symmetrical components to get:

$$IA_{012} = \left[ YSA_{012} + \frac{Y_{012}}{2} k \right] \Delta VA_{012} \quad (8.14)$$

$$IB_{012} = \left[ YSB_{012} + \frac{Y_{012}}{2} (1 - k) \right] \Delta VB_{012}$$

Expressing the phasor fault-point voltages ( $VF_{abc}$ ) in terms of  $\Delta VA_{abc}$  and  $\Delta VB_{abc}$  and then applying symmetrical transformation, we get:

$$VF_{012} = Z_{012} IA_{012} k + \Delta VA_{012} \quad (8.15)$$

$$VF_{012} = Z_{012} IB_{012} (1 - k) + \Delta VB_{012}$$

To derive equations independent of the post-fault current, we substitute  $IA_{012}$  and  $IB_{012}$  from (8.14) into (8.15) to obtain:

$$\begin{aligned} \left[ I_{3 \times 3} + kZ_{012} \left[ YSA_{012} + \frac{Y_{012}}{2}k \right] \right] \Delta VA_{012} = \\ \left[ I_{3 \times 3} + (1-k)Z_{012} \left[ YSB_{012} + \frac{Y_{012}}{2}(1-k) \right] \right] \Delta VB_{012} \end{aligned} \quad (8.16)$$

Equation (8.16) can be put in a form of (8.17) with complex coefficients as shown in (8.18):

$$ak^2 + bk + c = 0 \quad (8.17)$$

$$\begin{aligned} [a]_{3 \times 1} &= Z_{012} \frac{Y_{012}}{2} [\Delta VA_{012} - \Delta VB_{012}] \\ [b]_{3 \times 1} &= Z_{012} [YSA_{012} \Delta VA_{012} + YSB_{012} \Delta VB_{012}] + Z_{012} Y_{012} \Delta VB_{012} \end{aligned} \quad (8.18)$$

$$[c]_{3 \times 1} = [\Delta VA_{012} - \Delta VB_{012}] - Z_{012} \left[ YSB_{012} + \frac{Y_{012}}{2} \right] \Delta VB_{012}$$

Due to symmetric consideration of the system such as in generators, impedances, series impedance and parallel admittance of transmission line, equation (8.17) can be separated into three equations as:

$$a_i k^2 + b_i k + c_i; \quad i = 0, 1, 2 \quad (8.19)$$

It is clear that the proposed equations have unique solutions. By substituting  $k$  in (8.11), we obtain the estimated fault-point distance. The flow chart of the adaptive fault location algorithm is shown in Figure 8.20.

## 8.5 Simulation results of AFLA-2

This section presents the simulation results of AFLA-2 when applied to the 115 kV SEC system and discusses the effect of various factors on the algorithms accuracy.

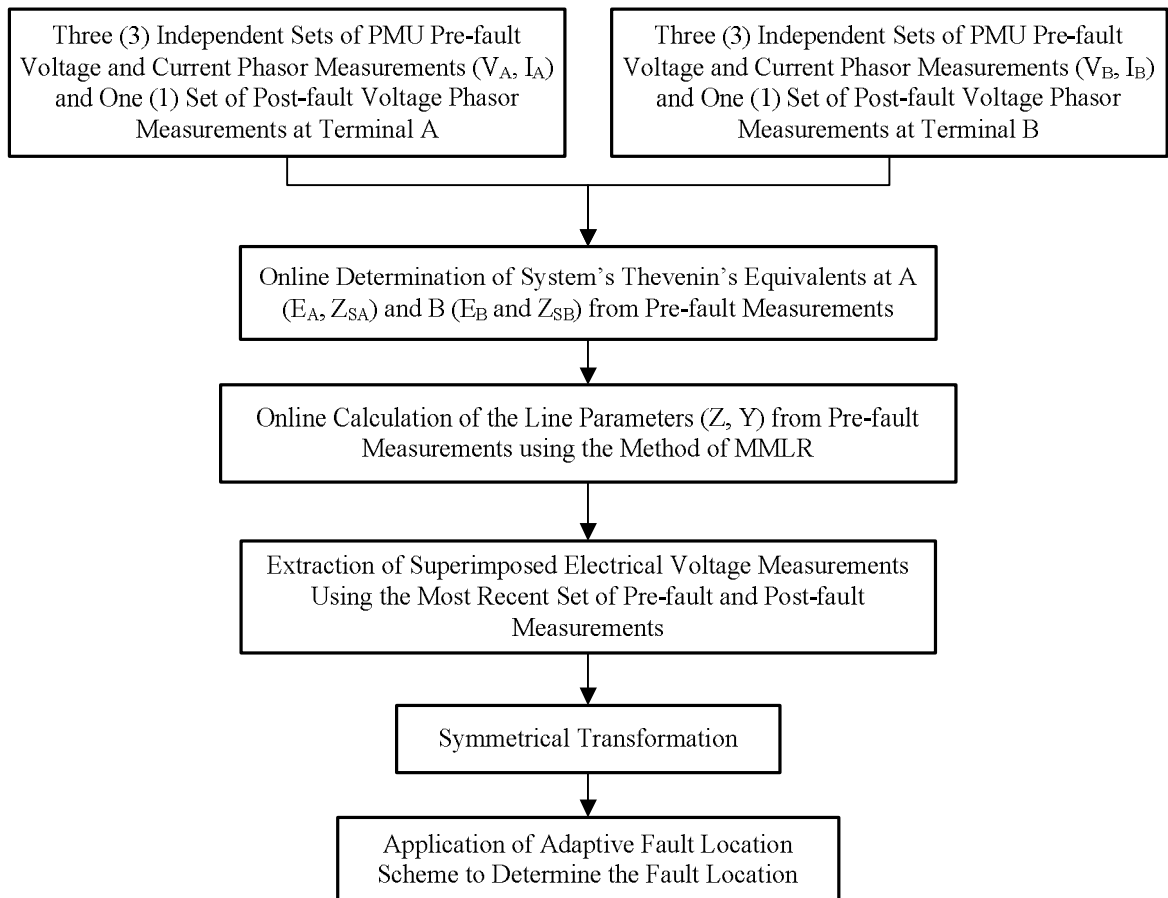


Figure 8.20: Flow chart of AFLA-2

### 8.5.1 Data generation and conditioning

The 115 kV SEC system, discussed in chapter 5, is considered under this study. The presented fault location algorithm has been evaluated using pre-fault and post-fault data obtained from reliable PSCAD/EMTDC simulations of faults assumed to occur on the line connecting bus-38 (A) and bus-30 (B). The line is modeled by the nominal- $\pi$  circuit and its parameters are as shown in Table 8.1. System's Thevenin's impedances at A and B are determined as described in chapter 7 and shown in Figure 7.8 and Figure 7.9 respectively. TE voltages are calculated using (7.1) and shown in Table 8.1. In order to show the errors of the presented algorithm itself, the CTs and VTs located at each line terminal are intentionally assumed as ideal devices. The three-phase voltage and current signals are sampled, as shown in Figure 7.3-7.5, at a frequency of 240 Hz which corresponds to 4 samples per cycle and are stored for post-processing. The DFT given by (3.3) is applied to extract the voltage and current phasors. The proposed algorithm is implemented in MATLAB. The percentage error used to measure the accuracy of fault location algorithm is as expressed in (8.10)

### 8.5.2 Accuracy analysis

To test the accuracy of the proposed algorithm, different type of faults with different fault locations and fault resistances have been simulated. Tables 8.16-8.19 present the fault location estimates obtained for the single line to ground (LG) faults, line to line (LL) faults, line to line to ground (LLG) faults and three phase (LLL) faults. The fault type, fault resistance and actual fault location are given in the first, second and third column respectively. The estimated distance to fault and the estimation errors resulting from the proposed algorithm are respectively displayed in the fourth and fifth column. From the

results obtained, it is observed that the proposed algorithm is very accurate as the maximum error is less than 0.9% for all type of faults.

TABLE 8.16  
AFLA-2: FAULT-LOCATION ESTIMATES FOR SINGLE-LINE-TO-GROUND FAULTS

<i><b>Fault Type</b></i>	<i><b>Fault Res. (<math>\Omega</math>)</b></i>	<i><b>Actual FL (p. u)</b></i>	<i><b>Estimated FL (p. u)</b></i>	<i><b>Error of Estimated FL (%)</b></i>
AG	10	0.2	0.19996	0.0037
		0.4	0.39989	0.0107
		0.6	0.59985	0.0146
		0.8	0.79983	0.0169
	100	0.2	0.19997	0.0025
		0.4	0.39993	0.0065
		0.6	0.59986	0.0136
		0.8	0.79978	0.0219
BG	10	0.2	0.19553	0.4465
		0.4	0.39612	0.3875
		0.6	0.59702	0.2977
		0.8	0.79823	0.1738
	100	0.2	0.19555	0.4446
		0.4	0.39619	0.3813
		0.6	0.59714	0.2857
		0.8	0.79829	0.1704
CG	10	0.2	0.19125	0.8751
		0.4	0.39260	0.7403
		0.6	0.59452	0.5477
		0.8	0.79697	0.3024
	100	0.2	0.19125	0.8751
		0.4	0.39258	0.7423
		0.6	0.59454	0.5458
		0.8	.79699	0.3009



TABLE 8.17  
AFLA-2: FAULT-LOCATION ESTIMATES FOR SINGLE-LINE-TO-LINE FAULTS

<i><b>Fault Type</b></i>	<i><b>Fault Res. (<math>\Omega</math>)</b></i>	<i><b>Actual FL (p. u)</b></i>	<i><b>Estimated FL (p. u)</b></i>	<i><b>Error of Estimated FL (%)</b></i>
AB	1	0.2	0.19755	0.2452
		0.4	0.39785	0.2146
		0.6	0.59845	0.1554
		0.8	0.79929	0.0711
	10	0.2	0.19743	0.2565
		0.4	0.39756	0.2438
		0.6	0.59798	0.2015
		0.8	0.79874	0.1262
BC	1	0.2	0.19312	0.6880
		0.4	0.39403	0.5966
		0.6	0.59553	0.4472
		0.8	0.79761	0.2388
	10	0.2	0.19311	0.6890
		0.4	0.39393	0.6065
		0.6	0.59532	0.4680
		0.8	0.79733	0.2669
CA	1	0.2	0.19733	0.2672
		0.4	0.39798	0.2019
		0.6	0.59859	0.1405
		0.8	0.79924	0.0764
	10	0.2	0.19732	0.2677
		0.4	0.39800	0.2001
		0.6	0.59867	0.1325
		0.8	0.79934	0.0654

TABLE 8.18  
AFLA-2: FAULT-LOCATION ESTIMATES FOR LINE-TO-LINE-TO-GROUND FAULTS

<i><b>Fault Type</b></i>	<i><b>Fault Res. (<math>\Omega</math>)</b></i>	<i><b>Actual FL (p. u)</b></i>	<i><b>Estimated FL (p. u)</b></i>	<i><b>Error of Estimated FL (%)</b></i>
ABG	5	0.2	0.19805	0.1950
		0.4	0.39854	0.1461
		0.6	0.59899	0.1006
		0.8	0.79959	0.0414
	50	0.2	0.19764	0.2360
		0.4	0.39796	0.2038
		0.6	0.59853	0.1471
		0.8	0.79933	0.0670
BCG	5	0.2	0.19362	0.6381
		0.4	0.39453	0.5469
		0.6	0.59591	0.4088
		0.8	0.79780	0.2196
	50	0.2	0.19321	0.6791
		0.4	0.39412	0.5883
		0.6	0.59558	0.4415
		0.8	0.79764	0.2360
CAG	5	0.2	0.19590	0.4094
		0.4	0.39659	0.3410
		0.6	0.59749	0.2511
		0.8	0.79863	0.1374
	50	0.2	0.19709	0.2908
		0.4	0.39777	0.2232
		0.6	0.59844	0.1561
		0.8	0.79916	0.0841

TABLE 8.19  
AFLA-2: FAULT-LOCATION ESTIMATES FOR THREE-PHASE FAULTS

<i><b>Fault Type</b></i>	<i><b>Fault Res. (<math>\Omega</math>)</b></i>	<i><b>Actual FL (p. u)</b></i>	<i><b>Estimated FL (p. u)</b></i>	<i><b>Error of Estimated FL (%)</b></i>
ABC	1	0.2	0.19599	0.4012
		0.4	0.39659	0.3413
		0.6	0.59745	0.2546
		0.8	0.79863	0.1366
	10	0.2	0.19597	0.4032
		0.4	0.39651	0.3492
		0.6	0.59735	0.2647
		0.8	0.79849	0.1507

### 8.5.3 Influence of the fault resistance

The effect of the variation of the fault resistance in the algorithm's accuracy for all types of LG, LL, LLG and LLL faults are shown respectively in Table 8.20-8.23 assuming that the fault occurs at a distance of 0.8 p. u. from bus-38. Faults involving ground have been investigated for fault resistance values varying from 0 to 500  $\Omega$ . This captures low- and high-resistance faults. Faults not involving ground have been investigated for resistance values ranging between 0 to 30  $\Omega$ . In all cases the local and remote source impedances are set equal to the system values. It can be easily seen that the fault location estimates are highly accurate and virtually independent of the fault resistance.

TABLE 8.20  
AFLA-2: INFLUENCE OF THE FAULT RESISTANCE ON THE ALGORITHM'S ACCURACY FOR  
SINGLE-LINE-TO-GROUND FAULTS (ACTUAL FL: 0.8 P.U.)

<i>Fault Res. (<math>\Omega</math>)</i>	<i>Fault Type</i>					
	<i>AG</i>		<i>BG</i>		<i>CG</i>	
	<i>Estim. FL (p. u)</i>	<i>Error of Estim. FL (%)</i>	<i>Estim. FL (p. u)</i>	<i>Error of Estim. FL (%)</i>	<i>Estim. FL (p. u)</i>	<i>Error of Estim. FL (%)</i>
0	0.80015	0.0150	0.79914	0.0861	0.79717	0.2828
1	0.80022	0.0216	0.79871	0.1293	0.79694	0.3055
5	0.79999	0.0010	0.79833	0.1669	0.79708	0.2916
10	0.79983	0.0169	0.79823	0.1738	0.79697	0.3024
20	0.79996	0.0037	0.79842	0.1576	0.79711	0.2887
50	0.79996	0.0038	0.79844	0.1560	0.79710	0.2902
100	0.79978	0.0219	0.79829	0.1704	0.79699	0.3009
200	0.79993	0.0072	0.79845	0.1551	0.79703	0.2967
400	0.79993	0.0070	0.79837	0.1626	0.79706	0.2943
500	0.79983	0.0169	0.79837	0.1627	0.79698	0.3018

TABLE 8.21  
AFLA-2: INFLUENCE OF THE FAULT RESISTANCE ON THE ALGORITHM'S ACCURACY FOR LINE-TO-LINE FAULTS (ACTUAL FL: 0.8 P.U.)

<b>Fault Res. (<math>\Omega</math>)</b>	<b>Fault Type</b>					
	<b>AB</b>		<b>BC</b>		<b>CA</b>	
	<b>Estim. FL (p. u)</b>	<b>Error of Estim. FL (%)</b>	<b>Estim. FL (p. u)</b>	<b>Error of Estim. FL (%)</b>	<b>Estim. FL (p. u)</b>	<b>Error of Estim. FL (%)</b>
0	0.79935	0.0650	0.79788	0.2121	0.79923	0.0764
0.5	0.79933	0.0673	0.79774	0.2258	0.79923	0.0771
1	0.79929	0.0711	0.79761	0.2388	0.79924	0.0764
2.5	0.79912	0.0879	0.79727	0.2731	0.79929	0.0705
5	0.79888	0.1119	0.79725	0.2750	0.79936	0.0640
7.5	0.79877	0.1228	0.79728	0.2716	0.79936	0.0639
10	0.79874	0.1262	0.79733	0.2669	0.79934	0.0654
15	0.79874	0.1263	0.79738	0.2620	0.79932	0.0678
20	0.79875	0.1252	0.79740	0.2598	0.79931	0.0686
30	0.79876	0.1242	0.79742	0.2581	0.79931	0.0692

TABLE 8.22  
AFLA-2: INFLUENCE OF THE FAULT RESISTANCE ON THE ALGORITHM'S ACCURACY FOR LINE-TO-LINE-TO-GROUND FAULTS (ACTUAL FL: 0.8 P.U.)

<b>Fault Res. (<math>\Omega</math>)</b>	<b>Fault Type</b>					
	<b>ABG</b>		<b>BCG</b>		<b>CAG</b>	
	<b>Estim. FL (p. u)</b>	<b>Error of Estim. FL (%)</b>	<b>Estim. FL (p. u)</b>	<b>Error of Estim. FL (%)</b>	<b>Estim. FL (p. u)</b>	<b>Error of Estim. FL (%)</b>
0	0.79959	0.0408	0.79816	0.1844	0.79876	0.1244
1	0.79959	0.0410	0.79817	0.1833	0.79862	0.1383
5	0.79959	0.0414	0.79780	0.2196	0.79863	0.1374
10	0.79943	0.0572	0.79780	0.2203	0.79898	0.1016
25	0.79937	0.0633	0.79769	0.2309	0.79912	0.0874
50	0.79933	0.0670	0.79764	0.2360	0.79916	0.0841
100	0.79931	0.0691	0.79763	0.2374	0.79921	0.0791
150	0.79930	0.0698	0.79762	0.2375	0.79922	0.0782
200	0.79930	0.0701	0.79762	0.2381	0.79922	0.0777
250	0.79930	0.0702	0.79762	0.2379	0.79922	0.0775

TABLE 8.23  
AFLA-2: INFLUENCE OF THE FAULT RESISTANCE ON THE ALGORITHM'S ACCURACY FOR THREE-PHASE FAULTS (ACTUAL FL: 0.8 P.U.)

<i><b>Fault Res. (<math>\Omega</math>)</b></i>	<i><b>Estimated FL (p. u)</b></i>	<i><b>Error of Estimated FL (%)</b></i>
0	0.79882	0.1174
0.5	0.79873	0.1267
1	0.79863	0.1366
2.5	0.79850	0.1499
5	0.79848	0.1523
7.5	0.79848	0.1521
10	0.79849	0.1507
15	0.79850	0.1498
20	0.79851	0.1494
30	0.79851	0.1494

#### 8.5.4 Influence of the fault inception angle

The effect of the variation of the fault inception angle on the algorithm's accuracy for AG, BC and CAG faults is shown in Table 8.24 assuming that the fault occurs at a distance of 0.6 p. u. from terminal A. Fault inception angle is varied from 0 to 150°. Considering all the cases simulated and presented in aforesaid tables, it is observed that the proposed algorithm is very accurate and virtually independent of the fault inception angle with an average error of 0.461%, 0.782% and 0.526% for AG, BC and CAG faults respectively. Figure 8.21 shows the effect of the variation of the fault inception angle on the algorithm's accuracy for aforesaid types of faults. It may be noted here that the fault location error changes nonlinearly with the change in the fault inception angle but it remains within a very much acceptable limit.

TABLE 8.24  
AFLA-2: INFLUENCE OF THE FAULT INCEPTION ANGLE ON THE ALGORITHM'S ACCURACY  
(ACTUAL FL: 0.6 P.U.)

<i>Fault Inception Angle (°)</i>	<i>Fault Type</i>					
	<i>AG</i>		<i>BC</i>		<i>CAG</i>	
	<i>Estim. FL (p. u)</i>	<i>Error of Estim. FL (%)</i>	<i>Estim. FL (p. u)</i>	<i>Error of Estim. FL (%)</i>	<i>Estim. FL (p. u)</i>	<i>Error of Estim. FL (%)</i>
0	0.6001	0.0090	0.5955	0.7477	0.5973	0.4499
30	0.5984	0.2651	0.5954	0.7700	0.5965	0.5897
45	0.6041	0.6874	0.5955	0.7445	0.5993	0.1088
60	0.6009	0.1501	0.5955	0.7570	0.5978	0.3736
90	0.6003	0.0511	0.5944	0.9377	0.5970	0.5005
120	0.5957	0.7238	0.5963	0.6238	0.5951	0.8095
135	0.6029	0.4888	0.5955	0.7556	0.5986	0.2382
165	0.5921	1.3107	0.5945	0.9176	0.5932	1.1382

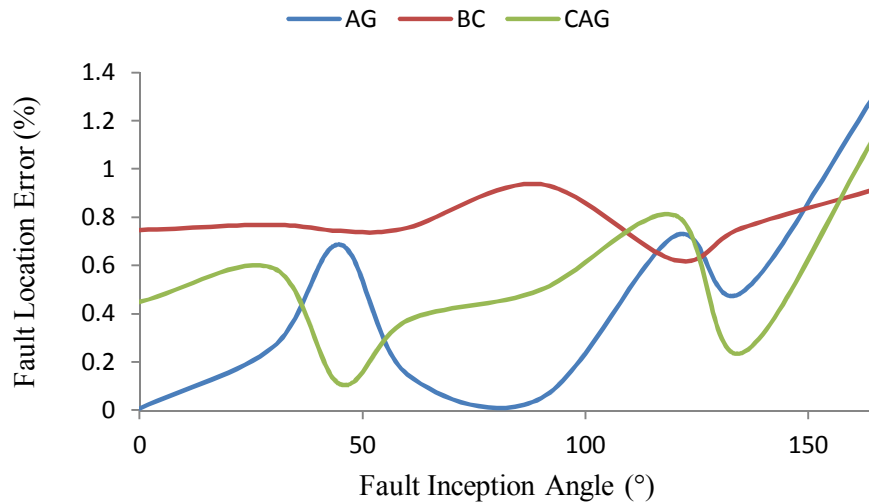


Figure 8.21: AFLA-2: Effect of fault inception angle on FL accuracy (Actual FL: 0.6 p.u.)

### 8.5.5 Influence of the pre-fault loading

Table 8.25 shows the influence of the pre-fault loading on the algorithm's accuracy for AG, BC and CAG faults assuming that these faults occur at 0.6 p.u. distance from terminal A. The pre-fault loading is varied from 0.5 to 3 times its original value.

Considering all the cases simulated and presented in aforesaid tables, it is observed that the proposed algorithm is very accurate with an average error of 0.674%, 0.648% and 0.679% for AG, BC and CAG faults respectively. Figure 8.22 depicts the effect of the variation of the pre-fault loading on the algorithm's accuracy for aforementioned types of faults.

TABLE 8.25  
INFLUENCE OF THE PRE-FAULT LOADING AT TERMINAL-A ON THE ALGORITHM'S ACCURACY  
(ACTUAL FL: 0.6 P.U.)

<i>Variation of Pre-fault Loading (%)</i>	<i>Fault Type</i>					
	<i>AG</i>		<i>BC</i>		<i>CAG</i>	
	<i>Estim. FL (p. u)</i>	<i>Error of Estim. FL (%)</i>	<i>Estim. FL (p. u)</i>	<i>Error of Estim. FL (%)</i>	<i>Estim. FL (p. u)</i>	<i>Error of Estim. FL (%)</i>
-50	0.5986	0.2279	0.5988	0.2025	0.5986	0.2347
-20	0.5977	0.3863	0.5978	0.3605	0.5976	0.3985
20	0.5969	0.5220	0.5970	0.4960	0.5969	0.5211
50	0.5960	0.6658	0.5962	0.6396	0.5960	0.6674
100	0.5946	0.8939	0.5948	0.8676	0.5946	0.8989
200	0.5919	1.3502	0.5921	1.3232	0.5919	1.3550

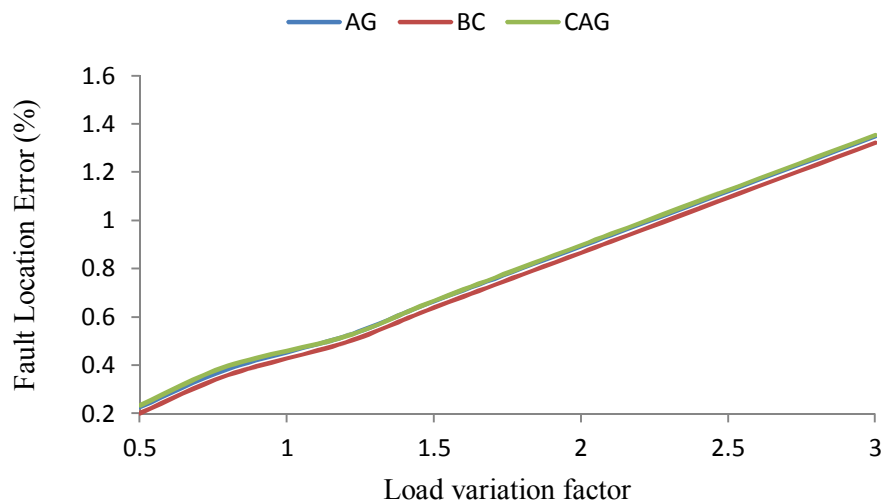


Figure 8.22: AFLA-2: Effect of load variation on FL accuracy (Actual FL: 0.6 p.u.)

### 8.5.6 Error analysis

Since both CTs and VTs may introduce errors in practice, we elect to carry out error analysis to study the impacts of measurement errors on the proposed algorithm. An error of 2% for magnitude and  $2^\circ$  for angle are added to the voltages and currents measured at the line ends. The worst case scenarios are considered where both sending end (A) and receiving end (B) measurements have the maximum error with the opposite sign in the magnitudes (+2% for  $V_A$ /-2% for  $V_B$  or +2% for  $I_A$ /-2% for  $I_B$ ) or angles ( $+2^\circ$  for  $V_A$ /- $2^\circ$  for  $V_B$  or  $+2^\circ$  for  $I_A$ /- $2^\circ$  for  $I_B$ ). Errors on fault location estimates are then investigated for all types of LG faults.

With the method of Multiple Measurement using Linear Regression (MMLR) applied for online calculation of the line parameters, Table 8.26 and 8.27 present the results for a 2% error in the magnitude and a  $2^\circ$  error in the angle of the voltage respectively. Similarly, Table 8.28 and 8.29 present the results for a 2% error in the magnitude and a  $2^\circ$  error in the angle of the current. If we assume that line parameters are determined by the method of Single Measurement (SM), then errors of estimated fault location due to 2% error in voltage/current magnitude and  $2^\circ$  error in voltage/current angle will be as shown in Table 8.30-8.33. It can be seen from the results presented in Tables 8.26-8.29 that the algorithm is desirably insensitive to measurement errors. Since the algorithm is independent of the fault current, the effect of current errors on the fault location accuracy is less compared to the effect of voltage errors. Figure 8.23-8.26 clearly indicate that the fault location algorithm performs much better in the presence of voltage and current errors when the method of MMLR is used for online calculation of the line parameters.



TABLE 8.26  
AFLA-2: INFLUENCE OF 2% VOLTAGE MAGNITUDE ERROR ON FAULT-LOCATION ESTIMATES  
FOR SINGLE-LINE-TO-GROUND FAULTS (MMLR)

<i><b>Fault Type</b></i>	<i><b>Fault Res. (<math>\Omega</math>)</b></i>	<i><b>Actual FL (p. u)</b></i>	<i><b>Estimated FL (p. u)</b></i>	<i><b>Error of Estimated FL (%)</b></i>
AG	10	0.2	0.18782	1.2180
		0.4	0.38206	1.7935
		0.6	0.57736	2.2637
		0.8	0.77470	2.5300
	100	0.2	0.18787	1.2126
		0.4	0.38211	1.7885
		0.6	0.57738	2.2619
		0.8	0.77468	2.5315
BG	10	0.2	0.18352	1.6482
		0.4	0.37840	2.1604
		0.6	0.57459	2.5408
		0.8	0.77314	2.6859
	100	0.2	0.18356	1.6439
		0.4	0.37843	2.1569
		0.6	0.57468	2.5320
		0.8	0.77319	2.6804
CG	10	0.2	0.17936	2.0640
		0.4	0.37496	2.5034
		0.6	0.57214	2.7860
		0.8	0.77187	2.8129
	100	0.2	0.17937	2.0625
		0.4	0.37497	2.5027
		0.6	0.57217	2.7827
		0.8	0.77186	2.8138

TABLE 8.27  
AFLA-2: INFLUENCE OF 2° VOLTAGE ANGLE ERROR ON FAULT-LOCATION ESTIMATES FOR  
SINGLE-LINE-TO-GROUND FAULTS (MMLR)

<i><b>Fault Type</b></i>	<i><b>Fault Res. (<math>\Omega</math>)</b></i>	<i><b>Actual FL (p. u)</b></i>	<i><b>Estimated FL (p. u)</b></i>	<i><b>Error of Estimated FL (%)</b></i>
AG	10	0.2	0.19370	0.6303
		0.4	0.39305	0.6951
		0.6	0.59251	0.7486
		0.8	0.79258	0.7416
	100	0.2	0.19371	0.6288
		0.4	0.39311	0.6893
		0.6	0.59253	0.7472
		0.8	0.79256	0.7444
BG	10	0.2	0.18196	1.0836
		0.4	0.38918	1.0816
		0.6	0.58962	1.0379
		0.8	0.79100	0.9002
	100	0.2	0.18920	1.0797
		0.4	0.38922	1.0776
		0.6	0.58973	1.0269
		0.8	0.79103	0.8966
CG	10	0.2	0.18477	1.5226
		0.4	0.38555	1.4449
		0.6	0.58705	1.2946
		0.8	0.78970	1.0301
	100	0.2	0.18478	1.5214
		0.4	0.38555	1.4448
		0.6	0.58707	1.2926
		0.8	0.78970	1.0299

TABLE 8.28  
AFLA-2: INFLUENCE OF 2% CURRENT MAGNITUDE ERROR ON FAULT-LOCATION ESTIMATES  
FOR SINGLE-LINE-TO-GROUND FAULTS (MMLR)

<i><b>Fault Type</b></i>	<i><b>Fault Res. (<math>\Omega</math>)</b></i>	<i><b>Actual FL (p. u)</b></i>	<i><b>Estimated FL (p. u)</b></i>	<i><b>Error of Estimated FL (%)</b></i>
AG	10	0.2	0.20431	0.4316
		0.4	0.40209	0.2088
		0.6	0.59989	0.0110
		0.8	0.79770	0.2298
	100	0.2	0.20435	0.4349
		0.4	0.40211	0.2111
		0.6	0.59988	0.0114
		0.8	0.79768	0.2323
BG	10	0.2	0.19994	0.0057
		0.4	0.39836	0.1636
		0.6	0.59709	0.2909
		0.8	0.79615	0.3850
	100	0.2	0.19999	0.0013
		0.4	0.39841	0.1585
		0.6	0.59716	0.2836
		0.8	0.79620	0.3795
CG	10	0.2	0.19571	0.4291
		0.4	0.39488	0.5120
		0.6	0.59462	0.5380
		0.8	0.79489	0.5113
	100	0.2	0.19574	0.4262
		0.4	0.39490	0.5099
		0.6	0.59464	0.5361
		0.8	0.79485	0.5148

TABLE 8.29  
AFLA-2: INFLUENCE OF 2° CURRENT ANGLE ERROR ON FAULT-LOCATION ESTIMATES FOR  
SINGLE-LINE-TO-GROUND FAULTS (MMLR)

<i><b>Fault Type</b></i>	<i><b>Fault Res. (<math>\Omega</math>)</b></i>	<i><b>Actual FL (p. u)</b></i>	<i><b>Estimated FL (p. u)</b></i>	<i><b>Error of Estimated FL (%)</b></i>
AG	10	0.2	0.20494	0.4943
		0.4	0.40402	0.4022
		0.6	0.60313	0.3130
		0.8	0.80224	0.2245
	100	0.2	0.20500	0.4997
		0.4	0.40405	0.4050
		0.6	0.60314	0.3143
		0.8	0.80220	0.2201
BG	10	0.2	0.20049	0.0495
		0.4	0.40022	0.0224
		0.6	0.60027	0.0266
		0.8	0.80066	0.0658
	100	0.2	0.20055	0.0556
		0.4	0.40029	0.0292
		0.6	0.60036	0.0363
		0.8	0.80071	0.0710
CG	10	0.2	0.19619	0.3810
		0.4	0.39666	0.3337
		0.6	0.59774	0.2258
		0.8	0.79936	0.0640
	100	0.2	0.19621	0.3785
		0.4	0.39667	0.3333
		0.6	0.59777	0.2227
		0.8	0.79937	0.0633

TABLE 8.30  
AFLA-2: INFLUENCE OF 2% VOLTAGE MAGNITUDE ERROR ON FAULT-LOCATION ESTIMATES  
FOR SINGLE-LINE-TO-GROUND FAULTS (SM)

<i><b>Fault Type</b></i>	<i><b>Fault Res. (<math>\Omega</math>)</b></i>	<i><b>Actual FL (p. u)</b></i>	<i><b>Estimated FL (p. u)</b></i>	<i><b>Error of Estimated FL (%)</b></i>
AG	10	0.2	0.21049	1.0494
		0.4	0.37909	2.0912
		0.6	0.54770	5.2299
		0.8	0.71631	8.3688
	100	0.2	0.21055	1.0555
		0.4	0.37910	2.0896
		0.6	0.54771	5.2290
		0.8	0.71626	8.3735
BG	10	0.2	0.20752	0.7517
		0.4	0.37669	2.3307
		0.6	0.54596	5.4039
		0.8	0.71537	8.4633
	100	0.2	0.20755	0.7549
		0.4	0.37673	2.3271
		0.6	0.54601	5.3988
		0.8	0.71538	8.4617
CG	10	0.2	0.20471	0.4706
		0.4	0.37456	2.5442
		0.6	0.54458	5.5420
		0.8	0.71474	8.5260
	100	0.2	0.20471	0.4705
		0.4	0.37457	2.5434
		0.6	0.54461	5.5389
		0.8	0.71470	8.5299

TABLE 8.31  
AFLA-2: INFLUENCE OF 2° VOLTAGE ANGLE ERROR ON FAULT-LOCATION ESTIMATES FOR  
SINGLE-LINE-TO-GROUND FAULTS (SM)

<i><b>Fault Type</b></i>	<i><b>Fault Res. (<math>\Omega</math>)</b></i>	<i><b>Actual FL (p. u)</b></i>	<i><b>Estimated FL (p. u)</b></i>	<i><b>Error of Estimated FL (%)</b></i>
AG	10	0.2	0.18741	1.2587
		0.4	0.39112	0.8882
		0.6	0.59420	0.5797
		0.8	0.79661	0.3391
	100	0.2	0.18742	1.2574
		0.4	0.39117	0.8829
		0.6	0.59421	0.5791
		0.8	0.79660	0.3399
BG	10	0.2	0.18286	1.7138
		0.4	0.38728	1.2720
		0.6	0.59136	0.8641
		0.8	0.79505	0.4949
	100	0.2	0.18290	1.7099
		0.4	0.38733	1.2672
		0.6	0.59146	0.8539
		0.8	0.79504	0.4955
CG	10	0.2	0.17846	2.1539
		0.4	0.38369	1.6308
		0.6	0.58885	1.1151
		0.8	0.79379	0.6213
	100	0.2	0.17846	2.1537
		0.4	0.38368	1.6318
		0.6	0.58888	1.1115
		0.8	0.79379	0.6213

TABLE 8.32  
AFLA-2: INFLUENCE OF 2% CURRENT MAGNITUDE ERROR ON FAULT-LOCATION ESTIMATES  
FOR SINGLE-LINE-TO-GROUND FAULTS (SM)

<i><b>Fault Type</b></i>	<i><b>Fault Res. (<math>\Omega</math>)</b></i>	<i><b>Actual FL (p. u)</b></i>	<i><b>Estimated FL (p. u)</b></i>	<i><b>Error of Estimated FL (%)</b></i>
AG	10	0.2	0.20035	0.0354
		0.4	0.40020	0.0197
		0.6	0.60006	0.0061
		0.8	0.79995	0.0050
	100	0.2	0.20040	0.0402
		0.4	0.40025	0.0250
		0.6	0.60008	0.0076
		0.8	0.79991	0.0085
BG	10	0.2	0.19593	0.4069
		0.4	0.39642	0.3580
		0.6	0.59723	0.2771
		0.8	0.79838	0.1620
	100	0.2	0.19596	0.4035
		0.4	0.39646	0.3539
		0.6	0.59732	0.2677
		0.8	0.79843	0.1564
CG	10	0.2	0.19165	0.8353
		0.4	0.39289	0.7110
		0.6	0.59473	0.5273
		0.8	0.79709	0.2907
	100	0.2	0.19165	0.8347
		0.4	0.39288	0.7120
		0.6	0.59476	0.5243
		0.8	0.79707	0.2927

TABLE 8.33  
AFLA-2: INFLUENCE OF 2° CURRENT ANGLE ERROR ON FAULT-LOCATION ESTIMATES FOR  
SINGLE-LINE-TO-GROUND FAULTS (SM)

<i>Fault Type</i>	<i>Fault Res. (<math>\Omega</math>)</i>	<i>Actual FL (p. u)</i>	<i>Estimated FL (p. u)</i>	<i>Error of Estimated FL (%)</i>
AG	10	0.2	0.20033	0.0331
		0.4	0.40018	0.0182
		0.6	0.60007	0.0068
		0.8	0.79996	0.0038
	100	0.2	0.20037	0.0373
		0.4	0.40019	0.0196
		0.6	0.60008	0.0076
		0.8	0.79996	0.0041
BG	10	0.2	0.19590	0.4099
		0.4	0.39641	0.3585
		0.6	0.59724	0.2763
		0.8	0.79839	0.1604
	100	0.2	0.19595	0.4050
		0.4	0.39647	0.3532
		0.6	0.59733	0.2667
		0.8	0.79842	0.1579
CG	10	0.2	0.19162	0.8383
		0.4	0.39288	0.7115
		0.6	0.59473	0.5267
		0.8	0.79711	0.2891
	100	0.2	0.19165	0.8346
		0.4	0.39289	0.7105
		0.6	0.59477	0.5232
		0.8	0.79711	0.2888

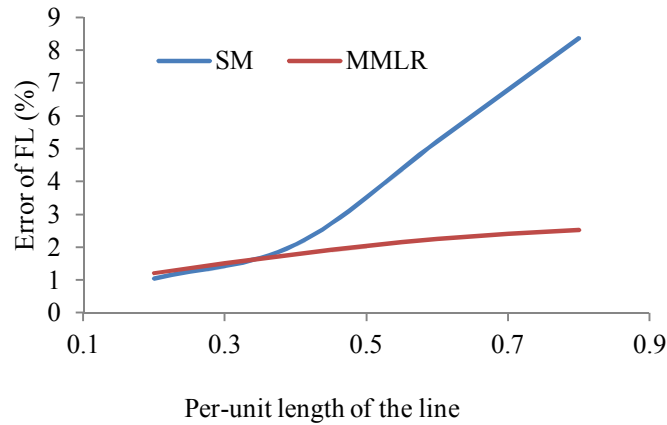


Figure 8.23: FL error with 2% error in voltage magnitude (AG-10)



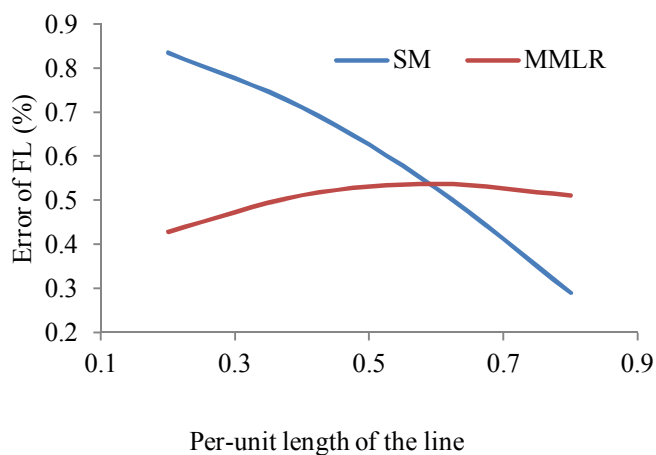


Figure 8.24: FL error with 2% error in current magnitude (CG-10)

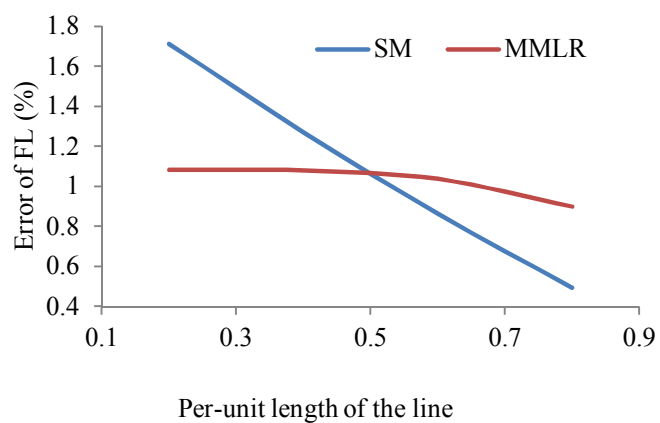


Figure 8.25: FL error with 2° error in voltage angle (BG-10)

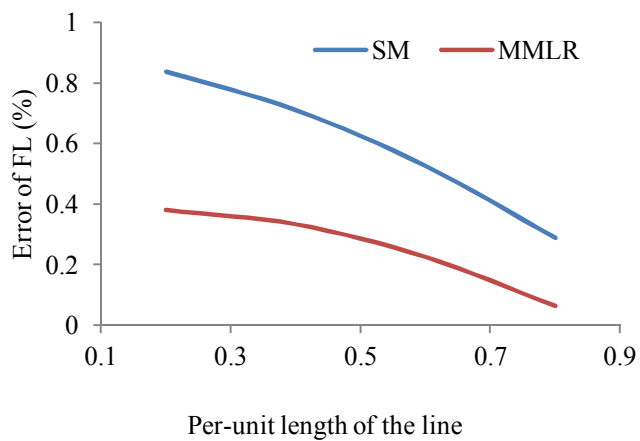


Figure 8.26: FL error with 2° error in current angle (CG-10)

## 8.6 Comparison with non-adaptive algorithm for two-terminal lines

In the proposed AFLA-1 and AFLA-2 for two-terminal lines, system impedance and line parameters are determined online and, thus, the effect of the surrounding environment and operation history on these parameters is nullified. System impedance and line parameters determined online from PMU synchronized measurements certainly reflect the system's practical operating conditions prior to and after the fault occurrence. In non-adaptive fault location algorithms, system impedance and line parameters are provided by the electric utility and assumed to be constant regardless of the environmental and system operating conditions. Such assumption, however, is a source of error that impacts the fault location accuracy.

In this section, we investigate the effect of system impedance and line parameters uncertainty on fault location accuracy assuming that they vary within  $\pm 25\%$  from their practical values. Table 8.34 shows the influence of the line parameters and system impedance variation on AFLA-2's accuracy for AG, BC, CAG and ABC faults assuming that these faults occur at 0.6 p.u. distance from terminal A. Considering all the cases simulated and presented in aforesaid table, one can easily observe that the effect of system impedance and parameters uncertainty on fault location can reach up to 10% if the parameters used in fault location vary 25% of the practical parameters. Figure 8.27 depicts the effect of the system impedance and line parameter variation on the algorithm's accuracy for aforementioned types of faults.

TABLE 8.34  
AFLA-2: INFLUENCE OF LINE PARAMETERS AND SYSTEM IMPEDANCE VARIATION ON THE  
ALGORITHM'S ACCURACY (ACTUAL FL: 0.6 P.U.)

Parameter Variation (%)	Fault Type							
	AG		CAG		BC		ABC	
	Estim. FL (p. u)	Error of Estim. FL (%)	Estim. FL (p. u)	Error of Estim. FL (%)	Estim. FL (p. u)	Error of Estim. FL (%)	Estim. FL (p. u)	Error of Estim. FL (%)
-25	0.6636	10.6012	0.6636	10.5951	0.6638	10.6259	0.6637	10.6136
-20	0.6493	8.2147	0.6493	8.2088	0.6494	8.2397	0.6494	8.2272
-15	0.6356	5.9258	0.6355	5.9201	0.6357	5.9509	0.6356	5.9383
-10	0.6224	3.7286	0.6223	3.7231	0.6225	3.7540	0.6224	3.7413
-5	0.6097	1.6181	0.6097	1.6127	0.6099	1.6436	0.6098	1.6308
0	0.5975	0.4107	0.5975	0.4159	0.5977	0.3851	0.5976	0.3979
5	0.5858	2.3623	0.5858	2.3674	0.5860	2.3367	0.5859	2.3495
10	0.5746	4.2409	0.5745	4.2459	0.5747	4.2153	0.5746	4.2281
15	0.5637	6.0504	0.5637	6.0553	0.5639	6.0248	0.5638	6.0376
20	0.5532	7.7945	0.5532	7.7993	0.5534	7.7689	0.5533	7.7817
25	0.5431	9.4765	0.5431	9.4812	0.5433	9.4510	0.5432	9.4638

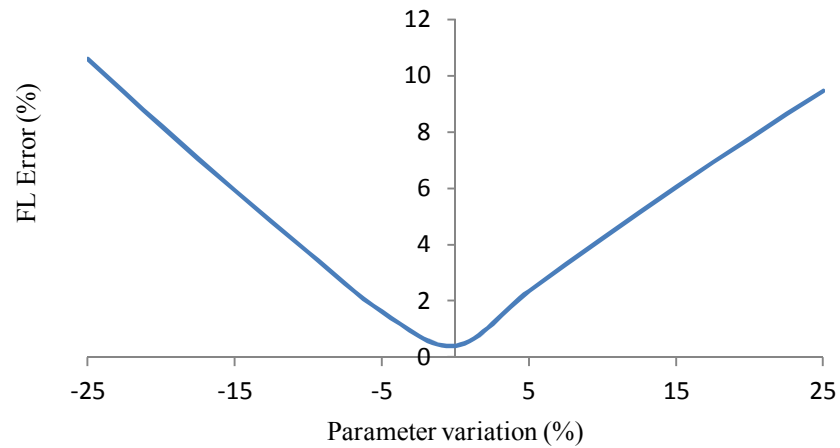


Figure 8.27: Influence of parameter variation on FL accuracy in two-terminal lines

## CHAPTER 9

### **Adaptive PMU-based Fault Location Algorithm for Three-terminal Lines**

Use is made of multi-terminal and tapped lines for economical or environmental-protection reasons. Multi-terminal lines are those having three or more terminals with substantial generation behind each. Based on the number of terminals we can distinguish three-terminal lines having three terminals, four-terminal lines having four terminals, and so on. Lines having three or more terminals with substantial power generation behind, at a maximum at two of them, are named tapped lines. The number of taps per line varies from one to even more than ten. The taps themselves feed only loads, which means that they are terminated by the passive networks, while at the remaining terminals there are active networks (with power generation). [2]

Fault location on multi-terminal and tapped lines relies on identifying the line section at which the fault occurred and determining the distance to fault for the faulted

section, usually measured from the respective bus towards the fault point. In this chapter, we propose an adaptive PMU-based fault location algorithm for three-terminal lines. The proposed algorithm will be described in details and simulation results will be presented and discussed.

## 9.1 PMU-based parameter estimation of a three-terminal line

The equivalent  $\pi$  model of a three-terminal transmission network is shown in Figure 9.1 [50] which can be represented, in steady state, by Figure 9.2. In this section, we propose a method to determine the parameters of a three-terminal line utilizing synchronized voltage and current phasor measurements obtained from PMUs installed at the three terminals A, B and C. Line parameters are determined for the case where the three sections have the same parameters per unit length and for the most general case where each section has parameters different from those of the other two sections.

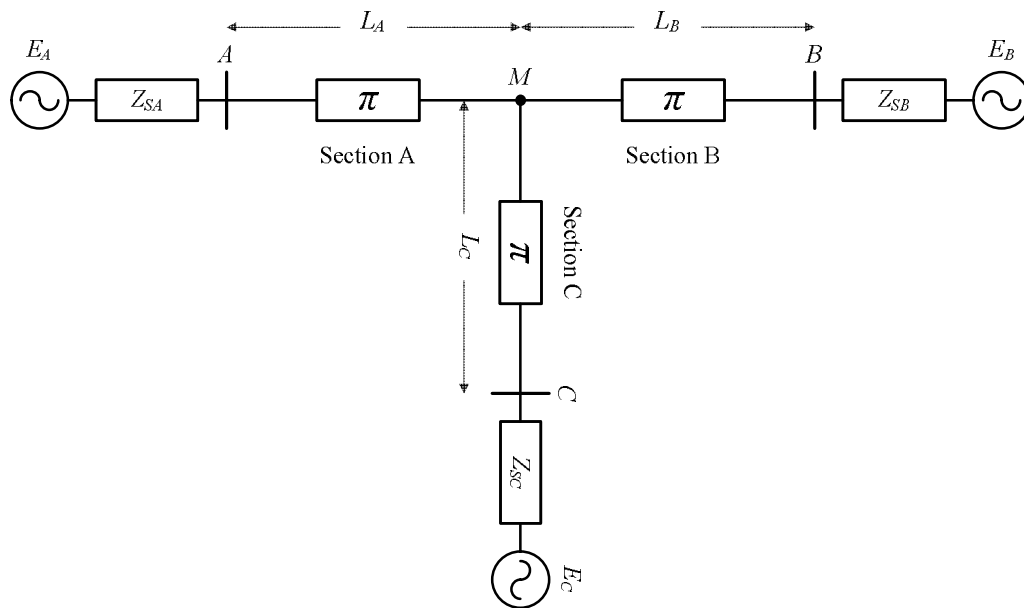


Figure 9.1: A three-terminal transmission network

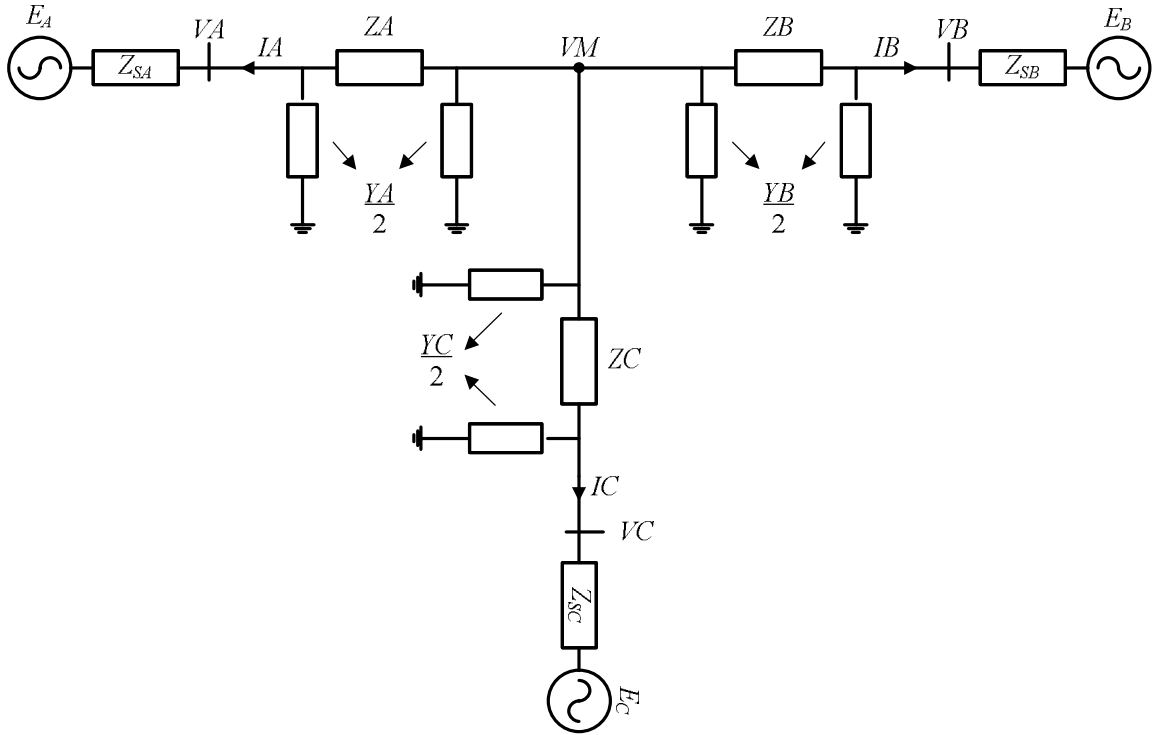


Figure 9.2: Steady state  $\pi$  equivalent model of a three-terminal transmission network

### 9.1.1 Line sections having the same parameters per unit length

For this case, we assume the three sections have the same impedance ( $z$ ) and the same admittance ( $y$ ) per unit length. With such assumption, we can write the following:

$$Z_A = L_A * z \quad (9.1)$$

$$Y_A = L_A * y \quad (9.2)$$

$$Z_B = L_B * z \quad (9.3)$$

$$Y_B = L_B * y \quad (9.4)$$

$$Z_C = L_C * z \quad (9.5)$$

$$Y_C = L_C * y \quad (9.6)$$

where

$L_A$  : Length of section A

$L_B$  : Length of section B

$L_C$  : Length of section C

$Z_A, Y_A$  : Impedance, admittance of section A

$Z_B, Y_B$  : Impedance, admittance of section B

$Z_C, Y_C$  : Impedance, admittance of section C

Considering Figure 9.2, we can write the following equations for section A, B and C:

$$VM - L_A * I_A * z - \frac{1}{2} * V_A * (L_A)^2 * y * z - V_A = 0 \quad (9.7)$$

$$VM - L_B * I_B * z - \frac{1}{2} * V_B * (L_B)^2 * y * z - V_B = 0 \quad (9.8)$$

$$VM - L_C * I_C * z - \frac{1}{2} * V_C * (L_C)^2 * y * z - V_C = 0 \quad (9.9)$$

Equation (9.7), and similarly (9.8) and (9.9), is a complex equation which can be written into two real equations as shown below:

$$Re[VM] - L_A * Re[I_A] * Re[z] + L_A * Im[I_A] * Im[z] + 0.5 * (L_A)^2 * Re[V_A] * \quad (9.10)$$

$$Im[z] * Im[y] + 0.5 * (L_A)^2 * Im[V_A] * Re[z] * Im[y] - Re[V_A] = 0$$

$$Im[VM] - L_A * Re[I_A] * Im[z] - L_A * Im[I_A] * Re[z] - 0.5 * (L_A)^2 * Re[V_A] * \quad (9.11)$$

$$Re[z] * Im[y] + 0.5 * (L_A)^2 * Im[V_A] * Im[z] * Im[y] - Im[V_A] = 0$$

Equations (9.10) and (9.11) are nonlinear equations with five unknowns, namely  $Re[z], Im[z], Im[y], Re[VM], Im[VM]$  and therefore five equations are needed to solve for the unknowns. Converting (9.8) and (9.9) into the corresponding real equations, we get four more equations in addition to (9.10) and (9.11) which are more than enough to solve for the five unknowns. So, for this case only one set of voltage and current phasor

measurements is needed to determine the line parameters for each section. Assuming that  $[X_1 \ X_2 \ X_3 \ X_4 \ X_5]' = [Re[z] \ Im[z] \ Im[y] \ Re[VM] \ Im[VM]]'$  then we need to solve the following set of nonlinear equations simultaneously to determine the line parameters per unit length:

$$\begin{aligned} X_4 - L_A * Re[I_A] * X_1 + L_A * Im[I_A] * X_2 + 0.5 * (L_A)^2 * Re[VA] * X_2 * X_3 + \\ 0.5 * (L_A)^2 * Im[VA] * X_1 * X_3 - Re[VA] = 0 \end{aligned} \quad (9.12)$$

$$\begin{aligned} X_5 - L_A * Re[I_A] * X_2 - L_A * Im[I_A] * X_1 - 0.5 * (L_A)^2 * Re[VA] * X_1 * X_3 + \\ 0.5 * (L_A)^2 * Im[VA] * X_2 * X_3 - Im[VA] = 0 \end{aligned} \quad (9.13)$$

$$\begin{aligned} X_4 - L_B * Re[I_B] * X_1 + L_B * Im[I_B] * X_2 + 0.5 * (L_B)^2 * Re[VB] * X_2 * X_3 + \\ 0.5 * (L_B)^2 * Im[VB] * X_1 * X_3 - Re[VB] = 0 \end{aligned} \quad (9.14)$$

$$\begin{aligned} X_5 - L_B * Re[I_B] * X_2 - L_B * Im[I_B] * X_1 - 0.5 * (L_B)^2 * Re[VB] * X_1 * X_3 + \\ 0.5 * (L_B)^2 * Im[VB] * X_2 * X_3 - Im[VB] = 0 \end{aligned} \quad (9.15)$$

$$\begin{aligned} X_4 - L_C * Re[I_C] * X_1 + L_C * Im[I_C] * X_2 + 0.5 * (L_C)^2 * Re[VC] * X_2 * X_3 + \\ 0.5 * (L_C)^2 * Im[VC] * X_1 * X_3 - Re[VC] = 0 \end{aligned} \quad (9.16)$$

Knowing the length of each section, equations (9.1)-(9.6) can be used to determine the line parameters pertaining to section A, B and C.

### 9.1.2 Line sections having different parameters

For this case, more unknowns are involved and, therefore, more sets of measurements are necessary. For the first set of measurements, we can form 6 equations as discussed earlier but we have a total of 11 unknowns, namely  $Re[ZA]$ ,  $Im[ZA]$ ,  $Im[YA]$ ,  $Re[ZB]$ ,  $Im[ZB]$ ,  $Im[YB]$ ,  $Re[ZC]$ ,  $Im[ZC]$ ,  $Im[YC]$ ,  $Re[VM]$ ,  $Im[VM]$ . For the second set of measurements, 6 more equations can be formed but 2 more unknowns, related to the voltage VM at the



tap point, are added. Thus, with 12 equations and 13 unknowns, a third set of measurement becomes mandatory. Proceeding in a similar fashion with the third set of measurement, 6 more equations can be formed and 2 more unknowns will be added to have a total of 18 equations which is more than enough to solve for 15 unknowns. If we consider the first set of measurements, the following equations can be written for section A, B and C based on Figure 9.2:

$$(VM)_1 - ZA * (IA)_1 - \frac{1}{2} * (VA)_1 * ZA * YA - (VA)_1 = 0 \quad (9.17)$$

$$(VM)_1 - ZB * (IB)_1 - \frac{1}{2} * (VB)_1 * ZB * YB - (VB)_1 = 0 \quad (9.18)$$

$$(VM)_1 - ZC * (IC)_1 - \frac{1}{2} * (VC)_1 * ZC * YC - (VC)_1 = 0 \quad (9.19)$$

The subscript (1) is used in equations (9.17)-(9.19) to denote the first set of measurements. Using the subscript (2) and (3) to denote respectively the second and the third sets of measurements, we write the following equations:

$$(VM)_2 - ZA * (IA)_2 - \frac{1}{2} * (VA)_2 * ZA * YA - (VA)_2 = 0 \quad (9.20)$$

$$(VM)_2 - ZB * (IB)_2 - \frac{1}{2} * (VB)_2 * ZB * YB - (VB)_2 = 0 \quad (9.21)$$

$$(VM)_2 - ZC * (IC)_2 - \frac{1}{2} * (VC)_2 * ZC * YC - (VC)_2 = 0 \quad (9.22)$$

$$(VM)_3 - ZA * (IA)_3 - \frac{1}{2} * (VA)_3 * ZA * YA - (VA)_3 = 0 \quad (9.23)$$

$$(VM)_3 - ZB * (IB)_3 - \frac{1}{2} * (VB)_3 * ZB * YB - (VB)_3 = 0 \quad (9.24)$$

$$(VM)_3 - ZC * (IC)_3 - \frac{1}{2} * (VC)_3 * ZC * YC - (VC)_3 = 0 \quad (9.25)$$

Equation (9.17), and similarly (9.18)-(9.25), is a complex equation which can be written into two real nonlinear equations as shown below:

$$\begin{aligned} Re[(VM)_1] - Re[ZA] * Re[(IA)_1] + Im[ZA] * Im[(IA)_1] + 0.5 * Re[(VA)_1] * \\ Im[ZA] * Im[YA] + 0.5 * Im[(VA)_1] * Im[YA] * Re[ZA] - Re[(VA)_1] = 0 \end{aligned} \quad (9.26)$$

$$\begin{aligned} Im[(VM)_1] - Re[ZA] * Im[(IA)_1] - Im[ZA] * Re[(IA)_1] - 0.5 * Re[(VA)_1] * \\ Im[YA] * Re[ZA] + 0.5 * Im[(VA)_1] * Im[ZA] * Im[YA] - Im[(VA)_1] = 0 \end{aligned} \quad (9.27)$$

Proceeding in the same manner, additional 16 equations can be written to have a total of 18 equations out of which 15 are needed to solve for 15 unknowns, namely  $Re[ZA]$ ,  $Im[ZA]$ ,  $Im[YA]$ ,  $Re[ZB]$ ,  $Im[ZB]$ ,  $Im[YB]$ ,  $Re[ZC]$ ,  $Im[ZC]$ ,  $Im[YC]$ ,  $Re[(VM)_1]$ ,  $Im[(VM)_1]$ ,  $Re[(VM)_2]$ ,  $Im[(VM)_2]$ ,  $Re[(VM)_3]$ ,  $Im[(VM)_3]$ .

## 9.2 Description of the proposed algorithm

The technique presented in chapter 8 for two-terminal transmission line can be extended for the three-terminal configuration. Consider that an unknown fault is occurred in the transmission line and its location is unknown. This fault may occur in one of the sections A or B or C. Based on Figure 9.1, the voltage of node M can be calculated in terms of the voltage of bus A or B or C.  $IA$  can be calculated as:

$$IA = \left[ YSA + \frac{YA}{2} \right] \Delta VA \quad (9.28)$$

and

$$VM = \Delta VA + ZAIA \quad (9.29)$$

Substituting 9.28 into 9.29, VM is obtained as:

$$VM = \left( I_{3 \times 3} + ZA \left( YSA + \frac{YA}{2} \right) \right) \Delta VA \quad (9.30)$$

VM can also be calculated as:

$$VM = \left( I_{3 \times 3} + ZB \left( YSB + \frac{YB}{2} \right) \right) \Delta VB \quad (9.31)$$

$$VM = \left( I_{3 \times 3} + ZC \left( YSC + \frac{YC}{2} \right) \right) \Delta VC \quad (9.32)$$

In this technique, fault location is determined in two stages: firstly, detection of faulted section and secondly, accurate estimation of fault point distance. Initially, consider that a fault is occurred in the network. Since the system model is changed VM cannot be calculated from the bus voltage of the faulted section. Therefore, VM can be calculated from the other two bus voltages. To detect the faulted section, it is sufficient to calculate VM by using Equations (9.30)-(9.32). Figure 9.3 shows the flowchart of the proposed method for the faulted section recognition.

In the second one, consider that an unknown fault is occurred in section B with the distance of  $l1$  from bus B. In this stage, the faulted section is obtained from the former stage. The Thevenin's model of the faulted system is shown in Figure 9.4. According to Equations (9.30) and (9.31), the voltage VM can be obtained by using the bus voltages of A or C. So, the faulted point voltage can be written as:

$$IM = IMA + IMC \quad (9.33)$$

The currents IMA and IMC can be obtained using the bus voltage of A and C:

$$IMA = IA + \frac{YA}{2} VM \quad (9.34)$$

$$IMC = IC + \frac{YC}{2} VM \quad (9.35)$$

and

$$IFM = IM + \frac{YB}{2} (1 - k) VM \quad (9.36)$$

$$VF = VM + ZB(1 - k) IFM \quad (9.37)$$

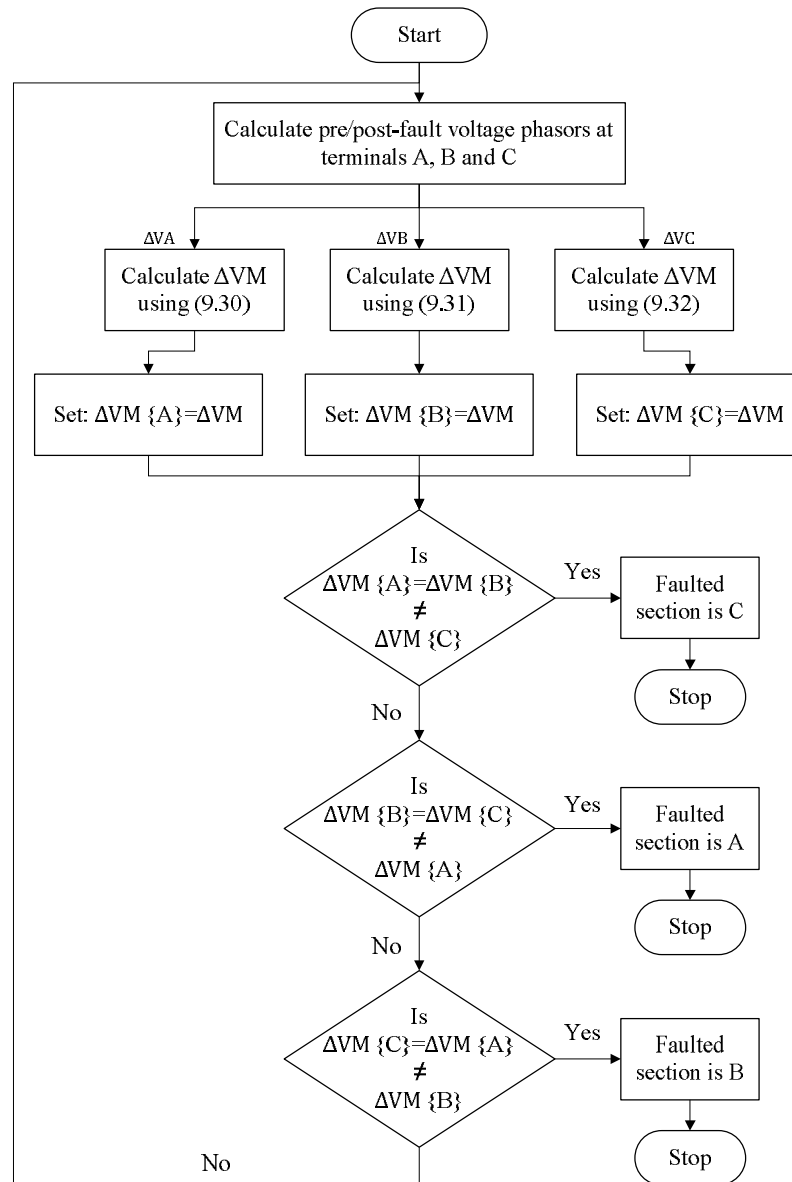
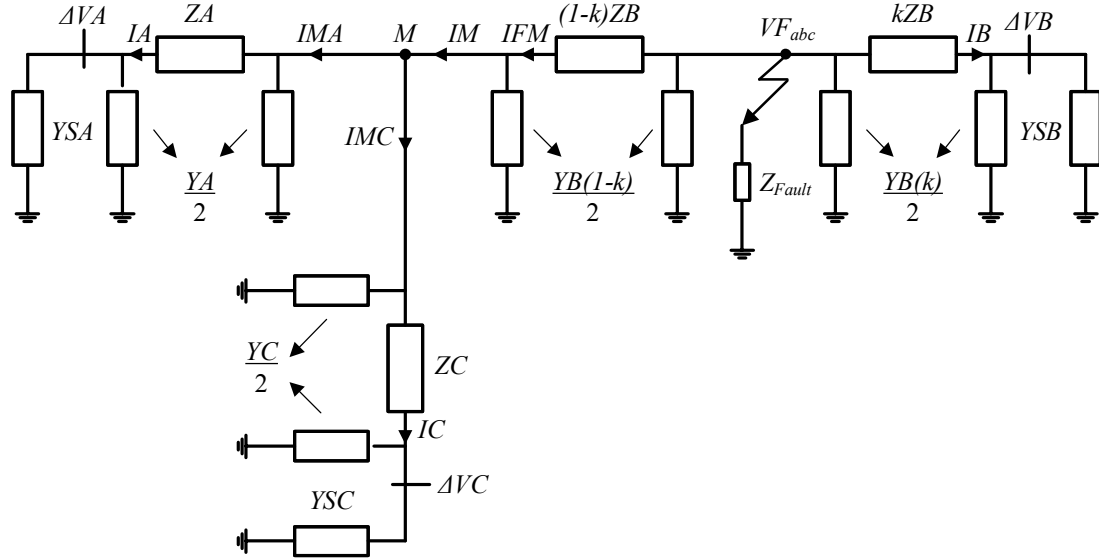


Figure 9.3: Flow chart showing the algorithm to identify the faulted section

Figure 9.4: Faulted three-terminal system in  $\pi$  equivalent model

Also, for the faulted section, the following equations can be written to obtain its bus voltage:

$$IB = \left[ Y_{SB} + \frac{Y_B}{2} k \right] \Delta VB \quad (9.38)$$

$$VF = \Delta VB + ZB k IB \quad (9.39)$$

Using (9.37) and (9.39), we can write:

$$\Delta VB + ZB k IB = VM + ZB(1 - k) IFM \quad (9.40)$$

So, k can be obtained as:

$$k = f(\Delta VA, \Delta VB, \Delta VC) \rightarrow ak^2 + bk + c = 0 \quad (9.41)$$

such that

$$a = ZB \frac{Y_B}{2} \Delta VB + ZB \frac{Y_A}{2} \Delta VA + ZB \frac{Y_C}{2} \Delta VC \quad (9.42)$$

$$b = ZBYSB\Delta VB - ZB \frac{YA}{2} \Delta VA - ZB \frac{YC}{2} \Delta VC + ZB \frac{YB}{2} VM + ZBYS A \Delta VA$$

$$+ ZBYS C \Delta VC + ZB \left( \frac{YA}{2} + \frac{YB}{2} + \frac{YC}{2} \right) VM$$

$$c = \Delta VB - VM - ZBYS A \Delta VA - ZBYS C \Delta VC - ZB \left( \frac{YA}{2} + \frac{YB}{2} + \frac{YC}{2} \right) VM$$

and  $VM$  is obtained using either (9.30) or (9.32). The estimated fault point distance can be calculated as:

$$l1 = k \times L_B \quad (9.43)$$

If we consider that an unknown fault is occurred in section A with the distance of  $l1$  from bus A, then the quadratic equation coefficients  $a$ ,  $b$  and  $c$  are given as:

$$a = ZA \frac{YA}{2} \Delta VA + ZA \frac{YB}{2} \Delta VB + ZA \frac{YC}{2} \Delta VC$$

$$b = ZAYS A \Delta VA - ZA \frac{YB}{2} \Delta VB - ZA \frac{YC}{2} \Delta VC + ZA \frac{YA}{2} VM + ZAYS B \Delta VB \\ + ZAYS C \Delta VC + ZA \left( \frac{YA}{2} + \frac{YB}{2} + \frac{YC}{2} \right) VM \quad (9.44)$$

$$c = \Delta VA - VM - ZAYS B \Delta VB - ZAYS C \Delta VC - ZA \left( \frac{YA}{2} + \frac{YB}{2} + \frac{YC}{2} \right) VM$$

and  $VM$  is obtained using either (9.31) or (9.32). The estimated fault point distance can be calculated:

$$l1 = k \times L_A \quad (9.45)$$

Finally, if we consider that an unknown fault is occurred in section C with the distance of  $l1$  from bus C, then the quadratic equation coefficients  $a$ ,  $b$  and  $c$  are given as:

$$a = ZC \frac{YC}{2} \Delta VC + ZC \frac{YA}{2} \Delta VA + ZC \frac{YB}{2} \Delta VB \quad (9.46)$$

$$b = ZCYSC\Delta VC - ZC \frac{YA}{2} \Delta VA - ZC \frac{YB}{2} \Delta VB + ZC \frac{YC}{2} VM + ZCYSA\Delta VA \\ + ZCYSB\Delta VB + ZC \left( \frac{YA}{2} + \frac{YB}{2} + \frac{YC}{2} \right) VM$$

$$c = \Delta VC - VM - ZCYSA\Delta VA - ZCYSB\Delta VB - ZC \left( \frac{YA}{2} + \frac{YB}{2} + \frac{YC}{2} \right) VM$$

and  $VM$  is obtained using either (9.30) or (9.31). The estimated fault point distance can be calculated:

$$l1 = k \times L_C \quad (9.47)$$

Based on the above and the AFLA-2 discussed in chapter 8 for two-terminal lines, AFLA for three-terminal lines is composed of the following steps:

1. Three (3) independent sets of PMU pre-fault voltage and current phasor measurements and one (1) set of post-fault voltage phasor measurements at terminal A, B and C are recorded and stored.
2. System's Thevenin's equivalent at terminal A, B and C are determined online, as described in chapter 7, utilizing above-mentioned PMU pre-fault measurements.
3. Aforesaid PMU pre-fault measurements are additionally utilized for online determination of parameters pertaining to section A, B and C as detailed in section 9.1.
4. Superimposed electrical voltage measurements at terminal A, B and C are extracted as the difference between the post-fault measurements and the most recent set of pre-fault measurements at each terminal respectively.
5. Symmetrical transformation is then applied to transform phasor quantities into zero, positive and negative sequence components.

6. The first stage of fault location in three-terminal lines is then implemented to identify the faulted section.
7. The second stage is then applied to determine the fault location using relevant equations for VM and quadratic equation coefficients as described previously.

Figure 9.5 is a flowchart of AFLA for a three-terminal line highlighting the main steps mentioned above.

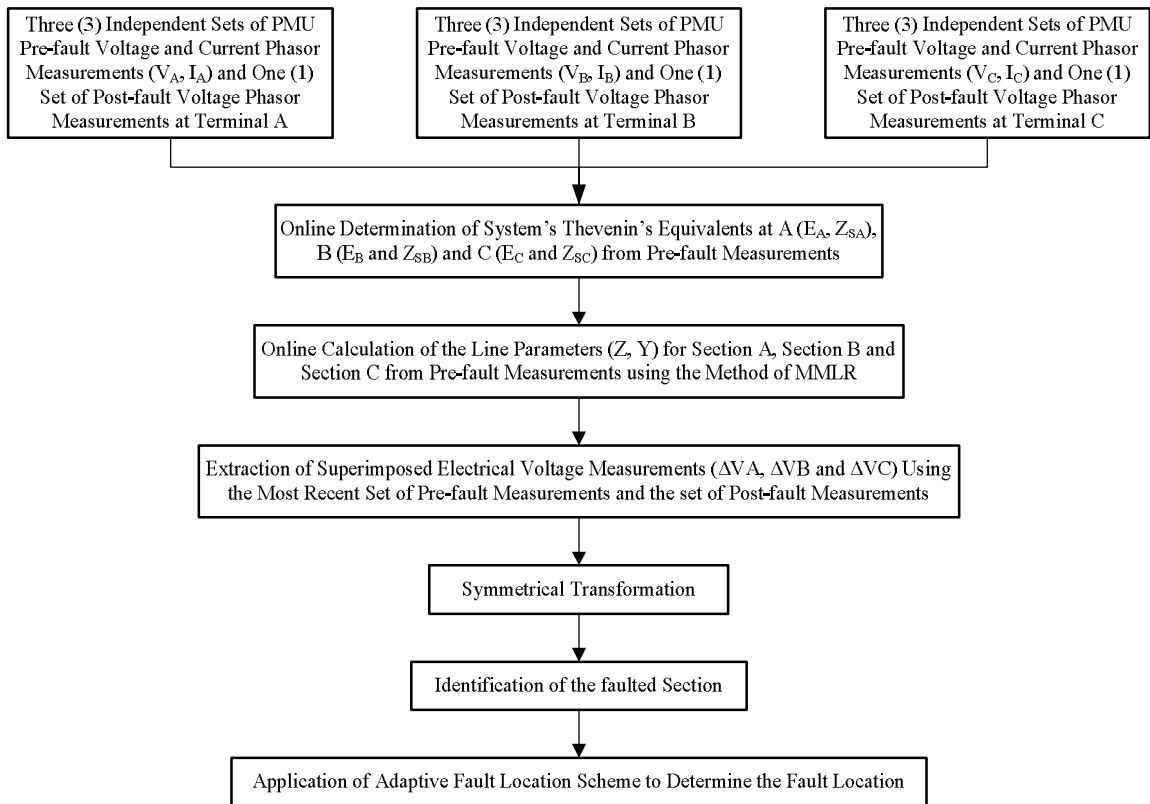


Figure 9.5: Flow chart of the proposed AFLA for a three-terminal line

### 9.3 Simulation results

This section presents PSCAD/EMTDC and MATLAB simulation results for a 500 kV three-terminal line, faulted in three sections A, B, C, when above-described algorithm is



applied to determine the fault location. Simulations are performed for LG, LL, LLG and LLL faults. Algorithm's accuracy is checked against fault type, location, fault resistance, pre-fault loading and fault inception angle.

### 9.3.1 Data generation and conditioning

A 500 kV three-terminal transmission network, represented by Figure 9.1, is considered under this study. The lengths of sections A, B, C are 150, 100 and 110 mile respectively. The presented fault location algorithm has been evaluated using pre-fault and post-fault data obtained from reliable PSCAD/EMTDC simulations of faults assumed to occur on sections A, B, C. Simulation parameters of the three-terminal transmission network are as shown in Table 9.1 where system's TEs at terminal A, B and C are determined as described in chapter 7.

TABLE 9.1: PARAMETERS OF THE 500 kV THREE-TERMINAL NETWORK

<i>Parameter</i>	<i>Value</i>
$R$	0.249168 $\Omega$ /mile
$L$	1.556277 mH/mile
$C$	19.469e-9 F/mile
$E_A$	500 kV $\angle 0^\circ$
$E_B$	475 kV $\angle -15^\circ$
$E_C$	472 kV $\angle -10^\circ$
$Z_{SA}$	5.7257 +j15.1762 $\Omega$
$Z_{SB}$	5.1033 +j15.3082 $\Omega$
$Z_{SC}$	5.4145 +j15.2422 $\Omega$

In order to show the errors of the presented algorithm itself, the CTs and VTs located at each line terminal are intentionally assumed as ideal devices. The three-phase voltage and current signals are sampled, as shown in Figure 9.6, at a frequency of 240 Hz which corresponds to 4 samples per cycle and are stored for post-processing. Sections A, B and

C are assumed to have the same impedance and the same admittance per unit length. With such assumption, only one set of pre-fault voltage and current phasor measurements at terminal A, B and C is utilized for online determination of the line parameters as detailed earlier. The DFT given by (3.3) is applied to extract the voltage and current phasors. The proposed algorithm is implemented in MATLAB. In this study, the percentage error used to measure the accuracy of fault location algorithm is as expressed in (8.10).

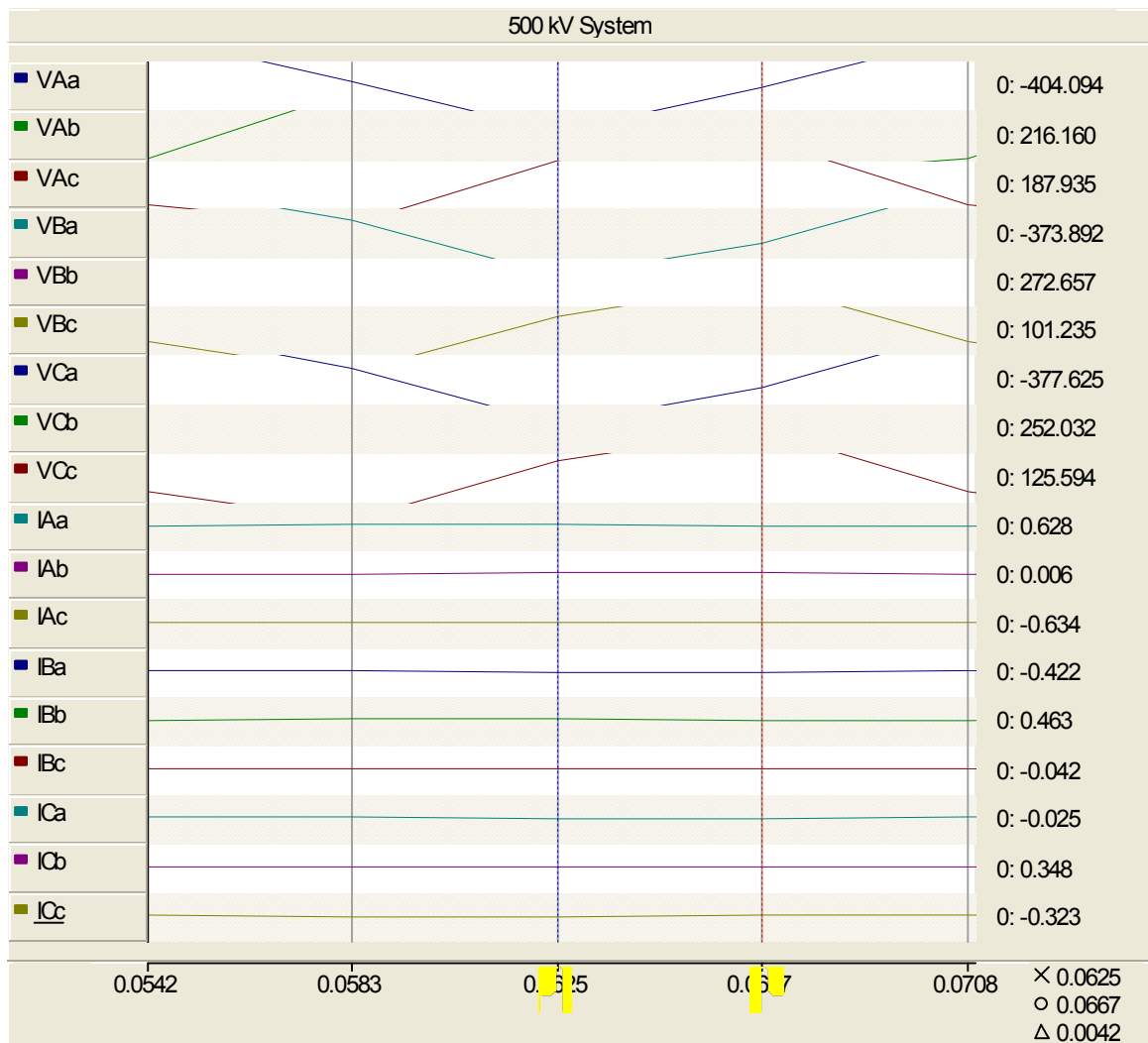


Figure 9.6: Sampling of voltage and current phasors at terminal A, B, C

### 9.3.2 Accuracy analysis

To test the accuracy of the proposed algorithm, different type of faults with different fault locations and fault resistances have been simulated. Tables 9.2-9.13 present the fault location estimates obtained for the single line to ground (LG) faults, line to line (LL) faults, line to line to ground (LLG) faults and three phase (LLL) faults occurred in section A, B and C. The fault type, fault resistance and actual fault location are given in the first, second and third column respectively. The estimated distance to fault and the estimation errors resulting from the proposed algorithm are respectively displayed in the fourth and fifth column. From the results obtained and considering all the cases simulated and presented in aforesaid tables, it is observed that the proposed algorithm is reasonably accurate with an average error of 0.785%, 0.572%, 0.561% and 0.563% for LG, LL, LLG and LLL faults occurred on section A. For faults on section B, the calculated average errors are 1.05%, 0.815%, 0.837% and 0.771% for LG, LL, LLG and LLL faults respectively. Finally, the calculated average errors for LG, LL, LLG and LLL faults on section C are 1.91%, 1.17%, 1.16% and 1.03%.

### 9.3.3 Influence of the fault resistance

The effect of the variation of the fault resistance in the algorithm's accuracy for all types of LG, LL, LLG and LLL faults are shown respectively in Table 9.14-9.25 assuming that the fault occurs at a distance of 0.4 p. u. from terminal A, B and C. Faults involving ground have been investigated for fault resistance values varying from 0 to 500  $\Omega$ . This captures low- and high-resistance faults. Faults not involving ground have been investigated for resistance values ranging between 0 to 30  $\Omega$ . In all cases the local and remote source impedances are set equal to the system values. Considering all the cases

simulated and presented in aforesaid tables, it is observed that the proposed algorithm is reasonably accurate and virtually independent of the fault resistance with an average error of 0.594%, 0.279%, 0.358% and 0.380% for LG, LL, LLG and LLL faults occurred on section A. For faults on section B, the calculated average errors are 0.972%, 0.928%, 0.992% and 1.069% for LG, LL, LLG and LLL faults respectively. Finally, the calculated average errors for LG, LL, LLG and LLL faults on section C are 1.066%, 1.099%, 1.229% and 1.173%.

TABLE 9.2  
FAULT-LOCATION ESTIMATES FOR SINGLE-LINE-TO-GROUND FAULTS ON SECTION A

<i><b>Fault Type</b></i>	<i><b>Fault Res. (<math>\Omega</math>)</b></i>	<i><b>Actual FL (p. u)</b></i>	<i><b>Estimated FL (p. u)</b></i>	<i><b>Error of Estimated FL (%)</b></i>
AG	10	0.2	0.1990	0.4838
		0.4	0.4010	0.2422
		0.6	0.6039	0.6464
		0.8	0.8084	1.0525
	100	0.2	0.1993	0.3516
		0.4	0.4017	0.4333
		0.6	0.6064	1.0650
		0.8	0.8115	1.4361
BG	10	0.2	0.1998	0.0909
		0.4	0.4018	0.4519
		0.6	0.6047	0.7907
		0.8	0.8088	1.1050
	100	0.2	0.2015	0.7626
		0.4	0.4050	1.2449
		0.6	0.6075	1.2493
		0.8	0.8113	1.4111
CG	10	0.2	0.1994	0.2918
		0.4	0.4023	0.5749
		0.6	0.6034	0.5667
		0.8	0.8086	1.0704
	100	0.2	0.1991	0.4433
		0.4	0.4028	0.7069
		0.6	0.6060	0.9943
		0.8	0.8110	1.3706

TABLE 9.3  
FAULT-LOCATION ESTIMATES FOR LINE-TO-LINE FAULTS ON SECTION A

<i><b>Fault Type</b></i>	<i><b>Fault Res. (<math>\Omega</math>)</b></i>	<i><b>Actual FL (p. u)</b></i>	<i><b>Estimated FL (p. u)</b></i>	<i><b>Error of Estimated FL (%)</b></i>
AB	1	0.2	0.1994	0.3054
		0.4	0.4008	0.2091
		0.6	0.6042	0.6933
		0.8	0.8083	1.0358
	10	0.2	0.1994	0.3241
		0.4	0.4009	0.2185
		0.6	0.6042	0.6996
		0.8	0.8083	1.0413
BC	1	0.2	0.1999	0.0733
		0.4	0.4020	0.5069
		0.6	0.6038	0.6299
		0.8	0.8087	1.0820
	10	0.2	0.1998	0.1145
		0.4	0.4021	0.5329
		0.6	0.6038	0.6268
		0.8	0.8086	1.0720
CA	1	0.2	0.1992	0.4180
		0.4	0.4015	0.3839
		0.6	0.6027	0.4462
		0.8	0.8080	1.0038
	10	0.2	0.1990	0.4771
		0.4	0.4015	0.3708
		0.6	0.6028	0.4642
		0.8	0.8081	1.0073

TABLE 9.4  
FAULT-LOCATION ESTIMATES FOR LINE-TO-LINE-TO-GROUND FAULTS ON SECTION A

<i><b>Fault Type</b></i>	<i><b>Fault Res. (<math>\Omega</math>)</b></i>	<i><b>Actual FL (p. u)</b></i>	<i><b>Estimated FL (p. u)</b></i>	<i><b>Error of Estimated FL (%)</b></i>
ABG	5	0.2	0.1994	0.2884
		0.4	0.4011	0.2847
		0.6	0.6038	0.6370
		0.8	0.8082	1.0291
	50	0.2	0.1996	0.1997
		0.4	0.4012	0.3036
		0.6	0.6042	0.7003
		0.8	0.8082	1.0307
BCG	5	0.2	0.1997	0.1738
		0.4	0.4018	0.4393
		0.6	0.6035	0.5899
		0.8	0.8085	1.0581
	50	0.2	0.1999	0.0652
		0.4	0.4020	0.5112
		0.6	0.6037	0.6125
		0.8	0.8086	1.0753
CAG	5	0.2	0.1993	0.3622
		0.4	0.4015	0.3727
		0.6	0.6030	0.4917
		0.8	0.8081	1.0082
	50	0.2	0.1994	0.2955
		0.4	0.4018	0.4469
		0.6	0.6029	0.4790
		0.8	0.8080	1.0029

TABLE 9.5  
FAULT-LOCATION ESTIMATES FOR THREE-PHASE FAULTS ON SECTION A

<i><b>Fault Type</b></i>	<i><b>Fault Res. (<math>\Omega</math>)</b></i>	<i><b>Actual FL (p. u)</b></i>	<i><b>Estimated FL (p. u)</b></i>	<i><b>Error of Estimated FL (%)</b></i>
ABC	1	0.2	0.1994	0.2774
		0.4	0.4014	0.3548
		0.6	0.6033	0.5524
		0.8	0.8082	1.0243
	10	0.2	0.1992	0.3952
		0.4	0.4014	0.3432
		0.6	0.6033	0.5451
		0.8	0.8081	1.0098

TABLE 9.6  
FAULT-LOCATION ESTIMATES FOR SINGLE-LINE-TO-GROUND FAULTS ON SECTION B

<i><b>Fault Type</b></i>	<i><b>Fault Res. (<math>\Omega</math>)</b></i>	<i><b>Actual FL (p. u)</b></i>	<i><b>Estimated FL (p. u)</b></i>	<i><b>Error of Estimated FL (%)</b></i>
AG	10	0.2	0.1996	0.1781
		0.4	0.4019	0.4770
		0.6	0.6056	0.9370
		0.8	0.8095	1.1834
	100	0.2	0.1975	1.2626
		0.4	0.4006	0.1619
		0.6	0.6061	1.0189
		0.8	0.8108	1.3546
BG	10	0.2	0.2004	0.2153
		0.4	0.4037	0.9337
		0.6	0.6053	0.8831
		0.8	0.8114	1.4224
	100	0.2	0.2022	1.0763
		0.4	0.4070	1.7611
		0.6	0.6108	1.8000
		0.8	0.8150	1.8744
CG	10	0.2	0.2011	0.5297
		0.4	0.4057	1.4190
		0.6	0.6053	0.8838
		0.8	0.8109	1.3595
	100	0.2	0.2004	0.1895
		0.4	0.4053	1.3343
		0.6	0.6085	1.4118
		0.8	0.8121	1.5071

TABLE 9.7  
FAULT-LOCATION ESTIMATES FOR LINE-TO-LINE FAULTS ON SECTION B

<i><b>Fault Type</b></i>	<i><b>Fault Res. (<math>\Omega</math>)</b></i>	<i><b>Actual FL (p. u)</b></i>	<i><b>Estimated FL (p. u)</b></i>	<i><b>Error of Estimated FL (%)</b></i>
AB	1	0.2	0.1998	0.1119
		0.4	0.4013	0.3339
		0.6	0.6051	0.8495
		0.8	0.8098	1.2263
	10	0.2	0.1997	0.1334
		0.4	0.4015	0.3811
		0.6	0.6051	0.8535
		0.8	0.8099	1.2376
BC	1	0.2	0.2009	0.4636
		0.4	0.4049	1.2180
		0.6	0.6041	0.6831
		0.8	0.8113	1.4180
	10	0.2	0.2010	0.5054
		0.4	0.4052	1.2981
		0.6	0.6045	0.7471
		0.8	0.8114	1.4213
CA	1	0.2	0.2006	0.3157
		0.4	0.4042	1.0453
		0.6	0.6050	0.8313
		0.8	0.8097	1.2118
	10	0.2	0.2005	0.2435
		0.4	0.4039	0.9826
		0.6	0.6051	0.8509
		0.8	0.8096	1.1996



TABLE 9.8  
FAULT-LOCATION ESTIMATES FOR LINE-TO-LINE-TO-GROUND FAULTS ON SECTION B

<i><b>Fault Type</b></i>	<i><b>Fault Res. (<math>\Omega</math>)</b></i>	<i><b>Actual FL (p. u)</b></i>	<i><b>Estimated FL (p. u)</b></i>	<i><b>Error of Estimated FL (%)</b></i>
ABG	5	0.2	0.2001	0.0619
		0.4	0.4023	0.5732
		0.6	0.6049	0.8197
		0.8	0.8100	1.2497
	50	0.2	0.2003	0.1536
		0.4	0.4022	0.5427
		0.6	0.6056	0.9332
		0.8	0.8102	1.2809
BCG	5	0.2	0.2008	0.3769
		0.4	0.4043	1.0722
		0.6	0.6042	0.7080
		0.8	0.8108	1.3477
	50	0.2	0.2011	0.5591
		0.4	0.4051	1.2651
		0.6	0.6043	0.7152
		0.8	0.8113	1.4101
CAG	5	0.2	0.2006	0.2789
		0.4	0.4038	0.9573
		0.6	0.6049	0.8156
		0.8	0.8099	1.2330
	50	0.2	0.2009	0.4699
		0.4	0.4044	1.1084
		0.6	0.6055	0.9085
		0.8	0.8100	1.2504

TABLE 9.9  
FAULT-LOCATION ESTIMATES FOR THREE-PHASE FAULTS ON SECTION B

<i><b>Fault Type</b></i>	<i><b>Fault Res. (<math>\Omega</math>)</b></i>	<i><b>Actual FL (p. u)</b></i>	<i><b>Estimated FL (p. u)</b></i>	<i><b>Error of Estimated FL (%)</b></i>
ABC	1	0.2	0.2004	0.2201
		0.4	0.4033	0.8354
		0.6	0.6045	0.7503
		0.8	0.8101	1.2631
	10	0.2	0.2004	0.1885
		0.4	0.4035	0.8674
		0.6	0.6048	0.7918
		0.8	0.8100	1.2558

TABLE 9.10  
FAULT-LOCATION ESTIMATES FOR SINGLE-LINE-TO-GROUND FAULTS ON SECTION C

<i><b>Fault Type</b></i>	<i><b>Fault Res. (<math>\Omega</math>)</b></i>	<i><b>Actual FL (p. u)</b></i>	<i><b>Estimated FL (p. u)</b></i>	<i><b>Error of Estimated FL (%)</b></i>
AG	10	0.2	0.2008	0.4191
		0.4	0.4036	0.9031
		0.6	0.6107	1.7763
		0.8	0.8146	1.8204
	100	0.2	0.2027	1.3470
		0.4	0.4051	1.2761
		0.6	0.6206	3.4265
		0.8	0.8218	2.7243
BG	10	0.2	0.2015	0.7681
		0.4	0.4045	1.1168
		0.6	0.6127	2.1249
		0.8	0.8141	1.7628
	100	0.2	0.2052	2.6231
		0.4	0.4090	2.2581
		0.6	0.6220	3.6661
		0.8	0.8221	2.7667
CG	10	0.2	0.2015	0.7319
		0.4	0.4059	1.4722
		0.6	0.6124	2.0622
		0.8	0.8139	1.7426
	100	0.2	0.2029	1.4520
		0.4	0.4073	1.8373
		0.6	0.6191	3.1814
		0.8	0.8204	2.5472

TABLE 9.11  
FAULT-LOCATION ESTIMATES FOR LINE-TO-LINE FAULTS ON SECTION C

<i><b>Fault Type</b></i>	<i><b>Fault Res. (<math>\Omega</math>)</b></i>	<i><b>Actual FL (p. u)</b></i>	<i><b>Estimated FL (p. u)</b></i>	<i><b>Error of Estimated FL (%)</b></i>
AB	1	0.2	0.2007	0.3727
		0.4	0.4027	0.6850
		0.6	0.6088	1.4593
		0.8	0.8126	1.5706
	10	0.2	0.2008	0.3815
		0.4	0.4029	0.7131
		0.6	0.6092	1.5363
		0.8	0.8128	1.6036
BC	1	0.2	0.2014	0.6895
		0.4	0.4047	1.1712
		0.6	0.6110	1.8366
		0.8	0.8119	1.4838
	10	0.2	0.2014	0.6952
		0.4	0.4050	1.2445
		0.6	0.6112	1.8694
		0.8	0.8122	1.5229
CA	1	0.2	0.2009	0.4480
		0.4	0.4046	1.1509
		0.6	0.6091	1.5232
		0.8	0.8125	1.5684
	10	0.2	0.2008	0.4058
		0.4	0.4045	1.1299
		0.6	0.6092	1.5349
		0.8	0.8127	1.5933

TABLE 9.12  
FAULT-LOCATION ESTIMATES FOR LINE-TO-LINE-TO-GROUND FAULTS ON SECTION C

<i><b>Fault Type</b></i>	<i><b>Fault Res. (<math>\Omega</math>)</b></i>	<i><b>Actual FL (p. u)</b></i>	<i><b>Estimated FL (p. u)</b></i>	<i><b>Error of Estimated FL (%)</b></i>
ABG	5	0.2	0.2008	0.4144
		0.4	0.4032	0.8079
		0.6	0.6085	1.4228
		0.8	0.8120	1.4998
	50	0.2	0.2011	0.5274
		0.4	0.4033	0.8145
		0.6	0.6087	1.4576
		0.8	0.8124	1.5526
BCG	5	0.2	0.2012	0.5838
		0.4	0.4043	1.0746
		0.6	0.6098	1.6417
		0.8	0.8116	1.4517
	50	0.2	0.2015	0.7475
		0.4	0.4048	1.2039
		0.6	0.6108	1.7967
		0.8	0.8118	1.4749
CAG	5	0.2	0.2009	0.4482
		0.4	0.4043	1.0644
		0.6	0.6088	1.4611
		0.8	0.8121	1.5106
	50	0.2	0.2012	0.5967
		0.4	0.4048	1.2122
		0.6	0.6092	1.5314
		0.8	0.8126	1.5774

TABLE 9.13  
FAULT-LOCATION ESTIMATES FOR THREE-PHASE FAULTS ON SECTION C

<i><b>Fault Type</b></i>	<i><b>Fault Res. (<math>\Omega</math>)</b></i>	<i><b>Actual FL (p. u)</b></i>	<i><b>Estimated FL (p. u)</b></i>	<i><b>Error of Estimated FL (%)</b></i>
ABC	1	0.2	0.2009	0.4328
		0.4	0.4037	0.9329
		0.6	0.6083	1.3816
		0.8	0.8113	1.4144
	10	0.2	0.2007	0.3415
		0.4	0.4038	0.9484
		0.6	0.6084	1.3927
		0.8	0.8115	1.4392

TABLE 9.14  
INFLUENCE OF THE FAULT RESISTANCE ON THE ALGORITHM'S ACCURACY FOR SINGLE-LINE-TO-GROUND FAULTS (ACTUAL FL: 0.4 P.U. FROM TERMINAL A)

<i>Fault Res.</i> ( $\Omega$ )	<i>Fault Type</i>					
	<i>AG</i>		<i>BG</i>		<i>CG</i>	
	<i>Estim. FL</i> (p. u)	<i>Error of Estim. FL</i> (%)	<i>Estim. FL</i> (p. u)	<i>Error of Estim. FL</i> (%)	<i>Estim. FL</i> (p. u)	<i>Error of Estim. FL</i> (%)
0	0.3998	0.0390	0.4004	0.0944	0.4018	0.4494
1	0.3998	0.0478	0.4004	0.1003	0.4018	0.4478
5	0.3997	0.0829	0.4005	0.1240	0.4018	0.4409
15	0.3993	0.1686	0.4007	0.1854	0.4017	0.4184
20	0.3992	0.2092	0.4009	0.2158	0.4016	0.4032
50	0.3983	0.4255	0.4015	0.3640	0.4011	0.2664
150	0.3961	0.9713	0.4022	0.5523	0.3985	0.3640
200	0.3952	1.1879	0.4023	0.5777	0.3973	0.6789
400	0.3928	1.8073	0.4026	0.6545	0.3931	1.7236
500	0.3920	2.0005	0.4029	0.7139	0.3915	2.1178

TABLE 9.15  
INFLUENCE OF THE FAULT RESISTANCE ON THE ALGORITHM'S ACCURACY FOR LINE-TO-LINE FAULTS (ACTUAL FL: 0.4 P.U. FROM TERMINAL A)

<i>Fault Res.</i> ( $\Omega$ )	<i>Fault Type</i>					
	<i>AB</i>		<i>BC</i>		<i>CA</i>	
	<i>Estim. FL</i> (p. u)	<i>Error of Estim. FL</i> (%)	<i>Estim. FL</i> (p. u)	<i>Error of Estim. FL</i> (%)	<i>Estim. FL</i> (p. u)	<i>Error of Estim. FL</i> (%)
0	0.4000	0.0014	0.4020	0.4901	0.4014	0.3593
0.5	0.4000	0.0010	0.4020	0.4915	0.4014	0.3571
1.5	0.4000	0.0004	0.4020	0.4944	0.4014	0.3527
2.5	0.4000	0.0002	0.4020	0.4972	0.4014	0.3483
5	0.4000	0.0018	0.4020	0.5043	0.4013	0.3372
7.5	0.4000	0.0034	0.4020	0.5114	0.4013	0.3262
15	0.4000	0.0076	0.4021	0.5326	0.4012	0.2925
20	0.4000	0.0098	0.4022	0.5465	0.4011	0.2698
25	0.4000	0.0115	0.4022	0.5599	0.4010	0.2468
30	0.3999	0.0128	0.4023	0.5728	0.4009	0.2236

TABLE 9.16  
INFLUENCE OF THE FAULT RESISTANCE ON THE ALGORITHM'S ACCURACY FOR LINE-TO-LINE-  
TO-GROUND FAULTS (ACTUAL FL: 0.4 P.U. FROM TERMINAL A)

<i>Fault Res. (<math>\Omega</math>)</i>	<i>Fault Type</i>					
	<i>ABG</i>		<i>BCG</i>		<i>CAG</i>	
	<i>Estim. FL (p. u)</i>	<i>Error of Estim. FL (%)</i>	<i>Estim. FL (p. u)</i>	<i>Error of Estim. FL (%)</i>	<i>Estim. FL (p. u)</i>	<i>Error of Estim. FL (%)</i>
0	0.4008	0.2002	0.4018	0.4443	0.4015	0.3789
1	0.4008	0.1986	0.4018	0.4457	0.4015	0.3774
2	0.4008	0.1973	0.4018	0.4474	0.4015	0.3763
10	0.4008	0.1912	0.4019	0.4662	0.4015	0.3822
25	0.4007	0.1824	0.4020	0.4967	0.4016	0.4096
75	0.4006	0.1524	0.4021	0.5253	0.4018	0.4494
100	0.4006	0.1416	0.4021	0.5280	0.4018	0.4547
150	0.4005	0.1260	0.4021	0.5291	0.4018	0.4577
200	0.4005	0.1151	0.4021	0.5283	0.4018	0.4566
250	0.4004	0.1065	0.4021	0.5269	0.4018	0.4537

TABLE 9.17  
INFLUENCE OF THE FAULT RESISTANCE ON THE ALGORITHM'S ACCURACY FOR THREE-PHASE  
FAULTS (ACTUAL FL: 0.4 P.U. FROM TERMINAL A)

<i>Fault Res. (<math>\Omega</math>)</i>	<i>Estimated FL (p. u)</i>	<i>Error of Estimated FL (%)</i>
0	0.4016	0.3988
0.5	0.4016	0.3980
1.5	0.4016	0.3966
2.5	0.4016	0.3952
5	0.4016	0.3916
7.5	0.4016	0.3881
15	0.4014	0.3432
20	0.4015	0.3773
25	0.4014	0.3610
30	0.4014	0.3516

TABLE 9.18  
INFLUENCE OF THE FAULT RESISTANCE ON THE ALGORITHM'S ACCURACY FOR SINGLE-LINE-TO-GROUND FAULTS (ACTUAL FL: 0.4 P.U. FROM TERMINAL B)

<i>Fault Res.</i> ( $\Omega$ )	<i>Fault Type</i>					
	<i>AG</i>		<i>BG</i>		<i>CG</i>	
	<i>Estim. FL</i> (p. u)	<i>Error of Estim. FL (%)</i>	<i>Estim. FL</i> (p. u)	<i>Error of Estim. FL (%)</i>	<i>Estim. FL</i> (p. u)	<i>Error of Estim. FL (%)</i>
0	0.4030	0.7513	0.4032	0.7935	0.4050	1.2493
1	0.4030	0.7376	0.4032	0.8032	0.4050	1.2517
5	0.4027	0.6845	0.4034	0.8437	0.4050	1.2577
15	0.4023	0.5639	0.4038	0.9430	0.4050	1.2507
20	0.4020	0.5083	0.4040	0.9877	0.4050	1.2377
50	0.4009	0.2129	0.4047	1.1788	0.4044	1.0885
150	0.3979	0.5285	0.4057	1.4232	0.4019	0.4862
200	0.3968	0.8038	0.4061	1.5294	0.4011	0.2633
400	0.3942	1.4460	0.4083	2.0772	0.3995	0.1351
500	0.3936	1.5993	0.4094	2.3557	0.3994	0.1564

TABLE 9.19  
INFLUENCE OF THE FAULT RESISTANCE ON THE ALGORITHM'S ACCURACY FOR LINE-TO-LINE FAULTS (ACTUAL FL: 0.4 P.U. FROM TERMINAL B)

<i>Fault Res.</i> ( $\Omega$ )	<i>Fault Type</i>					
	<i>AB</i>		<i>BC</i>		<i>CA</i>	
	<i>Estim. FL</i> (p. u)	<i>Error of Estim. FL (%)</i>	<i>Estim. FL</i> (p. u)	<i>Error of Estim. FL (%)</i>	<i>Estim. FL</i> (p. u)	<i>Error of Estim. FL (%)</i>
0	0.4024	0.6121	0.4044	1.1116	0.4043	1.0704
0.5	0.4024	0.6112	0.4045	1.1147	0.4043	1.0677
1.5	0.4024	0.6095	0.4045	1.1209	0.4042	1.0624
2.5	0.4024	0.6079	0.4045	1.1272	0.4042	1.0570
5	0.4024	0.6043	0.4046	1.1425	0.4042	1.0433
7.5	0.4024	0.6012	0.4046	1.1575	0.4041	1.0293
15	0.4024	0.5944	0.4048	1.2001	0.4039	0.9863
20	0.4024	0.5914	0.4049	1.2263	0.4038	0.9570
25	0.4024	0.5891	0.4050	1.2505	0.4037	0.9274
30	0.4023	0.5874	0.4051	1.2728	0.4036	0.8974

TABLE 9.20  
INFLUENCE OF THE FAULT RESISTANCE ON THE ALGORITHM'S ACCURACY FOR LINE-TO-LINE-  
TO-GROUND FAULTS (ACTUAL FL: 0.4 P.U. FROM TERMINAL B)

<i>Fault Res. (<math>\Omega</math>)</i>	<i>Fault Type</i>					
	<i>ABG</i>		<i>BCG</i>		<i>CAG</i>	
	<i>Estim. FL (p. u)</i>	<i>Error of Estim. FL (%)</i>	<i>Estim. FL (p. u)</i>	<i>Error of Estim. FL (%)</i>	<i>Estim. FL (p. u)</i>	<i>Error of Estim. FL (%)</i>
0	0.4031	0.7717	0.4041	1.0212	0.4040	1.0005
1	0.4031	0.7706	0.4041	1.0231	0.4040	1.0005
2	0.4031	0.7701	0.4041	1.0258	0.4040	1.0017
10	0.4031	0.7761	0.4043	1.0631	0.4041	1.0350
25	0.4032	0.7887	0.4045	1.1195	0.4044	1.1007
75	0.4031	0.7818	0.4047	1.1665	0.4047	1.1677
100	0.4031	0.7748	0.4047	1.1703	0.4047	1.1748
150	0.4030	0.7615	0.4047	1.1708	0.4047	1.1771
200	0.4030	0.7494	0.4047	1.1683	0.4047	1.1733
250	0.4030	0.7384	0.4047	1.1650	0.4047	1.1675

TABLE 9.21  
INFLUENCE OF THE FAULT RESISTANCE ON THE ALGORITHM'S ACCURACY FOR THREE-PHASE  
FAULTS (ACTUAL FL: 0.4 P.U. FROM TERMINAL B)

<i>Fault Res. (<math>\Omega</math>)</i>	<i>Estimated FL (p. u)</i>	<i>Error of Estimated FL (%)</i>
0	0.4040	1.0100
0.5	0.4041	1.0131
1.5	0.4041	1.0191
2.5	0.4041	1.0252
5	0.4042	1.0403
7.5	0.4042	1.0552
15	0.4044	1.0969
20	0.4045	1.1220
25	0.4046	1.1449
30	0.4047	1.1658



TABLE 9.22  
INFLUENCE OF THE FAULT RESISTANCE ON THE ALGORITHM'S ACCURACY FOR SINGLE-LINE-TO-GROUND FAULTS (ACTUAL FL: 0.4 P.U. FROM TERMINAL C)

<i>Fault Res.</i> ( $\Omega$ )	<i>Fault Type</i>					
	<i>AG</i>		<i>BG</i>		<i>CG</i>	
	<i>Estim. FL</i> (p. u)	<i>Error of Estim. FL</i> (%)	<i>Estim. FL</i> (p. u)	<i>Error of Estim. FL</i> (%)	<i>Estim. FL</i> (p. u)	<i>Error of Estim. FL</i> (%)
0	0.4038	0.9472	0.4039	0.9792	0.4056	1.3923
1	0.4037	0.9345	0.4039	0.9851	0.4056	1.3937
5	0.4035	0.8844	0.4040	1.0109	0.4056	1.3978
15	0.4031	0.7659	0.4043	1.0816	0.4056	1.3948
20	0.4028	0.7098	0.4045	1.1163	0.4055	1.3859
50	0.4016	0.4060	0.4051	1.2774	0.4050	1.2619
150	0.3985	0.3706	0.4059	1.4690	0.4026	0.6462
200	0.3973	0.6664	0.4061	1.5334	0.4015	0.3851
400	0.3944	1.4073	0.4077	1.9132	0.3992	0.2077
500	0.3936	1.6058	0.4085	2.1276	0.3987	0.3202

TABLE 9.23  
INFLUENCE OF THE FAULT RESISTANCE ON THE ALGORITHM'S ACCURACY FOR LINE-TO-LINE FAULTS (ACTUAL FL: 0.4 P.U. FROM TERMINAL C)

<i>Fault Res.</i> ( $\Omega$ )	<i>Fault Type</i>					
	<i>AB</i>		<i>BC</i>		<i>CA</i>	
	<i>Estim. FL</i> (p. u)	<i>Error of Estim. FL</i> (%)	<i>Estim. FL</i> (p. u)	<i>Error of Estim. FL</i> (%)	<i>Estim. FL</i> (p. u)	<i>Error of Estim. FL</i> (%)
0	0.4035	0.8813	0.4051	1.2654	0.4049	1.2343
0.5	0.4033	0.8178	0.4051	1.2676	0.4049	1.2319
1.5	0.4033	0.8153	0.4051	1.2721	0.4049	1.2272
2.5	0.4033	0.8129	0.4051	1.2766	0.4049	1.2224
5	0.4032	0.8072	0.4052	1.2880	0.4048	1.2104
7.5	0.4032	0.8018	0.4052	1.2993	0.4048	1.1982
15	0.4032	0.7876	0.4053	1.3328	0.4046	1.1606
20	0.4031	0.7796	0.4054	1.3543	0.4045	1.1348
25	0.4031	0.7726	0.4055	1.3748	0.4044	1.1085
30	0.4031	0.7663	0.4056	1.3943	0.4043	1.0817

TABLE 9.24  
INFLUENCE OF THE FAULT RESISTANCE ON THE ALGORITHM'S ACCURACY FOR LINE-TO-LINE-TO-GROUND FAULTS (ACTUAL FL: 0.4 P.U. FROM TERMINAL C)

<i>Fault Res. (<math>\Omega</math>)</i>	<i>Fault Type</i>					
	<i>ABG</i>		<i>BCG</i>		<i>CAG</i>	
	<i>Estim. FL (p. u)</i>	<i>Error of Estim. FL (%)</i>	<i>Estim. FL (p. u)</i>	<i>Error of Estim. FL (%)</i>	<i>Estim. FL (p. u)</i>	<i>Error of Estim. FL (%)</i>
0	0.4040	1.0091	0.4049	1.2325	0.4049	1.2158
1	0.4040	1.0116	0.4049	1.2374	0.4049	1.2185
2	0.4041	1.0144	0.4050	1.2429	0.4049	1.2221
10	0.4042	1.0402	0.4052	1.2921	0.4051	1.2667
25	0.4043	1.0650	0.4054	1.3513	0.4053	1.3358
75	0.4042	1.0566	0.4056	1.3911	0.4056	1.3983
100	0.4042	1.0476	0.4056	1.3929	0.4056	1.4040
150	0.4041	1.0321	0.4056	1.3912	0.4056	1.4051
200	0.4041	1.0191	0.4056	1.3877	0.4056	1.4010
250	0.4040	1.0079	0.4055	1.3840	0.4056	1.3952

TABLE 9.25  
INFLUENCE OF THE FAULT RESISTANCE ON THE ALGORITHM'S ACCURACY FOR THREE-PHASE FAULTS (ACTUAL FL: 0.4 P.U. FROM TERMINAL C)

<i>Fault Res. (<math>\Omega</math>)</i>	<i>Estimated FL (p. u)</i>	<i>Error of Estimated FL (%)</i>
0	0.4045	1.1368
0.5	0.4046	1.1385
1.5	0.4046	1.1420
2.5	0.4046	1.1455
5	0.4046	1.1544
7.5	0.4047	1.1633
15	0.4048	1.1894
20	0.4048	1.2053
25	0.4049	1.2196
30	0.4049	1.2325

### 9.3.4 Influence of the fault inception angle

The effect of the variation of the fault inception angle on the algorithm's accuracy for AG, BC and BCG faults are shown respectively in Table 9.26-9.28 assuming that the fault occurs at a distance of 0.4 p. u. from terminal A, B and C. Fault inception angle is varied from 0 to 150°. Considering all the cases simulated and presented in aforesaid tables, it is observed that the proposed algorithm is reasonably accurate and virtually independent of the fault inception angle with an average error of 0.234%, 0.745% and 0.642% for AG, BC and BCG faults occurred on section A. For faults on section B, the calculated average errors are 0.620%, 1.170% and 1.060% for AG, BC and BCG faults respectively. Finally, the calculated average errors for AG, BC and BCG faults on section C are 0.823%, 1.310% and 1.219%. Figure 9.7-9.9 show the effect of the variation of the fault inception angle on the algorithm's accuracy for different types of faults occurred at 0.4 p.u. from terminal A, B and C respectively.

TABLE 9.26  
INFLUENCE OF THE FAULT INCEPTION ANGLE ON THE ALGORITHM'S ACCURACY  
(ACTUAL FL: 0.4 P.U. FROM TERMINAL A)

<i>Fault Inception Angle (°)</i>	<i>Fault Type</i>					
	<i>AG</i>		<i>BC</i>		<i>BCG</i>	
	<i>Estim. FL (p. u)</i>	<i>Error of Estim. FL (%)</i>	<i>Estim. FL (p. u)</i>	<i>Error of Estim. FL (%)</i>	<i>Estim. FL (p. u)</i>	<i>Error of Estim. FL (%)</i>
0	0.4009	0.2232	0.4030	0.7490	0.4026	0.6460
30	0.4009	0.2225	0.4030	0.7535	0.4026	0.6509
45	0.4009	0.2241	0.4030	0.7510	0.4026	0.6483
60	0.4009	0.2206	0.4030	0.7466	0.4026	0.6431
90	0.4009	0.2233	0.4029	0.7192	0.4025	0.6151
120	0.4010	0.2400	0.4028	0.7121	0.4024	0.6110
135	0.4010	0.2604	0.4031	0.7644	0.4026	0.6575
150	0.4010	0.2604	0.4031	0.7643	0.4027	0.6662

TABLE 9.27  
INFLUENCE OF THE FAULT INCEPTION ANGLE ON THE ALGORITHM'S ACCURACY  
(ACTUAL FL: 0.4 P.U. FROM TERMINAL B)

<i>Fault Inception Angle (°)</i>	<i>Fault Type</i>					
	<i>AG</i>		<i>BC</i>		<i>BCG</i>	
	<i>Estim. FL (p. u)</i>	<i>Error of Estim. FL (%)</i>	<i>Estim. FL (p. u)</i>	<i>Error of Estim. FL (%)</i>	<i>Estim. FL (p. u)</i>	<i>Error of Estim. FL (%)</i>
0	0.4025	0.6224	0.4047	1.1722	0.4043	1.0631
30	0.4025	0.6215	0.4047	1.1778	0.4043	1.0694
45	0.4025	0.6250	0.4047	1.1690	0.4042	1.0592
60	0.4025	0.6173	0.4047	1.1739	0.4043	1.0649
90	0.4025	0.6178	0.4047	1.1634	0.4042	1.0563
120	0.4025	0.6275	0.4047	1.1859	0.4043	1.0790
135	0.4024	0.6111	0.4047	1.1766	0.4043	1.0635
150	0.4025	0.6169	0.4046	1.1390	0.4041	1.0214

TABLE 9.28  
INFLUENCE OF THE FAULT INCEPTION ANGLE ON THE ALGORITHM'S ACCURACY  
(ACTUAL FL: 0.4 P.U. FROM TERMINAL C)

<i>Fault Inception Angle (°)</i>	<i>Fault Type</i>					
	<i>AG</i>		<i>BC</i>		<i>BCG</i>	
	<i>Estim. FL (p. u)</i>	<i>Error of Estim. FL (%)</i>	<i>Estim. FL (p. u)</i>	<i>Error of Estim. FL (%)</i>	<i>Estim. FL (p. u)</i>	<i>Error of Estim. FL (%)</i>
0	0.4033	0.8240	0.4052	1.3106	0.4049	1.2190
30	0.4033	0.8241	0.4052	1.3082	0.4049	1.2160
45	0.4033	0.8260	0.4052	1.3076	0.4049	1.2158
60	0.4033	0.8253	0.4052	1.3122	0.4049	1.2212
90	0.4033	0.8217	0.4053	1.3349	0.4050	1.2474
120	0.4032	0.8041	0.4054	1.3400	0.4050	1.2512
135	0.4034	0.8493	0.4052	1.2942	0.4048	1.2053
150	0.4032	0.8079	0.4051	1.2712	0.4047	1.1733

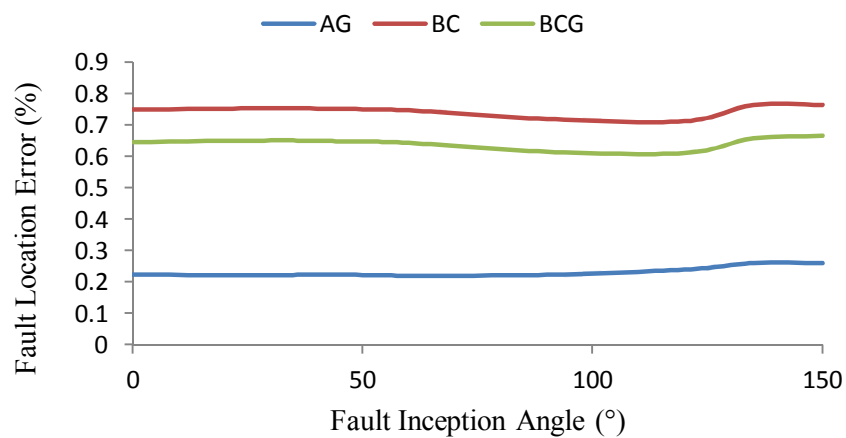


Figure 9.7: Effect of fault inception angle on FL accuracy (Actual FL: 0.4 p.u. from A)

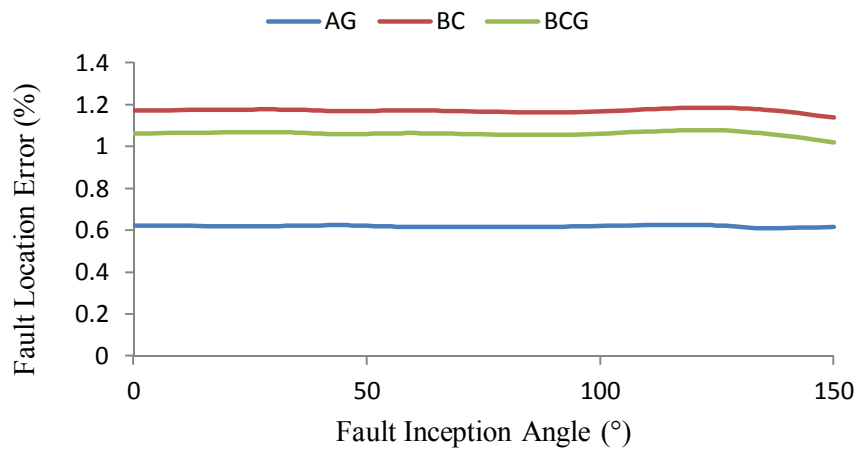


Figure 9.8: Effect of fault inception angle on FL accuracy (Actual FL: 0.4 p.u. from B)

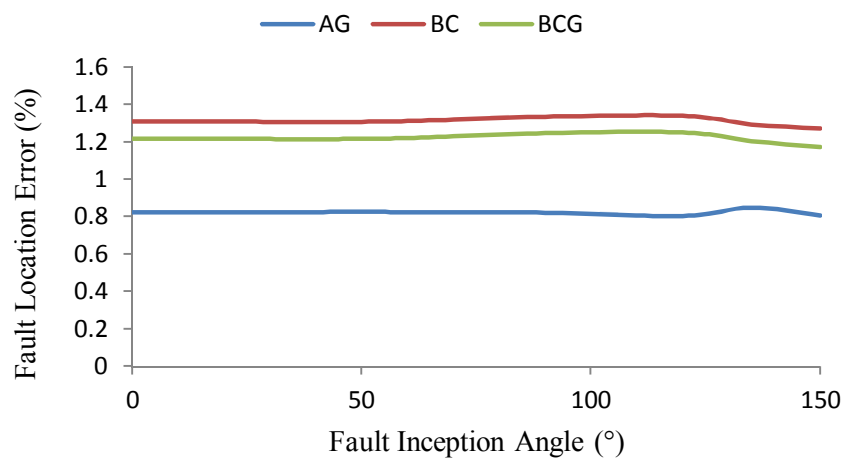


Figure 9.9: Effect of fault inception angle on FL accuracy (Actual FL: 0.4 p.u. from C)

### 9.3.5 Influence of the pre-fault loading

Table 9.29-9.31 show the influence of the pre-fault loading on the algorithm's accuracy for AG, BC and BCG faults assuming that these faults occur at 0.4 p.u. distance from terminal A, B and C respectively. The pre-fault loading is varied from 0.5 to 3 times its original value. Considering all the cases simulated and presented in aforesaid tables, it is observed that the proposed algorithm is reasonably accurate with an average error of 0.80%, 1.23% and 1.13% for AG, BC and BCG faults occurred on section A. For faults on section B, the calculated average errors are 1.18%, 1.72% and 1.61% for AG, BC and BCG faults respectively. Finally, the calculated average errors for AG, BC and BCG faults on section C are 1.45%, 1.92% and 1.83%.

TABLE 9.29  
INFLUENCE OF THE PRE-FAULT LOADING AT TERMINAL-A ON THE ALGORITHM'S ACCURACY  
(ACTUAL FL: 0.4 P.U. FROM TERMINAL A)

<i>Variation of Pre-fault Loading (%)</i>	<i>Fault Type</i>					
	<i>AG</i>		<i>BC</i>		<i>BCG</i>	
	<i>Estim. FL (p. u)</i>	<i>Error of Estim. FL (%)</i>	<i>Estim. FL (p. u)</i>	<i>Error of Estim. FL (%)</i>	<i>Estim. FL (p. u)</i>	<i>Error of Estim. FL (%)</i>
-50	0.3989	0.2625	0.4011	0.2696	0.4007	0.1652
-20	0.4001	0.0287	0.4022	0.5580	0.4018	0.4543
20	0.4017	0.4180	0.4038	0.9402	0.4034	0.8379
50	0.4028	0.7107	0.4049	1.2280	0.4045	1.1265
100	0.4048	1.1998	0.4068	1.7099	0.4064	1.6096
200	0.4087	2.1820	0.4107	2.6818	0.4103	2.5826

TABLE 9.30  
INFLUENCE OF THE PRE-FAULT LOADING AT TERMINAL-B ON THE ALGORITHM'S ACCURACY  
(ACTUAL FL: 0.4 P.U. FROM TERMINAL B)

<i>Variation of Pre-fault Loading (%)</i>	<i>Fault Type</i>					
	<i>AG</i>		<i>BC</i>		<i>BCG</i>	
	<i>Estim. FL (p. u)</i>	<i>Error of Estim. FL (%)</i>	<i>Estim. FL (p. u)</i>	<i>Error of Estim. FL (%)</i>	<i>Estim. FL (p. u)</i>	<i>Error of Estim. FL (%)</i>
-50	0.4003	0.0741	0.4025	0.6351	0.4021	0.5250
-20	0.4016	0.4025	0.4038	0.9569	0.4034	0.8474
20	0.4034	0.8429	0.4056	1.3882	0.4051	1.2795
50	0.4047	1.1750	0.4069	1.7137	0.4064	1.6054
100	0.4069	1.7313	0.4090	2.2599	0.4086	2.1522
200	0.4114	2.8529	0.4135	3.3648	0.4130	3.2574

TABLE 9.31  
INFLUENCE OF THE PRE-FAULT LOADING AT TERMINAL-C ON THE ALGORITHM'S ACCURACY  
(ACTUAL FL: 0.4 P.U. FROM TERMINAL C)

<i>Variation of Pre-fault Loading (%)</i>	<i>Fault Type</i>					
	<i>AG</i>		<i>BC</i>		<i>BCG</i>	
	<i>Estim. FL (p. u)</i>	<i>Error of Estim. FL (%)</i>	<i>Estim. FL (p. u)</i>	<i>Error of Estim. FL (%)</i>	<i>Estim. FL (p. u)</i>	<i>Error of Estim. FL (%)</i>
-50	0.4008	0.2108	0.4028	0.7078	0.4025	0.6155
-20	0.4023	0.5780	0.4043	1.0692	0.4039	0.9772
20	0.4043	1.0707	0.4062	1.5525	0.4058	1.4613
50	0.4058	1.4421	0.4077	1.9166	0.4073	1.8261
100	0.4083	2.0643	0.4101	2.5268	0.4097	2.4373
200	0.4133	3.3178	0.4150	3.7596	0.4147	3.6714

## 9.4 Comparison with non-adaptive algorithm for three-terminal lines

In the proposed adaptive fault location algorithm for three-terminal lines, system impedance and line parameters are determined online and, thus, the effect of the surrounding environment and operation history on these parameters is nullified. System

impedance and line parameters determined online from PMU synchronized measurements certainly reflect the system's practical operating conditions prior to and after the fault occurrence. In non-adaptive fault location algorithms, system impedance and line parameters are provided by the electric utility and assumed to be constant regardless of the environmental and system operating conditions. Such assumption, however, is a source of error that impacts the fault location accuracy.

In this section, we investigate the effect of system impedance and line parameters uncertainty on fault location accuracy assuming that they vary within  $\pm 25\%$  from their practical values. Table 9.32 shows the influence of the line parameters and system impedance variation on algorithm's accuracy for AG, BC, CAG and ABC faults assuming that these faults occur at 0.4 p.u. distance from terminal A. Considering all the cases simulated and presented in aforesaid table, one can easily observe that the effect of system impedance and parameters uncertainty on fault location can reach up to 14% if the parameters used in fault location vary 25% of the practical parameters. Figure 9.10 depicts the effect of the system impedance and line parameter variation on the algorithm's accuracy for aforementioned types of faults.



TABLE 9.32  
THREE-TERMINAL LINES: INFLUENCE OF LINE PARAMETERS AND SYSTEM IMPEDANCE  
VARIATION ON THE ALGORITHM'S ACCURACY (ACTUAL FL: 0.4 P.U. FROM TERMINAL A)

Parameter Variation (%)	Fault Type							
	AG		CAG		BC		ABC	
	Estim. FL (p. u)	Error of Estim. FL (%)	Estim. FL (p. u)	Error of Estim. FL (%)	Estim. FL (p. u)	Error of Estim. FL (%)	Estim. FL (p. u)	Error of Estim. FL (%)
-25	0.3425	14.3714	0.3437	14.0662	0.3443	13.9135	0.3436	14.1032
-20	0.3547	11.3209	0.3560	11.0108	0.3566	10.8551	0.3558	11.0480
-15	0.3666	8.3392	0.3679	8.0242	0.3685	7.8654	0.3678	8.0617
-10	0.3783	5.4232	0.3796	5.1034	0.3802	4.9417	0.3794	5.1411
-5	0.3897	2.5700	0.3910	2.2455	0.3917	2.0808	0.3909	2.2834
0	0.4009	0.2232	0.4022	0.5523	0.4029	0.7200	0.4021	0.5142
5	0.4118	2.9593	0.4132	3.2930	0.4139	3.4636	0.4130	3.2547
10	0.4226	5.6412	0.4239	5.9795	0.4246	6.1531	0.4238	5.9411
15	0.4331	8.2717	0.4345	8.6146	0.4352	8.7912	0.4343	8.5761
20	0.4434	10.8537	0.4448	11.2012	0.4455	11.3809	0.4447	11.1626
25	0.4536	13.3900	0.4550	13.7421	0.4557	13.9250	0.4548	13.7034

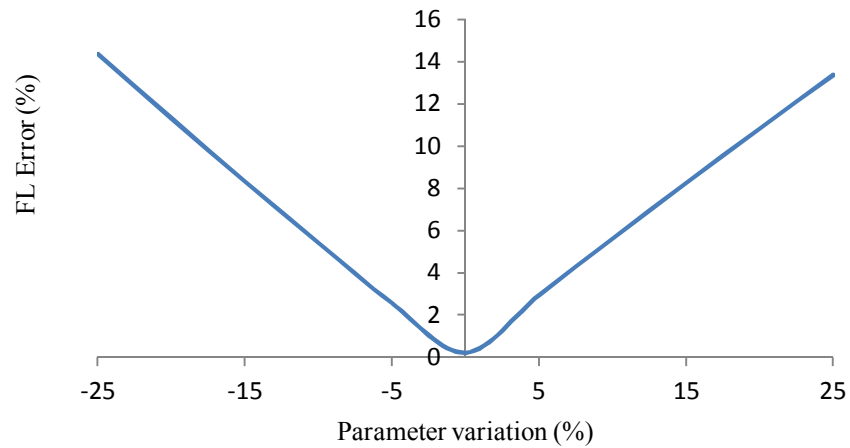


Figure 9.10: Influence of parameter variation on FL accuracy in three-terminal lines

## **CHAPTER 10**

### **Adaptive PMU-based Fault Location Algorithm for Series-compensated Lines**

AC power transmission in the overwhelming majority of cases is the established and the most cost effective option at hand for transmission of large amounts of electric power. During the last two decades, transmission of power generated from power plants to consumers has been vastly improved and expanded to every corner of the world. Recent development of series compensation in power systems can greatly increase power transfer capability, improve the transient stability and damp power oscillations if carefully designed. In cases of long distance transmission, care shall be taken for safeguarding of synchronism as well as stable system voltages, particularly in conjunction with system faults. With series compensation, the viable distances of AC power transmission become sufficiently large to eliminate altogether the issue of distance as a limiting factor for AC transmission in most cases. Thus, series compensated AC

power interconnectors transmitting bulk power over distances of more than 1000 kilometers are a reality today. Likewise, series compensation is an efficient means for minimizing the amount of transmission lines needed for a certain power transfer capability of an interconnector. In cases where the need for power transmission capability in a system is growing, the capability of already existing power lines can be increased considerably with series capacitors, thereby decreasing the need for building of new lines. Installing of series compensation on existing lines is generally less expensive and less time consuming than adding new lines. [184-186]

Fault location on SCLs is considered to be one of the most important tasks for the manufacturers, operators and maintenance engineers since these lines are usually spreading over a few hundreds of kilometers and are vital links between the energy production and consumption centers. However, SCLs are considered as especially difficult for fault location since series capacitors in these lines are equipped with metal-oxide varistors (MOV) for overvoltage protection. The non-linearity of MOV is well known and the accuracy in its model strongly affects the accuracy of the fault distance evaluation. MOVs, being highly non-linear elements, make measurement for such lines differ substantially in comparison to the non-compensated lines in both the static and dynamic characters. [186-190]

Recently, some research efforts have been focused on fault location in SCLs and different fault location algorithms have been published in the literature. The proposed algorithm by C. Yu et al. in [60, 62] can be applied to any series FACTS compensated line as it does not utilize the series device model and knowledge of its operation mode to compute the voltage drop during the fault period. Instead, it uses two-step algorithm, pre-

location step and correction step, to calculate the voltage drop and fault location. M. Al-Dabbagh et al. proposed in [63] a fault location algorithm for SCLs using time domain measurement of the instantaneous values and it can, therefore, be applied with minimum filtering of high frequencies. The proposed algorithm, which does not require the fault to be pure resistive or the knowledge of fault type, includes the MOV model in the fault equation and requires only a short duration of fault measurement data to estimate the location of fault. J. Sadah et al. proposed in [64] a fault location algorithm for SCLs that does not utilize the compensator device model and the knowledge of the compensator device operating mode to compute the voltage drop during fault. For this reason, the proposed technique can be easily applied to any series FACTS compensated line. The proposed algorithm is not sensitive to fault resistance and fault inception angle and does not require any knowledge of equivalent source impedances. The technique suggested in [191] uses the distributed time domain model for modeling of the transmission lines and takes advantage of only half cycle of the post-fault synchronized voltage and current samples taken from two ends of the line. The proposed algorithm considers two fault points; fault in front of series capacitors and fault behind series capacitors. This leads to two subroutines for the fault location. With applying these subroutines, two solutions are obtained for fault location and, then, a special procedure to select the correct solution is utilized. J. Izykowski et al. proposed in [187] a fault-location algorithm for double-circuit SCLs modeled with their distributed parameters. The algorithm applies two subroutines, designated for locating faults on particular line sections, and in addition, the procedure for selecting the valid subroutine. The subroutines are formulated with the use of the generalized fault-loop model. The distance to fault calculation is independent of the

compensating bank parameters. Only the position at which the bank is installed is required to be known. M. Kizilcay et al. proposed in [188] a two-terminal algorithm for locating faults on SCLs where the fault distance is determined in a general way using modal theory. The developed method requires only line parameters and source impedances at both ends of the line and it does not need any knowledge of fault resistance and fault type. It models the compensation stage with the protection device by current dependent equivalent impedance at power frequency. The algorithm introduces a new criterion to select correctly among two candidates of a solution assuming that the fault is in front of and behind the compensation stage. M. Fulczyk et al. proposed in [192, 193] a fault location algorithm for double-circuit SCLs modeled with their distributed parameters. The algorithm requires only the compensating bank installation position to be known. It consists of two subroutines, designated for locating faults at both sides of the compensating bank. The results consistent with the actual fault are obtained by selecting the valid subroutine. The subroutines of the algorithm have been formulated with use of the generalized fault loop model. The distance to fault calculation is independent on the compensating bank parameters. M. Saha et al. proposed in [189, 194] a one-end fault location algorithm for series-compensated transposed or untransposed parallel lines applying phase coordinates approach. The developed algorithm offsets the series compensation and the reactance effects and takes the countermeasure for the mutual coupling between parallel lines. Two subroutines are used for faults behind and in front of the compensating unit and the final estimate is obtained with the selection procedure. The algorithm does not require the source impedances and avoids pre-fault measurements. E. Rosolowski et al. proposed in [190] a one-end fault location algorithm

for SCLs based on differential equation approach which allows good reflection of the dynamic phenomena relevant for faults occurring behind the series compensating unit. This algorithm is recommended for application to the heavy fault cases with high level of noise components in the measured current and voltage signals, which appear as difficult for filtering out with using the fundamental frequency phasor approach. The algorithm is derived with use of the Clarke transformation for description of the network and the fault. The algorithm proposed by M. Saha et al. in [195] for locating faults on SCLs applies two-end currents and one-end voltage and thus can be applied with current differential protective relays. The algorithm applies two subroutines, formulated with use of the generalized fault loop model, and the procedure for selecting the valid subroutine. In this algorithm, the distance to fault calculations do not involve source impedances and the pre-fault measurements. The fault location algorithm proposed by S. Kapuduwage et al. in [186] is developed using linearized model of three-phase capacitor banks to represent the effects of compensation. Basically, the algorithm uses current and voltage measurements from both ends of the transmission network. In the developed algorithm, source impedances can be calculated on-line, which eliminates source mismatches substantially. The proposed algorithm can be applied to locate faults that may occur in front or behind the compensating unit in any type of transmission lines (multi-lines and multi-ends).

This chapter gives a brief introduction on series capacitor location and schemes. It then describes a proposed algorithm for online determination of the SC line parameters utilizing voltage and current synchronized measurements obtained from PMUs installed

at the two ends of the line. It also describes a proposed adaptive PMU-based fault location algorithm for a SCL and presents, in details, the associated simulation results.

## **10.1 Series capacitor location**

There are basically two principal locations at which series capacitors are installed today. They could be installed either in the middle or at both ends of the line as depicted in Figure 2.2 and Figure 2.3 respectively. Series capacitors located along the line are normally unattended. Due to the low fault current of this location, the required MOV rating will be comparatively low. Series capacitors located at the line ends are close to a substation or a switching station and therefore manned. Because of the high fault current of this location, the required MOV rating will be comparatively high. The location of series capacitor banks is important for several reasons. First, the compensation “effectiveness” of the series capacitor varies as a function of its location along the line. In addition, the series capacitor location affects the voltage profile along the line. Moreover, the transmission line protection and the series capacitor main circuit equipment are affected by the series capacitor location. Furthermore, the series capacitor location affects the maintainability of the series capacitor. Finally, for MOV protected series capacitors, the rating of the MOV depends upon the series capacitor location. [185]

## **10.2 Series capacitor scheme**

A series capacitor is not just a capacitor in series with the line. For proper functioning, series compensation requires control, protection and supervision to enable it to perform

as an integrated part of a power system. In addition, since the series capacitor is working at the same voltage level as the rest of the system, it needs to be fully insulated to ground. The main circuit diagrams of a state of the art series capacitor is shown in Figure 10.1 and Figure 10.2.

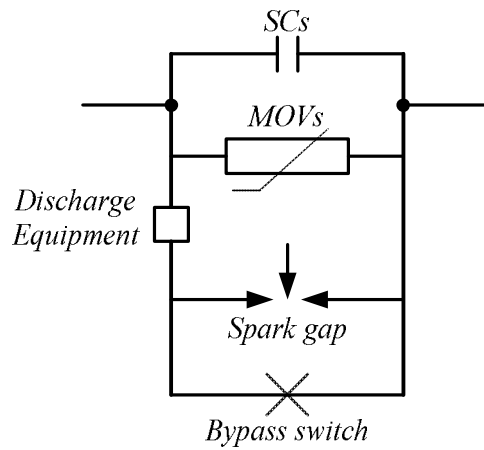


Figure 10.1: Series capacitor of a gapped scheme

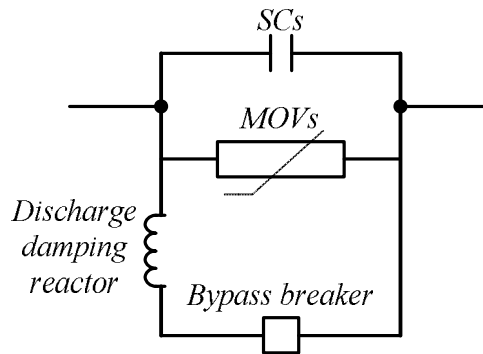


Figure 10.2: Series capacitor of a gapless scheme

The main protective device is MOV. The MOV is a non-linear resistor limiting the voltage across the capacitor to safe values in conjunction with system faults giving rise to large short circuit currents flowing through the line. During a fault, MOV operates to bypass fault current through the capacitor which would otherwise cause dangerously high voltage across the capacitor bank. A spark gap is utilized in many cases, to bypass the



series capacitor in situations where the MOV is not sufficient to absorb the excess current during a fault sequence. A bypass switch is incorporated in the scheme to enable bypassing and insertion of the series capacitor when needed. It is also necessary for extinguishing of the spark gap or, in the absence of a spark gap, for bypassing of the MOV in conjunction with faults close to the series capacitor. Finally a current limiting damping circuit (CLDC) is incorporated in the scheme to limit and damp the high frequency discharge current arising when the spark gap operates or the bypass switch is closed. The high frequency discharge current must be limited and damped to be within the withstand capabilities of the main circuit equipment of the SC. The CLDC normally consists of an air core reactor which together with the capacitor provides an LC discharge circuit. A parallel damping resistor is connected across the reactor in case a high damping of the capacitor discharge current is required. [185, 186]

### 10.2.1 Voltage-current relationship of MOV

The relationship between voltage and current of the MOV can be approximated by a non linear equation:

$$i_v = I_c \left( \frac{V_v}{V_p} \right)^\alpha \quad (10.1)$$

where

$i_v$  : The instantaneous current through the MOV

$I_c$  : The MOV coordination current

$V_v$  : The instantaneous voltage across the MOV

$V_p$  : The MOV protective level voltage usually defined at  $I_c$

$\alpha$  : A parameter related to the manufacturing process of the MOV material

A typical value of  $\alpha$  is in the order of 20 to 30. Referring to (10.1), as the applied voltage begins to increase above a certain voltage, the material will begin to conduct an increasing amount of current, while the voltage across the MOV is kept nearly constant. This very sharp V-I characteristic of the MOV allows it to provide direct overvoltage protection of the series capacitor during power system disturbances. The instantaneous and automatic reinsertion and restoration afforded by the MOV can considerably increase transfer limits dictated by the risk of transient instability. [63, 185, 187, 189, 191-195]

### 10.2.2 Internal and external faults

In designing of the series capacitor, it is necessary to distinguish between its required behavior in conjunction to internal as well as external faults. Internal faults, in relation to a series capacitor, are malfunctions of the power system that occur in the same section of the transmission line containing the series capacitor. External faults, on the other hand, are faults located outside of the segment of the line which contains the series capacitor. For normal external faults, it is generally required that the series capacitor is not bypassed in conjunction with the fault. In other words, the series capacitor has to stay in the circuit during and after the external fault sequence in the system and, therefore, it has to withstand that part of the fault current flowing through it without being damaged. To enable this, the MOV protecting the series capacitor must have sufficient thermal capacity to withstand the heating caused by the fault current for as long as it flows through the circuit. The voltage across the MOV drops after the fault has been cleared and the MOV stops conducting. This means that the series capacitor is instantaneously and automatically going back into operation. The inherent speed of this procedure, called

instantaneous series capacitor reinsertion, is crucial to system behavior after the fault. Fast reinsertion of the series capacitor is often a prerequisite for post-fault stability of the system and, as a matter of fact, may be one of the key reasons for having series compensation in the system in the first place. [185]

For internal faults, the requirements on the series capacitor are somewhat different. When the faulty line section is disconnected by opening of the line circuit breakers at both line sections ends, the series capacitor is taken out with it. As a result, the series capacitor is not required to carry any fault current once the line section has been disconnected. Prior to disconnecting the line section, however, the series capacitor must still carry the fault current. The disconnection of the faulty line will take some 60-100 ms to execute. In order to reduce the size of the MOV, it is generally permitted to bypass the series capacitor during an internal fault. Bypassing is carried out by the bypass switch alone for a gapless scheme and by the spark gap and the bypass switch for a gapped scheme. A gapped scheme is used when the fault duty for internal faults is high and when the fault duty for internal faults is low, a gapless scheme can be used. The fault duty for internal faults depends both on the short circuit capacity of the system and the location of the series capacitor. When the faulted and disconnected line section is successfully reclosed, the bypass switch is opened and the series capacitor is reinserted into operation. [185]

### **10.3 PMU-based parameter estimation of a SCL**

In order to develop an adaptive fault location algorithm for a SCL, we need first to determine the SCL parameters online instead of assuming fixed values of such

parameters regardless of the environmental and operating system conditions. Referring to [165], this section describes in detail how the positive-sequence parameters of a SCL are estimated utilizing synchronized voltage and current phasors measured at the two ends of the line.

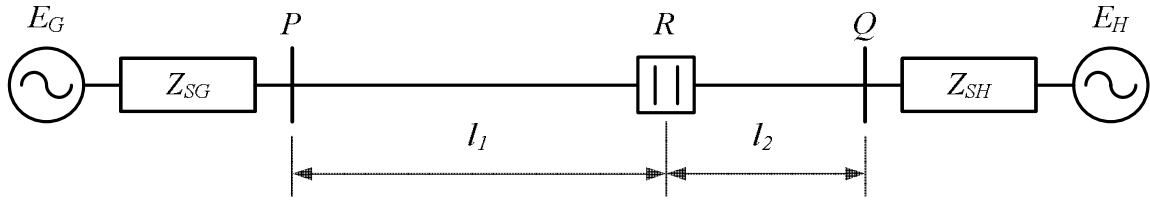


Figure 10.3: One line diagram of a series compensated line

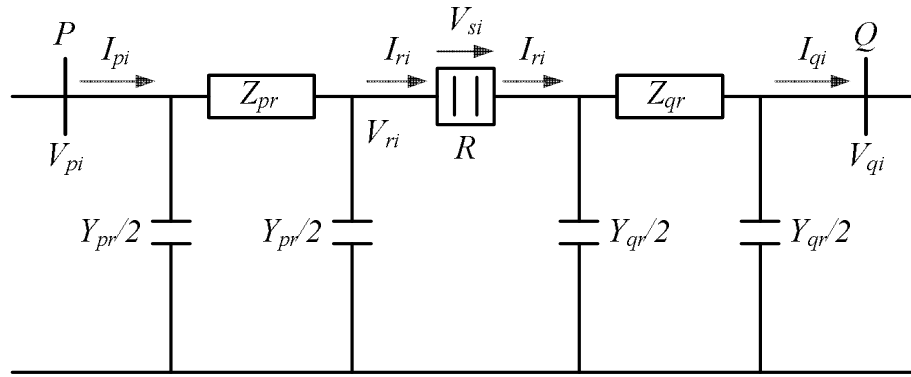


Figure 10.4: Positive sequence network of the system during normal operation

Consider a transposed line between terminal  $P$  and  $Q$  as shown in Figure 10.3 where  $E_G$  and  $E_H$  represent the TE sources at terminal  $P$  and  $Q$  respectively. The series compensation device is located at location  $R$ . The compensation device can be a simple capacitor bank or more complicated thyristor-controlled power flow controller. The distance of line segment  $PR$  and  $QR$  are  $l_1$  and  $l_2$  respectively. The aim is to estimate the positive sequence series resistance, series reactance and shunt susceptance of the SCL per unit length from the steady state voltage and current phasors at terminal  $P$  and  $Q$

measured at different moments during normal operations. It may be noted that zero sequence components in the circuit are usually negligible during normal operations. Nonetheless, the proposed algorithm will be equally applicable for estimating zero sequence parameters of the SCL if significant zero sequence components arise due to unbalanced load conditions or existence of external faults. Figure 10.4 depicts the positive sequence network of the system during normal operations. In the figure, the following notations are adopted:

$V_{pi}, I_{pi}$  : The  $i^{th}$  phasor measurement of positive sequence voltage and current at terminal  $P$  at  $i^{th}$  moment

$V_{qi}, I_{qi}$  : The  $i^{th}$  phasor measurement of positive sequence voltage and current at terminal  $Q$ ;  $i=1, 2, \dots, N$ ,  $N$  being the total number of measurement sets, with each set consisting of  $V_{pi}, I_{pi}, V_{qi}, I_{qi}$

$V_{ri}$  : The voltage at the left side of location  $R$

$V_{si}$  : The voltage drop across the series compensation device at location  $R$

$I_{ri}$  : The current flowing through the series compensation device at location  $R$

$Z_c$  : The characteristic impedance of the line

$\gamma$  : The propagation constant of the line

$Z_{pr}, Z_{qr}$  : The equivalent series impedance of the line segment  $PR$  and  $QR$

$Y_{pr}, Y_{qr}$  : The equivalent shunt admittance of the line segment  $PR$  and  $QR$

$l_1, l_2$  : Length of the line segment  $PR$  and  $QR$  in mile or km

The equivalent line parameters are expressed as

$$Z_{pr} = Z_c \sinh(\gamma l_1) \quad (10.2)$$

$$Z_{qr} = Z_c \sinh(\gamma l_2) \quad (10.3)$$

$$Y_{pr} = \frac{2}{Z_c} \tanh\left(\frac{\gamma l_1}{2}\right) \quad (10.4)$$

$$Y_{qr} = \frac{2}{Z_c} \tanh\left(\frac{\gamma l_2}{2}\right) \quad (10.5)$$

$$Z_c = \sqrt{\frac{z_1}{y_1}} \quad (10.6)$$

$$\gamma = \sqrt{z_1 y_1} \quad (10.7)$$

where

$z_1, y_1$  : Positive sequence series impedance and shunt admittance of the line per mile or km respectively

The real and imaginary parts of  $z_1$  and the imaginary part of  $y_1$  are the three parameters to be determined. Referring to Figure 10.4 and noting that the current is flowing from terminal  $P$  to terminal  $Q$ , we can derive the following equations:

$$V_{pi} = V_{ri} \cosh(\gamma l_1) + I_{ri} Z_c \sinh(\gamma l_1) \quad (10.8)$$

$$I_{pi} = I_{ri} \cosh(\gamma l_1) + \frac{V_{ri}}{Z_c} \sinh(\gamma l_1) \quad (10.9)$$

$$V_{ri} - V_{si} = V_{qi} \cosh(\gamma l_2) + I_{qi} Z_c \sinh(\gamma l_2) \quad (10.10)$$

$$I_{ri} = I_{qi} \cosh(\gamma l_2) + \frac{V_{qi}}{Z_c} \sinh(\gamma l_2) \quad (10.11)$$

Eliminating  $V_{ri}$  and  $I_{ri}$  and considering  $l=l_1+l_2$  to be the total length of the line, we get:

$$V_{pi} = V_{si} \cosh(\gamma l_1) + V_{qi} \cosh(\gamma l) + I_{qi} Z_c \sinh(\gamma l) \quad (10.12)$$

$$I_{pi} = V_{si} \frac{\sinh(\gamma l_1)}{Z_c} + I_{qi} \cosh(\gamma l) + \frac{V_{qi}}{Z_c} \sinh(\gamma l) \quad (10.13)$$

For one set of measurements, we can obtain the above two complex equations, which can be arranged into four real equations. We have five real unknowns, i.e. three parameters for the line, real and imaginary part of  $V_{si}$ . If we obtain another set of measurements, we have four more real equations and two more real unknowns for the new  $V_{si}$ . Then with eight equations, the seven real unknowns can be solved. It follows that, with more equations obtained according to different operation conditions, the classical least squares based method can be applied to obtain a more robust estimate. We define the unknown variables as:

$$X = [x_1, x_2, \dots, x_{2N}, x_{2N+1}, x_{2N+2}, x_{2N+3}]^T \quad (10.14)$$

where

$N$  : Total number of measurement sets

$x_{2i-1}, x_{2i}$  :  $i=1, 2, \dots, N$ , variables used to represent voltage across the compensation device, i.e.  $V_{si} = x_{2i-1} e^{jx_{2i}}$

$x_{2N+1}, x_{2N+2}, x_{2N+3}$  : Positive sequence transmission line series resistance, series reactance and shunt susceptance per unit length respectively

By employing the defined variables, equations (10.12) and (10.13) can be written in the form  $f_{2i-1}(X) = 0$  and  $f_{2i}(X) = 0$  respectively as follows:

$$f_{2i-1}(X) = x_{2i-1} e^{jx_{2i}} \cosh(\gamma l_1) + V_{qi} \cosh(\gamma l) + I_{qi} Z_c \sinh(\gamma l) - V_{pi} = 0 \quad (10.15)$$

$$f_{2i}(X) = x_{2i-1} e^{jx_{2i}} \frac{\sinh(\gamma l_1)}{Z_c} + I_{qi} \cosh(\gamma l) + \frac{V_{qi}}{Z_c} \sinh(\gamma l) - I_{pi} = 0 \quad (10.16)$$

where

$$Z_c = \sqrt{(x_{2N+1} + jx_{2N+2})/(jx_{2N+3})} \quad (10.17)$$

$$\gamma = \sqrt{(x_{2N+1} + jx_{2N+2})(jx_{2N+3})} \quad (10.18)$$

Define function vector  $F(X)$  as:

$$F_{2i-1}(X) = \text{Re}(f_i(X)), i = 1, 2, \dots, 2N \quad (10.19)$$

$$F_{2i}(X) = \text{Im}(f_i(X)), i = 1, 2, \dots, 2N \quad (10.20)$$

Then the unknown variable vector  $X$  can be derived as follows:

$$X_{k+1} = X_k + \Delta X \quad (10.21)$$

$$\Delta X = -(H^T H)^{-1} [H^T F(X_k)] \quad (10.22)$$

$$H = \frac{\partial F(X_k)}{\partial X} \quad (10.23)$$

where

$X_k, X_{k+1}$  : Variable vector before and after  $k^{th}$  iteration

$k$  : Iteration number starting from 1

$\Delta X$  : Variable update

$H$  : Matrix composed of the derivatives of the function with respect to the unknown variables

## 10.4 Description of the proposed algorithm

Referring to [195], we consider a line compensated with one three-phase bank of fixed series capacitors equipped with MOVs for overvoltage protection as depicted in Figure



10.5. A fault is of a random nature and therefore faults appearing at both sides of the three-phase capacitor compensating bank (faults  $F_A$  and  $F_B$  in Figure 10.5) shall be considered. As a result, two subroutines  $S_A$  and  $S_B$  are utilized for locating these hypothetical faults. Also, the selection procedure is applied for indicating the valid subroutine and, hence, the actual fault location.

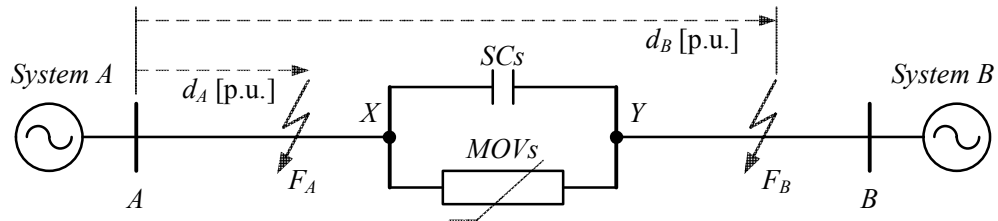


Figure 10.5: Diagram of a line compensated with series capacitors equipped with MOVs

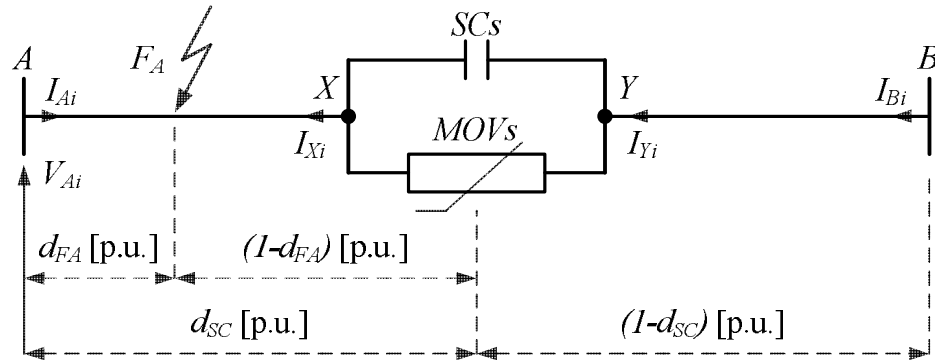


Figure 10.6: Subroutine  $S_A$  – scheme of SC line under fault  $F_A$

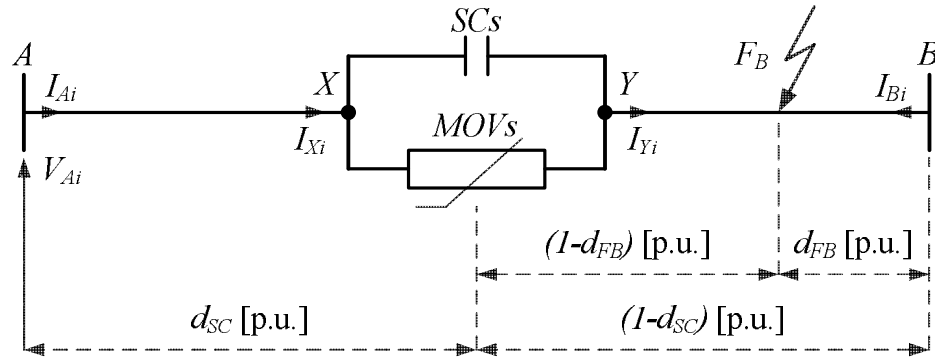


Figure 10.7: Subroutine  $S_B$  – scheme of SC line under fault  $F_B$

The compensating bank divides the line of the length  $l$  [km] into two line segments having the length:  $d_{SC}$  [p.u.] and  $(1-d_{SC})$  [p.u.], as shown in Figure 10.6 and Figure 10.7. The relative distances  $d_{FA}$ ,  $d_{FB}$  can be recalculated into the distances  $d_A$ ,  $d_B$  which are expressed in [p.u.] but related to the whole line length as follows:

$$d_A = d_{FA} \cdot d_{SC} \quad (10.24)$$

$$d_B = d_{SC} + (1 - d_{FB}) \cdot (1 - d_{SC}) \quad (10.25)$$

#### 10.4.1 Fault location subroutine $S_A$

The subroutine  $S_A$  is derived neglecting the line shunt capacitances effect which, however, can be accounted for in the next step. The subroutine  $S_A$  for fault  $F_A$  in the section A-X is based on the following generalized fault loop model:

$$V_{Ap} - d_{FA} Z_{1LA} I_{Ap} - R_{FA} I_{FA} = 0 \quad (10.26)$$

where

$d_{FA}$  : Unknown distance to fault [p.u.] on the section A-X

$R_{FA}$  : Unknown fault resistance for fault on section A-X

$V_{Ap}, I_{Ap}$  : Fault loop voltage and current for fault on section A-X

$I_{FA}$  : Total fault current for fault on section A-X

$Z_{1LA}$  : Positive sequence impedance of the line section A-X

Fault loop voltage and current, composed accordingly to the fault type, are expressed as follows:

$$V_{Ap} = a_1 V_{A1} + a_2 V_{A2} + a_0 V_{A0} \quad (10.27)$$

$$I_{Ap} = a_1 I_{A1} + a_2 I_{A2} + a_0 \frac{Z_{0LA}}{Z_{1LA}} I_{A0} \quad (10.28)$$

where

$a_1, a_2, a_0$  : Weighting coefficients (Table 10.1)

$V_{A1}, V_{A2}, V_{A0}$  : Positive, negative and zero sequence components of side-A voltage

$I_{A1}, I_{A2}, I_{A0}$  : Positive, negative and zero sequence components of side-A current

$Z_{0LA}$  : Zero sequence impedance of the line section A-X

The total fault current in (10.26) is determined using the following generalized fault model:

$$I_{FA} = a_{F1}I_{FA1} + a_{F2}I_{FA2} + a_{F0}I_{FA0} \quad (10.29)$$

where

$a_{F1}, a_{F2}, a_{F0}$  : Weighting coefficients (Table 10.2)

The  $i^{th}$  sequence component of the total fault current is determined as a sum of the  $i^{th}$  sequence components of currents from both ends of the faulted section A-X:

$$I_{FAi} = I_{Ai} + I_{Xi} \quad (10.30)$$

where

$i$  : Index of a symmetrical component (1 for positive, 2 for negative and 0 for zero sequence component)

$I_{Ai}$  :  $i^{th}$  sequence component of current at bus A

$I_{Xi}$  :  $i^{th}$  sequence component of current at point X

When neglecting the line shunt capacitances,  $I_{Xi}$  is equal to the current  $I_{Bi}$ , and thus one obtains:

$$I_{FAi} = I_{Ai} + I_{Bi} \quad (10.31)$$

To assure high accuracy of fault location, it is recommended to use negative sequence components for phase-to-earth and phase-to-phase faults, negative and zero

sequence components for phase-to-phase-to-earth faults and superimposed positive sequence components for three phase symmetrical faults. In the case of three-phase balanced faults the total fault current is determined taking the superimposed positive sequence currents from both line ends A, B, respectively:

$$I_{FA1} = I_{A1}^{superimp.} + I_{B1}^{superimp.} \quad (10.32)$$

where the superimposed (superscript: ‘superimp.’) positive sequence currents are calculated by subtracting the pre-fault quantity (superscript: ‘pre’) from the fault quantity:

$$I_{FA1} = (I_{A1} - I_{A1}^{pre}) + (I_{B1} - I_{B1}^{pre}) \quad (10.33)$$

In this way, an accurate calculation of the total fault current is assured since the positive-sequence components, for which the shunt capacitance effect is the most distinct, are excluded for all fault types (Table 10.2). After resolving (10.26) into the real and imaginary parts, and eliminating the unknown fault resistance, the sought fault distance is determined as follows:

$$d_{FA} = \frac{real(V_{Ap}) imag(I_{FA}) - imag(V_{Ap}) real(I_{FA})}{real(Z_{1LA} I_{Ap}) imag(I_{FA}) - imag(Z_{1LA} I_{Ap}) real(I_{FA})} \quad (10.34)$$

Having the fault distance calculated, the fault resistance can be also determined.

TABLE 10.1: WEIGHTING COEFFICIENTS

<b><i>Fault Type</i></b>	<b><i>a<sub>1</sub></i></b>	<b><i>a<sub>2</sub></i></b>	<b><i>a<sub>0</sub></i></b>
AG	1	1	1
BG	$-0.5 - j0.5\sqrt{3}$	$-0.5 + j0.5\sqrt{3}$	1
CG	$-0.5 + j0.5\sqrt{3}$	$-0.5 - j0.5\sqrt{3}$	1
AB, ABG, ABC	$1.5 + j0.5\sqrt{3}$	$1.5 - j0.5\sqrt{3}$	0
BC, BCG	$-j\sqrt{3}$	$j\sqrt{3}$	0
CA, CAG	$-1.5 + j0.5\sqrt{3}$	$-1.5 - j0.5\sqrt{3}$	0

TABLE 10.2: SHARE COEFFICIENTS

<b><i>Fault Type</i></b>	<b><i>a<sub>F1</sub></i></b>	<b><i>a<sub>F2</sub></i></b>	<b><i>a<sub>F0</sub></i></b>
AG	0	3	0
BG	0	$-1.5 + j1.5\sqrt{3}$	0
CG	0	$-1.5 - j1.5\sqrt{3}$	0
AB	0	$1.5 - j0.5\sqrt{3}$	0
BC	0	$j\sqrt{3}$	0
CA	0	$-1.5 - j0.5\sqrt{3}$	0
ABG	0	$3 - j\sqrt{3}$	$j\sqrt{3}$
BCG	0	$j2\sqrt{3}$	$j\sqrt{3}$
CAG	0	$3 + j\sqrt{3}$	$j\sqrt{3}$
ABC	$1.5 + j0.5\sqrt{3}$	$1.5 - j0.5\sqrt{3}$	0

#### 10.4.2 Fault location subroutine $S_B$

Assuming that the fault location function is also available at terminal B, the distance to the fault, occurring in section B-Y, can be calculated without representing the bank at all. Proceeding with such assumption, fault location subroutine  $S_B$  can be applied in a similar way as done previously for fault location subroutine  $S_A$ . The subroutine  $S_B$  for fault  $F_B$  in the section B-Y is based on the following generalized fault loop model:

$$V_{Bp} - d_{FB}Z_{1LB}I_{Bp} - R_{FB}I_{FB} = 0 \quad (10.35)$$

where

- $d_{FB}$  : Unknown distance to fault [p.u.] on the section B-Y
- $R_{FB}$  : Unknown fault resistance for fault on section B-Y
- $V_{Bp}, I_{Bp}$  : Fault loop voltage and current for fault on section B-Y
- $I_{FB}$  : Total fault current for fault on section B-Y
- $Z_{1LB}$  : Positive sequence impedance of the line section B-Y

Fault loop voltage and current, composed accordingly to the fault type, are expressed as follows:

$$V_{Bp} = a_1 V_{B1} + a_2 V_{B2} + a_0 V_{B0} \quad (10.36)$$

$$I_{Bp} = a_1 I_{B1} + a_2 I_{B2} + a_0 \frac{Z_{0LB}}{Z_{1LB}} I_{B0} \quad (10.37)$$

where

$V_{B1}, V_{B2}, V_{B0}$  : Positive, negative and zero sequence components of side-B voltage

$I_{B1}, I_{B2}, I_{B0}$  : Positive, negative and zero sequence components of side-B current

$Z_{0LB}$  : Zero sequence impedance of the line section B-Y

The total fault current in (10.35) is determined using the following generalized fault model:

$$I_{FB} = a_{F1} I_{FB1} + a_{F2} I_{FB2} + a_{F0} I_{FB0} \quad (10.38)$$

The  $i^{th}$  sequence component of the total fault current is determined as a sum of the  $i^{th}$  sequence components of currents from both ends of the faulted section B-Y:

$$I_{FBi} = I_{Bi} + I_{Yi} \quad (10.39)$$

where

$I_{Bi}$  :  $i^{th}$  sequence component of current at bus B

$I_{Yi}$  :  $i^{th}$  sequence component of current at point Y

When neglecting the line shunt capacitances,  $I_{Yi}$  is equal to the current  $I_{Ai}$ , and thus one obtains:

$$I_{FBi} = I_{Ai} + I_{Bi} \quad (10.40)$$

In the case of three-phase balanced faults the total fault current is determined taking the superimposed positive sequence currents from both line ends A, B, respectively:

$$I_{FB1} = I_{A1}^{superimp.} + I_{B1}^{superimp.} \quad (10.41)$$

As done earlier, (10.41) can be put in the following form:

$$I_{FB1} = (I_{A1} - I_{A1}^{pre}) + (I_{B1} - I_{B1}^{pre}) \quad (10.42)$$

After resolving (10.35) into the real and imaginary parts, and eliminating the unknown fault resistance, the sought fault distance is determined as follows:

$$d_{FB} = \frac{\text{real}(V_{Bp}) \text{imag}(I_{FB}) - \text{imag}(V_{Bp}) \text{real}(I_{FB})}{\text{real}(Z_{1LB} I_{Bp}) \text{imag}(I_{FB}) - \text{imag}(Z_{1LB} I_{Bp}) \text{real}(I_{FB})} \quad (10.43)$$

Having the fault distance calculated, the fault resistance can be also determined.

### 10.4.3 Selection procedure

To determine the fault location correctly, we adopt [195] procedure for selecting the valid subroutine. To select among subroutines  $S_A$  and  $S_B$ , we first reject the subroutine yielding a fault distance outside the section range and/or a negative fault resistance. In vast majority of the cases this allows to select the valid subroutine. If this is not so, then one has to proceed with further selection. For this purpose, the circuit diagrams of the network for the negative-sequence, relevant for both subroutines are considered. In the case of three-phase balanced faults the superimposed positive-sequence components are considered. The particular subroutine is selected as the valid one if the determined remote source impedance has an  $R$ - $L$  character and its value is close to the actual source impedance.

## 10.5 Simulation results

This section presents PSCAD/EMTDC and MATLAB simulation results for a 400 kV transmission network with a series compensated line as depicted in Figure 10.8. The

series compensated line is faulted at both sides of the series compensating unit in sections A-X and B-Y. Simulations are performed for LG, LL, LLG and LLL faults. Fault location algorithm's accuracy is checked against fault type, location, fault resistance, line parameters and fault inception angle.

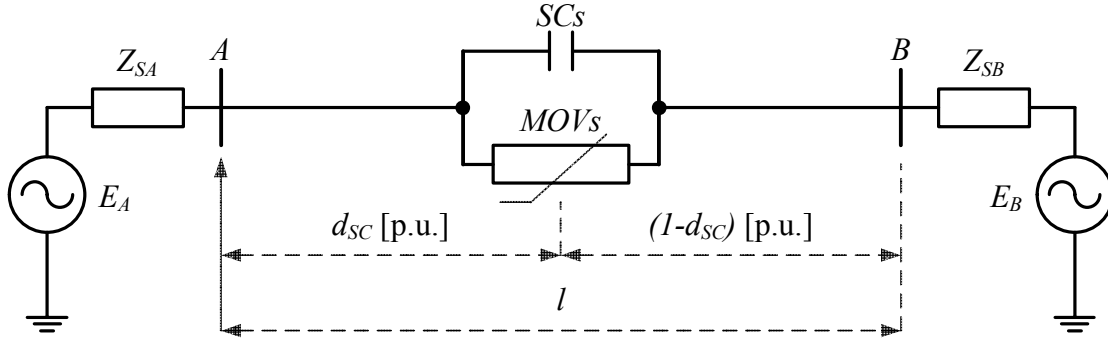


Figure 10.8: Test system with a SC line

### 10.5.1 Data generation and conditioning

The 400 kV line, compensated in the middle at 70% degree of compensation, is modeled in PSCAD/EMTDC with its distributed parameters. Table 10.3 shows the simulation parameters of the 400 kV series compensated transmission network where system's TEs at terminal A, B are determined as described in chapter 7. The CTs and VTs located at each line terminal are assumed as ideal devices. The three-phase voltage and current signals are sampled, as shown in Figure 10.9-10.11, at a frequency of 240 Hz which corresponds to 4 samples per cycle and are stored for post-processing. The DFT given by (3.3) is applied to extract the voltage and current phasors. The proposed algorithm is implemented in MATLAB. In this study, the percentage error used to measure the accuracy of fault location algorithm is as expressed in (8.10).



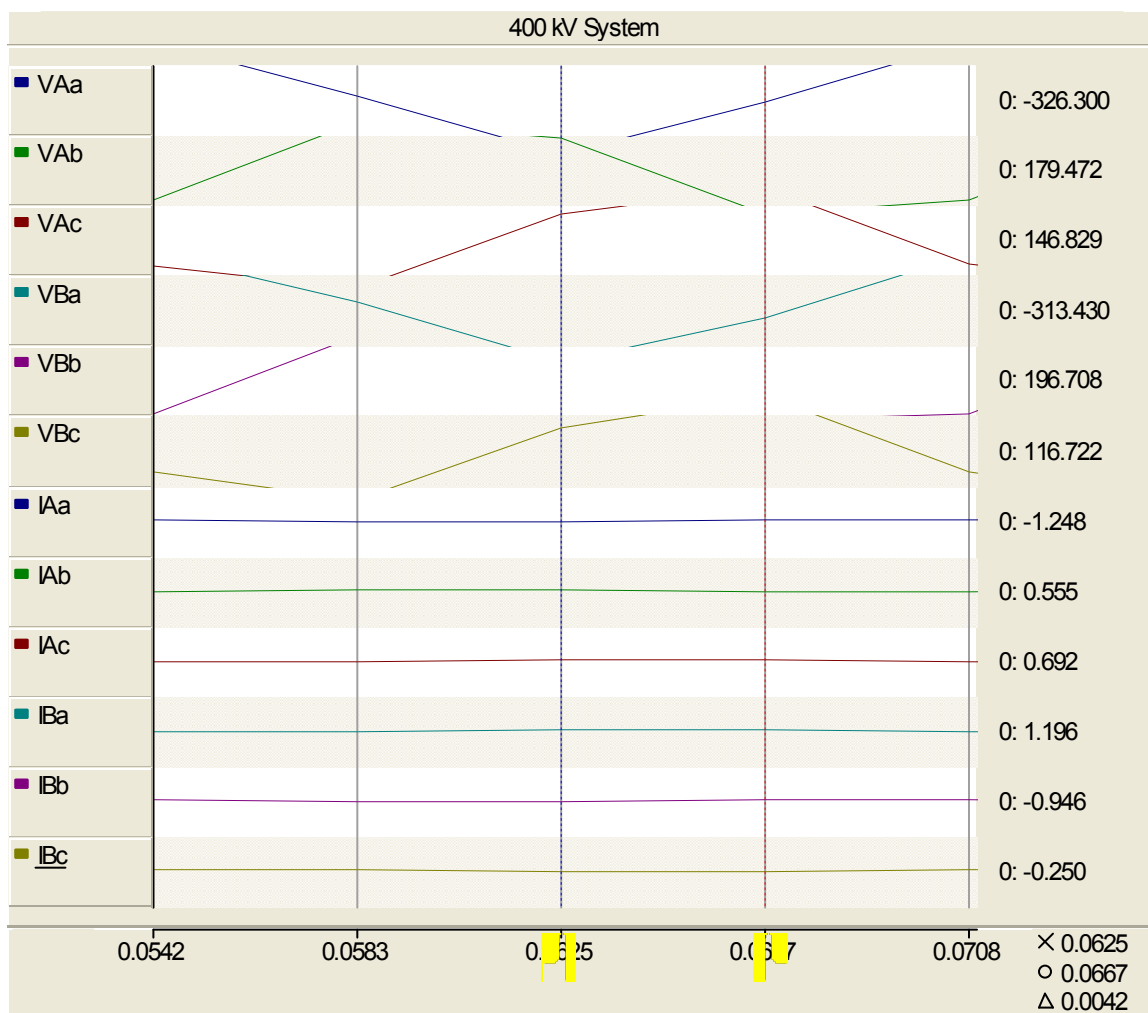


Figure 10.9: Sampling of 1<sup>st</sup> set of PMU phasor measurements at bus A & bus B

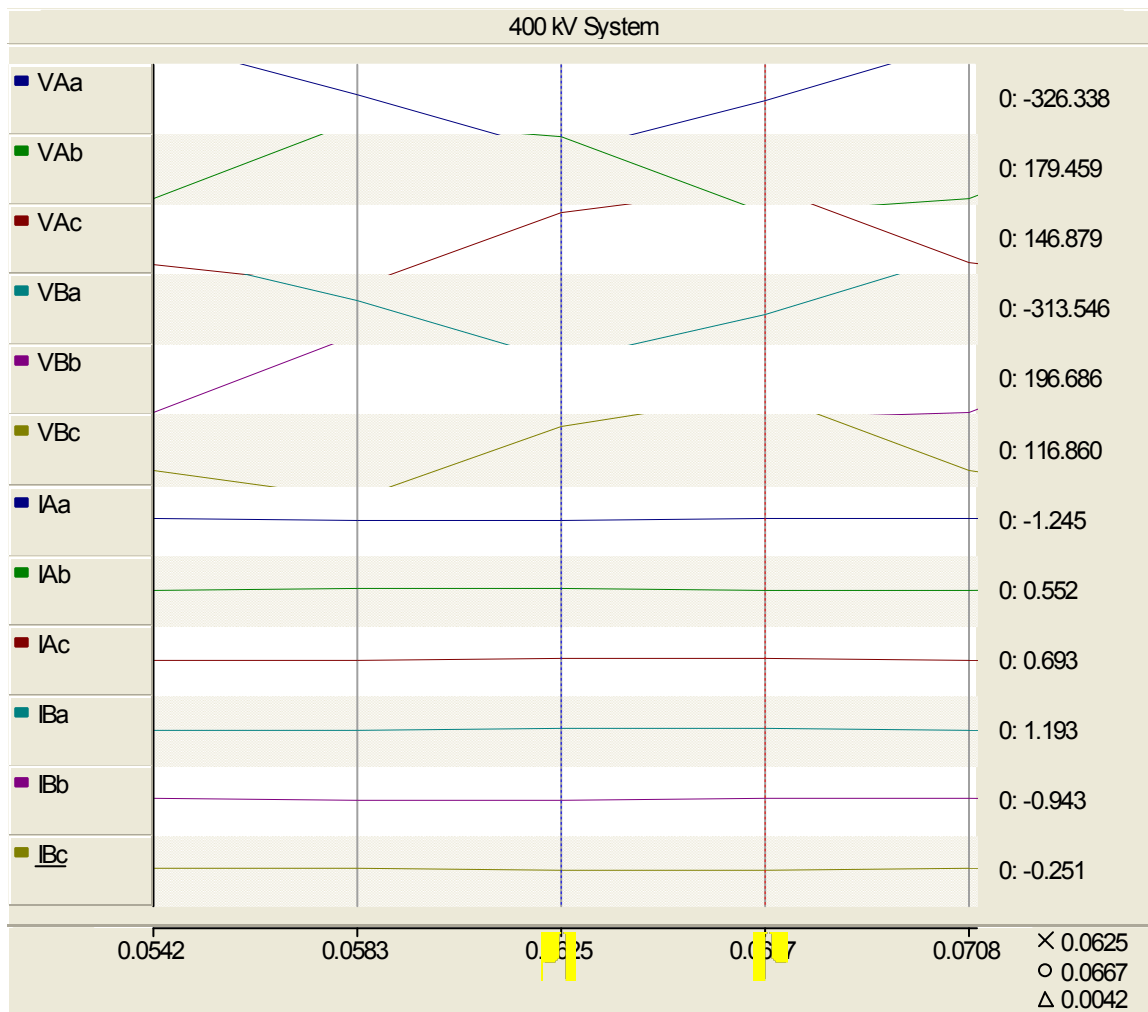


Figure 10.10: Sampling of 2<sup>nd</sup> set of PMU phasor measurements at bus A & bus B

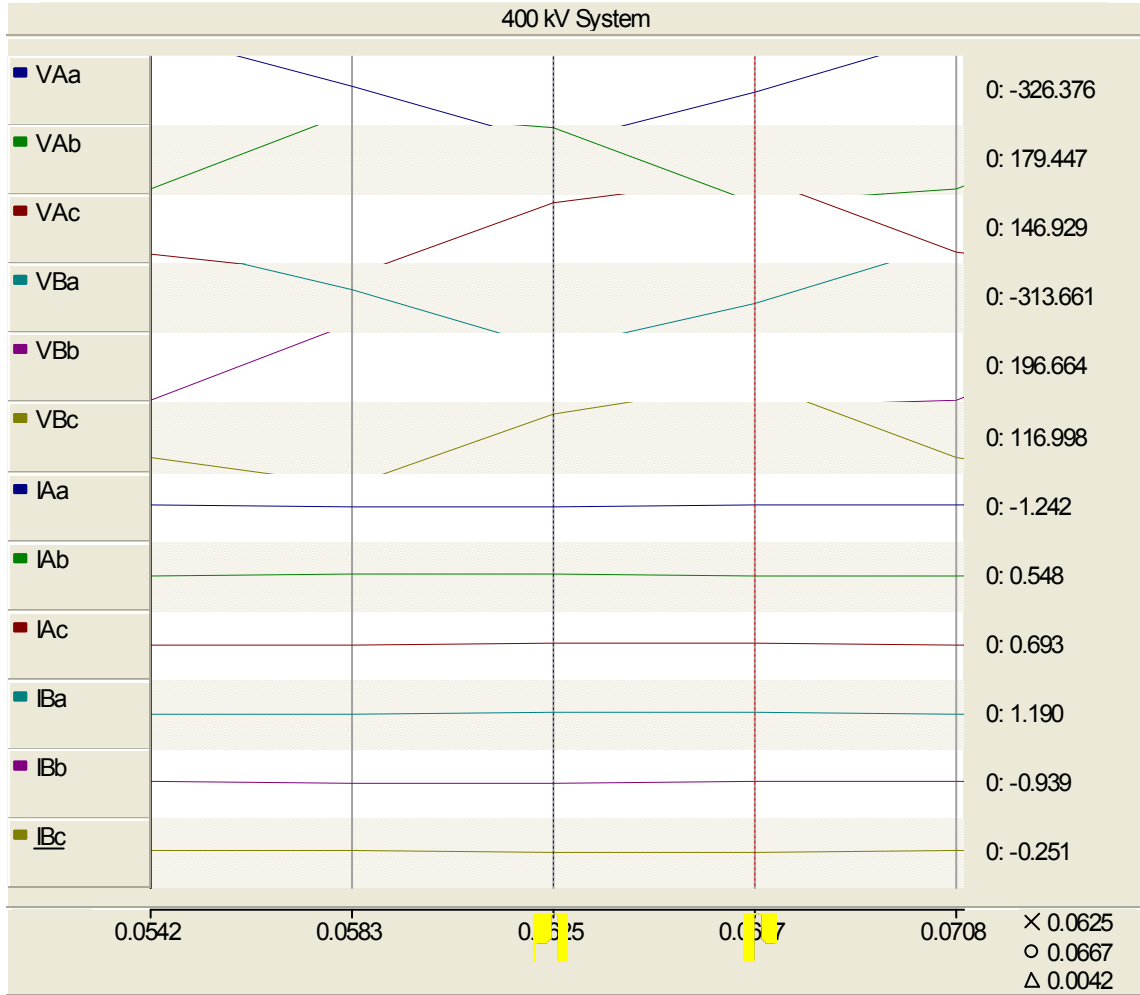


Figure 10.11: Sampling of 3<sup>rd</sup> set of PMU phasor measurements at bus A & bus B

TABLE 10.3: PARAMETERS OF THE 400 kV SERIES COMPENSATED NETWORK

<i>Parameter</i>	<i>Value</i>
$l$	300 km
$d_{SC}$	0.5 p.u.
$Z_{1L}$	$8.28+j94.5 \Omega$
$Z_{0L}$	$82.5+j307.9 \Omega$
$C_{1L}$	13 nF/km
$C_{0L}$	8.5 nF/km
$Z_{1SA}, Z_{1SB}$	$1.31+j15 \Omega$
$Z_{0SA}, Z_{0SB}$	$2.33+j22.5 \Omega$
$E_A$	400 kV $\angle 0^\circ$
$E_B$	390 kV $\angle -10^\circ$
$I_c$	1 kA
$V_p$	150 kV
$\alpha$	23

### 10.5.2 Accuracy analysis

To test the accuracy of the proposed algorithm, different type of faults with different fault locations and fault resistances have been simulated. Tables 10.4-10.7 present the fault location estimates obtained for the single line to ground (LG) faults, line to line (LL) faults, line to line to ground (LLG) faults and three phase (LLL) faults occurred in sections A-X and B-Y.

TABLE 10.4  
FAULT-LOCATION ESTIMATES FOR SINGLE-LINE-TO-GROUND FAULTS ON SECTIONS A-X & B-Y

<i><b>Fault Type</b></i>	<i><b>Fault Res. (<math>\Omega</math>)</b></i>	<i><b>Actual FL (p. u)</b></i>	<i><b>Estimated FL (p. u)</b></i>	<i><b>Error of Estimated FL (%)</b></i>
AG	10	0.2	0.1992	0.3781
		0.4	0.4009	0.2282
		0.6	0.6047	0.7757
		0.8	0.8005	0.0601
	100	0.2	0.1990	0.5202
		0.4	0.4050	1.2450
		0.6	0.6075	1.2459
		0.8	0.7943	0.7180
BG	10	0.2	0.2032	1.5769
		0.4	0.4094	2.3518
		0.6	0.5948	0.8610
		0.8	0.7960	0.4940
	100	0.2	0.2035	1.7500
		0.4	0.4083	2.0750
		0.6	0.5932	1.1333
		0.8	0.7953	0.5875
CG	10	0.2	0.2013	0.6626
		0.4	0.4068	1.7103
		0.6	0.5927	1.2193
		0.8	0.7997	0.0401
	100	0.2	0.1989	0.5478
		0.4	0.4001	0.0129
		0.6	0.5972	0.4600
		0.8	0.8026	0.3271

The fault type, fault resistance and actual fault location are given in the first, second and third column respectively. The estimated distance to fault and the estimation errors resulting from the proposed algorithm are respectively displayed in the fourth and fifth column. From the results obtained, it is observed that the proposed algorithm gives very accurate results for all type of faults.

TABLE 10.5  
FAULT-LOCATION ESTIMATES FOR LINE-TO-LINE FAULTS ON SECTIONS A-X & B-Y

<i><b>Fault Type</b></i>	<i><b>Fault Res. (<math>\Omega</math>)</b></i>	<i><b>Actual FL (p. u)</b></i>	<i><b>Estimated FL (p. u)</b></i>	<i><b>Error of Estimated FL (%)</b></i>
AB	1	0.2	0.2005	0.2298
		0.4	0.4032	0.7964
		0.6	0.5968	0.5364
		0.8	0.7995	0.0603
	10	0.2	0.2007	0.3689
		0.4	0.4043	1.0704
		0.6	0.5960	0.6590
		0.8	0.7995	0.0602
BC	1	0.2	0.2016	0.7921
		0.4	0.4054	1.3575
		0.6	0.5945	0.9191
		0.8	0.7984	0.1962
	10	0.2	0.2021	1.0405
		0.4	0.4053	1.3206
		0.6	0.5960	0.6743
		0.8	0.7989	0.1364
CA	1	0.2	0.2007	0.3467
		0.4	0.4038	0.9473
		0.6	0.5955	0.7501
		0.8	0.7991	0.1148
	10	0.2	0.2007	0.3596
		0.4	0.4061	1.5241
		0.6	0.5940	1.0040
		0.8	0.7978	0.2713

TABLE 10.6  
FAULT-LOCATION ESTIMATES FOR LINE-TO-LINE-TO-GROUND FAULTS ON SECTION A-X & B-Y

<i><b>Fault Type</b></i>	<i><b>Fault Res. (<math>\Omega</math>)</b></i>	<i><b>Actual FL (p. u)</b></i>	<i><b>Estimated FL (p. u)</b></i>	<i><b>Error of Estimated FL (%)</b></i>
ABG	5	0.2	0.2005	0.2640
		0.4	0.4033	0.8264
		0.6	0.5968	0.5359
		0.8	0.7995	0.0567
	50	0.2	0.2005	0.2498
		0.4	0.4033	0.8239
		0.6	0.5969	0.5097
		0.8	0.7996	0.0515
BCG	5	0.2	0.2014	0.6984
		0.4	0.4054	1.3455
		0.6	0.5946	0.8983
		0.8	0.7986	0.1744
	50	0.2	0.2014	0.6810
		0.4	0.4054	1.3465
		0.6	0.5947	0.8862
		0.8	0.7985	0.1841
CAG	5	0.2	0.2009	0.4570
		0.4	0.4042	1.0420
		0.6	0.5957	0.7178
		0.8	0.7988	0.1442
	50	0.2	0.2008	0.3992
		0.4	0.4038	0.9387
		0.6	0.5957	0.7108
		0.8	0.7991	0.1143

TABLE 10.7  
FAULT-LOCATION ESTIMATES FOR THREE-PHASE FAULTS ON SECTIONS A-X & B-Y

<i><b>Fault Type</b></i>	<i><b>Fault Res. (<math>\Omega</math>)</b></i>	<i><b>Actual FL (p. u)</b></i>	<i><b>Estimated FL (p. u)</b></i>	<i><b>Error of Estimated FL (%)</b></i>
ABC	1	0.2	0.1995	0.2277
		0.4	0.4019	0.4638
		0.6	0.5985	0.2572
		0.8	0.8007	0.0871
	10	0.2	0.1957	2.1477
		0.4	0.3968	0.8035
		0.6	0.6063	1.0547
		0.8	0.8052	0.6521

### 10.5.3 Influence of the fault resistance

The effect of the variation of the fault resistance in the algorithm's accuracy for all types of LG, LL, LLG and LLL faults are shown respectively in Table 10.8-10.11 assuming that the fault occurs at a distance of 0.6 p. u. from terminal A, B and C. Faults involving ground have been investigated for fault resistance values varying from 0 to 500  $\Omega$ . This captures low- and high-resistance faults. Faults not involving ground have been investigated for resistance values ranging between 0 to 30  $\Omega$ . In all cases the local and remote source impedances are set equal to the system values. It can be easily seen that the fault location estimates are highly accurate and virtually independent of the fault resistance.

TABLE 10.8  
INFLUENCE OF THE FAULT RESISTANCE ON THE ALGORITHM'S ACCURACY FOR SINGLE-LINE-TO-GROUND FAULTS ON SECTION B-Y (ACTUAL FL: 0.6 P.U. FROM TERMINAL A)

<i>Fault Res.</i> ( $\Omega$ )	<i>Fault Type</i>					
	<i>AG</i>		<i>BG</i>		<i>CG</i>	
	<i>Estim. FL</i> (p. u)	<i>Error of Estim. FL</i> (%)	<i>Estim. FL</i> (p. u)	<i>Error of Estim. FL</i> (%)	<i>Estim. FL</i> (p. u)	<i>Error of Estim. FL</i> (%)
0	0.5969	0.5087	0.5955	0.7470	0.5948	0.8673
1	0.5972	0.4740	0.5946	0.9034	0.5945	0.9193
5	0.5999	0.0128	0.5929	1.1866	0.5943	0.9518
10	0.6047	0.7757	0.5948	0.8610	0.5927	1.2193
20	0.6055	0.9157	0.6028	0.4595	0.5822	2.9706
50	0.5864	2.2594	0.6022	0.3667	0.6075	1.250
100	0.6075	1.2459	0.6018	0.3001	0.5972	0.4600
200	0.6049	0.8180	0.6013	0.2167	0.5849	2.5167
400	0.5863	2.2827	0.5975	0.4167	0.5859	2.350
500	0.5792	3.4676	0.5960	0.6667	0.5381	1.9833

TABLE 10.9  
INFLUENCE OF THE FAULT RESISTANCE ON THE ALGORITHM'S ACCURACY FOR LINE-TO-LINE  
FAULTS ON SECTION B-Y (ACTUAL FL: 0.6 P.U. FROM TERMINAL A)

<i>Fault Res.</i> <i>(<math>\Omega</math>)</i>	<i>Fault Type</i>					
	<i>AB</i>		<i>BC</i>		<i>CA</i>	
	<i>Estim.</i> <i>FL</i> <i>(p. u)</i>	<i>Error of</i> <i>Estim.</i> <i>FL (%)</i>	<i>Estim.</i> <i>FL</i> <i>(p. u)</i>	<i>Error of</i> <i>Estim.</i> <i>FL (%)</i>	<i>Estim.</i> <i>FL</i> <i>(p. u)</i>	<i>Error of</i> <i>Estim.</i> <i>FL (%)</i>
0	0.5969	0.5193	0.5947	0.8832	0.5959	0.6846
0.5	0.5969	0.5244	0.5946	0.9058	0.5957	0.7226
1	0.5968	0.5364	0.5945	0.9191	0.5955	0.7501
2.5	0.5966	0.5607	0.5943	0.9483	0.5950	0.8360
5	0.5964	0.5943	0.5945	0.9248	0.5943	0.9435
7.5	0.5963	0.6244	0.5950	0.8290	0.5940	0.9993
10	0.5960	0.6590	0.5960	0.6743	0.5940	1.0040
15	0.5953	0.7757	0.5983	0.2760	0.5947	0.8834
20	0.5939	1.0113	0.6007	0.1126	0.5964	0.5996
30	0.5893	1.7786	0.6033	0.5459	0.6022	0.3613

TABLE 10.10  
INFLUENCE OF THE FAULT RESISTANCE ON THE ALGORITHM'S ACCURACY FOR LINE-TO-LINE-  
TO-GROUND FAULTS ON SECTION B-Y (ACTUAL FL: 0.6 P.U. FROM TERMINAL A)

<i>Fault Res.</i> <i>(<math>\Omega</math>)</i>	<i>Fault Type</i>					
	<i>ABG</i>		<i>BCG</i>		<i>CAG</i>	
	<i>Estim.</i> <i>FL</i> <i>(p. u)</i>	<i>Error of</i> <i>Estim.</i> <i>FL (%)</i>	<i>Estim.</i> <i>FL</i> <i>(p. u)</i>	<i>Error of</i> <i>Estim.</i> <i>FL (%)</i>	<i>Estim.</i> <i>FL</i> <i>(p. u)</i>	<i>Error of</i> <i>Estim.</i> <i>FL (%)</i>
0	0.5967	0.5423	0.5946	0.8966	0.5960	0.6660
1	0.5968	0.5414	0.5946	0.8972	0.5959	0.6797
5	0.5968	0.5359	0.5946	0.8983	0.5957	0.7178
10	0.5969	0.5239	0.5946	0.9017	0.5957	0.7148
25	0.5969	0.5116	0.5946	0.8986	0.5957	0.7202
50	0.5969	0.5097	0.5947	0.8862	0.5957	0.7108
100	0.5969	0.5167	0.5946	0.8927	0.5958	0.6974
150	0.5969	0.5129	0.5947	0.8905	0.5958	0.6993
200	0.5969	0.5097	0.5947	0.8757	0.5958	0.6931
250	0.5970	0.5076	0.5947	0.8794	0.5959	0.6857



TABLE 10.11  
INFLUENCE OF THE FAULT RESISTANCE ON THE ALGORITHM'S ACCURACY FOR THREE-PHASE  
FAULTS ON SECTION B-Y (ACTUAL FL: 0.6 P.U. FROM TERMINAL A)

<i><b>Fault Res. (<math>\Omega</math>)</b></i>	<i><b>Estimated FL (p. u)</b></i>	<i><b>Error of Estimated FL (%)</b></i>
0	0.5969	0.5171
0.5	0.5973	0.4507
1	0.5985	0.2572
2.5	0.5989	0.1871
5	0.6011	0.1825
7.5	0.6036	0.5998
10	0.6063	1.0547
15	0.6121	2.0149
20	0.6179	2.9878
30	0.6286	4.7724

#### 10.5.4 Influence of the fault inception angle

The effect of the variation of the fault inception angle on the algorithm's accuracy for AG, BC and ABG faults is shown in Table 10.12 assuming that the fault occurs at a distance of 0.6 p. u. from terminal A. Fault inception angle is varied from 0 to 150°. Considering all the cases simulated and presented in aforesaid tables, it is observed that the proposed algorithm is very accurate and virtually independent of the fault inception angle with an average error of 0.523%, 1.139% and 0.552% for AG, BC and ABG faults respectively. Figure 10.12 shows the effect of the variation of the fault inception angle on the algorithm's accuracy for above-mentioned types of faults.

#### 10.5.5 Influence of the pre-fault loading

Table 10.13 shows the influence of the pre-fault loading on the algorithm's accuracy for AG, BC and ABG faults assuming that these faults occur at 0.6 p.u. distance from terminal A. The pre-fault loading is varied from 0.5 to 3 times its original value.

Considering all the cases simulated and presented in aforesaid tables, it is observed that the proposed algorithm is highly accurate with an average error of 0.496%, 0.909% and 0.529% for AG, BC and ABG faults respectively. Figure 10.13 depicts the effect of pre-fault loading on the algorithm's fault location accuracy.

TABLE 10.12  
INFLUENCE OF THE FAULT INCEPTION ANGLE ON THE ALGORITHM'S ACCURACY  
(ACTUAL FL: 0.6 P.U. FROM TERMINAL A)

<b>Fault Inception Angle (°)</b>	<b>Fault Type</b>					
	<b>AG</b>		<b>BC</b>		<b>ABG</b>	
	<b>Estim. FL (p. u)</b>	<b>Error of Estim. FL (%)</b>	<b>Estim. FL (p. u)</b>	<b>Error of Estim. FL (%)</b>	<b>Estim. FL (p. u)</b>	<b>Error of Estim. FL (%)</b>
0	0.5969	0.5087	0.5947	0.8832	0.5967	0.5423
30	0.5969	0.5184	0.5950	0.8376	0.5968	0.5375
45	0.5967	0.5450	0.5951	0.8135	0.5968	0.5303
60	0.5965	0.5892	0.5951	0.8209	0.5969	0.5204
90	0.5960	0.6632	0.5936	1.0698	0.5969	0.5165
120	0.5965	0.5821	0.5910	1.5064	0.5967	0.5577
135	0.5972	0.4640	0.5903	1.6202	0.5965	0.5907
150	0.5981	0.3136	0.5906	1.5641	0.5963	0.6186

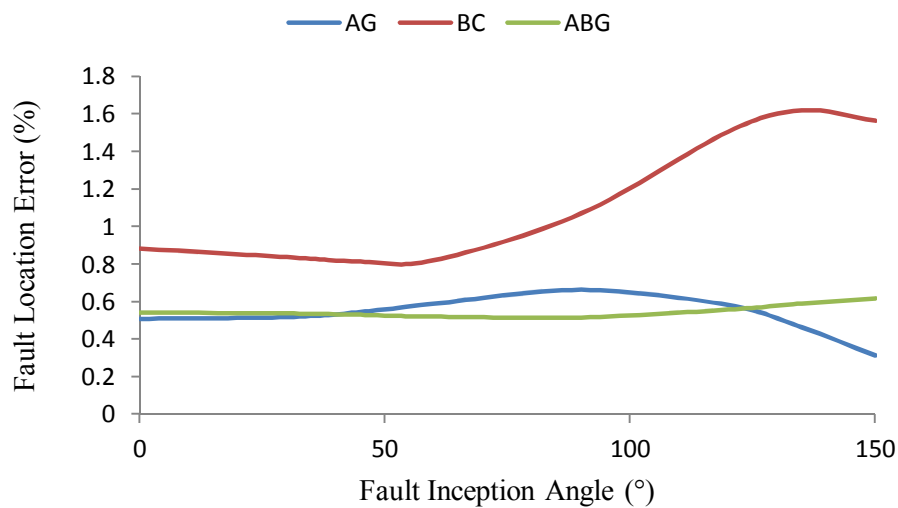


Figure 10.12: Effect of fault inception angle on FL accuracy (Actual FL: 0.6 p.u. from A)

TABLE 10.13  
INFLUENCE OF THE PRE-FAULT LOADING AT TERMINAL-A ON THE ALGORITHM'S ACCURACY  
(ACTUAL FL: 0.6 P.U. FROM TERMINAL A)

<i>Variation of Pre-fault Loading (%)</i>	<i>Fault Type</i>					
	<i>AG</i>		<i>BC</i>		<i>ABG</i>	
	<i>Estim. FL (p. u)</i>	<i>Error of Estim. FL (%)</i>	<i>Estim. FL (p. u)</i>	<i>Error of Estim. FL (%)</i>	<i>Estim. FL (p. u)</i>	<i>Error of Estim. FL (%)</i>
-50	0.5970	0.4934	0.5945	0.9088	0.5968	0.5294
-20	0.5970	0.4951	0.5945	0.9139	0.5968	0.5289
20	0.5970	0.4967	0.5945	0.9117	0.5968	0.5286
50	0.5970	0.4975	0.5945	0.9126	0.5968	0.5285
100	0.5970	0.4982	0.5946	0.9077	0.5968	0.5285
200	0.5970	0.4978	0.5946	0.8990	0.5968	0.5288

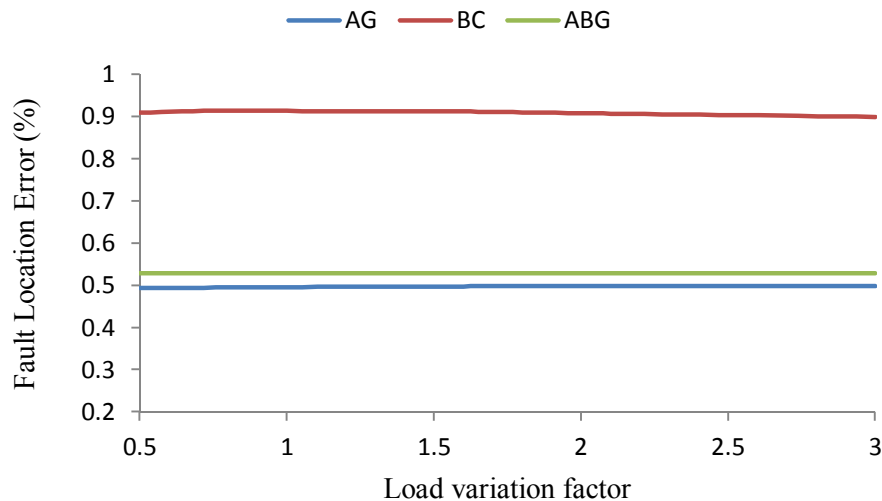


Figure 10.13: Effect of load variation on FL accuracy (Actual FL: 0.6 p.u. from A)

### 10.5.6 Influence of the compensation degree

Table 10.14 shows the influence of the compensation degree on the algorithm's accuracy for AG, BC and ABG faults assuming that these faults occur at 0.6 p.u. distance from terminal A. The compensation degree is varied from 50 % to 90 %. Considering all the cases simulated and presented in aforesaid table, it is observed that the proposed

algorithm is highly accurate and virtually independent on the compensation degree with an average error of 0.519%, 0.886% and 0.532% for AG, BC and ABG faults respectively. Figure 10.14 depicts the effect of compensation degree on the algorithm's fault location accuracy.

TABLE 10.14  
INFLUENCE OF THE COMPENSATION DEGREE ON THE ALGORITHM'S ACCURACY  
(ACTUAL FL: 0.6 P.U. FROM TERMINAL A)

<b>Compensation Degree (%)</b>	<b>Fault Type</b>					
	<b>AG</b>		<b>BC</b>		<b>ABG</b>	
	<b>Estim. FL (p. u)</b>	<b>Error of Estim. FL (%)</b>	<b>Estim. FL (p. u)</b>	<b>Error of Estim. FL (%)</b>	<b>Estim. FL (p. u)</b>	<b>Error of Estim. FL (%)</b>
50	0.5967	0.5451	0.5950	0.8398	0.5969	0.5213
60	0.5968	0.5309	0.5947	0.8839	0.5969	0.5230
70	0.5969	0.5087	0.5947	0.8832	0.5967	0.5423
80	0.5969	0.5136	0.5945	0.9118	0.5967	0.5436
90	0.5970	0.4960	0.5945	0.9140	0.5968	0.5287

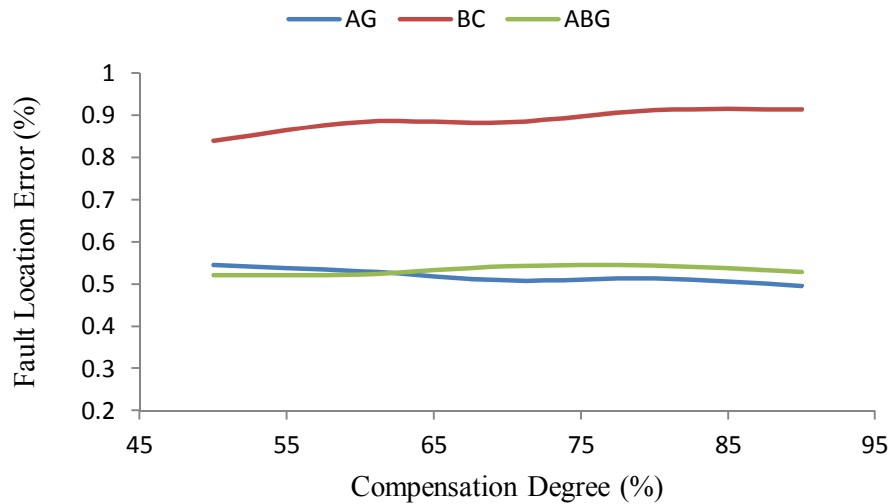


Figure 10.14: Effect of compensation degree on FL accuracy (Actual FL: 0.6 p.u. from A)

## 10.6 Comparison with non-adaptive algorithm for series-compensated lines

In the proposed adaptive fault location algorithm for SCLs, system impedance and line parameters are determined online and, thus, the effect of the surrounding environment and operation history on these parameters is nullified. System impedance and line parameters determined online from PMU synchronized measurements certainly reflect the system's practical operating conditions prior to and after the fault occurrence. In non-adaptive fault location algorithms, system impedance and line parameters are provided by the electric utility and assumed to be constant regardless of the environmental and system operating conditions. Such assumption, however, is a source of error that impacts the fault location accuracy.

In this section, we investigate the effect of system impedance and line parameters uncertainty on fault location accuracy assuming that they vary within  $\pm 25\%$  from their practical values. Table 10.15 shows the influence of the line parameters and system impedance variation on algorithm's accuracy for AG, BC, CAG and ABC faults assuming that these faults occur at 0.6 p.u. distance from terminal A. Considering all the cases simulated and presented in aforesaid table, one can easily observe that the effect of system impedance and parameters uncertainty on fault location can reach up to 23% if the parameters used in fault location vary 25% of the practical parameters. Figure 10.15 depicts the effect of the system impedance and line parameter variation on the algorithm's accuracy for aforementioned types of faults.

TABLE 10.15  
 SCLs: INFLUENCE OF LINE PARAMETERS AND SYSTEM IMPEDANCE VARIATION ON THE  
 ALGORITHM'S ACCURACY (ACTUAL FL: 0.6 P.U. FROM TERMINAL A)

Parameter Variation (%)	Fault Type							
	AG		CAG		BC		ABC	
	Estim. FL (p. u)	Error of Estim. FL (%)	Estim. FL (p. u)	Error of Estim. FL (%)	Estim. FL (p. u)	Error of Estim. FL (%)	Estim. FL (p. u)	Error of Estim. FL (%)
-25	0.4626	22.9009	0.4613	23.1150	0.4595	23.4087	0.4626	22.8971
-20	0.4962	17.3029	0.4950	17.5037	0.4933	17.7790	0.4962	17.2994
-15	0.5258	12.3635	0.5247	12.5525	0.5231	12.8116	0.5258	12.3602
-10	0.5522	7.9730	0.5511	8.1514	0.5496	8.3961	0.5522	7.9698
-5	0.5757	4.0446	0.5747	4.2136	0.5733	4.4455	0.5758	4.0416
0	0.5969	0.5090	0.5960	0.6696	0.5947	0.8899	0.5970	0.5062
5	0.6161	2.6899	0.6152	2.5369	0.6140	2.3271	0.6162	2.6925
10	0.6336	5.5979	0.6327	5.4519	0.6315	5.2516	0.6336	5.6004
15	0.6495	8.2531	0.6487	8.1134	0.6475	7.9219	0.6495	8.2555
20	0.6641	10.6870	0.6633	10.5531	0.6622	10.3696	0.6641	10.6893
25	0.6776	12.9261	0.6768	12.7976	0.6757	12.6214	0.6776	12.9284

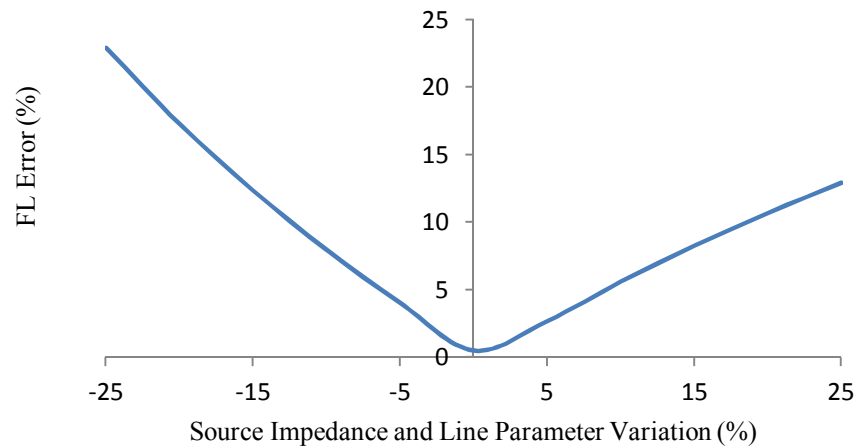


Figure 10.15: Influence of parameter variation on FL accuracy in SCLs

## **CHAPTER 11**

### **RTDS Implementation of the Proposed PMU-based Fault Locator**

In this chapter, the experimental work associated with designing a prototype PMU-based fault locator and testing its performance using real time digital simulator (RTDS) will be discussed. After an introductory section on RTDS, the fault locator design is detailed. Experimental results obtained for different cases are then presented and discussed.

#### **11.1 Real-time digital simulator (RTDS)**

The RTDS solution algorithm represents power system in the basis of nodal analysis techniques. In order to calculate the instantaneous voltages at various nodes within the system, the inverse conductance matrix is multiplied by a column vector of current injections. The conductance matrix is generally a square, rather sparse matrix whose entries depend on the circuit components connected to the nodes. The ability to separate

the conductance matrix into block diagonal pieces enables the simultaneous solution of the node voltages associated with each block. This so-called *subsystem* solution method is an important consideration in the parallel processing implemented in the RTDS. Each subsystem is simultaneously solved by different portions of the specialized hardware. The concept of mathematically isolated subsystems proved to be a significant consideration during the development of an interface to the analog simulator. [196]

The RTDS simulator is a powerful computer that accomplishes the task of real-time simulation via parallel computation. Using trapezoidal integration and exploiting the delay in travelling waves on transmission lines, the system is capable of performing time domain simulation at real-time speed using time steps less than 50 $\mu$ s. Such small time steps enable the RTDS to accurately and reliably simulate power system phenomena in the range of 0 to 3 kHz. [196, 197]

### 11.1.1 RTDS hardware

The RTDS hardware [198-202] is based on digital signal processor (DSP) and reduced instruction set computer (RISC) and utilizes advanced parallel processing techniques in order to achieve computational speeds required to maintain continuous real-time operation. The design is modular so that different size power systems can be accommodated by adding units (racks) to the simulator. Each rack of hardware includes both communication and processor cards which are linked together through a common communication backplane. In case a network exceeds the capabilities of one rack it can be divided into different racks by splitting the network into subsystems and each rack then becomes responsible for the calculation of one subsystem. Racks are identical and



each rack contains three distinct types of cards, namely tandem processor card (TPC), workstation interface card (WIC) and inter-rack communication card (IRC).

There are eighteen TPCs residing in each RTDS rack and each TPC contains two digital signal processors with a combined computing speed of approximately 44 MFLOPS (millions of floating point operations per second). TPC function in any simulation case is purely defined by software. Depending on the type of function allocated to a particular TPC during a simulation, its two processors may operate independently or in unison and, therefore, an increased processing power for component models can be achieved with more complicated algorithms. Each TPC is provided with analogue and digital input/output (I/O) in order to minimize internal data communication and to facilitate interconnection to the RTDS to measurement, control and protection devices. Half of the I/O on each TPC is generally assigned to each processor so that locally computed quantities can be directly output (input). However, under certain circumstances signals can be passed to output ports belonging to the adjacent processor or to ports on other TPCs since the system is fully programmable. Each TPC contains eight scalable analogue output ports, two 16-bit digital output ports, two 16-bit digital input ports and two analogue input ports (optional). The actual function allocated to an I/O port will vary depending on the particular model assigned to the processor during any given simulation.

Each RTDS rack also contains one WIC whose main task is to regulate communication both between the TPCs and the host computer workstation. The WIC does not actively participate in the power system solution but instead functions as an interface and simulation control device. Connection between the RTDS rack(s) and the

workstation is made via standard Ethernet based local area network. An Ethernet controller on the WIC is able to interpret data packets which are intended for its use and respond back to the originating workstation. Incoming data can be redirected by the WIC and sent on the interconnecting backplane to TPCs. In this way, control actions such as fault application or set point adjustment can be made dynamically on the workstation.

The last type of card in the RTDS architecture is the IRC. In multi-rack simulation cases, the data exchange between processors residing on separate racks is accomplished through special high-speed communication channels mounts on the IRCs. Each IRC includes up to four separate transmitted receiver channels hence allowing direct connection to as many as four other racks. RTDS simulators comprised of more than five racks are therefore not fully connected if only one IRC is used per rack.

The existing RTDS has two GPC cards with two processors in each card, analogue output component (GTAO), digital input component (GTDI) and digital output component (GTDO). Figure 11.1 shows the existing RTDS simulator.



Figure 11.1: Existing RTDS simulator

### 11.1.2 RTDS software

There are several levels of software involved with the RTDS simulator. At the lower level are the component models that have been optimized for real time operation. The highest level of software is the graphical user interface (GUI) known as RSCAD which allows simulation circuits to be constructed, run, operated and results to be recorded and documented. [200-202]

RSCAD consists of many modules including *Filemanager*, *Draft* and *Runtime*. The *Filemanager* module represents the top level of RSCAD through which the user enters the graphically driven system. This icon-based file management system aids the user in maintaining a large number of studies and the many files associated with them. All other RSCAD modules are invoked from within the *Filemanager* level. *Draft* is a pre-processing module used to assemble the power system circuit and enter its associated parameters. The user simply needs to draw a picture of the circuit instead of creating a text-based file describing the interconnection of the network under study. Icons representing individual power system components are arranged on one side of the workstation screen in the form of a user-defined library and the circuit is assembled on the other side. Assembly is accomplished by choosing and copying library components, dragging them to the circuit assembly area and interconnecting them appropriately. Operation of the RTDS is accomplished using the *Runtime* module. One or more operator's consoles can be created through which individual simulation cases can be downloaded, started and controlled. During the simulation the user can monitor specified system quantities using graphical icons of meters and plots. It is also possible to dynamically interact with the simulation as it runs by creating push buttons, sliders,

switches etc. As an example, a fault can be applied at a predefined point in the power system using a push button. The type, location and duration of the fault are defined in *Draft* before compiling the case. In addition, other events associated with the fault application (e.g. timed breaker operation) are defined prior to compiling through the *Draft* sequencer. [198, 199]

The RTDS has a specially designed compiling system representing an important link between the GUI software and the DSP code which runs on it. The RTDS compiler takes the circuit layout and parameters, entered through *Draft*, and produces all of the parallel processing code required by the digital signal processors. Moreover, the compiler automatically assigns the role that each DSP will play during the simulation based on the required circuit layout and the available RTDS hardware. The compiler follows a number of general rules when allocating processors. However, it is not always obvious to the user which processor is performing which tasks. Since under many circumstances interconnection to analogue and digital I/O is required, the user must know where to access the appropriate signals. Due to this, the compiler produces a user-readable file indicating the function of each processor in the particular case being considered in addition to producing the DSP code. This so-called MAP File also directs the user to I/O points which might be required for interfacing of physical measurement, protection or control equipment. [198, 199]

In order to produce the DSP code, the compiler accesses a library of predefined and pre-assembled power system component models. Some power system component models currently exist with RTDS include passive components, transmission lines, transformers, circuit breakers, faults, synchronous machines, MOV-protected series

capacitors, SVCs, measurement transducers, etc. Since these software models will directly impact the minimum simulation time steps achievable, they are written in low level machine language code. All of the code used in conjunction with the component models is hand assembled and optimized. Although this approach is somewhat labor intensive, it needs only be done once for each component. The optimized models are then stored in the library for access by the compiler. [198, 199]

## 11.2 RTDS applications

The RTDS technology combines the real-time operating properties of analogue simulators with the flexibility and accuracy of digital simulation programs. Due to this, the RTDS simulator has found widespread applications in power systems. It is currently applied to many areas of development, testing and studying of power system planning, feasibility studies, system operation and behavior, integrated protection and control, etc. Furthermore, since the RTDS responds in real-time to events initiated through the user interface software (i.e. operator's console), it provides an excellent method for training operators and educating engineers in the principles of power system operation. In addition, because the RTDS is housed in one or more standard 19 inch cubicles, it can conveniently be taken to substation where equipment, such as protective relays, can be easily tested. [196-199, 203]

When the RTDS is combined with suitable voltage and current amplification systems it can be used to perform closed-loop relay tests. A wide variety of tests can be performed, ranging from application of simple voltage and current waveforms through to complicated sequencing within a detailed power system model. Due to the availability of

an extensive power system component library, including measurement transducers, the relay can be tested under system conditions similar to those it will encounter in the real life. During all tests, the relay can be connected via analogue output channels to voltage and current amplifiers. Relay output contacts can in turn be connected back to circuit breaker models using the RTDS digital input ports. Closed-loop testing is unique to real-time simulation systems in that it provides a method of evaluating not only the performance of the relay, but also the response of the system to its reaction. [198, 199]

Many of the wide area protection and control schemes proposed are based on or utilize PMU data. A PMU model has been developed for the RTDS simulator so new designs can be thoroughly tested under realistic network conditions. The PMU model allows eight PMU's to be represented per instance so an extensive WAMS can be simulated. A mechanism has been developed to synchronize the simulation time step to 1 pulse per second (PPS) timing signal so the RTDS simulator can be used for benchmark testing of PMU devices. The recent trend to adopt distributed generation schemes is another opportunity for the RTDS simulator. A number of manufacturers and utilities are now using the RTDS simulator to investigate the impact of distributed generation and smart grid concepts on their existing networks. With detailed models of wind, solar, fuel cell, etc. and implementation of required communication protocols, the RTDS is well suited for simulation of today's modern power systems. [200, 204-206]

In a manner similar to that described for protection system testing, the RTDS simulator can be applied to the evaluation and testing of physical control equipment. Required analogue and digital signals produced during simulation of the power system can be connected directly to the control equipment. The controller outputs are then

connected to input points on the particular power system component model being simulated. This again closes the test loop and allows evaluation of control equipment performance on the system to which the equipment is tested. [198-200]

If appropriate interfacing points and methods are chosen, the RTDS can be used to expand and enhance the capabilities of traditional analogue simulators. A particular attention has been recently paid to expansion of HVDC analogue simulators to permit representation of larger ac networks at either end of the HVDC link. Because of the inherent difficulties associated with ac system modeling in analogue simulators, interfacing the RTDS to an analogue simulator offers a simple and relatively inexpensive alternative. [198-199]

### 11.3 Experimental work and simulation results

A two-terminal 400 kV transmission network, shown in Figure 11.2, is considered for RTDS implementation with terminal A being the sending end and terminal B being the receiving end. The transmission line connecting both terminals is represented with its equivalent nominal- $\pi$  model since it is a medium-length line. System parameters are listed in Table 11.1.

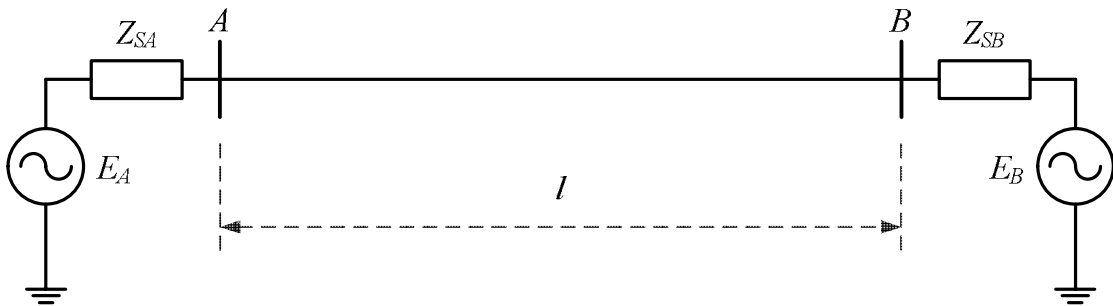
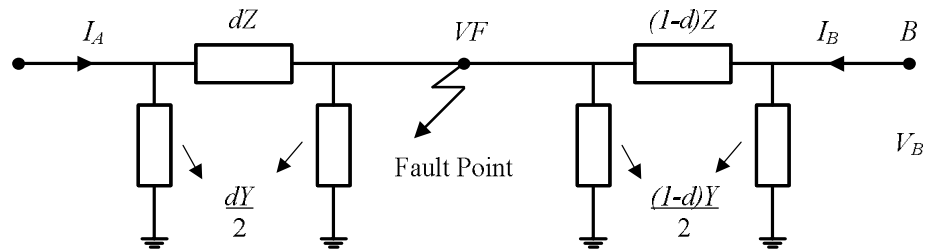


Figure 11.2: A two terminal 400 kV transmission network for RTDS implementation

TABLE 11.1: PARAMETERS OF THE 400 kV NETWORK IMPLEMENTED IN RSCAD

<i>Parameter</i>	<i>Value</i>
$l$	100 km
$Z_{1L}$	$2.76+j31.5 \Omega$
$Z_{0L}$	$27.5+j102.63 \Omega$
$C_{1L}$	13 nF/km
$C_{0L}$	8.5 nF/km
$Z_{1SA}, Z_{1SB}$	$1.31+j15 \Omega$
$Z_{0SA}, Z_{0SB}$	$2.33+j22.5 \Omega$
$E_A$	400 kV $\angle 0^\circ$
$E_B$	390 kV $\angle -10^\circ$

When the system is faulted at a per-unit distance of  $d$  from terminal A, then it can be represented as shown in Figure 11.3.

Figure 11.3: A faulted system at a distance  $d$  (p.u.) from terminal A

Applying KVL between terminal A and the fault point, we get:

$$V_F = V_A - dZ \left( I_A - V_A \frac{dY}{2} \right) \quad (11.1)$$

which can be re-written as:

$$V_F = \left( 1 + \frac{d^2ZY}{2} \right) V_A - dZI_A \quad (11.2)$$

Similarly, applying KVL between terminal B and the fault point, we get:

$$V_F = V_B - (1-d)Z \left( I_B - V_B \frac{(1-d)Y}{2} \right) \quad (11.3)$$



which can be re-written as:

$$V_F = \left(1 + \frac{(1-d)^2 ZY}{2}\right) V_B - (1-d) ZI_B \quad (11.4)$$

Equating (11.2) and (11.4) and re-arranging the terms, we get:

$$\frac{ZY}{2} (V_A - V_B) d^2 + Z(YV_B - I_A - I_B) d + \left(V_A - \left(1 + \frac{ZY}{2}\right) V_B + ZI_B\right) = 0 \quad (11.5)$$

Equation (11.5) is a quadratic equation having two solutions for d given by:

$$d = \frac{-b \pm \sqrt{b^2 - 4ac}}{2a} \quad (11.6)$$

with

$$\begin{aligned} a &= \frac{ZY}{2} (V_A - V_B) \\ b &= Z(YV_B - I_A - I_B) \\ c &= V_A - \left(1 + \frac{ZY}{2}\right) V_B + ZI_B \end{aligned} \quad (11.7)$$

In the design of the proposed fault locator, we consider the positive sequence components in calculating the coefficients a, b and c since they are present in all types of faults. The solution with an absolute value less than 1 is selected as the per unit distance (d) of the fault measured from terminal A.

The system is modeled in RSCAD as depicted in Figure 11.4. In RSCAD implementation, two PMUs are installed at the sending end (terminal A) and the receiving end (terminal B). Fault location, duration and resistance are treated as variables during the simulation. Also, the model is developed to account for all types of faults and any fault inception angle. A subsystem to control aforesaid fault parameters is shown in Figure 11.5.

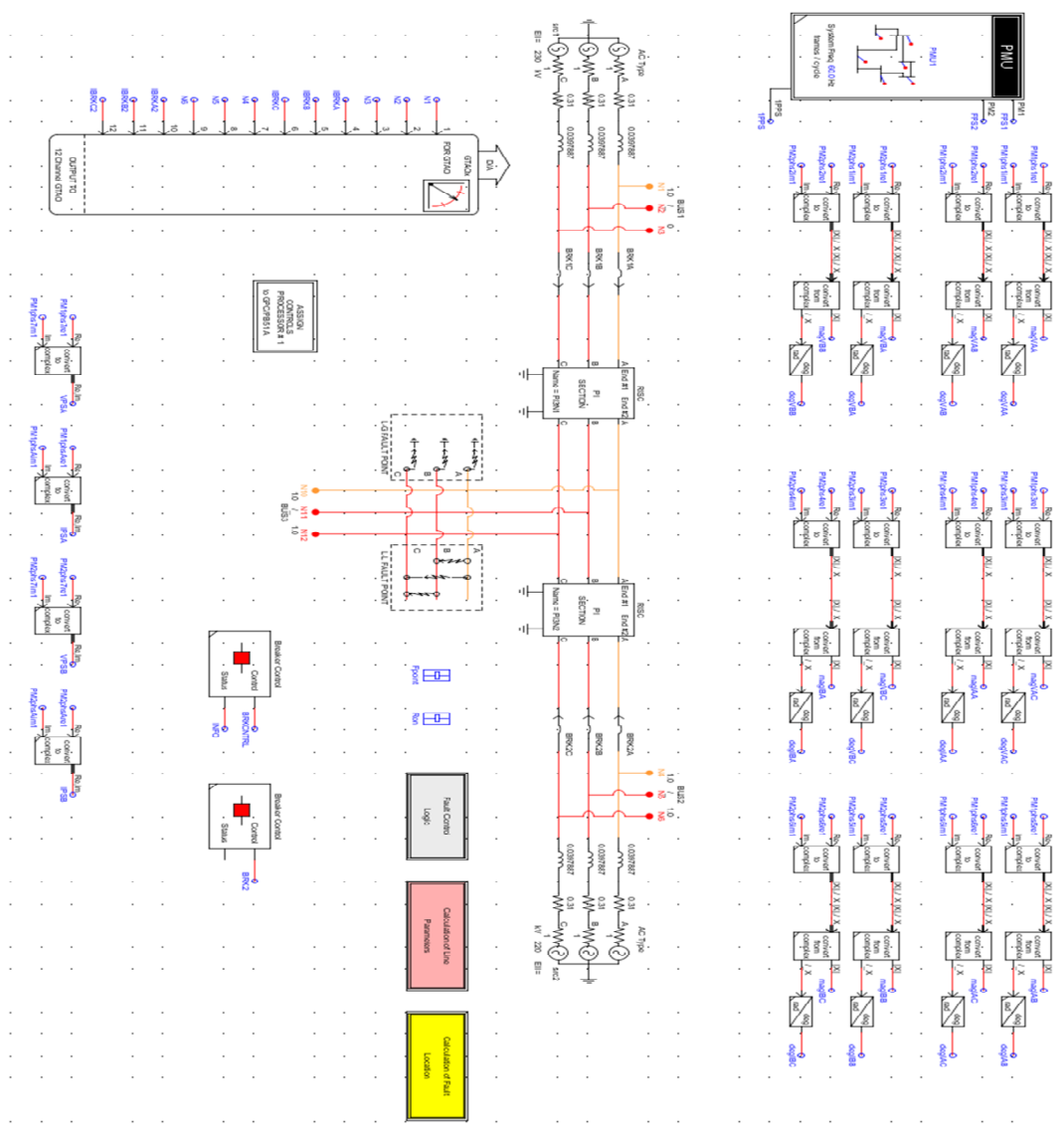


Figure 11.4: A 400 kV transmission system model in RSCAD

The diagram illustrates a neural network architecture for system identification. It features four input nodes: IPSA, IPSP, VPSA, and VPSB. These inputs feed into a series of processing blocks. The network includes summation nodes (circles with '+' or '-' signs), multiplication nodes (circles with 'x'), and a gain block (rectangle with '2.0' and '0.0'). The connections are labeled with expressions like  $|X|/X$  and  $1/X$ . The final output is ZPS.

Figure 11.6: Calculation of line parameters

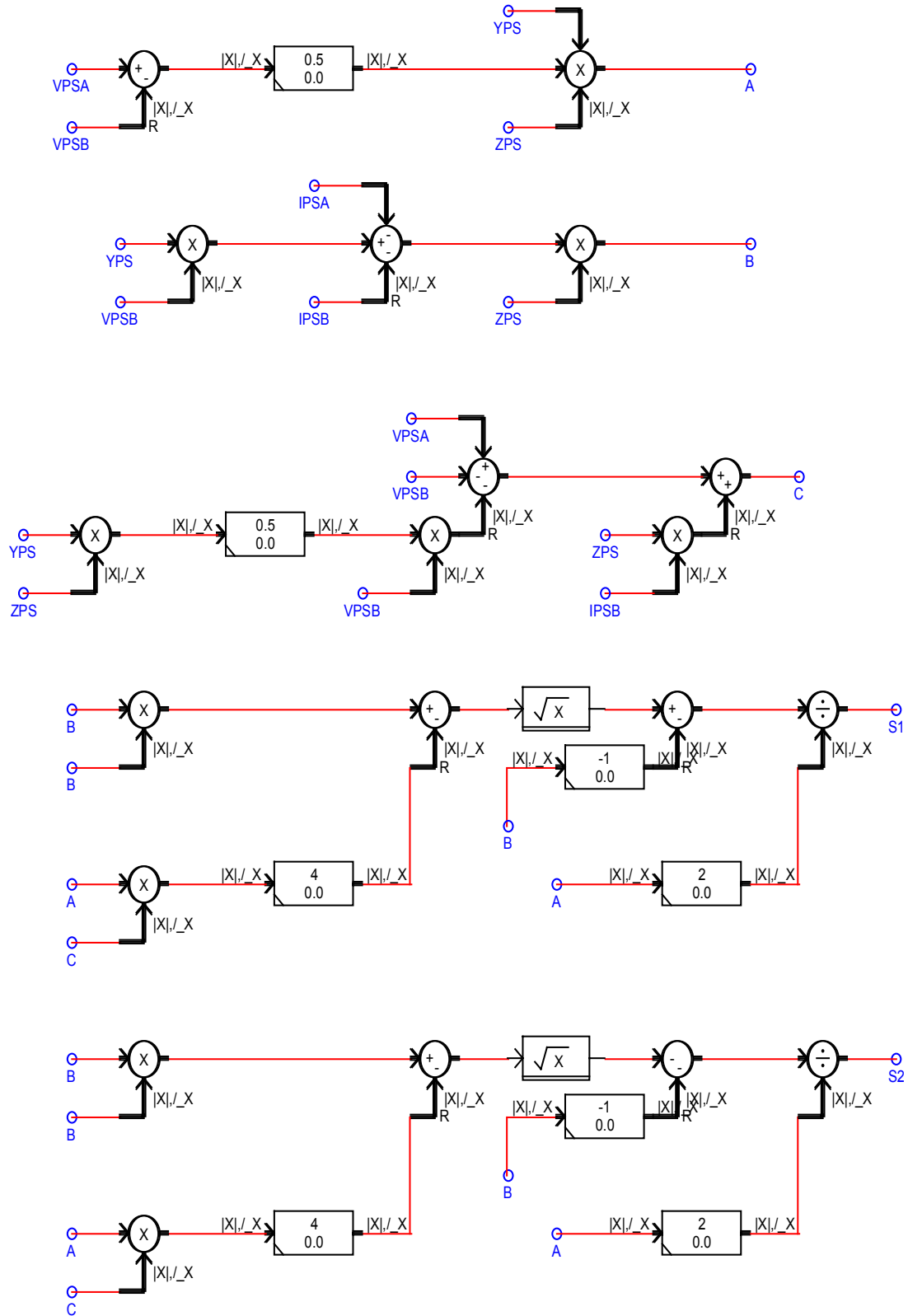


Figure 11.7: Calculation of fault location

PMUs are configured to give voltage and current phasors and their corresponding symmetrical components. The positive sequence components of pre-fault voltage and current phasors at terminal A and terminal B are utilized for online determination of the line resistance, series reactance and shunt admittance using (6.1) and (6.2). This function is incorporated in the subsystem named “Calculation of line Parameters” as shown in Figure 11.6. Figure 11.7 shows the fault location calculation based on (11.6) and (11.7). A 12-input GTAO device is incorporated in the model to allow sending voltage and current signals to external devices for further processing. The pre-fault voltages and currents at terminal A and terminal B are depicted in Figure 11.8-11.11.

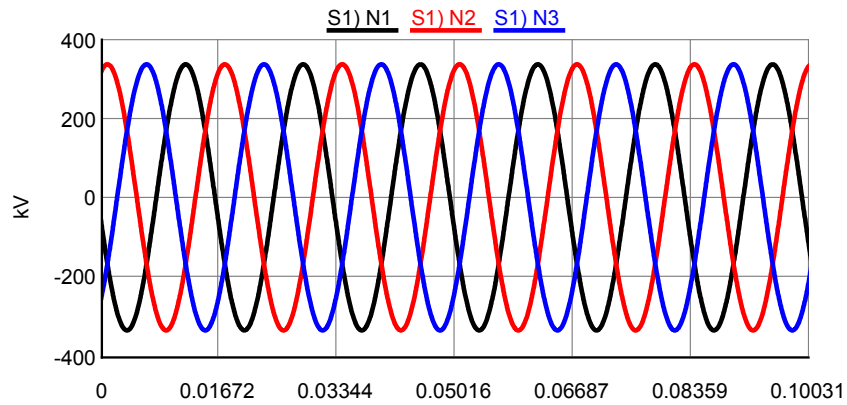


Figure 11.8: Pre-fault voltages at terminal A

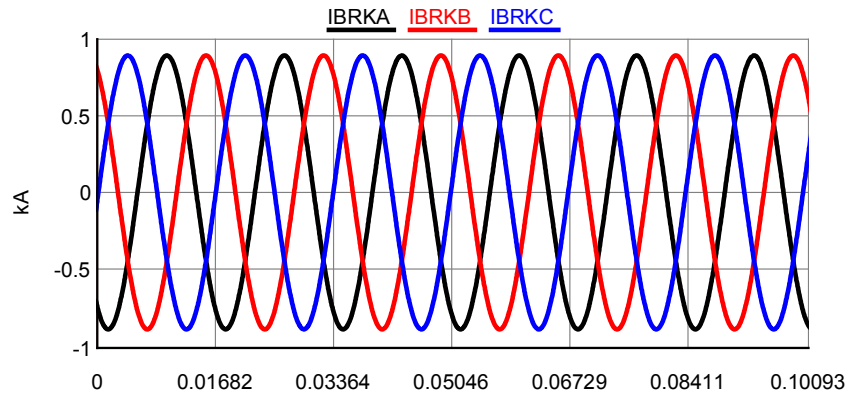


Figure 11.9: Pre-fault currents at terminal A

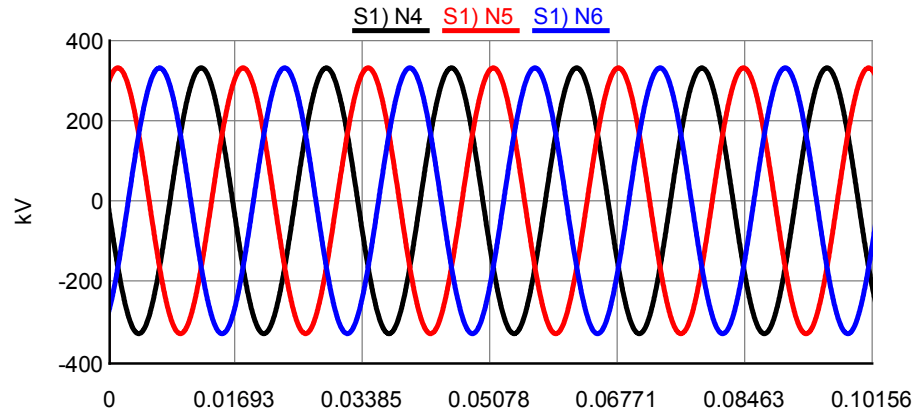


Figure 11.10: Pre-fault voltages at terminal B

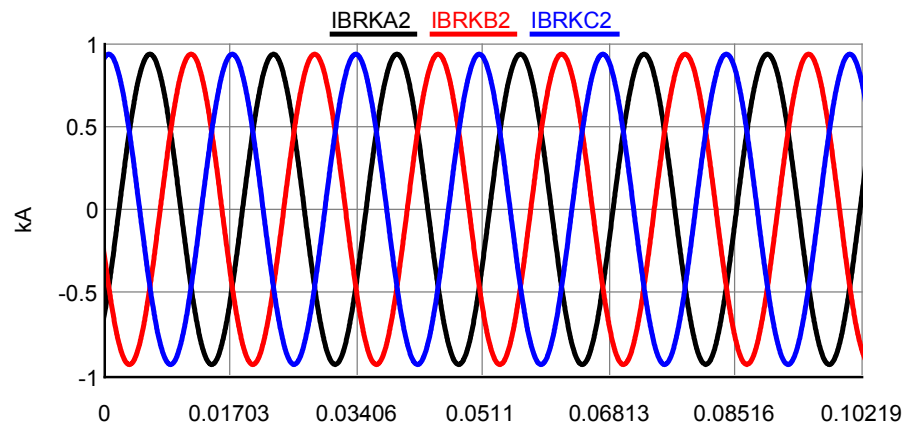


Figure 11.11: Pre-fault currents at terminal B

RSCAD has a great plotting capability. Vectors, for instance, can be plotted either in rectangular coordinates, with the real and imaginary parts of the vector, or in polar coordinates with the magnitude and angle of the vector. Figure 11.12 displays the voltage and current phasors at both terminal A and B and Figure 11.13 depicts their corresponding symmetrical components. In this study, we select phase A to ground (AG), phase B to phase C (BC), phase C to phase A to ground (CAG) and three phase (ABC) faults in order to represent LG, LL, LLG and LLL types of faults and their fault voltage and current waveforms at terminal A and terminal B are shown in Figure 11.14-11.17.

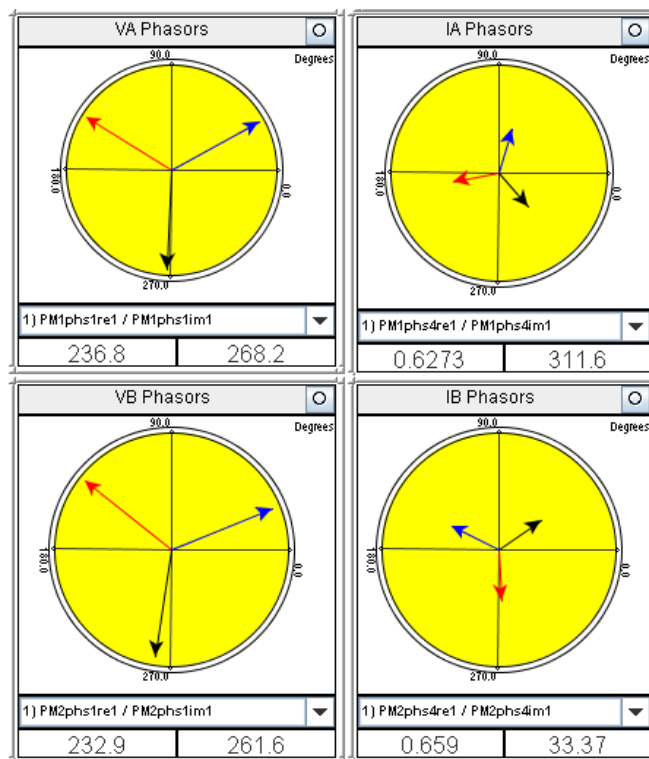


Figure 11.12: Pre-fault voltage and current phasors at terminal A and B

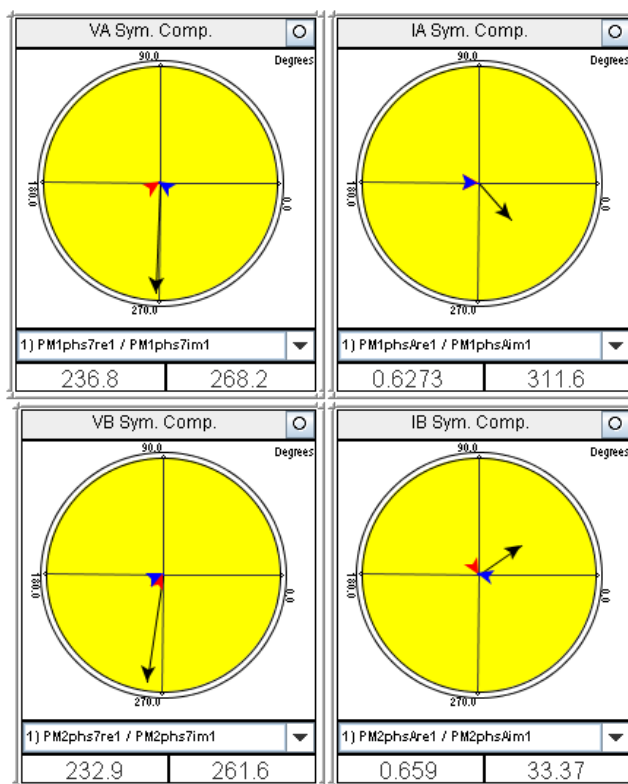


Figure 11.13: Symmetrical components of pre-fault voltage and current phasors at A and B

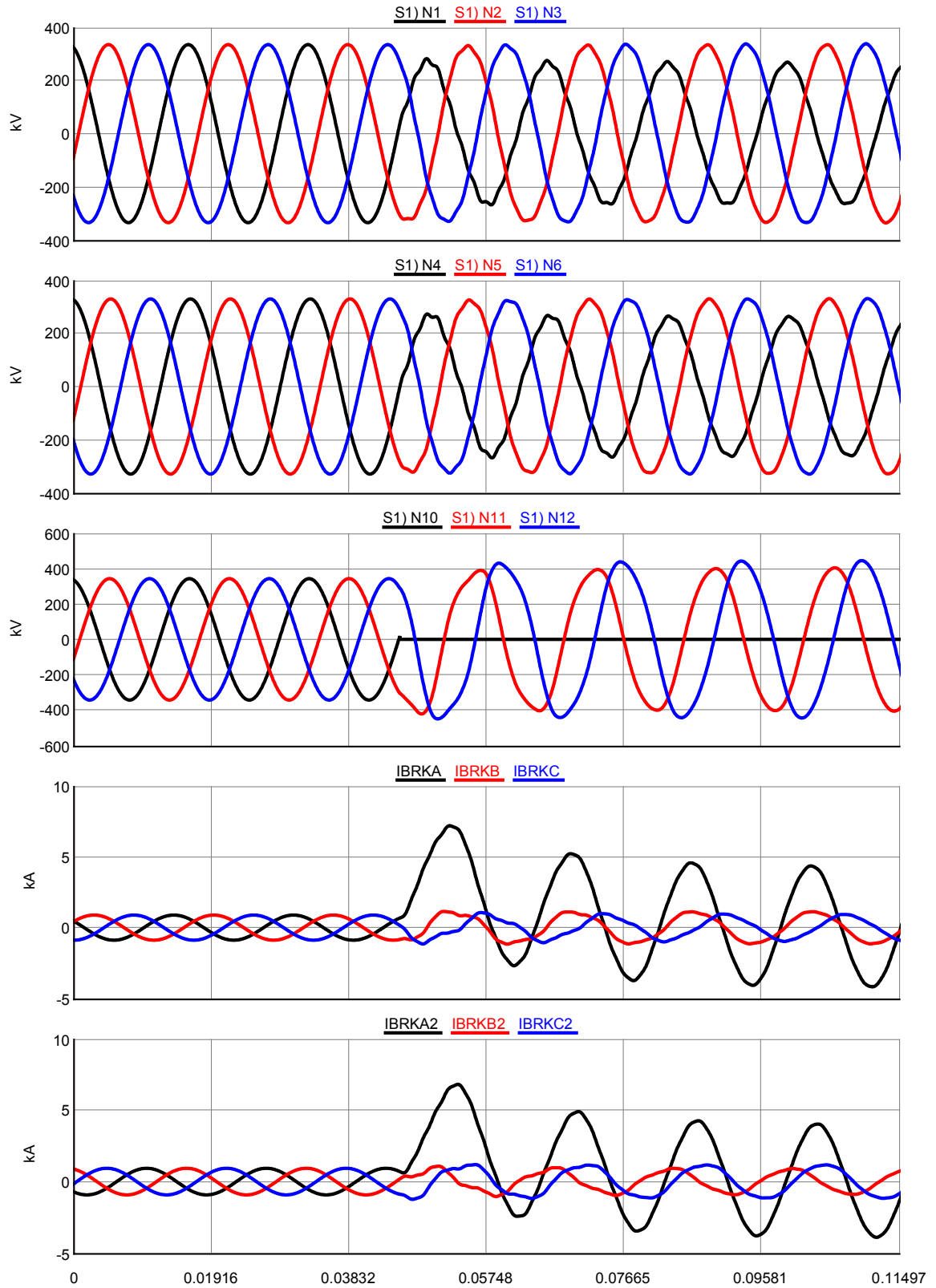


Figure 11.14: Waveforms pertaining to AG Fault



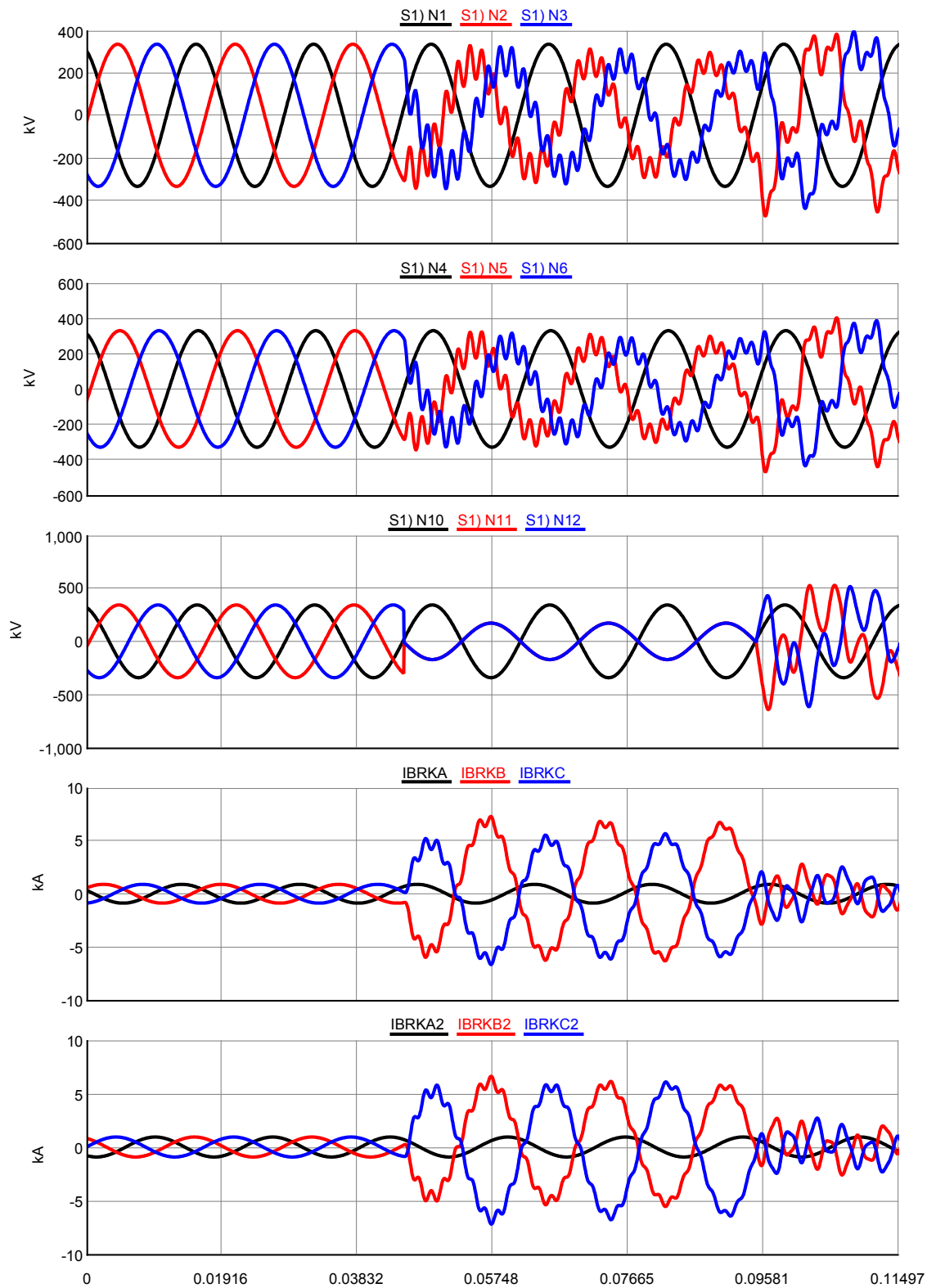


Figure 11.15: Waveforms pertaining to BC Fault

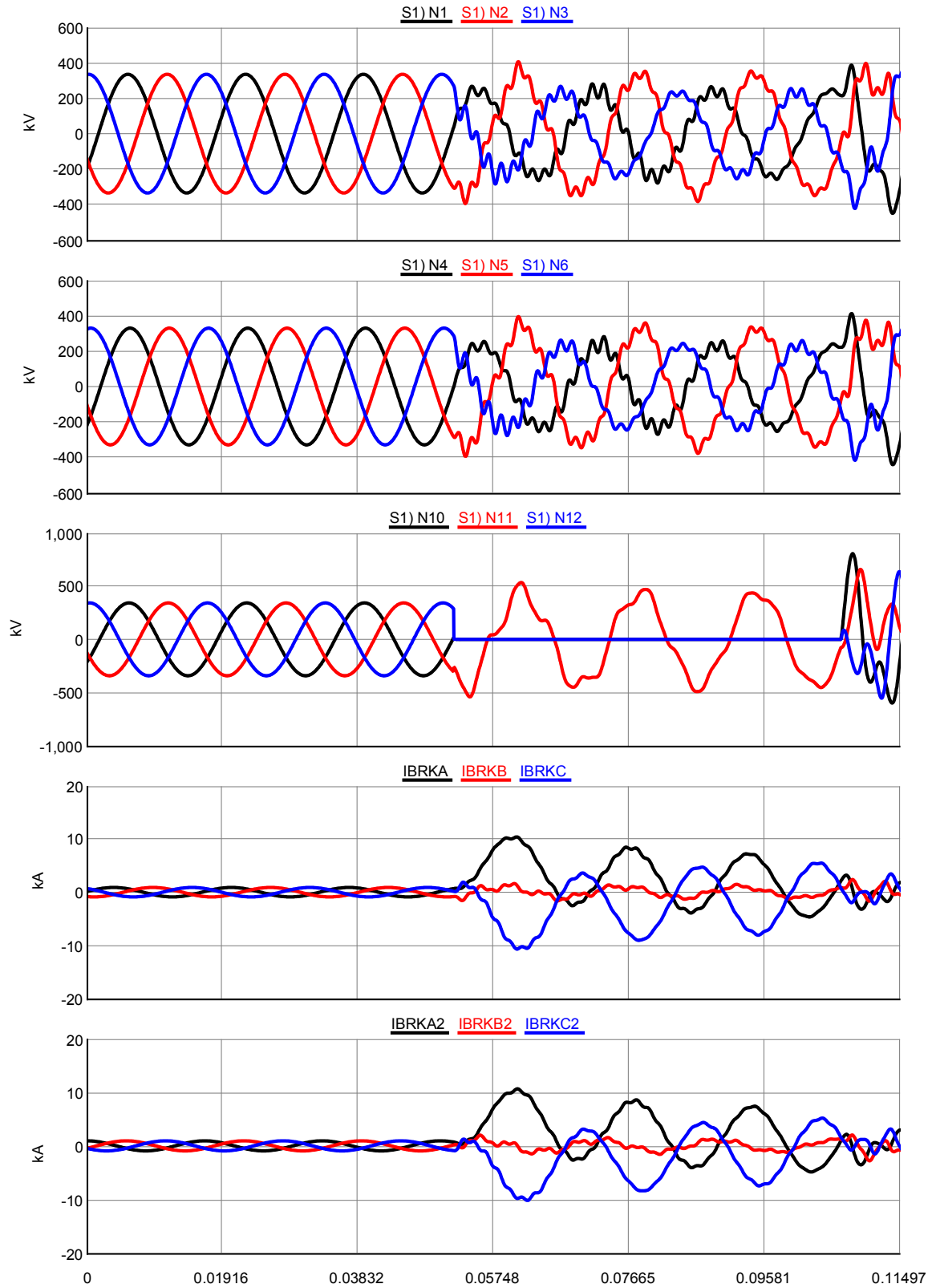


Figure 11.16: Waveforms pertaining to CAG Fault

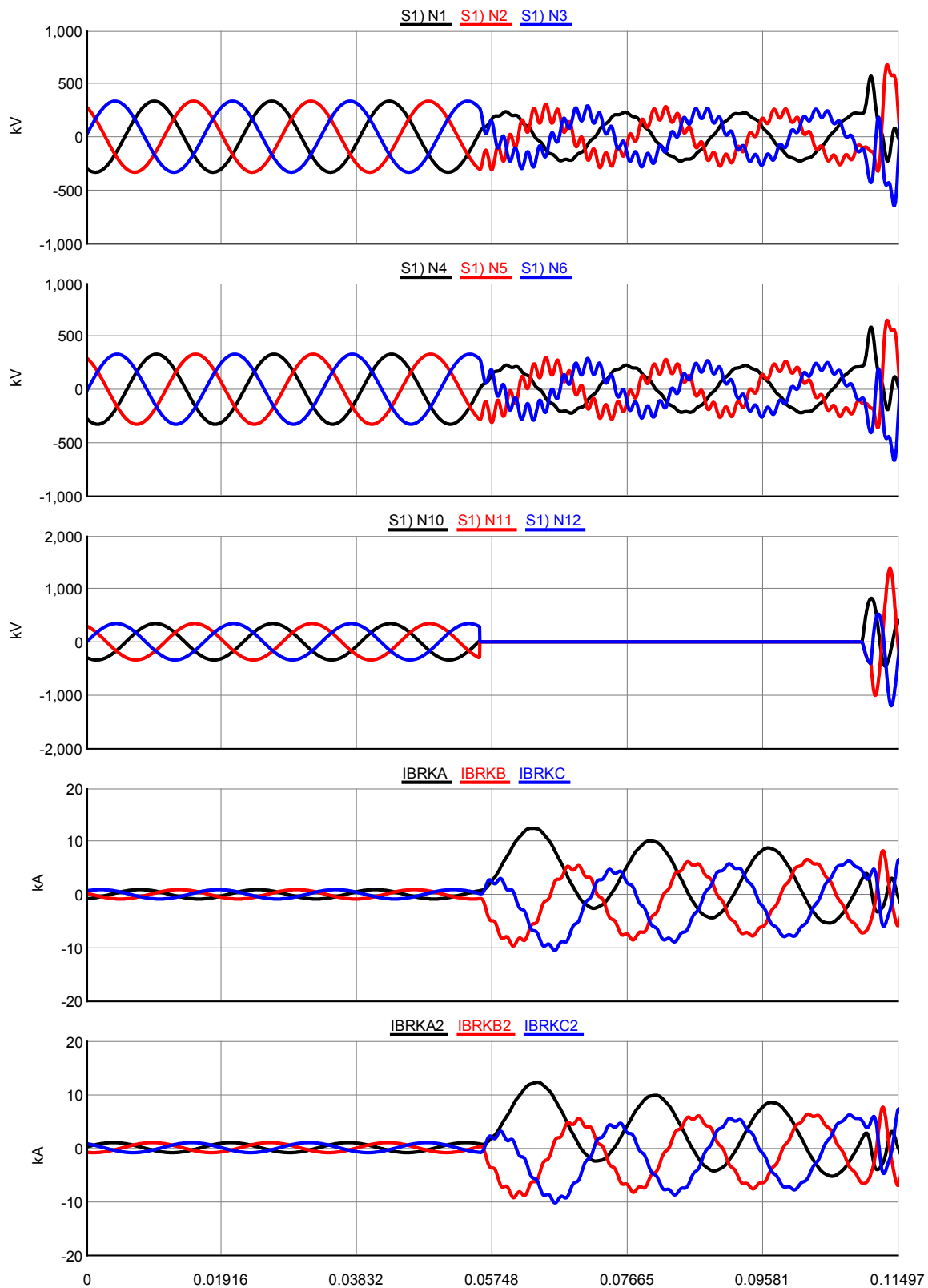


Figure 11.17: Waveforms pertaining to ABC Fault

Table 11.2 shows the accuracy of the implemented algorithm when different types of faults occur at various locations along the line. To study the influence of the fault resistance on the algorithm's accuracy, different fault resistance values are considered as shown in Table 11.3. Similarly, to study the influence of the fault inception angle on the algorithm's accuracy, different fault inception angles are considered as shown in Table 11.4. As one can see, the algorithm is highly accurate and independent of the fault type, fault location, fault resistance and fault inception angle.

TABLE 11.2  
INFLUENCE OF THE FAULT TYPE AND LOCATION ON THE ALGORITHM'S ACCURACY

<i>Fault Location (p. u)</i>	<i>Fault Type</i>							
	<i>AG</i>		<i>CAG</i>		<i>BC</i>		<i>ABC</i>	
	<i>Estim. FL (p. u)</i>	<i>Error of Estim. FL (%)</i>	<i>Estim. FL (p. u)</i>	<i>Error of Estim. FL (%)</i>	<i>Estim. FL (p. u)</i>	<i>Error of Estim. FL (%)</i>	<i>Estim. FL (p. u)</i>	<i>Error of Estim. FL (%)</i>
0.2	0.2004	0.2059	0.2000	0.0199	0.1998	0.1085	0.2001	0.0392
0.4	0.4002	0.0516	0.4001	0.0138	0.4000	0.0117	0.4001	0.0128
0.6	0.5999	0.0113	0.6000	0.0030	0.6001	0.0194	0.6000	0.0004
0.8	0.7997	0.0372	0.8000	0.0030	0.8002	0.0287	0.8000	0.0062

TABLE 11.3  
INFLUENCE OF THE FAULT RESISTANCE ON THE ALGORITHM'S ACCURACY (FL=0.6 p.u.)

<i>Fault Resist. (<math>\Omega</math>)</i>	<i>Fault Type</i>							
	<i>AG</i>		<i>CAG</i>		<i>BC</i>		<i>ABC</i>	
	<i>Estim. FL (p. u)</i>	<i>Error of Estim. FL (%)</i>	<i>Estim. FL (p. u)</i>	<i>Error of Estim. FL (%)</i>	<i>Estim. FL (p. u)</i>	<i>Error of Estim. FL (%)</i>	<i>Estim. FL (p. u)</i>	<i>Error of Estim. FL (%)</i>
0.01	0.5999	0.0113	0.6000	0.0030	0.6001	0.0194	0.6000	0.0004
1	0.5999	0.0150	0.6000	0.0071	0.6002	0.0341	0.6000	0.0038
5	0.5999	0.0102	0.6000	0.0058	0.6002	0.0268	0.6000	0.0028
10	0.6001	0.0138	0.5999	0.0118	0.6001	0.0086	0.6000	0.0064
20	0.6003	0.0432	0.5999	0.0085	0.6001	0.0167	0.6000	0.0008
30	0.6004	0.0685	0.6000	0.0022	0.6002	0.0338	0.6000	0.0073
50	0.6007	0.1201	0.6001	0.0189				
100	0.6015	0.2494	0.6003	0.0520				
200	0.6030	0.5066	0.6007	0.1185				
250	0.6038	0.6339	0.6009	0.1516				

TABLE 11.4  
INFLUENCE OF THE FAULT INCEPTION ANGLE ON THE ALGORITHM'S ACCURACY (FL=0.6 p.u.)

<i>Fault Inception Angle (°)</i>	<i>Fault Type</i>							
	<i>AG</i>		<i>CAG</i>		<i>BC</i>		<i>ABC</i>	
	<i>Estim. FL (p. u)</i>	<i>Error of Estim. FL (%)</i>	<i>Estim. FL (p. u)</i>	<i>Error of Estim. FL (%)</i>	<i>Estim. FL (p. u)</i>	<i>Error of Estim. FL (%)</i>	<i>Estim. FL (p. u)</i>	<i>Error of Estim. FL (%)</i>
0	0.5999	0.0113	0.6000	0.0030	0.6001	0.0194	0.6000	0.0004
30	0.6007	0.1240	0.6004	0.0699	0.6005	0.0769	0.6006	0.0958
45	0.5996	0.0736	0.6002	0.0355	0.5998	0.0297	0.5997	0.0558
60	0.6004	0.0598	0.6020	0.3307	0.6019	0.3119	0.6011	0.1816
90	0.5996	0.0695	0.5986	0.2334	0.5997	0.0530	0.5996	0.0681
120	0.6054	0.9049	0.6021	0.3569	0.5942	0.9647	0.5998	0.0294
135	0.5979	0.3532	0.5986	0.2370	0.6006	0.0934	0.5992	0.1361
150	0.5962	0.6313	0.5964	0.5925	0.5994	0.1036	0.5977	0.3756

## 11.4 Comparison with RTDS simulation results

In order to have a comparison with the results obtained using RTDS, the same system shown in Figure 11.2 has been modeled in PSCAD/EMTDC. AFLA-2 MATLAB code is used to simulate different fault cases for this system. Table 11.5 shows the accuracy of the implemented algorithm for all types of faults at different locations. As in the case when RTDS is used, results obtained are highly accurate with a maximum average error of 0.06%. To study the effect of the fault resistance on the algorithm's accuracy, different fault resistance values are considered as shown in Table 11.6. A maximum average error of 0.025% is observed here against a maximum average error of 0.167% obtained using RTDS. To study the influence of the fault inception angle on the algorithm's accuracy, different fault inception angles are considered as shown in Table 11.7. A maximum average error of 0.542% is observed here against a maximum error of 0.278% obtained using RTDS. From the results obtained, one may conclude that both methods are considered to be of a high accuracy.

TABLE 11.5  
INFLUENCE OF THE FAULT TYPE AND LOCATION ON THE ALGORITHM'S ACCURACY

<i>Fault Location (p. u)</i>	<i>Fault Type</i>							
	<i>AG</i>		<i>CAG</i>		<i>BC</i>		<i>ABC</i>	
	<i>Estim. FL (p. u)</i>	<i>Error of Estim. FL (%)</i>	<i>Estim. FL (p. u)</i>	<i>Error of Estim. FL (%)</i>	<i>Estim. FL (p. u)</i>	<i>Error of Estim. FL (%)</i>	<i>Estim. FL (p. u)</i>	<i>Error of Estim. FL (%)</i>
0.2	0.2003	0.1538	0.2003	0.1472	0.2003	0.1676	0.2003	0.1607
0.4	0.4001	0.0353	0.4001	0.0323	0.4001	0.0214	0.4001	0.0284
0.6	0.5999	0.0154	0.5999	0.0164	0.5999	0.0145	0.5999	0.0149
0.8	0.7997	0.0348	0.7997	0.0349	0.7997	0.0429	0.7997	0.0389

TABLE 11.6  
INFLUENCE OF THE FAULT RESISTANCE ON THE ALGORITHM'S ACCURACY (FL=0.6 P.U.)

<i>Fault Resist. (<math>\Omega</math>)</i>	<i>Fault Type</i>							
	<i>AG</i>		<i>CAG</i>		<i>BC</i>		<i>ABC</i>	
	<i>Estim. FL (p. u)</i>	<i>Error of Estim. FL (%)</i>	<i>Estim. FL (p. u)</i>	<i>Error of Estim. FL (%)</i>	<i>Estim. FL (p. u)</i>	<i>Error of Estim. FL (%)</i>	<i>Estim. FL (p. u)</i>	<i>Error of Estim. FL (%)</i>
0.01	0.5999	0.0154	0.5999	0.0164	0.5999	0.0145	0.5999	0.0149
1	0.5999	0.0153	0.5999	0.0178	0.5999	0.0163	0.5999	0.0169
5	0.5999	0.0157	0.5999	0.0197	0.5999	0.0239	0.5999	0.0221
10	0.5999	0.0162	0.5999	0.0199	0.5998	0.0285	0.5999	0.0243
20	0.5999	0.0170	0.5999	0.0197	0.5998	0.0324	0.5998	0.0268
30	0.5999	0.0176	0.5999	0.0196	0.5998	0.0347	0.5998	0.0285
50	0.5999	0.0185	0.5999	0.0195				
100	0.5999	0.0206	0.5999	0.0192				
200	0.5998	0.0260	0.5999	0.0191				
250	0.5998	0.0308	0.5999	0.0191				

TABLE 11.7  
INFLUENCE OF THE FAULT INCEPTION ANGLE ON THE ALGORITHM'S ACCURACY (FL=0.6 p.u.)

<i>Fault Inception Angle (°)</i>	<i>Fault Type</i>							
	<i>AG</i>		<i>CAG</i>		<i>BC</i>		<i>ABC</i>	
	<i>Estim. FL (p. u)</i>	<i>Error of Estim. FL (%)</i>	<i>Estim. FL (p. u)</i>	<i>Error of Estim. FL (%)</i>	<i>Estim. FL (p. u)</i>	<i>Error of Estim. FL (%)</i>	<i>Estim. FL (p. u)</i>	<i>Error of Estim. FL (%)</i>
0	0.5999	0.0154	0.5999	0.0164	0.5999	0.0145	0.5999	0.0149
30	0.6013	0.2244	0.6006	0.1068	0.6010	0.1604	0.6012	0.1918
45	0.5988	0.2043	0.6000	0.0074	0.5994	0.0929	0.5991	0.1504
60	0.6006	0.1079	0.6036	0.5992	0.6033	0.5535	0.6020	0.3253
90	0.5989	0.1755	0.5972	0.4635	0.5998	0.0397	0.5993	0.1174
120	0.6114	1.8963	0.6039	0.6504	0.5873	2.1201	0.5993	0.1106
135	0.5972	0.4674	0.5972	0.4632	0.6004	0.0684	0.5988	0.1931
150	0.5925	1.2492	0.5917	1.3820	0.5969	0.5249	0.5947	0.8770

# **CHAPTER 12**

## **Conclusions and Future Work**

In this chapter, some conclusions are drawn and contributions of this thesis work are summarized. Future research in the area of adaptive fault location using synchronized phasor measurements is highlighted.

### **12.1 Summary and conclusions**

A new formulation for OPP problem is proposed considering not only the new PMUs to be installed but also the existing ones to be retained or relocated. The aim is to achieve full network observability with the minimum number of PMUs while taking into account practical constraints and limitations of the network. Examples of such constraints include the locations at which PMUs must be installed and the places at which PMU installation must be avoided. This problem formulation is further extended by combining dual contradicting objectives; to minimize the required number of PMUs and to maximize the



PMU measurement redundancy. The existence of zero-injection buses is considered in this extended formulation and accounted for by applying some topological observability rules to assess the network observability. A solution based on differential evolution (DE) algorithm is coded in MATLAB and used to solve OPP problem. The proposed DE-based algorithm is tested on various IEEE systems and a real-life system and its performance is analyzed.

PMU-based algorithms are proposed for online determination of transmission line parameters and Thevenin's equivalent of the system at designated terminals to cope up with the requirements of adaptive fault location. Several PMU-based adaptive fault location algorithms (AFLAs) are proposed for two-terminal, three-terminal and series-compensated transmission networks. The transmission networks are modeled in PSCAD/EMTDC and the proposed AFLAs are coded in MATLAB. The fault-location accuracy evaluation is performed for these algorithms considering different factors. These include the fault type, fault location, fault resistance, fault inception angle, pre-fault loading and the compensation degree in case of series-compensated lines. Experimental work to design a prototype of a PMU-based adaptive fault locator using RTDS is carried out as well. Based on the research work presented in this thesis, the following conclusions can be drawn:

1. The comprehensive literature survey presented in this thesis has revealed the high interest in fault location based on synchronized phasor measurements.
2. It has been noticed that a power system can be made fully observable by installing PMUs at approximately one third of its buses. Consideration of the zero-injection buses in the OPP problem formulation always results in reducing the optimal

number of PMUs. Depending on the system's topology and the number of zero-injection buses, the optimal number of PMUs can go down to one fifth of the buses.

3. In comparison with published results obtained by other optimization techniques for different IEEE systems, it has been observed that solutions obtained by DE algorithm are either as good as or better in terms of the number of PMUs. When dual objectives are considered, DE algorithm produced new solutions where PMU measurement redundancy is maximized at the same minimum number of PMUs.
4. Through a number of simulation studies, it was found that designing a DE-based algorithm to solve OPP problem while avoiding PMU installation at the zero-injection buses has an advantage in producing a higher quality solution at a faster convergence of the algorithm. Similarly, avoiding PMU installation at buses that have only one incident line has the same advantage.
5. Through a number of simulation studies, it has been observed that designing a DE-based algorithm to solve the OPP problem with a constraint to get PMUs installed at buses having the highest number of incident lines may sometimes lead to solutions of a lower quality. In some other times, this may not be the case depending on the system topology.
6. Through a number of simulation studies, it has been observed that designing a DE-based algorithm to solve the OPP problem with a variable scaling factor can sometimes enhance the quality of the optimal solution and lead to a faster convergence. Also, it is found empirically that selecting the population size to be 2-3 times the number of power system buses under study is sufficient to obtain

high-quality solutions. Moreover, it is found that selecting crossover rates in the range of 0.7-0.9 usually produces solutions of a higher quality compared to the solutions obtained using smaller crossover rates in the range of 0.4-0.6.

7. The first aspect of PMU-based adaptive fault location is to determine the transmission line parameters online. This can be achieved via three different methods utilizing single, double or multiple sets of PMU synchronized measurements. It has been observed that all the three methods perform well in case if the measurements are noise-free. In the case if either a random noise or bias errors are present in PMU voltage or current measurements, the line resistance, reactance or shunt susceptance could be determined incorrectly. Through a number of simulation studies considering the presence of random noise and bias errors, the multiple measurement method has been observed to perform better than the other two methods.
8. The second aspect of PMU-based adaptive fault location is to determine the Thevenin's equivalent of the system at a particular node online. This can be achieved when at least three independent sets of PMU measurements are available. Any two sets are used to form a circle in the impedance plane and the third set is used with either the first or the second set to form another circle. The intersection point of the two circles defines the Thevenin's impedance value at that node. The Thevenin's voltage is determined from the knowledge of Thevenin's impedance and the local PMU measurements at that node. It is noticed that this technique is accurate and reflects the practical operating conditions of the system.

9. Two adaptive fault location algorithms have been proposed to locate faults in two-terminal lines. The AFLA-1, which utilizes synchronized voltage and current phasor measurements prior to and during the fault, proved to be highly accurate with a maximum fault location error of less than 0.6%. The AFLA-2, which utilizes synchronized voltage and current phasor measurements prior to the fault and only voltage measurements during the fault, proved to be highly accurate with a maximum fault location error of less than 0.9%. Both algorithms were found independent of the fault type, fault location, fault resistance, fault inception angle and pre-fault loading.
10. For two-terminal transmission networks, it has been observed that the effect of system impedance and parameters uncertainty on fault location can reach up to 10% if the parameters used in fault location vary 25% of the practical parameters.
11. The adaptive fault location algorithm proposed for three-terminal transmission networks utilizes synchronized voltage and current phasor measurements prior to the fault and only voltage measurements during the fault. It proved to be reasonably accurate with a maximum average fault location error of 1.9%. The proposed algorithm is virtually independent of the fault type, fault location, fault resistance, fault inception angle and pre-fault loading.
12. For three-terminal transmission networks, it has been observed that the effect of system impedance and parameters uncertainty on fault location can reach up to 14% if the parameters used in fault location vary 25% of the practical parameters.
13. The adaptive fault location algorithm proposed for transmission networks with a series-compensated line utilizes synchronized voltage and current phasor

measurements prior to and during the fault. The algorithm does not require any knowledge on the exact model of the series-compensation elements and, therefore, can be applied to transmission networks with any type of series-compensation units. It proved to be accurate and virtually independent of the fault type, fault location, fault resistance, fault inception angle, pre-fault loading and line compensation degree.

14. For transmission networks with a series-compensated line, it has been observed that the effect of system impedance and parameters uncertainty on fault location can reach up to 23% if the parameters used in fault location vary 25% of the practical parameters

## 12.2 Future work

The following potential future works are recommended to aid and expand the work of this thesis:

1. In case two-end synchronized measurements are utilized for fault location, it is possible to formulate more equations than the number of unknowns. The resulting redundancy may be explored to obtain certain improvements in fault location. Taking this into account, some new and highly accurate fault location algorithms may be developed.
2. New adaptive fault location techniques suiting all types of faults and not requiring line parameters and source impedances may be developed.
3. The work of designing a fault location approach capable of detecting, identifying and removing the possible bad measurements seems interesting as it helps achieve

better fault-location accuracy. A future work in this area may be developed accordingly.

4. Application of expert systems for fault location in power systems may also be an area for future research.
5. In addition to measurement noise addressed in Chapter 6, other real world challenges exist. These challenges include problems with phase angle shifting, mutual coupling between the lines and untransposed lines with unbalanced loads. The effect of such factors on parameter estimation utilizing synchronized phasor measurements may be investigated.
6. PMU-based algorithms to determine parameters of combined transmission systems composed of an overhead transmission line in series with an underground cable with two PMUs installed at only the sending and receiving ends may be developed. This enables development of adaptive fault location algorithms for such systems instead of the conventional impedance-based approaches as the one presented in [207, 208].
7. Knowing that the average temperature and sag of selected spans of a line, which can be utilized for dynamic thermal rating for increased power transfer, can be calculated based on estimated line parameters, a future research on utilizing PMUs for this application may be investigated since this work has already demonstrated the use of PMUs for line parameter determination. With regard to determination of conductor temperature, one may examine feasibility of estimating line temperature based on estimated resistance and find out meter accuracy requirements for desired temperature estimation. Various factors

affecting line resistance such as skin effects shall be considered when performing validation studies.

8. The effect of strength of equivalent sources behind the line terminals on fault location accuracy may be investigated.
9. Actual PMU measurements may be utilized to monitor the line parameters throughout the year and evaluate the variation in these parameters under different ambient temperatures and loading conditions. This future work may be used as a base to assess the need to revise the relay settings and carry out various power system's planning and operation studies.

## References

- [1] *Phasor Measurement Unit (PMU) Implementation and Applications*, EPRI, Palo Alto, CA: 2007. 1015511.
- [2] M. Saha, J. Izykowski and E. Rosolowski, “*Fault Location on Power Network*,” Springer, New York, 2010.
- [3] M. Kezunovic and B. Perunicic, “Synchronized sampling improves fault location,” *IEEE Computer Applications in Power*, vol. 8, no. 2, pp. 30-33, 1995.
- [4] V. Madani, “Western interconnection experience with phasor measurements,” *IEEE PES Power Systems Conference and Exposition*, pp. 343-352, 2006.
- [5] A. G. Phadke and J. S. Thorp, “*Synchronized Phasor Measurements and Their Applications*,” Springer, New York, 2008.
- [6] L. Chih-Wen, S. Mu-chun, T. Shuenn-Shing and W. Yi-Jen, “Application of a novel fuzzy neural network to real-time transient stability swings prediction based on synchronized phasor measurements,” *IEEE Trans. Power Syst.*, vol. 14, no. 2, pp. 685-692, 1999.
- [7] N. Zhang and M. Kezunovic, “A study of synchronized sampling based fault location algorithm performance under power swing and out-of-step conditions,” *IEEE Russia Power Tech*, pp. 1-7, 2005.
- [8] N. Zhang and M. Kezunovic, “Improving real-time fault analysis and validating relay operations to prevent or mitigate cascading blackouts,” *IEEE PES Transmission and Distribution Conference and Exhibition*, pp. 847-852, 2006.
- [9] J. Altman, “*A Practical Comprehensive Approach to PMU Placement for Full Observability*,” M.S Thesis, Faculty of the Virginia Polytechnic Institute and State University, Blacksburg, Virginia, 2007.
- [10] Y. Makarov, C. Miller, T. Nguen and M. Jian, “Characteristic ellipsoid method for monitoring power system dynamic behavior using phasor measurements,” *Bulk Power System Dynamics and Control - VII. Revitalizing Operational Reliability, IREP Symposium*, pp. 1-5, 2007
- [11] M. El-Hadidy, D. Helmi, H. Negm and H. El-Shaer, “Starting synchrophasor measurements in Egypt: a pilot project using fault recorders,” *12<sup>th</sup> International Middle-East Power System Conference*, pp. 157-161, 2008.
- [12] K. Martin, “Precise timing in electric power systems,” *Proceedings of the IEEE International Frequency Control Symposium*, pp. 15-22, 1993.
- [13] R. Burnett, M. Butts and P. Sterlina, “Power system applications for phasor measurement units,” *IEEE Computer Applications in Power*, vol. 7, no. 1, pp. 8-13, 1994.
- [14] R. Wilson, “PMUs [phasor measurement unit],” *IEEE Potentials*, vol. 13, no. 2, pp. 26-28, 1994.



- [15] J. Tlustý, A. Kasembe, Z. Müller, J. Švec, T. Šykora, A. Popelka, E. Mgaya and O. Diallo, "The monitoring of power system events on transmission and distribution level by the use of phasor measurements units (PMU)," *20<sup>th</sup> International Conference and Exhibition on Electricity Distribution*, pp. 1-4, 2009.
- [16] S. Lopez, J. Gomez, R. Cimadevilla, and O. Bolado, "Synchrophasor applications of the national electric system operator of Spain," *61<sup>st</sup> Annual Conference for Protective Relay Engineers*, pp. 436-456, 2008.
- [17] M. Kezunovic, C. Zheng, and C. Pang, "Merging PMU, operational, and non-Operational data for interpreting alarms, locating faults and preventing cascades," *43<sup>rd</sup> Hawaii International Conference on System Sciences (HICSS)*, pp. 1-9, 2010
- [18] S. Brahma, "New fault location scheme for a two-terminal transmission line using synchronized phasor measurements," *IEEE PES Transmission and Distribution Conference and Exhibition*, pp. 853-857, 2006.
- [19] S. Samantaray, L. Tripathy and P. Dash, "Differential equation-based fault locator for unified power flow controller-based transmission line using synchronised phasor measurements," *IET Generation, Transmission & Distribution*, vol. 3, no. 1, pp. 86-98, 2009.
- [20] S. El Safty, M. Nasr and M. Mansour, "New technique for fault location in interconnected networks using phasor measurement unit," *12<sup>th</sup> International Middle-East Power System Conference*, pp. 6-10, 2008.
- [21] C. Zheng, L. Chengmu, S. Jinxi and W. Xinrong, "A fault location algorithm for transmission line based on distributed parameter", *IEE International Conference on Developments in Power System Protection*, pp. 411-413, 2001.
- [22] L. Ying-Hong, L. Chih-Wen and C. Ching-Shan, "A new PMU-based fault detection/location technique for transmission lines with consideration of arcing fault discrimination-part I: theory and algorithms," *IEEE Trans. Power Del.*, vol. 19, no. 4, pp. 1587-1593, 2004.
- [23] M. Gilany, E. El Din, M. Abdel Aziz and D. Ibrahim, "An accurate scheme for fault location in combined overhead line with underground power cable," *IEEE Power Engineering Society General Meeting*, vol. 3, pp. 2521-2527, 2005.
- [24] M. Kezunovic and B. Perunicic, "Automated transmission line fault analysis using synchronized sampling at two ends," *IEEE Trans. Power Syst.*, vol. 11, no. 1, pp. 441-447, 1996.
- [25] J. Izykowski, E. Rosolowski, P. Balcerek, M. Fulczyk and M. Saha, "Accurate noniterative fault-location algorithm utilizing two-end unsynchronized measurements," *IEEE Trans. Power Del.*, vol. PP, no. 99, pp. 1-9, 2009.
- [26] Z. Radojevic, and V. Terzija, "Two terminals numerical algorithm for fault distance calculation and fault analysis," *IEEE PES Power Systems Conference and Exposition*, pp. 1037-1042, 2006.

- [27] J. Izykowski, E. Rosolowski, P. Balcerek, M. Fulczyk and M. Saha, "Accurate noniterative fault location algorithm utilizing two-end unsynchronized measurements," *IEEE Trans. Power Del.*, vol. 25, no. 1, pp. 72-80, 2010.
- [28] M. Kezunovic and B. Perunicic, "Automated transmission line fault analysis using synchronized sampling at two ends," *Proceedings of IEEE Power Industry Computer Application Conference*, pp. 407-413, 1995.
- [29] A. Gopalakrishnan, M. Kezunovic, S. McKenna and D. Hamai, "Fault location using the distributed parameter transmission line model," *IEEE Trans. Power Del.*, vol. 15, no. 4, pp. 1169-1174, 2000.
- [30] Z. Radojevic and V. Terzija, "Numerical algorithm for overhead lines protection and disturbance records analysis," *IET Generation, Transmission & Distribution*, vol. 1, no. 2, pp. 357-363, 2007.
- [31] V. Terzija, N. Elkalashy, G. Preston, V. Stanojevic and G. Strbac, "Detection of arcing faults: modelling, simulation, testing and algorithms aspects," *IEEE Lausanne Power Tech*, pp. 1147-1152, 2007.
- [32] M. Djurić, V. Terzija and Z. Radojević, "Overhead lines fault location and arc voltage estimation numerical algorithm derived in time domain," *Electrical Engineering*, vol. 81, no. 1, 1998.
- [33] C. Lee, J. Park, J. Shin and Z. Radojević, "A new two-terminal numerical algorithm for fault location, distance protection, and arcing fault recognition," *IEEE Trans. Power Syst.*, vol. 21, no. 3, pp. 1460-1462, 2006.
- [34] H. Kim, C. Lee, Z. Radojević, J. Park and J. Shin, "An improved two-terminal numerical algorithm for fault location estimation considering shunt capacitance," *IEEE Power Engineering Society General Meeting*, 2006.
- [35] S. Urano, T. Yamada, Y. Ooura, X. Youheng and Y. Yamaguchi, "Development of the high accuracy impedance type fault locator using a mode transformation," *IEEE/PES Transmission and Distribution Conference and Exhibition: Asia and Pacific*, pp. 1-6, 2005.
- [36] L. Ying-Hong, L. Chih-Wen and C. Ching-Shan, "A new PMU-based fault detection/location technique for transmission lines with consideration of arcing fault discrimination-part II: performance evaluation," *IEEE Trans. Power Del.*, vol. 19, no. 4, pp. 1594-1601, 2004.
- [37] T. El Sayed, M. Abdel Aziz, D. Ibrahim and M. Gilany, "Fault location scheme for combined overhead line with underground power cable," *Electric Power Systems Research*, vol. 76, no. 11, pp. 928-935, 2006.
- [38] L. Chan-Joo, Z. Radojević, K. Hyun-Hong, P. Jong-Bae and S. Joong-Rin, "A new numerical algorithm for fault location estimation using two-terminal synchronized voltage and current phasors," *Power Plants and Power Systems Control*, pp. 131-136, 2007.

- [39] N. Zhang and M. Kezunovic, "Complete fault analysis for long transmission line using synchronized sampling," *Power Plants and Power Systems Control*, pp 137-142, 2007.
- [40] F. Chunju, C. Huarong and Y. Weiyong, "Application of six-sequence fault components in fault location for joint parallel transmission line," *Tsinghua Science & Technology*, vol. 10, no. 2, pp. 247-253, 2005.
- [41] M. Shiroei, S. Daniar, and M. Akhbari, "A new algorithm for fault location on transmission lines," *IEEE Power & Energy Society General Meeting, PES '09*, pp. 1-5, 2009.
- [42] K. Firouzjah and A. Sheikholeslami, "A current independent synchronized phasor measurement based method for fault location on transmission lines," *ICEE '07 International Conference on Electrical Engineering*, pp. 1-5, 2007.
- [43] S. Brahma and A. Girgis, "Fault location on a transmission line using synchronized voltage measurements," *IEEE Trans. Power Del.*, vol. 19, no. 4, pp. 1619-1622, 2004.
- [44] W. Chun, D. Chun-Xia, L. Xin-Bin and J. Qing-Quan, "A WAMS/PMU-based fault location technique," *Electric Power Systems Research*, vol. 77, no. 8, pp. 936-945, 2007.
- [45] W. Chun, J. Qing-Quan, L. Xin-Bin and D. Chun-Xia, "Fault location using synchronized sequence measurements," *International Journal of Electrical Power & Energy Systems*, vol. 30, no. 2, pp. 134-139, 2008.
- [46] J. Izykowski, E. Rosolowski, M. Saha, M. Fulczyk and P. Balcerek, "A fault-location method for application with current differential relays of three-terminal lines," *IEEE Trans. Power Del.*, vol. 22, no. 4, pp. 2099-2107, 2007.
- [47] R. Aggarwal, D. Coury, A. Johns and A. Kalam, "Computer-aided design and testing of an accurate fault locator for EHV teed feeders," *Fifth International Conference on Developments in Power System Protection*, pp. 60-64, 1993.
- [48] L. Ying-Hong, L. Chih-Wen and Y. Chi-Shan, "A new fault locator for three-terminal transmission lines using two-terminal synchronized voltage and current phasors," *IEEE Trans. Power Del.*, vol. 17, no. 2, pp. 452-459, 2002.
- [49] Y. Lin, C. Liu and C. Yu, "A new fault locator for three-terminal transmission lines using two terminal synchronized voltage and current phasors," *IEEE Power Engineering Review*, vol. 21, no. 11, pp. 58-58, 2001.
- [50] K. Firouzjah and A. Sheikholeslami, "A current independent method based on synchronized voltage measurement for fault location on transmission lines," *Simulation Modeling Practice and Theory*, volume 17, no. 4, pp. 692-707, 2009.
- [51] T. Funabashi, H. Otoguro, Y. Mizuma, T. Kai, N. Takeuchi, S. Akiyama, L. Dube and A. Ametani, "Digital fault location for high resistance grounded transmission lines," *IEEE Trans. Power Del.*, vol. 14, no. 1, pp. 80-85, 1999.

- [52] A. Esmaeilian et al., "A precise PMU based fault location method for multi terminal transmission line using voltage and current measurement," *10<sup>th</sup> International Conference on Environment and Electrical Engineering*, pp. 1-4, 2011
- [53] S. Brahma, "New fault-location method for a single multiterminal transmission line using synchronized phasor measurements," *IEEE Trans. Power Del.*, vol. 21, no. 3, pp. 1148-1153, 2006.
- [54] S. Brahma, "Fault location scheme for a multi-terminal transmission line using synchronized Voltage measurements," *IEEE Trans. Power Del.*, vol. 20, no. 2 , pp. 1325-1331, 2005.
- [55] Y. Chi-Shan, L. Chih-Wen and L. Ying-Hong, "A fault location algorithm for transmission lines with tapped leg-PMU based approach," *IEEE Power Engineering Society Summer Meeting*, vol. 2, pp. 915-920, 2001.
- [56] L. Chih-Wen, L. Kai-Ping, C. Ching-Shan and J. Joe-Air, "A universal fault location technique for n-terminal ( $N \geq 3$ ) transmission lines," *IEEE Trans. Power Del.*, vol. 23, no. 3, pp. 1366-1373, 2008.
- [57] L. Kai-Ping, L. Chih-Wen, J. Jiang, C. Ching-Shan and Y. Chi-Shan, "A novel fault location algorithm for multi-terminal lines using phasor measurement units," *Proceedings of the 37<sup>th</sup> Annual North American Power Symposium*, pp. 576-581, 2005.
- [58] M. Abe, N. Otsuzuki, T. Emura and M. Takeuchi, "Development of a new fault location system for multi-terminal single transmission lines," *Proceedings of the IEEE Power Engineering Society Transmission and Distribution Conference*, pp. 259-268, 1994.
- [59] M. Abe, N. Otsuzuki, T. Emura and M. Takeuchi, "Development of a new fault location system for multi-terminal single transmission lines," *IEEE Trans. Power Del.*, vol. 10 , no. 1, pp. 159-168, 1995.
- [60] Y. Chi-Shan, L. Chih-Wen and J. Joe-Air, "A new fault location algorithm for series compensated lines using synchronized phasor measurements," *IEEE Power Engineering Society Summer Meeting*, vol. 3, pp 1350-1354, 2000.
- [61] C. Yu, C. Liu, S. Yu and J. Jiang, "A new PMU-based fault location algorithm for series compensated lines," *IEEE Power Engineering Review*, vol. 21, no. 11, pp. 58-58, 2001.
- [62] Y. Chi-Shan, L. Chih-Wen, Y. Sun-Li and J. Jiang, "A new PMU-based fault location algorithm for series compensated lines," *IEEE Transactions on Power Delivery*, vol. 17, no.1, pp. 33-46, 2002.
- [63] M. Al-Dabbagh and S. Kapuduwage, "Using instantaneous values for estimating fault locations on series compensated transmission lines," *Electric Power Systems Research*, vol. 76, no.1-3, pp. 25-32, 2005.

- [64] J. Sadeh and A. Adinehzadeh, "Accurate fault location algorithm for transmission line in the presence of series connected FACTS devices," *International Journal of Electrical Power & Energy Systems*, vol. 32, no. 4, pp. 323-328, 2010
- [65] G. Jyh-Cherng, S. Kun-Yuan, Y. Sun-Li and Y. Chi-Shan, "Removal of dc offset and subsynchronous resonance in current signals for series compensated transmission lines using a novel Fourier filter algorithm," *Electric Power Systems Research*, vol. 76, no. 5, pp. 327-335, 2006.
- [66] F. Chunju, D. Xiuhua, L. Shengfang and Y. Weiyong, "An adaptive fault location technique based on PMU for transmission line," *IEEE Power Engineering Society General Meeting*, pp. 1-6, 2007.
- [67] D. Shi, D. Tylavsky, N. Logic and K. Koellner, "Identification of short transmission-line parameters from synchrophasor measurements," *40<sup>th</sup> North American Power Symposium*, NAPS '08, pp. 1-8, 2008.
- [68] J. Jiang, C. Chen and C. Liu, "A new protection scheme for fault detection, direction discrimination, classification, and location in transmission lines," *IEEE Power Engineering Review*, vol. 22, no. 7, pp. 60-60, 2002.
- [69] J. Jiang, C. Ching-Shan and L. Chih-Wen, "A new protection scheme for fault detection, direction discrimination, classification, and location in transmission lines," *IEEE Trans. Power Del.*, vol. 18, no.1, pp. 34-42, 2003.
- [70] E. Din, M. Gilany, M. Aziz, D. Ibrahim, "An PMU double ended fault location scheme for aged power cables," *IEEE Power Engineering Society General Meeting*, vol. 1, pp. 80-86, 2005.
- [71] J. Joe-Air, L. Ying-Hong, L. Chih-Wen, Y. Jun-Zhe and T. Tong-Ming, "An adaptive fault locator system for transmission lines," *IEEE Power Engineering Society Summer Meeting*, vol. 2, pp 930-936, 1999.
- [72] C. Chen, C. Liu and J. Jiang, "A new adaptive PMU-based protection scheme for transposed/untransposed parallel transmission lines," *IEEE Power Engineering Review*, vol. 22, no. 3, pp. 61-62, 2002.
- [73] C. Ching-Shan, L. Chih-Wen and J. Joe-Air, "A new adaptive PMU based protection scheme for transposed/untransposed parallel transmission lines," *IEEE Trans. Power Del.*, vol. 17, no. 2, pp. 395-404, 2002.
- [74] J. Jiang, L. Chih-Wen and C. Ching-Shan, "A novel adaptive PMU-based transmission-line relay-design and EMTP simulation results," *IEEE Trans. Power Del.*, vol. 17, no. 4, pp. 930-937, 2002.
- [75] J. Jiang, C. Liu and C. Chen, "A novel adaptive PMU based transmission line relay: design and EMTP simulation results," *IEEE Power Engineering Review*, vol. 22, no. 7, pp. 61-61, 2002.
- [76] J. Jiang; Y. Lin; J. Yang; T. Too and C. Liu, "An adaptive PMU based fault detection/location technique for transmission lines. II. PMU implementation and performance evaluation," *IEEE Trans. Power Del.*, vol. 15, no. 4, pp. 1136-1146, 2000.

- [77] J. Jiang, J. Yang, Y. Lin, C. Liu and J. Ma, "An adaptive PMU based fault detection/location technique for transmission lines. I. theory and algorithms," *IEEE Trans. Power Del.*, vol. 15, no.2, pp. 486-493, 2000.
- [78] H. Khorashadi-Zadeh and L. Zuyi, "A novel PMU-based transmission line protection scheme design," *39<sup>th</sup> North American Power Symposium, NAPS '07*, pp. 13-19, 2007.
- [79] E. Tag Eldin, M. Gilany, M. Abdelaziz and D. Ibrahim, "An accurate fault location scheme for connected aged cable lines in double-fed systems," *Electrical Engineering*, vol. 88, no.1, 2006.
- [80] Y. Lin, C. Liu and J. Jiang, "An adaptive fault locator for transmission lines tapped with a source of generation-using synchronized voltage and current phasors," *IEEE Power Engineering Society Summer Meeting*, vol. 3, pp. 1379-1383, 2000.
- [81] L. Shengfang, F. Chunju, Y. Weiyong, C. Huarong and K. Li, "A new phase measurement unit (PMU) based fault location algorithm for double circuit lines," *Eighth IEE International Conference on Developments in Power System Protection*, vol. 1, pp. 188-191, 2004.
- [82] Z. Liang, Y. Mu, Q. Wu and W. Lu, "A new method about location for single-phase grounding fault in distribution network," *20<sup>th</sup> International Conference and Exhibition on Electricity Distribution*, pp 1-4, 2009.
- [83] K. Lien, C. Liu, C. Yu and J. Jiang, "Transmission network fault location observability with minimal PMU placement," *IEEE Trans. Power Del.*, vol. 21, no. 3, pp. 1128-1136, 2006.
- [84] Z. Guo-fang and L. Yu-ping, "Development of fault location algorithm for distribution networks with DG," *IEEE International Conference on Sustainable Energy Technologies, ICSET 2008*, pp. 164-168, 2008.
- [85] S. Abdul Gafoor and R. Rao, "Wavelet based fault detection, classification and location in transmission lines," *IEEE International Power and Energy Conference, PECon '06*, pp. 114-118, 2006.
- [86] S. Javadian, A. Nasrabadi, M. Haghighifam and J. Rezvantalab, "Determining fault's type and accurate location in distribution systems with DG using MLP neural networks," *International Conference on Clean Electrical Power*, pp. 284-289, 2009.
- [87] W. Bo, Q. Jiang and Y. Cao, "Transmission network fault location using sparse PMU measurements," *International Conference on Sustainable Power Generation and Supply*, pp. 1-6, 2009.
- [88] S. Geramian, H. Abyane and K. Mazlumi, "Determination of optimal PMU placement for fault location using genetic algorithm," *13<sup>th</sup> International Conference on Harmonics and Quality of Power*, pp. 1-5, 2008.

- [89] K. Mazlumi, H. Abyaneh, S. Sadeghi and S. Geramian, "Determination of optimal PMU placement for fault-location observability," *Third International Conference on Electric Utility Deregulation and Restructuring and Power Technologies*, pp. 1938-1942, 2008.
- [90] Y. Zhang, J. Zhang, J. Ma and Z. Wang, "Fault detection based on discriminant analysis theory in electric power system," *International Conference on Sustainable Power Generation and Supply*, pp. 1-5, 2009.
- [91] Z. Yagang, M. Jing, Z. Jinfang and W. Zengping, "Fault diagnosis based on cluster analysis theory in wide area backup protection system," *Asia-Pacific Power and Energy Engineering Conference*, pp. 1-4, 2009.
- [92] W. Zhao, X. Chen, Y. Cao and M. Peng, "A novel method of fault diagnosis based on synchronized phasor measuring and flow fingerprint identification technology," *International Conference on Sustainable Power Generation and Supply*, pp. 1-5, 2009.
- [93] Z. Yagang, Z. Jinfang, M. Jing and W. Zengping, "Fault detection and identification based on DFS in electric power network," *IEEE International Symposium on Knowledge Acquisition and Modeling Workshop*, pp. 742-745, 2008.
- [94] R. Pereira, L. da Silva and J. Mantovani, "PMUs optimized allocation using a tabu search algorithm for fault location in electric power distribution system," *IEEE/PES Transmission and Distribution Conference and Exposition: Latin America*, pp. 143-148, 2004.
- [95] D. Dustegor, S. Poroseva, M. Hussaini and S. Woodruff, "Automated graph-based methodology for fault detection and location in power systems," *IEEE Trans. Power Del.*, vol. 25, no. 2, pp. 638-646, 2010.
- [96] N. Rezaei and M. Haghifam, "Protection scheme for a distribution system with distributed generation using neural networks," *International Journal of Electrical Power & Energy Systems*, vol. 30, no. 4, pp. 235-241, 2008.
- [97] G. Kim, H. Kim and H. Choi, "Wavelet transform based power transmission line fault location using GPS for accurate time synchronization," *The 27<sup>th</sup> Annual Conference of the IEEE Industrial Electronics Society*, vol. 1, pp. 495-499, 2001.
- [98] M. Gilany, D. Ibrahim and T. El Sayed, "Traveling-wave-based fault-location scheme for multiend-aged underground cable system," *IEEE Trans. Power Del.*, vol. 22, no. 1, pp. 82-89, 2007.
- [99] H. Nouri, W. Chun and T. Davies, "An accurate fault location technique for distribution lines with tapped loads using wavelet transform," *IEEE Porto Power Tech Proceedings*, vol. 3, 2001.
- [100] M. Da Silva, M. Oleskovicz and D. Coury, "A fault locator for three-terminal lines based on wavelet transform applied to synchronized current and voltage

- signals,” *IEEE/PES Transmission & Distribution Conference and Exposition: Latin America*, pp. 1-6, 2006.
- [101] C. Evrenosoglu and A. Abur, “Fault location for teed circuits with mutually coupled lines and series capacitors,” *Proceedings of IEEE Bologna Power Tech Conference*, 2003.
  - [102] M. Da Silva, D. Coury, M. Oleskovicz and E. Segatto, “An alternative fault location algorithm based on wavelet transforms for three-terminal lines,” *IEEE Power and Energy Society General Meeting - Conversion and Delivery of Electrical Energy in the 21<sup>st</sup> Century*, pp. 1-7, 2008.
  - [103] A. G. Phadke, R.M. de Moraes, “The wide world of wide-area measurement,” *IEEE Power and Energy Magazine*, vol. 6, no. 5, pp. 52-65, 2008
  - [104] J. De La Ree, V. Centeno, J. S. Thorp, A. G. Phadke, “Synchronized phasor measurement applications in power systems,” *IEEE Trans. Smart Grid.*, vol. 1, no. 1, pp. 20-27, 2010.
  - [105] K. Martin, J. Carroll, “Phasing in the technology,” *IEEE Power and Energy Magazine*, vol. 6, no. 5, pp. 24-33, 2008
  - [106] C. Borda, A. Olarte and H. Diaz, "PMU-based line and transformer parameter estimation," *IEEE/PES Power Systems Conference and Exposition*, pp. 1-8, 2009
  - [107] A. H. Al-Mohammed and M. M. Mansour, "Fault location in SEC interconnected network based on synchronized phasor measurements," *GCC Power 2010 Conference*, pp. 1-6, October 2010
  - [108] F. Ding and C. Booth, “Protection and stability assessment in future distribution networks using PMUs,” *11<sup>th</sup> International Conference on Developments in Power Systems Protection*, pp.1-6, 2012.
  - [109] F. Ding and C. Booth, “Applications of PMUs in power distribution networks with distributed generation,” *Proceedings of 46<sup>th</sup> International Universities’ Power Engineering Conference*, pp. 1-5, 2011
  - [110] Z. Radojevic, C. Kim, M. Popov, G. Preston and V. Terzija, “New approach for fault location on transmission lines not requiring line parameters,” *International Conference on Power Systems Transients*, pp. 1-6, 2009
  - [111] Z. Dong, P. Zhang et al., “*Emerging Techniques in Power System Analysis*,” Springer, New York, 2010.
  - [112] M. Wache and D. Murray, “Application of synchrophasor measurements for distribution networks,” *IEEE Power and Energy Society General Meeting*, pp. 1-4, 2011
  - [113] M. Khederzadeh, “Wide-area protection in smart grids,” *11<sup>th</sup> International Conference on Developments in Power Systems Protection*, pp.1-4, 2012.
  - [114] P. Navalkar and S. Soman, “Secure remote backup protection of transmission lines using synchrophasors,” *IEEE Trans. Power Del.*, vol. 26, no. 1, pp. 87-96, 2011.



- [115] M. Jing et al., "Design of global power systems stabilizer to damp interarea oscillations based on wide-area collocated control technique," *IEEE Power and Energy Society General Meeting*, pp. 1-7, 2011
- [116] M. Cvetkovic and M. Ilic, "PMU based transient stabilization using FACTS," *IEEE/PES Power Systems Conference and Exposition*, pp. 1-6, 2011
- [117] S. Chakrabarti, E. Kyriakides, T. Bi, "Measurements get together," *IEEE Power and Energy Magazine*, vol. 7, no. 1, pp. 41-49, 2009
- [118] A. Bose, "Smart transmission grid applications and their supporting infrastructure," *IEEE Trans. Smart Grid.*, vol. 1, no. 1, pp. 11-19, 2010.
- [119] Available online: [http://www.ece.cmu.edu/~electricityconference/2006/Adamia-k\\_Premarlani\\_Kasztenny%20SynchroPhasors.pdf](http://www.ece.cmu.edu/~electricityconference/2006/Adamia-k_Premarlani_Kasztenny%20SynchroPhasors.pdf)
- [120] J. Chow, "Power system measurement data and their applications," *European Trans. Electr. Power*, vol. 21, no. 4, pp. 1493-1495, 2011.
- [121] R. Kavasseri and S. Srinivasan, "Joint optimal placement of PMU and conventional measurements in power systems," *Proceedings of the IEEE International Symposium on Circuits and Systems*, pp. 3449-3452, 2010.
- [122] F. Aminifar, C. Lucas, A. Khodaei and M. Fotuhi-Firuzabad, "Optimal placement of phasor measurement units using immunity genetic algorithm," *IEEE Trans. Power Del.*, vol. 24, no. 3, pp. 1014-1020, 2009.
- [123] R. Kavasseri and S. Srinivasan, "Joint placement of phasor and conventional power flow measurements for fault observability of power systems," *IET Generation, Transmission & Distribution*, vol. 5, no. 10, pp. 1019-1024, 2011.
- [124] D. Gyllstrom et al., "On the impact of PMU placement on observability and cross-validation," *3<sup>rd</sup> International Conference on Future Energy Systems*, pp. 1-10, 2012
- [125] P. SreenivasaReddy, S. P. Chowdhury and S. Chowdhury, "Power system PMU placement – a comparative survey report," *IET-UK International Conference on Information and Communication Technology in Electrical Sciences*, pp. 249-255, 2007.
- [126] B. Gou, "Generalized integer linear programming formulation for optimal PMU placement," *IEEE Trans. Power Syst.*, vol. 23, no. 3, pp. 1099-1104, 2008.
- [127] R. Sodhi, S. Srivastava and S. Singh, "Optimal PMU placement to ensure system observability under contingencies," *IEEE Power & Energy Society General Meeting*, pp. 1-6, 2009.
- [128] D. Dua, S. Dambhare, R. Gajbhiye and S. Soman, "Optimal multistage scheduling of PMU placement: an ILP approach," *IEEE Trans. Power Del.*, vol. 23, no. 4, pp. 1812-1820, 2008.
- [129] B. Ivatloo and S. Hosseini, "Optimal PMU placement for power system observability considering secondary voltage control," *Canadian Conference on Electrical and Computer Engineering*, pp. 365-368, 2008.

- [130] S. Chakrabarti, G. Venayagamoorthy and E. Kyriakides, "PMU placement for power system observability using binary particle swarm optimization," *Australasian Universities Power Engineering Conference*, pp. 1-5, 2008.
- [131] A. Sadu, R. Kumar and R. Kavasseri, "Optimal placement of phasor measurement units using particle swarm optimization," *World Congress on Nature and Biologically Inspired Computing*, pp. 1708-1713, 2009.
- [132] S. Chakrabarti, E. Kyriakides and D. Eliades, "Placement of synchronized measurements for power system observability," *IEEE Trans. Power Del.*, vol. 24, no. 1, pp. 12-19, 2009.
- [133] S. Chakrabarti and E. Kyriakides, "Optimal placement of phasor measurement units for power system observability," *IEEE Trans. Power Syst.*, vol. 23, no. 3, pp. 1433-1440, 2009.
- [134] A. Ketabi, S. M. Nosratabadi and M. R. Sheibani, "Optimal PMU placement based on mean square error using differential evolution algorithm," *First Power Quality Conference*, pp. 1-6, 2010.
- [135] V. Kekatos et al., "Optimal placement of phasor measurement units via convex relaxation," *IEEE Trans. Power Syst.*, vol. 27, no. 3, pp. 1521-1530, 2012.
- [136] F. Aminifar, M. Fotuhi-Firuzabad and A. Safdarian, "Optimal PMU placement based on probabilistic cost/benefit analysis," *IEEE Trans. Power Syst.*, vol. PP, no. 99, pp. 1-2, 2012.
- [137] A. Zadeh et al., "Optimal placement of a defined number of phasor measurement units in power systems," *2<sup>nd</sup> Iranian Conference on Smart Grids*, pp. 1-9, 2012.
- [138] L. Junqi et al., "Trade-offs in PMU deployment for state estimation in active distribution grids," *IEEE Trans. Smart Grid*, vol. 3, no. 2, pp. 915-924, 2012.
- [139] K. Lee and M. El-Sharkawi, *Modern Heuristic Optimization Techniques*, John Wiley & Sons, New Jersey, 2008.
- [140] F. Aminifar, A. Khodaei, M. Fotuhi-Firuzabad and M. Shahidehpour, "Contingency-constrained PMU placement in power networks," *IEEE Trans. Power Syst.*, vol. 25, no.1, pp. 516-523, 2010.
- [141] P. Chunhua and X. Xuesong, "A hybrid algorithm based on BPSO and immune mechanism for PMU optimization placement," *Proceedings of the 7<sup>th</sup> World Congress on Intelligent Control and Automation*, pp. 7036-7040, 2008.
- [142] M. Hajian, A. M. Ranjbar, T. Amraee and A. R. Shirani, "Optimal placement of phasor measurement units: particle swarm optimization approach," *International Conference on Intelligent Systems Applications to Power Systems*, pp. 1-6, 2007.
- [143] P. Chunhua and X. Xuesong, "A hybrid algorithm based on immune BPSO and N-1 principle for PMU multi-objective optimization placement," *Third International Conference on Electric Utility Deregulation and Restructuring and Power Technologies*, pp. 610-614, 2008.

- [144] A. A. Abou El Ela, M. A. Abido and S. R. Spea, "Optimal power flow using differential evolution algorithm," *Electric Power System Research*, vol. 80, no. 7, pp. 878-885, 2010.
- [145] M. A. Abido and N. A. Al-Ali, "Multi-objective differential evolution for optimal power flow," *International Conference on Power Engineering, Energy and Electrical Drives*, pp. 101-106, 2009.
- [146] A. H. Al-Mohammed, M. A. Abido, M. M. Mansour, "Optimal PMU placement for power system observability using differential evolution," *11<sup>th</sup> International Conference on Intelligent Systems Design and Applications*, Spain, November 22-24, 2011
- [147] R. Storn, "System design by constraint adaptation and differential evolution," *IEEE Trans. Evolutionary Computation*, vol. 3, no. 1, pp. 22-34, 1999.
- [148] K. Price, "Differential evolution: a fast and simple numerical optimizer," *Biennial Conference of the North American Fuzzy Information Processing Society*, pp. 524-527, 1996.
- [149] R. Storn, "Differential evolution design of an IIR-filter," *Proceedings of IEEE International Conference on Evolutionary Computation*, pp. 268-273, 1996.
- [150] J. Chiou and F. Wang, "A hybrid method of differential evolution with application to optimal control problems of a bioprocess system," *IEEE World Congress on Computational Intelligence*, pp. 627-632, 1998.
- [151] T. Sum-Im, "A Novel Differential Evolution Algorithmic Approach to Transmission Expansion Planning," M.S Thesis, Department of Electronic and Computer Engineering, Brunel University, 2009
- [152] B. Allagui et al., "Optimal placement of phasor measurement units by genetic algorithm," *First International Conference on Renewable Energies and Vehicular Technology*, pp. 434-439, 2012
- [153] M. Hajian, A. M. Ranjbar, T. Amraee and B. Mozafari, "Optimal placement of PMUs to maintain network observability using a modified BPSO algorithm," *Electrical Power and Energy Systems*, vol. 33, no. 1, pp. 1-6, 2011.
- [154] M. Zhou et al., "A preprocessing method for effective PMU placement studies," *Third International Conference on Electric Utility Deregulation and Restructuring and Power Technologies*, pp. 2862-2867, 2008.
- [155] J. Grainger and W. Stevenson, *Power System Analysis*, New York, McGraw-Hill, 1994
- [156] S. Chan, "Computing overhead line parameters," *Comput. Appl. Power*, vol. 6, no. 1, pp. 43-45, 1993
- [157] H. Dommel, "Overhead line parameters from handbook formulas and computer programs," *IEEE Trans. Power Appar. Syst.*, vol. PAS-104, no. 4, pp. 366-370, 1985
- [158] R. Wilson, G. Zevenbergen and D. Mah, "Calculation of transmission line parameters from synchronized measurements," *Electric Machines and Power Systems*, vol. 27, no. 12, pp. 1269-1278, 1999

- [159] C. Indulkar and K. Ramalingam, "Estimation of transmission line parameters from measurements," *International Journal of Electrical Power & Energy Systems*, vol. 30, no. 5, pp. 337-342, 2008
- [160] Y. Liao, "Algorithms for fault location and line parameter estimation utilizing voltage and current data during the fault," *40<sup>th</sup> Southeastern Symposium on System Theory*, pp. 183 - 187, 2008
- [161] Y. Liao, "Power transmission line parameter estimation and optimal meter placement," *Proceedings of the IEEE SoutheastCon 2010*, pp.250-254, 2010
- [162] Y. Liao, "Algorithms for power system fault location and line parameter estimation," *Thirty-Ninth Southeastern Symposium on System Theory*, pp. 189-193, 2007
- [163] Y. Liao and M. Kezunovic, "Online optimal transmission line parameter estimation for relaying applications," *IEEE Transactions on Power Delivery*, vol. 24, no. 1, pp. 96-102, 2009
- [164] Y. Liao and M. Kezunovic, "Optimal estimate of transmission line fault location considering measurement errors," *IEEE Transactions on Power Delivery*, vol. 22, no. 3, pp. 1335-1341, 2007
- [165] Y. Liao, "Some algorithms for transmission line parameter estimation," *4<sup>1st</sup> Southeastern Symposium on System Theory*, pp. 127-132, 2009
- [166] B. Tianshu, C. Jinmeng, W. Jingtao and Y. Qixun, "Synchronized phasor based on-line parameter identification of overhead transmission line," *Third International Conference on Electric Utility Deregulation and Restructuring and Power Technologies*, pp. 1657-1662, 2008
- [167] Y. Liao and N. Kang, "Fault location algorithms without utilizing line parameters based on the distributed parameter line model," *IEEE Transactions on Power Delivery*, vol. 24, no. 2, pp. 579-584, 2009
- [168] R. Che and J. Liang, "An accurate fault location algorithm for two-terminal transmission lines combined with parameter estimation," *Asia-Pacific Power and Energy Engineering Conference*, pp. 1-4, 2009
- [169] S. Zocholl and D. Smaha, "Current transformer concepts," Proc. Of 19<sup>th</sup> Annual Western Protective Relay Conference, Spokane, WA, 1992
- [170] J. Linders, C. Barnett and J. Chadwick, "Relay performance considerations with low-ratio CTs and high fault currents," *IEEE Trans. Ind. Appl.*, vol. 31, no. 2, pp. 392-404, 1995
- [171] S. Abdelkader, "Online Thevenin's equivalent using local PMU measurements," *International Conference on Renewable Energies and Power Quality*, Spain, pp. 1-4, 2010
- [172] C. Chuang, J. Jiang, Y. Wang, C. Chen and Y. Hsiao, "An adaptive PMU-based fault location estimation system with a fault-tolerance and load-balancing communication network," *IEEE Lausanne Power Tech*, pp. 1197-1202, 2007
- [173] E. Tag El Din, M. Abdel Aziz, D. Ibrahim and M. Gilany, "Fault location scheme for combined overhead line with underground power cable," *Electric Power Systems Research*, vol. 76, no. 11, pp. 928-935, 2006
- [174] C. Apostolopoulos and G. Korres, "A novel algorithm for locating faults on transposed/untransposed transmission lines without utilizing line parameters," *IEEE Trans. Power Del.*, vol. 25, no. 4, pp. 2328-2338, 2010

- [175] C. Wang, Q. Jia, X. Li and C. Dou, "Fault location using synchronized sequence measurements," *International Journal of Electrical Power & Energy Systems*, vol. 30, no. 2, pp. 134-139, 2008
- [176] C. Wang, C. Dou, X. Li and Q. Jia, "A WAMS/PMU-based fault location technique," *Electric Power Systems Research*, vol. 77, no. 8, pp. 936-945, 2007
- [177] J. Quanyuan, L. Xingpeng, W. Bo and W. Haijiao, "PMU-based fault location using voltage measurements in large transmission networks," *IEEE Trans. Power Del.*, vol. 27, no. 3, pp. 1644-1652, 2012.
- [178] E. Nashawati, R. Garcia and T. Rosenberger, "Using synchrophasor for fault location identification," *65<sup>th</sup> Annual Conference for Protective Relay Engineers*, pp. 14-21, 2012
- [179] Y. Lin, C. Liu and C. Chen, "A new PMU-based fault detection/location technique for transmission lines with consideration of arcing fault discrimination-Part I: theory and algorithms," *IEEE Trans. Power Del.*, vol. 19, no. 4, pp. 1587-1593, 2004
- [180] Y. Lin, C. Liu and C. Chen, "A new PMU-based fault detection/location technique for transmission lines with consideration of arcing fault discrimination-Part II: performance evaluation," *IEEE Trans. Power Del.*, vol. 19, no. 4, pp. 1594-1601, 2004
- [181] C. Apostolopoulos and G. Korres, "A novel fault-location algorithm for double-circuit transmission lines without utilizing line parameters," *IEEE Trans. Power Del.*, vol. 26, no. 3, pp. 1467-1478, 2011
- [182] C. Chen, C. Liu and J. Jiang, "A new adaptive PMU based protection scheme for transposed/untransposed parallel transmission lines," *IEEE Trans. Power Del.*, vol. 17, no. 2, pp. 395-404, 2002
- [183] W. Zengping et al., "Principal components fault location based on WAMS/PMU measure system," *IEEE Power and Energy Society General Meeting*, pp. 1-5, 2011
- [184] G. Jancke, N. Fahlen and O. Nerf, "Series capacitors in power systems," *IEEE Trans. Power Apparatus and Systems*, vol. PAS-94, no. 3, pp. 915-925, 1975
- [185] R. Grunbaum and J. Samuelsson, "Series capacitors facilitate long distance AC power transmission," *2005 IEEE Russia Power Tech*, pp. 1-6, 2005
- [186] Available online: <http://itee.uq.edu.au/~aupec/aupec02/Final-Papers/SK-Kapuduwage.pdf>
- [187] J. Izykowski et al., "Fault location on double-circuit series-compensated lines using two-end unsynchronized measurements," *IEEE Trans. Power Del.*, vol. PP, no. 99, 2011
- [188] M. Kizilcay and P. La Seta, "A new unsynchronized two-terminals fault location method on series compensated lines," *2005 IEEE Russia Power Tech*, pp. 1-7, 2005
- [189] M. Saha, K. Wikstrom, J. Izykowski and E. Rosolowski, "New concept for fault location in series-compensated parallel lines," *IEEE Power Engineering Society Winter Meeting*, vol. 2, pp. 769-774, 2001
- [190] Available online: <http://www.montefiore.ulg.ac.be/services/stochastic/pscc05/papers/fp56.pdf>

- [191] J. Sadeh, N. Hadjsaid, A.M. Ranjbar and R. Feuillet, "Accurate fault location algorithm for series compensated transmission lines," *IEEE Trans. Power Del.*, vol. 15, no. 3, pp. 1027-1033, 2000
- [192] M. Fulczyk et al., "Fault locator using two-end unsynchronized measurements for UHV series compensated parallel lines," *International Conference on High Voltage Engineering and Application*, pp. 88-91, 2008
- [193] M. Fulczyk et al., "Two-end unsynchronized fault location algorithm for double-circuit series compensated lines," *IEEE Power and Energy Society General Meeting- Conversion and Delivery of Electrical Energy in the 21<sup>st</sup> Century*, pp. 1-9, 2008
- [194] R. Dutra, L. Fabiano, M. Saha and S. Lidstrom, "Fault location on parallel transmission lines with series compensation," *IEEE/PES Transmission and Distribution Conference and Exposition: Latin America*, pp. 591-597, 2004
- [195] M. Saha, J. Izykowski and E. Rosolowski, "A fault location method for application with current differential protective relays of series-compensated transmission line," *10<sup>th</sup> IET International Conference on Developments in Power System Protection (DPSP 2010), Managing the Change*, pp. 1-5, 2010
- [196] C. Seung et al., "A real-time simulation platform for power system operation," *IPEC Conference Proceedings*, pp. 909-914, 2010
- [197] G. Jackson et al., "A real-time platform for teaching power system control design," *International Conference on Power Systems Transients*, pp. 1-5, 2005.
- [198] R. Kuffel et al., "RTDS – a fully digital power system simulator operating in real time," *IEEE WESCANEX '95 Proceedings*, vol. 2, pp. 300-305, 1995.
- [199] R. Kuffel et al., "RTDS – a fully digital power system simulator operating in real time," *EMPD '95 Proceedings*, vol. 2, pp. 498-503, 1995.
- [200] Available online: [http://www.aesieap0910.org/upload/File/PDF/5-Poster%20Sessions/PP/PP0202/PP0202007/PP0202007\\_FP.pdf](http://www.aesieap0910.org/upload/File/PDF/5-Poster%20Sessions/PP/PP0202/PP0202007/PP0202007_FP.pdf)
- [201] A. Saran et al., "Real time power system simulation using RTDS and NI PXI," *40<sup>th</sup> North American Power Symposium*, pp.1-6, 2008.
- [202] C. Apostolopoulos and G. Korres, "Real-time implementation of digital relay models using MATLAB/SIMULINK and RTDS," *Euro. Trans. Electr. Power*, pp. 1-15, 2008.
- [203] Available online: <http://soa.asee.org/paper/conference/paper-view.cfm?id=11825>
- [204] D. Ouellette et al., "Using a real time digital simulator with phasor measurement unit technology," *International Conference on Advanced Power System Automation and Protection*, vol. 3, pp. 2472-2476, 2011.
- [205] P. Tatcho, Y. Zhou, H. Li and L. Liu, "A real time digital test bed for a smart grid using RTDS," *2<sup>nd</sup> IEEE International Symposium on Power Electronics for Distributed Generation Systems*, pp. 658-661, 2010
- [206] Available online: <http://www.aesieap0910.org/upload/File/Exhibitor%20News/RDTS.pdf>
- [207] P. Eguia, I. Martin, I. Zamora and R. Cimadevilla, "Fault location in combined transmission lines using PMUs for recloser control," *IEEE Trondheim Power Tech*, pp. 1-8, 2011
- [208] L. Chih-Wen, L. Tzu-Chiao, Y. Chi-Shan and Y. Jun-Zhe, "A fault location technique for two-terminal multisection compound transmission lines using

synchronized phasor measurements,” *IEEE Trans. Smart Grid*, vol. 3, no. 1, pp. 113-121, 2012.

## Extracted Papers

### **Published Papers**

1. A. H. Al-Mohammed, M. M. Mansour, "Fault location in SEC interconnected network based on synchronized phasor measurements," *GCC Power 2010 Conference*, Doha, Qatar, October 18-20, 2010, vol. 2, pp. 1-6.
2. A. H. Al-Mohammed, M. M. Mansour, M. A. Abido, "Application of phasor measurement units (PMUs) for fault location in SEC-EOA interconnected network," *IEEE International Energy Conference and Exhibition*, Bahrain, 2010, pp. 435-439.
3. A. H. Al-Mohammed, M. A. Abido, M. M. Mansour, "Transmission line parameter identification in SEC network using synchronized phasor measurements," *GCC Power 2011 Conference*, Kuwait, November 22-24, 2011, pp. 226-232.
4. A. H. Al-Mohammed, M. A. Abido, M. M. Mansour, "Optimal PMU placement for power system observability using differential evolution," *11<sup>th</sup> International Conference on Intelligent Systems Design and Applications*, Spain, November 22-24, 2011
5. A. H. Al-Mohammed, M. A. Abido, M. M. Mansour, "Optimal placement of synchronized phasor measurement units based on differential evolution algorithm" *IEEE PES ISGT Middle East 2011*, Saudi Arabia, December 18-20, 2011
6. A. H. Al-Mohammed, M. M. Mansour, M. A. Abido, "Fault location in SEC interconnected network based on synchronized phasor measurements," *GIGRE 2012*, Paris, France, August 2012 (Paper # C4-205)

### **Papers under Submission**

1. "Fault Location Based on Synchronized Measurements - A Comprehensive Survey" submitted to *Energy Conversion & Management* on January 2012
2. "An Adaptive Current Independent PMU Based Fault Location Algorithm for Power System Networks" submitted to *IEEE Trans. Smart Grid* on February 2012

### **Papers under Preparation**

1. "An Adaptive Fault Location Algorithm for Power System Networks Based on Synchrophasor Measurements"
2. "An adaptive PMU-based Fault Location Algorithm for a Three-terminal Transmission Network"
3. "An adaptive PMU-based Fault Location Algorithm for Series-compensated Lines"



4. "Parameter Identification for Combined Transmission Systems Using Synchronized Phasor Measurements"

**Appendix-A: NASPI's Synchrophasor Applications Table**

<i>Topics</i>	<i>Applications</i>	<i>Description</i>
Reliability Operations	Wide-area grid monitoring and visualization	Use phasor data to monitor and alarm for metrics across entire inter-connection (frequency stability, voltage, angle differences, MW and MVAR flows).
	Power plant monitoring and integration	Use real-time data to track and integrate power plant operation (including intermittent renewables and distributed energy resources).
	Alarming for situational awareness tools	Use real-time data and analysis of system conditions to identify and alert operators to potential grid problems
	State estimation	Use actual measured system condition data in place of modeled estimates.
	Inter-area oscillation monitoring, analysis and control	Use phasor data and analysis to identify frequency oscillations and initiate damping activities.
	Automated real-time control of assets	Use phasor data and analysis to identify frequency oscillations and initiate damping activities.
	Wide-area adaptive protection and system integrity protection	Real-time phasor data allow identification of grid events and adaptive design, execution and evaluation of appropriate system protection measures
	Planned power system separation	Improve planned separation of power system into islands when instability occurs, and dynamically determine appropriate islanding boundaries for island-specific load and generation balances.
	Dynamic line ratings and VAR support	Use PMU data to monitor or improve transmission line rating in real time
	Day-ahead and hour-ahead operations planning	Use phasor data and improved models to understand current, hour-ahead, and day-ahead system operating conditions under a range of normal and potential contingency operating scenarios.
	Automatically manage frequency and voltage response from load	System load response to voltage and frequency variations.
	System reclosing and power system restoration	Use phasor data to bring equipment back into service without risking stability or unsuccessful reclosing attempts.
	Protection system and device commissioning	
Market Operation	Congestion analysis	Synchronized measurements make it possible to operate the grid according to true real-time dynamic limits, not conservative limits derived from off-line studies for worst-case scenarios.
Planning	Static model benchmarking	Use phase data to better understand system operations, identify errors in system modeling data, and fine-tune power system models for on-line and off-line applications (power flow, stability, short circuit, OPF, security assessment, modal frequency response, etc.).
	Dynamic model benchmarking	Phasor data record actual system dynamics and can be used to validate and calibrate dynamic models.
	Generator model validation	
	Stability model validation	
	Performance validation	Use phasor data to validate planning models, to understand observed system behavior and predict future behavior under assumed conditions.
Others	Forensic event analysis	Use phasor data to identify the sequence of events underlying an actual system disturbance, to determine its causes.
	Phasor applications vision, road mapping & planning	

## Appendix-B: IEEE Test Systems

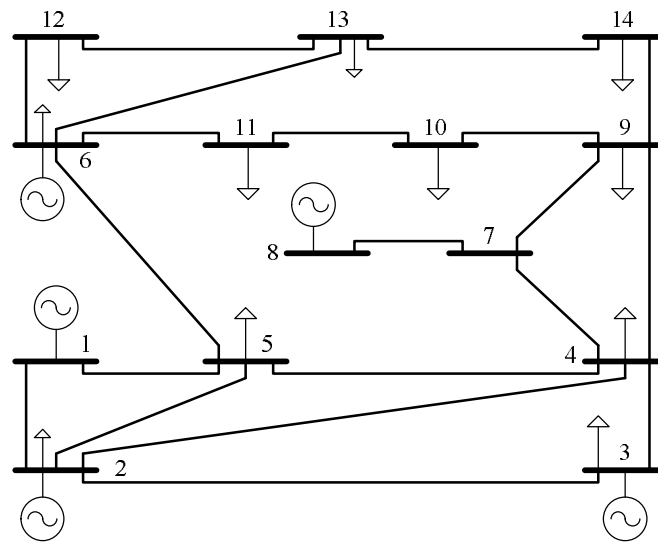


Figure A.1: IEEE 14-bus test system

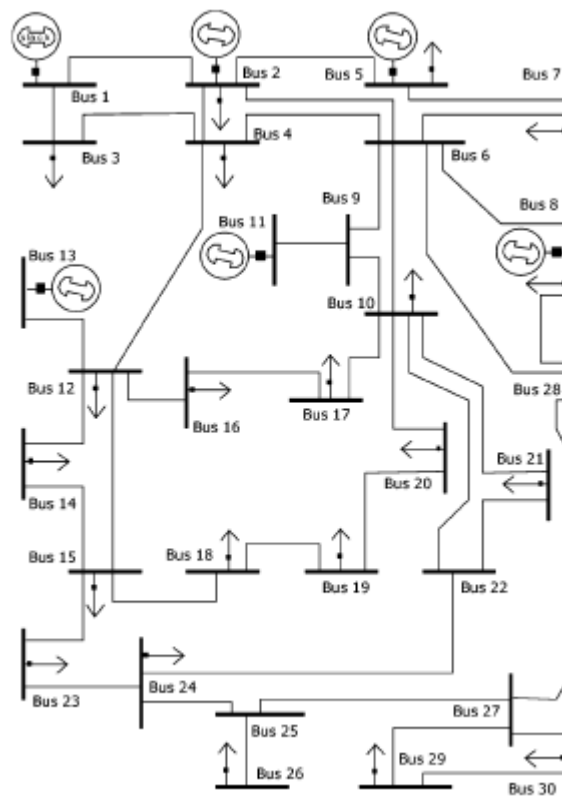


Figure A.2: IEEE 30-bus test system

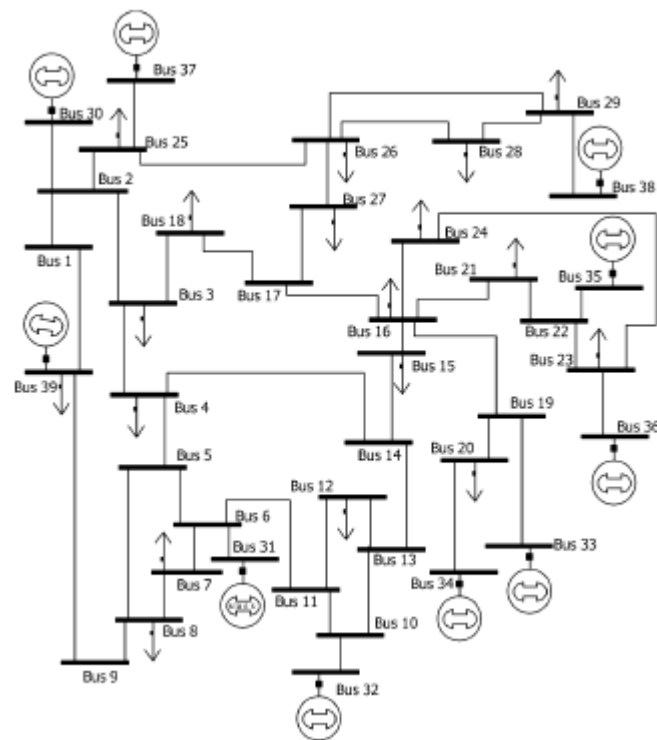


Figure A.3: IEEE 39-bus test system

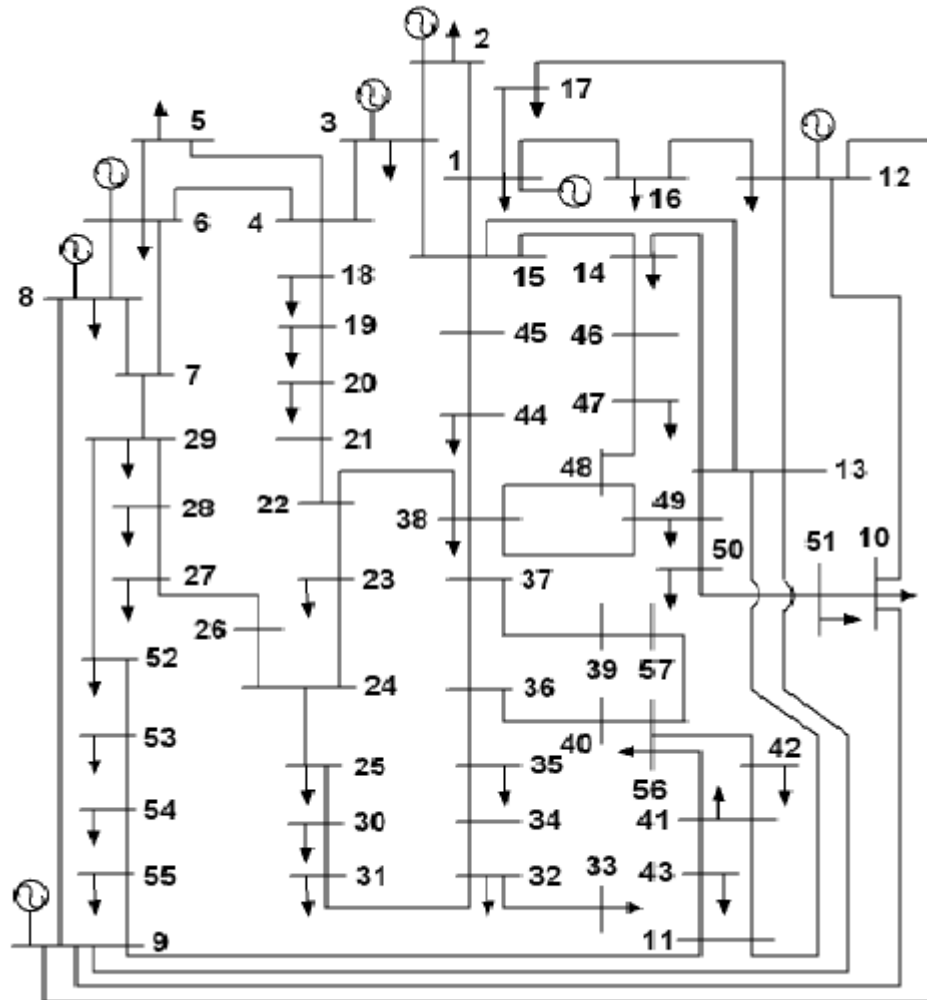


Figure A.4: IEEE 57-bus test system

## Vita

Name : Ali Hassan Al-Mohammed

Birth Date : August 5, 1972

Birth Place : Al-Hassa, Saudi Arabia

Status : Married

Nationality : Saudi

Address : SEC-EOA  
E&DD/E&DD-EOA  
P.O.Box:5190  
Dammam-31422  
Saudi Arabia

Telephone No. : 00966 3 8585326

E-mail : ali200ahm@yahoo.com

Education : Master's degree in Electrical Engineering from King Fahd University of Petroleum and Minerals, Dhahran, Saudi Arabia in 1999.

Bachelor's degree with highest honors in Electrical Engineering from King Fahd University of Petroleum and Minerals, Dhahran, Saudi Arabia in 1994.

Area of Interest : Power system planning, Wide-area monitoring and control of power systems, PMU applications in power systems, High voltage engineering